

FEASIBILITY AND IMPLICATIONS OF A ROCK COATING CATENA:
ANALYSIS OF A DESERT HILLSLOPE

by

R. Evan Palmer

A Thesis Presented in Partial Fulfillment
of the Requirements for the Degree
Master of Arts

ARIZONA STATE UNIVERSITY

August 2002

Report Documentation Page		
Report Date 01AUG2002	Report Type N/A	Dates Covered (from... to) -
Title and Subtitle Feasibility and Implications of a Rock Coating Catena: Analysis of a Desert Hillslope	Contract Number	
	Grant Number	
	Program Element Number	
Author(s) Palmer, Ronald E.	Project Number	
	Task Number	
	Work Unit Number	
Performing Organization Name(s) and Address(es) Arizona State University	Performing Organization Report Number	
Sponsoring/Monitoring Agency Name(s) and Address(es) The Department of the Air Force AFIT/CIA, Bldg. 125 2950 P. St. Wright-Patterson AFB, OH 45433	Sponsor/Monitor's Acronym(s)	
	Sponsor/Monitor's Report Number(s)	
Distribution/Availability Statement Approved for public release, distribution unlimited		
Supplementary Notes The original document contains color images.		
Abstract		
Subject Terms		
Report Classification unclassified	Classification of this page unclassified	
Classification of Abstract unclassified	Limitation of Abstract UU	
Number of Pages 209		

FEASIBILITY AND IMPLICATIONS OF A ROCK COATING CATENA:

ANALYSIS OF A DESERT HILLSLOPE

by

R. Evan Palmer

has been approved

July 2002

APPROVED:

_____, Chair

Supervisory Committee

ACCEPTED:

Department Chair

Dean, Graduate College

In loving memory of

Larry Knight Palmer

ACKNOWLEDGMENTS

My heartfelt thanks goes to many special people who have helped make this possible, only a few of which I am able to mention. First, to my chair, Dr. Ron Dorn. Thank you for your willingness to take me on as a student, despite the odds against me. I appreciate your patience, expert guidance and editing, and help in order to finish on time. I thank Dr. Steve Gordon, not only for serving on my committee and helping me to get in contact with the right folks here at ASU, but for your friendship throughout the last three years. I also thank Niccole Cerverny and Dr. Robert Balling for being willing to be a part of my committee. Both of you played important roles in helping me excel.

A very special thanks goes to LTC Daniel Gilewitch and family. You have been an excellent role model for as a senior officer, even though I have yet to see you in uniform! Thank you for your friendship and intellectual encouragement. LTC Gilewitch obtained the TMS imagery and converted it to a readable format (VICAR) and made the atmospheric correction (MODTRAN) before sharing it with me. The ASU Department of Geography provided facility and software support. To my good friend Jeremy Williams, thanks for your assistance in the field.

I am so grateful to my family—Misty, Brandon, and Quinn. Misty, thank you for your amazing love and companionship. Brandon, thanks for helping me find the ‘dark’ rocks and the ‘light’ rocks. Quinn, thanks for joining us and being so cute. It has been a fun and interesting road together. I also thank my wonderful parents, brothers, and sisters, for their help and encouragement.

Finally, I thank the Air Force for extending me this opportunity to spend a year studying geography and geomorphology.

ABSTRACT

This research analyzes rock coatings on a basaltic hill in the western Mojave Desert using a combination of aerial imagery, a new method of digital ‘in-field’ ground-based image processing, and statistical analyses. In addition, this research resulted in the development of a new rock coating index (RCI) to generalize changes in rock coatings along a slope, applied here to 2,760 individual clasts.

RCI values reveal variations of different types of rock coatings on different particle sizes, in this case rock varnish, iron films, and rocks eroding too fast to host any coating. Larger particles host more rock varnish, iron films do not prefer a particular particle size, and highly weathered ‘no-coating’ rocks are relatively smaller.

Hillslope position in a catena strongly influences the nature of rock coatings. Although slope angle did not reveal statistically significant relationships with particle sizes in any of the transects, rock varnish dominates on hilltops. Iron films occur at all slope positions, but dominance is apparent where varnish influence is minimal at the lower slope positions. "High albedo" (no coating) rocks occur throughout the catena without a clear slope position signal. Young's model of soil horizon character along a slope fits these data in that positions of least transport mobility correspond with rock varnish dominance, suggesting that maps of rock coating character can be a proxy for slope stability.

A fundamental question is whether field-based observations link statistically to observations gathered from aerial or satellite platforms. Results show statistically significant correlations between RCI ground values and three separate Thematic Mapper

Simulator (TMS) wavebands: mid infrared (2.08-2.35 μ m), near infrared (0.76-0.90 μ m), and visible (0.45-0.52 μ m).

Variables in a discriminant analysis represent a combination of low-resolution data from TMS, medium resolution data from the orthophotograph albedo, and higher resolution field data, separated by slope position. A combined plot of canonical discriminant functions shows distinct discriminant fences between the top convex, middle straight, and bottom concave sections of the studied transect slopes.

Driven by the need for data on slope stability, future researchers can now predict surficial rock coating catenas using remotely sensed values, at least for homogenous hills of basaltic lithologies. Obviously, this first study has been limited to a feasibility test using one lithology and one location. However, the success of the multi-scale approach justifies expansion into other settings.

Disclaimer: The views expressed in this thesis are those of the author and do not reflect the official policy or position of the United States Air Force, Department of Defense, or the U.S. Government.

TABLE OF CONTENTS

	Page
LIST OF TABLES	ix
LIST OF FIGURES	x
CHAPTER 1. Introduction	1
1.1. Interface of geomorphology and remote sensing	1
1.2. Issues of scale and resolution	3
1.3. Case study: rock coating distribution on a desert hillslope.	4
1.4. Problem statement.	7
1.5. Broader implications of the study.	9
1.6. Organization of the thesis	10
CHAPTER 2. Introducing the concept of a rock coating catena.	11
2.1. Remote sensing of desert slopes.	11
2.2. Catena studies in desert geomorphology.	18
CHAPTER 3. Methods	26
3.2. Digital image sampling.	28
3.3. Rock coating index, GIS, and data matrix creation	37
3.4. Method results in this study.	43
CHAPTER 4. Results and discussion	44
4.1. Introduction	44
4.2. Data matrix	44
4.3. Results	45
4.4. Discussion	60
CHAPTER 5. Conclusion	66

	Page
REFERENCES.....	69
APPENDIX	
A. DIGITAL IMAGES.....	77
B. DATA TABLE.....	171

LIST OF TABLES

Table	Page
1.1. 15 known types of rock coatings and their descriptions.	6
2.1. Options in the Multi-approach.	14
2.2. TMS and LANDSAT TM Bands and Wavelengths.	17
3.1. Several important studies of particle size measurement and sampling schemes applied to the field sampling and digital image processing method in this study	30
3.2. NIH or Scion Image instructions	36
4.1 Descriptive statistics	46
4.2. Kolmogorov-Smirnov test.	47
4.3. Difference of means test	50
4.4. Structure Matrices for B1 (left), B2 (center), and B3 (right). Function 1 is renamed “stability”, in terms of slope position, or distance from the top of the hill and Function 2 relabeled “rock coating horizons”. Note the inverse relationship in the structure coefficients for rock coating and iron skins RCI variables	58
B.1. Partial data table from digital field sampling and digital image processing of 2760 basalt clasts	172

LIST OF FIGURES

Figure	Page
1.1. Venn Diagram showing the interconnectedness of rock weathering in the subfield of geomorphology, remote sensing, and GIS	5
2.1. Conceptual diagram of desert geomorphology's potentially greater percent of interaction with remote sensing, due to a more direct view of the surface, than geomorphology as a whole.	12
2.2. Cross-sectional diagrams of simple catenas. 'A' is representative of arid regions, 'B' is representative of semi-arid regions	19
2.3. Young's model describing the possible ways that soils horizons can vary along a catena: 'A' remain constant; 'B' increase; 'C' decrease; 'D' deepen; 'E' rise; 'F' end or begin, 'G' and 'H' be replaced; or 'I' gradually change in terms of properties but maintain the same identity.	21
2.4. Picture of <i>in situ</i> weathering in a basalt clast from study site. The shell of altered rock around the edge, reddish brown on the outside and a dark purple as it transitions from parent material, is about 2-5mm thick. Hand provides scale. There is also a micro-thin iron film on this sample	23
3.1. Study site in the western Mojave Desert. The arrow points to the basalt hill on as seen in a USGS digital orthophotograph. Highway 58 at the bottom of the image gives scale. North is to the top.	27
3.2. Establishing a scale in Step 2 by counting the number of pixels that spans one inch on the inset ruler. Drawing an object, in this case a line set at an appropriate weight, so that its edges touch tick marks quickly gives photo scale. The scale for this picture is 39 pixels inch ⁻¹	32
3.3. Steps 3-5. 'A' is an Adobe Photoshop window showing the semi-grid for selecting particles in Step 3. 'B' is the resulting 'cut-out' image of extracted particles from Step 4. Note that the rocks in 'B' are in the exact, to near exact, location as in the original image. Before Step 5, particles are filled in with black, 'C', and saved as a TIFF file. 'D' is the way the now outlined and cataloged particles appear after analysis in Scion Image. 'E' shows corresponding results, in this case area (mm ²), perimeter length (mm), two-dimensional major axis (mm), and two-dimensional minor axis (mm), which may be pasted into a spreadsheet program such as Microsoft Excel.	33

Figure		Page
3.4.	Rock Coating Index (RCI) continuum for rock varnish, iron films (or iron skins), and particles eroding too fast to have either varnish or iron films. Each field observation at a field of view of approximately 0.5 meters can have a RCI score of 0-120 for varnish and iron skins, and a score between 0-30 for no coating RCI. RCI is an indicator for rock coating strength.	39
3.5.	ArcGIS map showing the line theme representing transects beginning at origin (intersection) on the top of the hill and extending in (magnetic) north, west, south, and east directions for transects B1, B2, B3, and B4, respectively. The image is a 1-meter resolution digital orthophotograph. As depicted here, the line for transect B1 extends roughly 800 feet.	41
3.6.	Close-up view of higher resolution (~0.5 meter) observation points (small squares) ‘overlaid’ on top of TMS data (larger gray squares) at 25 meter resolution. This is a visual depiction of how a GIS can integrate isolated field observations and contiguous remotely sensed data of different scales. Transect B1 extends from bottom to top and a portion of B2 is in the lower left corner	42
4.1.	Plot of mean particle size (mm^2) and standardized values for slope angle (degrees). This relationship is not statistically significant ($p=0.426$).	49
4.2.	Plot of mean varnish area, iron film area, and high albedo area and standard error bars at the 90% confidence interval, showing a statistically significant difference between the three. Varnished rocks are generally larger, and thus more resistant to overland flow (sheetwash). Iron films are, on average, not as large. Rocks without a coating are undergoing weathering at faster rates and are the smallest	51
4.3.	RCI toposequence (A) for three rock coating types and % area toposequence (B) for three rock coating types. Note that in both case varnish is dominant at the top, iron films are present from top to bottom but increase in strength towards the bottom, and no coating rocks lack a slope position signal. ‘A’ is an average of RCI values every 30 meters (100 feet), and ‘B’ derives from a single observation every 30 meters.	52
4.4.	Scatterplots of multiple regressions for weighted least squares corrected TMS band 10 (top right), TMS band 7 (top right), and TMS band 2 (bottom) against the three ‘smoothed’ RCI variables. These suggest a good correlation between isolated field observations of rock coatings and remotely sensed data, despite the jump in scale.	54

Figure		Page
4.5.	Combined plot of the first two cononical discriminant functions for the north- facing catena (B1) showing an obvious separation (discriminant fence) between upper, middle, and lower slope positions. N=27	55
4.6.	Combined plot of the first two cononical discriminant functions for the west-facing catena (B2) showing an obvious separation (discriminant fence) between upper, middle, and lower slope positions. N=30	56
4.7.	Combined plot of the first two cononical discriminant functions for the south-facing catena (B3) showing an obvious separation (discriminant fence) between upper, middle, and lower slope positions. N=24	57
4.8.	Diagram showing the dicriminant analysis grouping variable, slope position—top convex (1), middle straight (2), and bottom concave (3)	59
A.1.	B1_01	79
A.2.	B1_02	80
A.3.	B1_03	81
A.4.	B1_04	82
A.5.	B1_05	83
A.6.	B1_06	84
A.7.	B1_07	85
A.8.	B1_08	86
A.9.	B1_09	87
A.10.	B1_10	88
A.11.	B1_11	89
A.12.	B1_12	90
A.13.	B1_13	91

A.14.	B1_14	92
Figure		Page
A.15.	B1_15	93
A.16.	B1_17	94
A.17.	B1_18	95
A.18.	B1_19	96
A.19.	B1_20	97
A.20.	B1_21	98
A.21.	B1_22	99
A.22.	B1_24	100
A.23.	B1_25	101
A.24.	B1_26	102
A.25.	B2_32	103
A.26.	B2_33	104
A.27.	B2_34	105
A.28.	B2_35	106
A.29.	B2_36	107
A.30.	B2_37	108
A.31.	B2_38	109
A.32.	B2_39	110
A.33.	B2_40	111
A.34.	B2_41	112
A.35.	B2_42	113
A.36.	B2_43	114
A.37.	B2_44	115

A.38.	B2_45	116
Figure		Page
A.39.	B2_46	117
A.40.	B2_47	118
A.41.	B2_48	119
A.42.	B2_49	120
A.43.	B2_55	121
A.44.	B2_56	122
A.45.	B2_57	123
A.46.	B2_58	124
A.47.	B2_59	125
A.48.	B2_60	126
A.49.	B2_61	127
A.50.	B2_62	128
A.51.	B2_63	129
A.52.	B2_64	130
A.53.	B2_65	131
A.54.	B2_68	132
A.55.	B2_73	133
A.56.	B3_80	134
A.57.	B3_81	135
A.58.	B3_82	136
A.59.	B3_83	137
A.60.	B3_84	138
A.61	B3_85	139

A.62.	B3_86	140
Figure		Page
A.63.	B3_87	141
A.64.	B3_89	142
A.65.	B3_90	143
A.66.	B3_91	144
A.67.	B3_92	145
A.68.	B3_93	146
A.69.	B3_94	147
A.70.	B3_95	148
A.71.	B3_96	149
A.72.	B3_97	150
A.73.	B3_98	151
A.74.	B3_99	152
A.75.	B3_100	153
A.76.	B3_101	154
A.77.	B3_102	155
A.78.	B3_103	156
A.79.	B3_104	157
A.80.	B3_108	158
A.81.	B4_109	159
A.82.	B4_110	160
A.83.	B4_111	161
A.84.	B4_112	162
A.85.	B4_113	163

A.86.	B4_114	164
Figure		Page
A.87.	B4_115	165
A.88.	B4_116	166
A.89.	B4_117	167
A.90.	B4_118	168
A.92.	B4_119	169
A.92.	B4_120	170

1. Introduction

My basic research question is how rock coatings vary spatially from the top to the bottom of a desert hillslope. Although anecdotal observations exist on this topic, this research question has not been asked previously in a systematic fashion (Dorn, 1998).

Rock coatings rest within the subfield of weathering in the multidisciplinary arena of geomorphology. My approach to answering this question involves field methods in geomorphology, remote sensing methods, and geographic information science as an approach to integrate contiguous and spatially isolated data. This introductory chapter explains the connection between these different topics and justifies the importance of the research question.

1.1. Interface of geomorphology and remote sensing

Geomorphology remains a mostly observational science (Rhoads and Thorn, 1996) filled with isolated spatial data. These observations are then extrapolated and used to produce meaningful conclusions over an entire area for which it is not feasible or, perhaps, possible to collect data at every point. Graf, for example, studied the sediment budget of a river in Los Alamos Canyon, New Mexico where plutonium distribution is based on a series of isolated samples. His methodology rested on ‘observed evidence’ to describe the distinct and predictable geographies of contamination controlled by fluvial transport processes over time (Graf, 1996). Leopold et al. (1966) previously exemplified how isolated observations in the field build theory. However, “[e]xtrapolation of experimental-plot data to the whole contributing area [is] difficult, and in any case the

observations [are] not comprehensive” (Cooke et al., 1993, pp. 113). In summary, field geomorphologists make isolated observations that, ideally, represent a spatially continuous condition. Most often a new map can be created or, in light of Geographic Information Systems (GIS), observations are compiled to make mappable polygons (Heywood et al., 1998; Legg, 1992).

Remote sensing provides an alternative to fieldwork whereby geomorphic conditions can be observed at a variety of scales (Walsh et al., 1998). Distinct from discrete field observations, remote sensing continuously samples the geomorphic condition (Lillesand and Kiefer, 2000) as long as the subject(s) in study are known to a reasonable degree and can be verified, or ground truthed. Remotely sensed data communicates the observed surface quantitatively in a fashion allowing digital image processing (Jensen, 1996) and correlation with field measurements of surface phenomena. In other words, if the investigator successfully identifies the geomorphic feature, the spatial information gained is, ideally, contiguous.

Geomorphologists have long adopted remote sensing techniques (Short and Blair, 1986). Some examples include glacial monitoring studies (Bayr et al., 1994; Bishop et al., 1998; Espizua and Bengochea, 1990; Krimmel and Meier, 1973; Scambos et al., 1992); river studies (Gupta et al., 2002; Fouache et al., 2001; Johnson, 1994; Kalliola et al., 1991); alluvial fan studies (Farr and Chadwick, 1996; White, 1991); terrestrial and extraterrestrial aeolian studies (Arvidson, 1974; Breed and Grow, 1979; Sagan and Pollack, 1969); and studies of sediment transport and desert slopes (Kenea, 2001; McDermid and Franklin, 1995; Milana, 2000; Pickup and Marks, 2000; Spatz et al., 1989; Sultan et al., 1987; White, 1993; White et al., 1997; Wood et al., 1989). This study

follows this deep tradition in geomorphology by exploring the interface of remote sensing and the study of rock weathering.

1.2. Issues of scale and resolution

Rock weathering research traditionally uses microscopic scales of 1000:1 or even 100,000:1. In contrast, remote sensing scales of analysis traditionally rest in the range of 1:1000 to smaller scales. Thus, interfacing remote sensing and weathering requires the linkage of vastly divergent spatial resolutions.

Consider the problem of using a 30-meter x 30-meter pixel in weathering research. Complex, heterogeneous surfaces often create ‘mixed’ signals, integrating multiple landforms into a single digital signal — making linkage between scales difficult. A way to isolate a research subject is to increase spatial resolution by reducing the amount of surface area per pixel. However, there is a trade-off between spectral and spatial resolutions; relatively high spatial resolutions (ex. 1 meter) generally have lower spectral resolutions (ex. one band in the visible portion of the electromagnetic spectrum). Imagery with high resolutions in both areas is often extremely expensive or is unavailable to the public for national security reasons.

Spatial resolution remains a crucial issue in the study of weathering processes occurring at microscopic levels. For instance, 120 meters permits measurement of vegetation cover and analysis of urban areas; 60 meter and 30-meter pixel sizes provide more precision sufficient to study larger buildings and landforms, but nowhere near enough to study weathering. Other platforms, such as IKONOS-2, have resolutions near 1 meter— facilitating some ability to zoom in and out. Eventually, resolutions of remote

sensors will facilitate the study of weathering, but not in the near future. Thus, there is a need to link remotely sensed imagery with data collected in the field.

The linkage is a combination of fieldwork and Geographic Information Science (Jensen, 1996). The combination permits the researcher to address spatial variability and complexity in geomorphic systems with increasing precision. In summary, the overall structure of my research problem can be described by three interconnected circles in a Venn diagram: remote sensing as a tool to gather contiguous spatial data; GIS as a tool to integrate contiguous spatial data at different scales; and rock weathering as a subfield of geomorphology (Fig. 1.1).

1.3. Case study: rock coating distribution on a desert hillslope

The particular aspect of rock weathering most amenable to creating a bridge with remote sensing is the study of rock coatings in deserts. The limited vegetation cover permits remote sensing platforms the ability to sense surface characteristics, and in particular rock coatings. Rock coatings are paper-thin accretions of minerals, clays, and biotic agents in varied combinations on the surfaces of rocks in many different environments and settings at terrestrial and even extra-terrestrial surfaces (Dorn, 1998). Table 1.1 shows 15 different known types.

The Mojave Desert offers an excellent general study area to explore the interface of remote sensing, GIS, and the study of rock coatings. Many different types of rock coatings occur in the Mojave Desert. For example, case hardening allows the boulders of Joshua Tree National Monument to preserve bizarre cavernous forms. Lichens, a type of lithobiontic coatings, provide a canvas of colors on steep well-shaded northeast facing

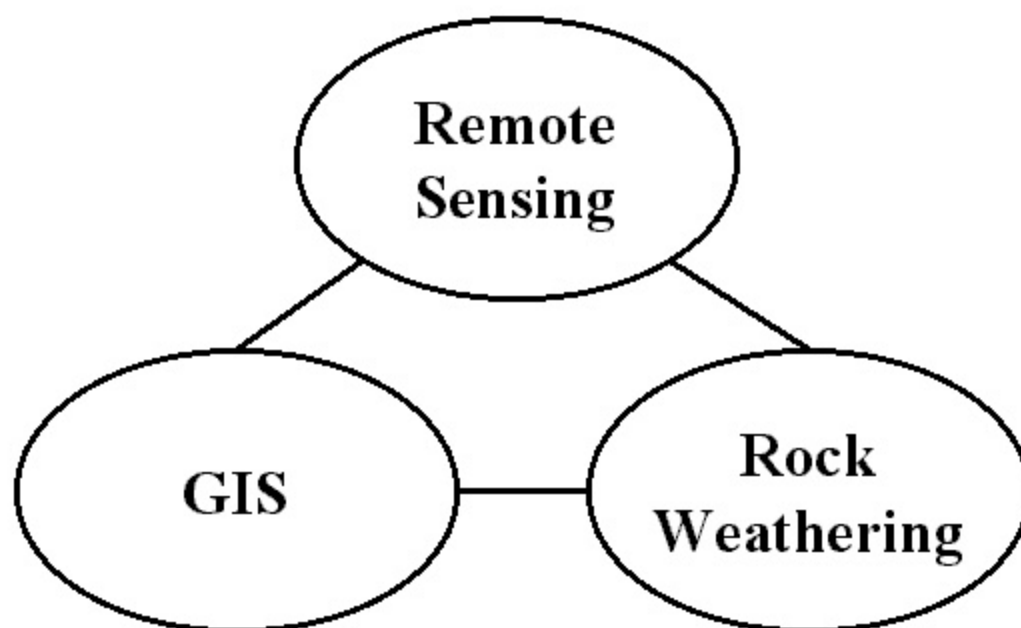


Fig. 1.1. Venn Diagram showing the interconnectedness of rock weathering in the subfield of geomorphology, remote sensing, and GIS.

Table 1.1. 15 known types of rock coatings and their descriptions. Adapted from Dorn (1998).

Coating	Description
Carbonate Skin	Coating composed primarily of carbonate, usually calcium carbonate, but could be combined with magnesium or other cations.
Case Hardening Agents	Addition of cementing agent to rock matrix material; the agent may be manganese, sulfate, carbonate, silica, iron, oxalate, organisms, or anthropogenic.
Dust Film	Light powder of clay- and silt-sized particles attached to rough surfaces and in rock fractures.
Heavy Metal Skins	Coatings of iron, manganese, copper, zinc, nickel, mercury, lead and other heavy metals on rocks in natural and human-altered settings.
Iron Film	Composed primarily of iron oxides or oxyhydroxides; unlike orange rock varnish because it does not have clay as a major constituent.
Lithobiontic Coatings	Organic remains form the rock coating, for example lichens, moss, fungi, cyanobacteria, algae.
Nitrate Crust	Potassium and calcium nitrate coatings on rocks, often in caves and rock shelters in limestone areas.
Oxalate Crust	Mostly calcium oxalate and silica with variable concentrations of magnesium, aluminum, potassium, phosphorus, sulfur, barium, and manganese. Often found forming near or with lichens. Usually dark in color, but can be as light as ivory
Phosphate Skin	Various phosphate minerals (e.g. iron phosphates or apatite) that are mixed with clays and sometimes manganese.
Pigment	Human-manufactured material placed on rock surfaces by people.
Rock Varnish	Clay minerals, Mn and Fe oxides, and minor and trace elements; color ranges from orange to black in color produced by variable concentrations of different manganese and iron oxides.
Salt Crust	The precipitation of sodium chloride on rock surfaces
Silica Glaze	Usually clear white to orange shiny luster, but can be darker in appearance, composed primarily of amorphous silica and aluminum, but often with iron.
Sulfate Crust	Composed of the superposition of sulfates (e.g., barite, gypsum) on rocks; not gypsum crusts that are sedimentary deposits

rocks. Manganiferous rock varnish, also known as desert varnish, readily appears on the boulders of stable hillslopes and dramatically affects the aesthetic appearance of the desert. The limited vegetation cover in the western Mojave Desert facilitates sensor examination of these coated rock surfaces. Furthermore, I have obtained publicly available Thematic Mapper Simulator (TMS) data (25-meter spatial resolution) and a digital orthophotograph (1-meter spatial resolution) of a basaltic knob in the western Mojave Desert. Of particular interest is TMS band 10 (2.08-2.35 μ m), which discriminates between minerals and rock types (Lillesand and Kiefer, 2000).

1.4. Problem statement

The basic research question is how rock coatings vary spatially from the top to the bottom of a desert hillslope. Such a simple question has not yet been answered, perhaps in part to cautions that oversimplification of the tremendous variance existing in rock coatings in desert environments results in erroneous mapping of what are truly complex relations between geomorphic conditions and coatings (Dorn, 1998). The tendency, most often, is to either ignore or simplify them as being the same.

Despite our increasing understanding of many types of rock coatings, there are still vast amounts left to discover. Several studies have attempted to develop gross field measurements to understand the overall development of rock varnish as an indicator of time (Derbyshire et al., 1984; Espizua, 1993; Hurst and Kelly, 1961; Lui and Dorn, 1996; Whitley et al., 1984). Iron films, also known as iron skins, have been analyzed to provide clues about the environmental character of prehistoric petroglyphs (Campbell, 1991) and in relation to such environmental stresses as fires (Dragovich, 1993). While rock

coatings have certainly been identified as being associated with particular landforms on hillslopes (Dorn and Krinsley, 1994), no prior study of rock coatings has attempted to characterize systematic changes along a slope. Thus, the overall focus of my research rests in understanding rock coating distributions at the field, or local scale.

In order to answer the basic research question of spatial variability in rock coatings, the research design necessarily links observations at a variety of scales, including micron-scale insights from the laboratory, millimeter to meter-scale observations from the field, and meter to kilometer-scale data from remote sensors. Rock coatings have been the subject of a wide variety of remote sensing investigations (Farr and Chadwick, 1996; Kenea, 2001; Milana, 2000; Spatz et al., 1989; Sultan et al., 1987; White, 1993; White et al., 1997; Wood et al., 1989). While considerable attention rests at the interface of separating the signature of rock coatings and the underlying rocks, the abundant remote sensing research has not yet turned to variability seen along a hillslope. This variability is a confounding factor in the remote sensing objectives of mapping geologic units (Dorn, 1998). For example, Christensen and Harrison (1993) connects satellite views to electron microscope observations of rock varnish without consideration of their signals at millimeter and meter-scale distributions. Until now, “[there] has been no effort to generalize microscopic information at the millimeter scale, which will be necessary to make the leap to meter-scale airborne and satellite data (Dorn, 1998, pp. 379). Thus, the second goal of my research is to provide some preliminary insight for this ‘middle’ step, making it more possible in the future to make successful, critical jumps from micro to meso, and meso to macro.

1.5. Broader implications of the study

The significance of this research exists at several different levels, explored here from the narrowly focused researcher to broader societal issues. Researchers focused on rock coatings and rock weathering obtain a new method to understand spatial variability of this weathering phenomenon, as well as a case study of rock coating variability along a particular location in the Mojave Desert. This thesis also develops a new method of studying particles on slopes with a digital camera.

More broadly, the general concept of mapping rock coating variability has implications for helping desert land-use planners, preservation of petroglyphs, and specialists in remote sensing and the physical sciences. Desert regions comprise one-third of global land surface areas (Thomas, 1989). As more people live in or near deserts, understanding geomorphic processes such as rock coatings assists in the assessment of disturbance, anthropogenic or otherwise. The Phoenix Metropolitan area in the Sonoran Desert, Arizona is a good example of the rapid expansion of urban populations in a desert region. Similarly, the western Mojave Desert is now experiencing rapid population growth adjacent to the Los Angeles Metropolitan region. Development in deserts requires environmental impact assessments, and understanding the nature of slopes can generate tools to analyze environmental change. Rock coating maps will aide in land-use planning or in the initial assessment and monitoring of restoration efforts in damaged desert environments, which sometimes involves the application of ‘artificial’ rock coatings. Also, archaeologists may use maps of rock coating regimes in the immediate area around rock art and rock monuments to detect those most in danger of being worn away by weathering and erosion. Lastly, as the remote sensing community accounts for

the variability of rock coating distribution signals in image data, lithologic and other related mapping practices will rest on more solid ground.

1.6. Organization of the thesis

This first chapter provides a brief intellectual framework and isolates the research question. The second chapter provides an overview of the literature at the interface of rock coatings, geomorphology, and remote sensing in order to help focus the specific research problem. The third chapter presents a new method of studying rock coatings on surficial clasts on desert slopes, as a means of interfacing ground data with remotely sensed data. The fourth chapter presents results and statistical analyses of the ground and aerial remotely sensed data, while the fifth chapter concludes the thesis.

2. Introducing the concept of a rock coating catena

2.1. Remote sensing of desert slopes

Slopes are the most extensive part of the earth's surface, transporting weathered debris to river, glacial, coastal, or aeolian transport corridors. Variation of processes and forms down a slope, thus, form a core concern in geomorphology. In desert geomorphology slopes and variation in slopes have long been a primary concern for geomorphologists (Cooke et al., 1993; Doehring, 1980; Oberlander, 1989). This thesis focuses on lateral variability of rock coatings down desert slopes, and in particular the interface between remote sensing and geomorphic studies. However, the interface I explore has not yet been the focus of scientific study. Thus, this chapter lays out prior relevant literature in, 1) briefly highlighting examples in the literature where multi-approach remote sensing has been used to study weathering and slopes in deserts, and, 2) focusing on the concept of a catena as it might apply to rock coatings.

2.1.1. Multi-approach remote sensing for desert geomorphologists

Shared by a host of scientific disciplines, yet without an outright owner, remote sensing provides invaluable insights to the geomorphologist, even those concerned with processes at small scales. Remote sensing is particularly suited to the analysis of desert regions, largely because the relative lack of vegetation and cloud cover reveals the surface in all of its detail (Cooke et al., 1993). Conceptually, while all geomorphologists have a potential use for remote sensing, desert geomorphologists may benefit by the potential capability for a greater percent of 'integration' (Fig. 2.1). Particularly, the

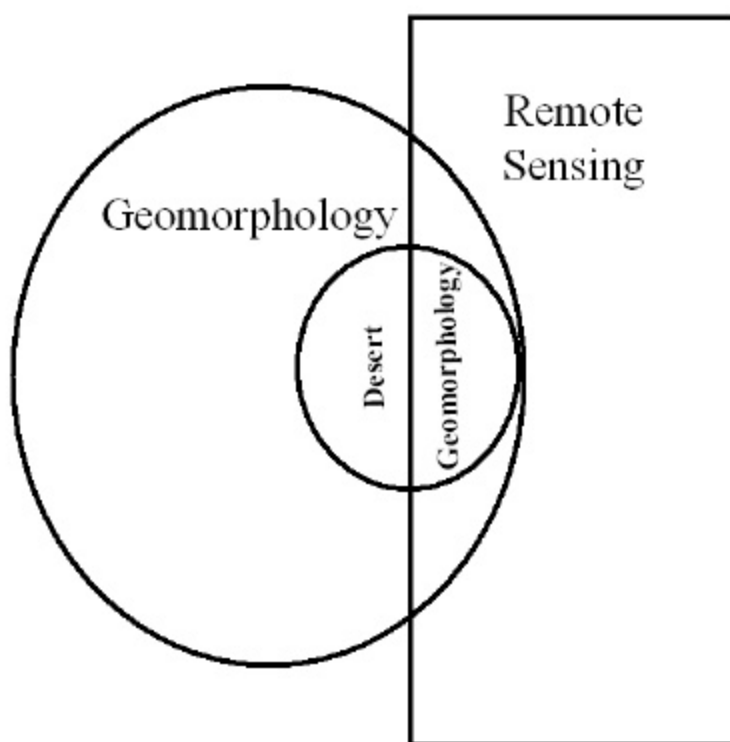


Fig. 2.1. Conceptual diagram of desert geomorphology's potentially greater percent of interaction with remote sensing, due to a more direct view of the surface, than geomorphology as a whole.

ability to collect data using the “multi”-approach (Short, 1999), or “multiple-view” approach (Lillesand and Kiefer, 2000) or the “multi-concept” (Jensen, 1996; Simonett, 1983) provides a powerful tool (Table 2.1).

The multiple-approach concept of remote sensing is fairly simple, involving analysis of remotely sensed information obtained from more than one source in more than one form of analysis. Gathering data in multiple spatial and temporal resolutions, multiple bands, with the prospect of sophisticated image analysis procedures on a computer, provide geomorphologists extremely attractive tools, evidenced by a variety of recent multi-approach studies (Asner et al., 2000; Graef et al., 1998; Langley et al., 2001; Prigent et al., 1999; Zumsprekel and Prinz, 2000; Farr and Chadwick, 1996; Abrams et al., 1991), two of which are detailed below.

2.1.2. Examples of multi-approach remote sensing techniques in desert geomorphology

Farr and Chadwick (1996) combined field observations with the ‘multiple-view’ remote sensing approach to study alluvial fans in the Kun Lun Mountains, China. They used data from the French satellite, SPOT, at high spatial resolution in the visible bands, combined with radar images taken with the Spaceborne Radar Laboratory, that have a different spatial resolutions (Farr and Chadwick, 1996). The synergistic combination of these sensors isolated several different types of forms generated by processes on the fans: salt weathering; rock varnish accretion; aeolian deposition; and fluvial dissection (Farr and Chadwick, 1996). In the case of these fans, remote sensing analysis indicated that salt weathering was the dominant, overriding process responsible for fan appearance,

Table 2.1. Options in the Multi-approach. Compiled from Jensen (1996); Lillesand and Kiefer (2000); Short (1999); Simonett (1983).

Type	Description	Example
Multi-spectral	Data consisting of several bandwidths within the electromagnetic spectrum	A combination of visible, near infrared, short-wave infrared, thermal infrared, or radar
Multi-temporal	Data collected on more than one occasion	Satellite images of the same location taken days, months or years apart
Multi-spatial resolutions	Data of the same location at more than one spatial resolution	1-meter resolution aerial photo and 30-meter resolution satellite image
Multi-platform	Using different types of Sensors from different platforms, independent of each other	Combination of Landsat Multispectral Scanner (MSS) image with Shuttle Imaging Radar (SIR) C/X—Synthetic Aperture Radar (SAR)

whereas varnishing and pavement processes tend to dominate in the southwest deserts of the United States (Farr and Chadwick, 1996).

Abrams et al. (1991) present another good example of the multiple-approach with application to desert geomorphology. Their study took place at basaltic lava flows in a semi-arid region in Hawaii. Abrams et al. (1991) monitored surface changes caused by weathering processes acting on these flows including: the physical breakdown of surface chill coats; the development and erosion of silica coatings; the oxidation of mafic minerals; and the development of vegetation. They employed a multi-approach by analyzing images of multiple platforms at multiple resolutions, and by using images with numerous spectral bands. Specifically, they used thermal infrared images taken by the Thermal Infrared Multispectral Scanner (TIMS) and the NS-001 scanner with bands in the visible, near-infrared, and short-wave infrared (Abrams et al., 1991). The result was the ability to map quantitatively changes in flows over time. They wrote: “...data from the [various] wavelength regions show more than [they do] separately” (Abrams et al., 1991, pp. 475).

Both of these examples provide an important foundation for my research. Both studies employ multi-approach remote sensing to study spatial variability in weathering processes in arid regions. Instead of studying alluvial fan or lava flow morphogenesis, my study focuses on a systematic changes from top to bottom of a hill.

2.1.3. Background on multi-approach sensors employed in this study

This study employs TMS data and a black and white digital orthophotograph to study a basaltic slope in the Mojave Desert. This section, therefore, provides background information on these sensors.

TMS is a by-product of the National Aeronautics and Space Administration (NASA) and Jet Propulsion Laboratory and Daedalus Enterprises, Inc.'s combined efforts to develop a number of multispectral scanners flown aboard NASA aircraft. TMS is usually flown on a NASA ER-2 (civilian equivalent of a United States Air Force U-2). Designed to simulate LANDSAT Thematic Mapper (TM), TMS maintains a slightly higher spatial resolution (25 meters at operation altitude of 65,000ft) with a spectral resolution of 11 channels (the 12th is a duplicate of band 11 at higher gain) covering visible and infrared regions of the electromagnetic spectrum (Table 2.2). Data (NASA, 1992) containing my study site came from NASA Research Center, located at Moffit Field, California. These data are also available for purchase, via the Internet, from the United States Geological Society Earth Resources Observation Systems Distributed Active Archive Center (USGS EROS EDC DAAC).

A digital orthophotograph of my study site from the USGS provides an aerial view in the visible spectrum. This panchromatic view portrays visual albedo with a spatial resolution of 1-meter. Together, these two sources, TMS at specific channels and the orthophotograph at high spatial resolution provide 'multi' analysis capability.

A key issue in the selection of multi-approach sensors must be qualified. Individual researchers must articulate the timing of image acquisition to the frequency of changes under study. In this case, the temporal resolution variations between TMS and

Table 2.2. TMS and LANDSAT TM Bands and Wavelengths (NASA, 1992).

Channel	Wavelength Range (microns)	LANDSAT Thematic Mapper Equivalent Band
1	0.42 - 0.45 micrometers	equates to non-TM band A
2	0.45 - 0.52 micrometers	equates to TM band 1
3	0.52 - 0.60 micrometers	equates to TM band 2
4	0.60 - 0.62 micrometers	equates to non-TM band B
5	0.63 - 0.69 micrometers	equates to TM band 3
6	0.69 - 0.75 micrometers	equates to non-TM band C
7	0.76 - 0.90 micrometers	equates to TM band 4
8	0.91 - 1.05 micrometers	equates to non-TM band D
9	1.55 - 1.75 micrometers	equates to TM band 5
10	2.08 - 2.35 micrometers	equates to TM band 7
11	8.50 - 14.0 micrometers (low gain)	equates to TM band 6
12	8.50 - 14.0 micrometers (high gain)	equates to TM band 6

orthophoto platforms are unimportant because the object of study, the distribution of rock coatings, change very slowly (Dorn, 1998).

2.2. *Catena studies in desert geomorphology*

Soil geomorphologists arrange characteristics of different soils in ‘soil catenas’ to describe systematic change down a slope (Beach, 1998; Birkeland and Gerson, 1991; Kochis and Lasca, 1994; McCalpin and Berry, 1996; Miller and Birkeland, 1992; Simon et al., 2000). A catena thus links soil horizonation and landform processes (Birkeland, 1991). “Soils related in a catena are seen to have properties that can be related to their position on the landscape” (Buol et al., 1973, pp. 122, who quotes Ruhe). Milne (1935) formalized the catena concept. Ollier (1976) describes catenas of different climates. Although there has been some debate on the utility of the catena concept, viewing soils in a slope continuum has provided insight into slope processes. The title of one of earth science’s major academic journals, *Catena*, is partial testimony to the broad utility of this concept.

A common way to portray a soil catena (Fig. 2.2) is to depict a series of soil profiles as they correspond to different positions on the slope, often illustrated in the form of a cross-sectional diagram (Gerrard, 1992). It is not, however, the end-product appearance of a catena that is important; rather, it is the implication that its order provides for the presence of pedogenic and geomorphologic processes. A simple catena, for example, is the examination of the change in soil characteristics on a convex-concave hillslope, where the convex portion is generally a zone of erosion, straight sections are zones of transport, and concave sections areas of deposition. Young (1976) outlined possible

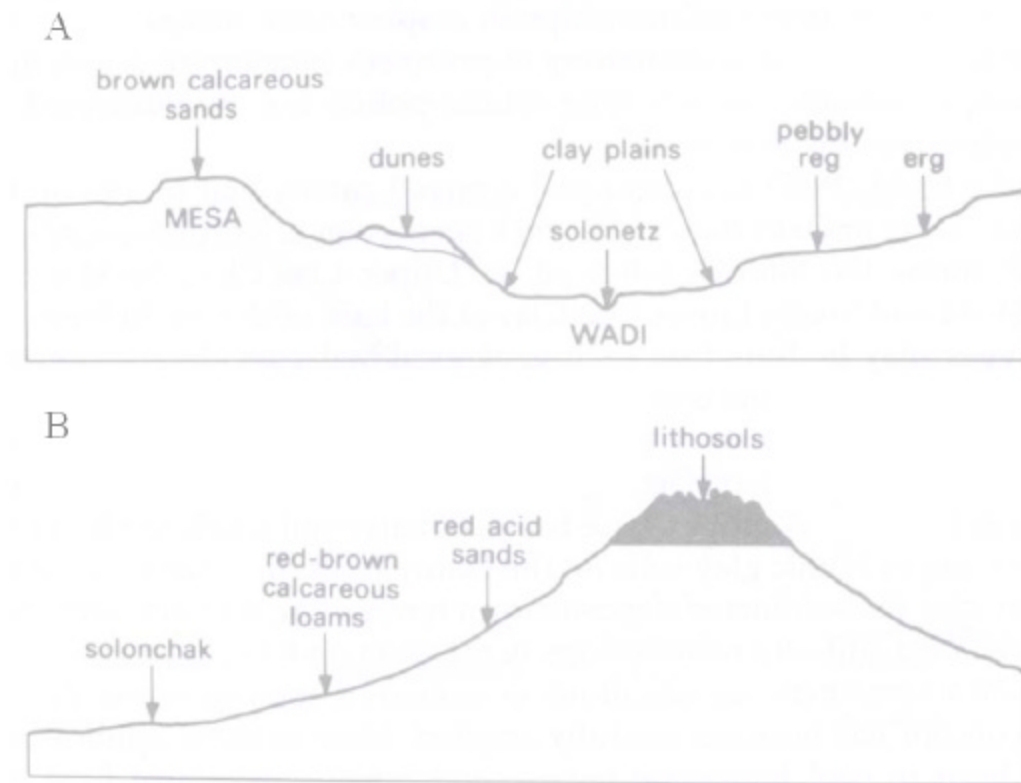


Fig. 2.2. Cross-sectional diagrams of simple catenas. 'A' is representative of arid regions, 'B' is representative of semi-arid regions. Adapted from (Bunting, 1965).

catenary variations; the depth, color, and content of soil horizons from topographic highs can remain constant, increase or decrease, or abruptly end or begin as one proceeds down slope, indicating the influence of slope on soil and weathering processes (Fig 2.3). Also, catenas occur at all levels of scale, as long as a continual slope exists (Gerrard, 1992). Knowledge of one part of the catena thus facilitates prediction of other positions along a slope.

2.3. *Rock coatings on clasts as a possible catena*

Desert slopes often maintain lags of rock particles on slopes (Sharon 1962). These rock particles are almost entirely covered by rock coatings (Dorn, 1998). No prior researcher has explored variations in these rock coatings down a slope. This section connects the concept of a soil catena to the rock coating literature.

Subaerial particles (surficial regolith) are usually not included as part of the make up of a soil. Certainly, soil scientists include desert pavements as a part of soil descriptions in deserts, but rock coatings themselves are not included in the description of a soil. However, weathering evidenced in rocks at the surface and rock coatings on them are *not unlike* a soil. This section posits the perspective that rock coatings and the underlying weathering rind are as tiny ‘suburb soils’ with layered zones and horizons of their own, yet formed in concert with the biogeochemical conditions leading to the formation of the soil. Splitting clasts of basalt in the field, for example, reveals these ‘mini-soils’, exposing an outward zone of chemical weathering and superimposed microlaminations.

A weathering rind is a common feature in weathered rocks and is a result of *in situ* decay (Colman, 1982; Dorn, 1998) much in the same way that rocks weather to form the

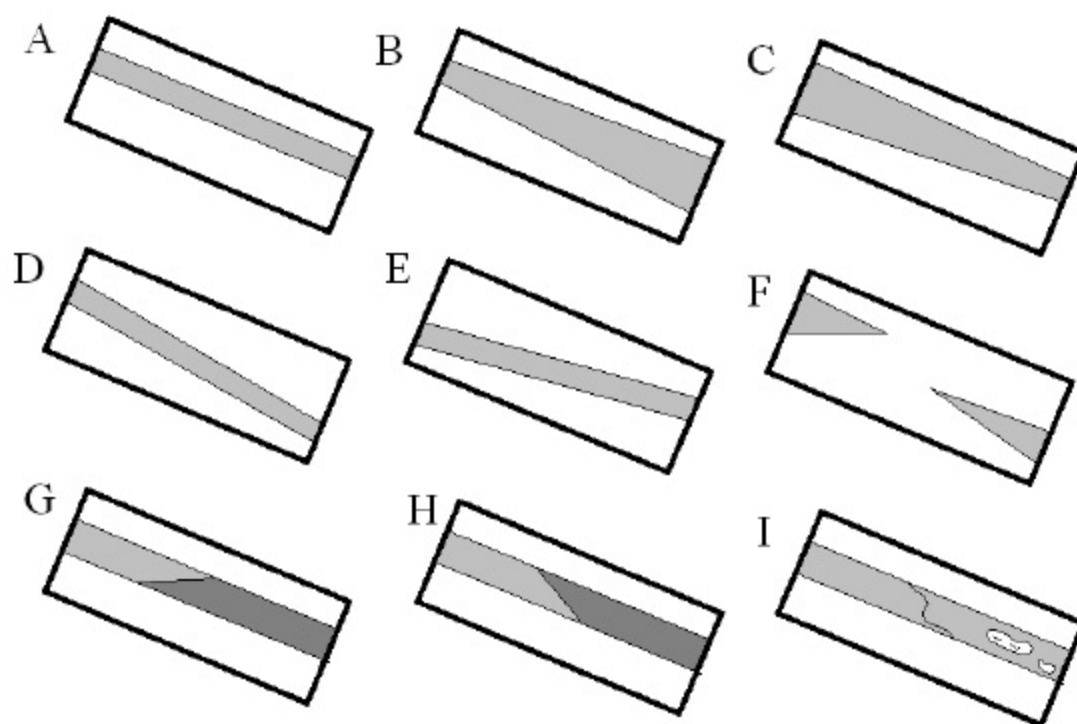


Fig. 2.3. Young's model describing the possible ways that soils horizons can vary along a catena: 'A' remain constant; 'B' increase; 'C' decrease; 'D' deepen; 'E' rise; 'F' end or begin, 'G' and 'H' be replaced; or 'I' gradually change in terms of properties but maintain the same identity. Adapted from Young (1976).

regolith or "C weathered rock horizon" of soils. Weathering rinds appear as discolored layers or as a millimeter-scale shell around the outside of a clast (Fig. 2.4). Weathering rinds start to form while the rock is still beneath the surface. The nature and thickness of rind formation depends on a variety of weathering factors outlined by Pope et al. (1995).

Rock coatings form on top of weathering rinds and can express weathering variability in desert surfaces (Cooke et al., 1993; Thomas, 1989), thus showing the potential to indicate slope stability. Consider a road cut in a new development in Phoenix or in the Mojave Desert. The high-albedo of carbonate-coated or less weathered rock stands out in contrast to the darker rock coatings, providing an intuitive clue to ongoing disturbance.

Each coating informs on the environmental conditions of its formation. For each rock coating is a unique combination of minerals, weathered by-products, and other materials that have been translocated from microns to kilometers formed under a specific set of geomorphic conditions. Rock coatings may dissolve and disappear when the climate changes from drier to wetter conditions, or may be abraded off through transport movements when slopes become unstable. In some cases, rock coatings are stronger than their host rocks. Some rocks may be weathering-limited, meaning that disintegrating or spalling rates of rocks undergoing weathering must be slower than coating accumulation rates. The formative and destructive conditions enables coatings, such as rock varnish, to serve as indicators of geomorphic stability.

The current paradigm that geomorphologists and rock coating specialists employ to explore rock coatings is analyzing them in terms of a geochemical framework (Dixon et al., 2002; Dorn, 1998). The vast array of chemical interactions and physical processes that occur at the molecular level are then used to inform on broader scale processes. A

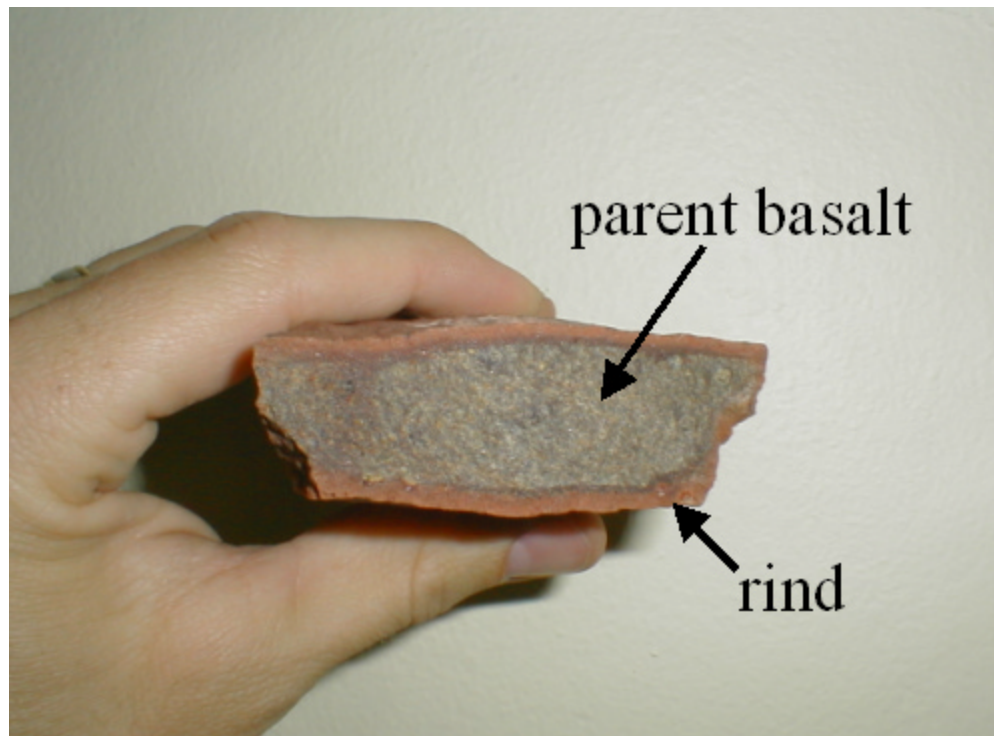


Figure 2.4. Picture of *in situ* weathering in a basalt clast from study site. The shell of altered rock around the edge, reddish brown on the outside and a dark purple as it transitions from parent material, is about 2-5mm thick. Hand provides scale. There is also a micro-thin iron film on this sample.

carefully prepared sample of rock varnish on basalt placed under a secondary electron microscope (SEM), for example, reveals that the varnish forms as molecular flakes of iron and magnesium rich clay materials are cemented together via a biotic agent, beginning in the micro-fissures and jointings of the rock and, over time, eventually covering the surface of the rock (Dorn 1998). Such research shows that varnish is 'deposited' and not derived from within the host rock (Dorn, 1998) as premature logic might suggest. Dorn (1998) writes:

Weathering is the breakdown and decay of minerals in place. In contrast, rock coatings are accretions on top of the rock. In most cases, rock coatings are not directly derived from the underlying rock. The formation of weathering rinds and rock coatings are distinct phenomena, although they are in direct physical juxtaposition. (pp. 12)

A good analogy for rock coatings and weathering rinds is a glazed doughnut, where the baking process (hot oil) turns the outer portion to a golden brown but the glaze is applied separately through 'other' processes taking place in the kitchen.

While minerals that are weathered from regolith into the soil most definitely contribute to the geochemical environment of a region suitable for the formation of certain types of rock coatings, they generally do not form in direct response. The separate formation of coatings as geochemical agglomerations at rock surfaces and weathering rinds from internal decay are thus analogous to a soil. The general model of a soil profile consists of a sequence of horizons (A,B,C) that transition between the topsoil and bedrock below. The differing zones of eluviation and illuviation (leaching and

depositional zones, respectively) in a soil create darker/lighter or colored horizons that are discernable in the field (Christopherson, 2000).

Weathering rinds can be considered small zones of eluviation and rock coatings as micro-zones of illuviation. The link becomes even stronger when considering typical soils in deserts, where the Av horizon accumulates on top of the weathered soil. I contend that the nature of rock coatings and weathering rinds are enough like soils to merit their spatial distributions to be described in the same manner—as a catena. There is no prior research in the literature involving rock coating catenas.

Anytime an investigator proposes a new way of examining prior phenomenon, the change in approach should have side benefits, applicable to connected arenas of research. In this case, the greatest power of a catena interpretation of rock coatings rests in a new tool to assist in the analysis of slope stability. Traditional geomorphological methods employ detailed monitoring field studies (Abrahams et al., 1988; Schick, 1980; Young, 1960) whereby sediment flows are measured over days to decades. Rock coating catenas have the potential to monitor slope stability, not through laborious and expensive field monitoring sites limited in spatial extend, but through changes in the aerial distribution of rock coatings. In other words, rock coatings have the potential to provide a nominal signal that slopes are stable or unstable—which can then provide the basis for site selection for more expensive monitoring.

3. Methods

This research employs a unique combination of traditional field techniques and a new type of digital image sampling to quantify systematic change of rock coatings along a desert hillslope in the western Mojave Desert, California. Instead of physically handling and measuring particles sizes and rock coatings in the field, this methodology uses digital image processing techniques to capture data efficiently in the field and assess them later in the laboratory.

The end product of the data processing is the generation of a rock coating index, created through an objective procedure. These data are compared with the multi-approach remotely sensed data within a GIS framework and subject to statistical analysis. This chapter, thus, outlines the study site and methods used to obtain and comparatively analyze rock coating index data.

3.1. Study site

The extreme complexity of rock coatings (Table 1.1) can pose problems for conducting the first research project on a 'catena' of rock coatings over a hillslope. Thus, the research design of my project must be able to constrain this complexity. Basalt knobs in the western Mojave provide a way to simplify the complexity. My study site lies approximately two miles north of North Edwards, CA along State Highway 58 near Edwards Air Force Base and Roger's Dry Lake at a basaltic knob (Figure 3.1). The hill rises roughly 90 feet (27 meters) from the flat desert floor, is 2450 feet (747 meters) in elevation, and the smaller member of a family of basaltic knobs in the immediate area.



Fig. 3.1. Study site in the western Mojave Desert. The arrow points to the basalt hill on as seen in a USGS digital orthophotograph. Highway 58 at the bottom of the image gives scale. North is to the top.

Only two rock coatings dominate on the basalt hills in the western Mojave to be readily noticeable at the field scale: rock varnish and iron films. Rock varnish appears as a dark brown or black coating, while the iron films appear as orange. There are also whitish-colored rocks, but these are too weathered to hold rock coatings. Weathering rinds are present in the surface particles. Vegetation, mainly Creosote Bush (*Larrea tridentate*) and Brittlebrush (*Ensilia farinosa*), is both constant in distribution and abundance and minimal.

3.2 Digital image sampling

Improvements in technology facilitate changes in the way field scientists approach research questions. In almost every case, field researchers employ sampling techniques (Gardiner and Dackombe, 1983) in order to maximize their rate of data return for time spent in the field. Sampling while in the field, however, can often be the limiting factor in successful and effective fieldwork, requiring numerous measurements, a multitude of field equipment, and time. In concert with another colleague, Kevin Green, I developed a technique for, but not limited to, gathering particle size and rock coating data at the local field scale that lifts these time and labor constraints—facilitating sampling of field data to be processed later (Bull, 1981). This method only requires a digital camera and scale to be included in the digital image, and an image-processing program such as publicly available NIH Image (1997) or its Windows equivalent (2002). Benefits of this method include the ability to collect larger data sets for a given amount of time in the field, and digital precision and consistency. This strategy is similar in concept to a method Dorn (1995), Gordon (1996), and Cervený (2000) use to directly measure in situ chemical

weathering at the microscale. This method builds upon slope particle size studies, compiled by Green in Table 3.1, and ultimately being modified from Cooke and Reeves (1972) and Vincent and Sadah (1995). Butler et al. (2001) recently developed and tested the method for automatically extracting clast-size data from digital imagery of streambed gravels. In contrast, I manually extract particles size data from digital imagery of basalt clasts on a slope.

This digital image sampling method consists of five general steps:

- 1) field imaging
- 2) measuring embedded scale
- 3) particle sampling
- 4) particle extraction
- 5) particle size analysis

Step 1 requires a digital camera and scale with a fine-enough resolution to permit matching of pixel width with real-world length. Steps 2 through 4 require an image-processing program, for example, Adobe Photoshop (2002). Step 5 requires a free image processing package developed by the National Institute of Health called NIH Image or its Windows equivalent Scion Image™ available at the following websites:

<http://rsb.info.nih.gov/nih-image/> or <http://www.scioncorp.com/>.

3.2.1. Field work

Step 1, Field imaging. I made observations along four transects of a basaltic knob. Previous to selecting this location, in order to prevent bias, I decided that these transects would be in the magnetic north, west, south, and east directions (Brunson compass), originate from the top of the hill, and extend downslope until the hill's influence is no longer dominant in terms of slope or particle distribution. Using a metal transect tape I

Table 3.1. Several important studies of particle size measurement and sampling schemes applied to the field sampling and digital image processing method in this study. Green compiled these sources.

Reference	Research Problem	Methods
Dury (1966)	Particle size/slope on pediments	Measure b-axis of particle at toe for every step for 100 ft. interval
Cooke and Reeves (1972)	Debris size/slope on mountain fronts/pediments	Randomly sample the b-axis of 50 particles within a (.9 m) grid at 100 ft intervals (mountain fronts) and 200 ft. intervals (pediments)
Akagi (1980)	Debris size/slope angle on pediments	Measure b-axis for ten largest particles within a 9 m ² area at 50 m intervals on mountain fronts and 100 m on pediments
Kesel (1977)	Thickness of waste cover/slope on inselberg slopes	Calculate thickness of waste cover at 15.2 m intervals (for particles > 4 mm using a portable seismic timer) and measure b-axis of particles within a 1 m circle (for gravel and cobbles)
Abrahams and Parsons (1985)	Influence of hydrologic processes on particle size/slope on debris slopes	Measure b-axis of 50 to 200 particles sampled within a grid and take a bulk sample of particles > 2 mm when these particles represent more than 5% of the total sample
Vincent and Sadah (1995)	Particle size/slope on pediments and inselbergs	Bulk sample of 0.8 kg for particles finer than 3.5 phi (using dry sieving and pipette analysis) and use photographic technique for particles coarser than -3.5 phi (take a photograph of a 50 cm ² cross-wired grid and measure particles on enlargements using calipers)

took a high-resolution (2.0 mega-pixels) digital photograph with a Olympus D-520 Zoom digital camera every 20 feet along these transects (Appendix A). Each image includes an embedded scale provided by a yardstick set perpendicular to the transect tape at the appropriate tick-marks, serving as the upper boundary of the observation. Another marker two feet below the yardstick clearly indicates the lower boundary. The transect tape is the left boundary. Maintaining a constant distance from ground to camera keeps the focal length fairly consistent and shortens processing time in step 2.

The rapid speed of primary data capture facilitates the gathering of other supplementary data. These supplementary data and field notes correspond to a specific frame number assigned by the camera, drastically reducing the amount of information that has to be recorded with a pencil and paper. The ‘pre-view’ option available with this digital camera allows a field check to ensure that each photo is suitable for later processing (i.e. is focus correct?, is coverage as desired?).

3.2.2. Laboratory work

Step 2, Measuring Imbedded Scale. Upon saving digital imagery onto a computer, step 2 requires an image-processing program such as Adobe Photoshop 6.0. The first stage in step 2 sets an average scale (e.g. pixels per millimeter) for each image. This is necessary because small curvatures of the surface, as well as varying focal lengths causes each photograph to vary slightly in scale. Viewing each picture on a computer screen in Adobe Photoshop 6.0 allows the number of pixels spanning a length measure (in this case, one inch) to be counted and averaged them across several locations in the

photograph. Photoshop's "line tool" set at appropriate line weights expedites this process (Fig. 3.2).

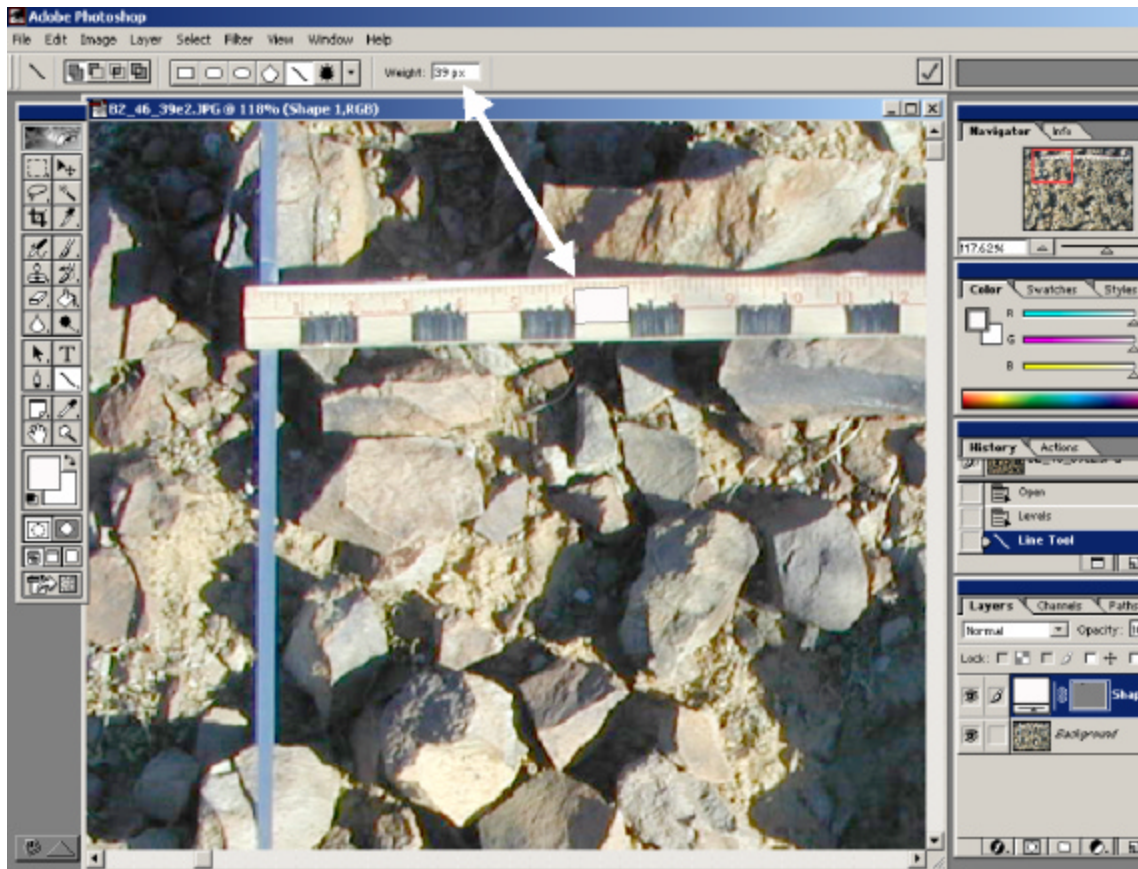


Fig. 3.2. Establishing a scale in Step 2 by counting the number of pixels that spans one inch on the inset ruler. Drawing an object, in this case a line set at an appropriate weight, so that its edges touch tick marks quickly gives photo scale. The scale for this picture is 39 pixels inch⁻¹.

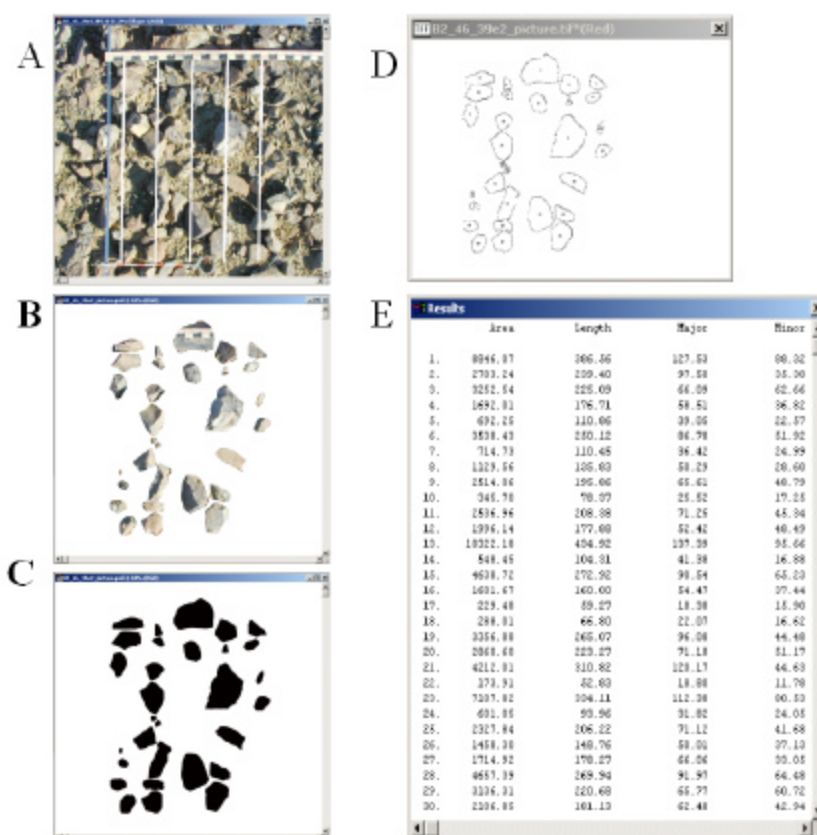


Fig. 3.3. Steps 3-5. 'A' is an Adobe Photoshop window showing the semi-grid for selecting particles in Step 3. 'B' is the resulting 'cut-out' image of extracted particles from Step 4. Note that the rocks in 'B' are in the exact, to near exact, location as in the original image. Before Step 5, particles are filled in with black, 'C', and saved as a TIFF file. 'D' is the way the now outlined and cataloged particles appear after analysis in Scion Image. 'E' shows corresponding results, in this case area (mm^2), perimeter length (mm), two-dimensional major axis (mm), and two-dimensional minor axis (mm), which may be pasted into a spreadsheet program such as Microsoft Excel.

The resulting average scale for each frame forms the basis for particle size measurement later in step 4. The mean scale and standard deviation for the 92 digital observations I used in the analysis is 36.22 ± 1.9 pixels inch⁻¹.

Step 3, Particle Sampling. Unlike previous studies, I applied a sampling scheme *after* returning from the field (Figure 3.3a). Representative samples of the particles in each photo can be obtained by overlaying a ‘semi-grid’ in Adobe Photoshop as a new layer—hence this grid is not directly placed on the raw image. Setting the line tool to a small weight (6 pixels), I drew vertical parallel lines stretching downward (2 feet) and spaced them evenly at an interval of four inches across the photograph, always beginning at the same starting point. The copy/paste function of the software package enables the grid exact in terms of length and angle. My sampling scheme required the selection of the first 30 particles that were touched or crossed by the lines, as long as the entire portion of the particle appears in the photograph. I did include rocks that are covered partially by the yardstick or the transect tape as long as their outlines are discernable. Generally, I selected particles by beginning at the top of the left-most grid line, follow it downward, and then move to the top of the next line, and so on. Particles large enough to be intersected by two or more grid lines are ‘captured’ only once. This step, then, identified the particles to be systematically extracted in the following step.

Step 4, Particle Extraction. The goal of this step is to save only the selected particles as a new image. The edges of each particle are traced manually using Photoshop’s “lasso tool”. The step requires a steady hand and a responsive mouse, as well as a considerable amount of time and patience. The brightness level of an image taken when the sun is at lower angles should be adjusted so that dark shadows do not obscure particle edges.

After tracing a particle, I found it was best to copy to a new layer (“layer via copy” function) until new ‘particle layers’ totaled 30. With the background layer (raw image) turned off, the outlined particles that remain can be moved and adjusted where necessary so that they do not touch or overlap each other and then “flattened” the image. This permanently removes the grid and background layers, resulting in a ‘cookie-cut’ image of particles in their exact or near geographical position over a white background (Fig. 3.3b).

Before moving on to step 5, I filled-in each particle (Fig. 3.3c) with Photoshop’s “paint fill” tool set at its highest tolerance setting (255). (This is easily done by first clicking over the white (background) area of the image with the “wand” tool set at zero (lowest) tolerance and then choosing the ‘select inverse’ option in the right-mouse button pop-down menu before performing the fill). This image of black particles on a white background must then be saved in the TIFF format.

Step 5, Particle Size Analysis. A key advantage in using this method is that NIH/Scion Image calculates numerous types of measurements when given an image and its pre-determined scale (in unit length or simply pixels). This analysis package offers advanced particle size measurement capabilities that can be set to suit the specific needs of the user and his/her data. Detailed steps for using these softwares in a manner similar to this study appear in Table 3.2. Again, the imported image represents a series of distinct particles that are colored black. NIH/Scion Image analysis produces a new image where each particle is outlined and numerically cataloged (Fig. 3.3d). I copied and pasted the measurement results (Fig. 3.3e) into a Microsoft Excel spreadsheet and printed the new image (Appendix A). The ability to electronically transfer results to a data spreadsheet saves time and allows the instant creation of data matrix.

Table 3.2. NIH or Scion Image instructions

Steps:	Location on Screen:	What to do:	Reason:
1 Import	Toolbar under File menu, labeled 'Import'	Select and Open TIFF file	Imports TIFF file for use in NIH/Scion Image
2 Threshold	Toolbar under Options menu, labeled 'Threshold'	Click menu item	Creates a binary image to distinguish between particle pixels (black) and non-particle pixels (white)
3 Set Scale	Toolbar under Analyze menu, labeled 'Set Scale...'	Enter the scale in the appropriate units/pixel obtained from the embedded ruler, click 'OK'	Applies the scale to the image in units/pixel
4 Set Measurement Options	Toolbar under Analyze, labeled 'Options...'	Choose one or more types of desired measurements, click 'OK'	Allows user to indicate which types of measurements are to be included in the output table
5 Measure Particles	Toolbar under Analyze, labeled 'Analyze Particles...'	After confirming measurement modes, click 'OK'	Measures all particles
6 View Results (optional)	Toolbar under Analyze, labeled 'Show Results'	Click menu item	New window appears displaying measurement table
7 Save Results	Toolbar under Edit, labeled 'Copy Measurements'	Click menu item	Saves results by copying table onto computers 'clipboard' to be pasted into a spreadsheet program, such as Microsoft Excel

3.2.3. Digital image processing limitations

There are limitations to this method. The primary limitation is that only two axes of a rock's flattened (2-dimensional) image can be measured. "In-field" sampling would enable the measurement of a third dimension, the b-axis, and allow a researcher to calculate other metrics, for example, sphericity. Also, there is a propensity for larger rocks to be selected with the semi-grid system over smaller ones (Dunkerley, 1996). However, I did not feel that this was detrimental to my study, which ultimately looked at the correlation between field observations and remotely sensed imagery, where larger particles would have an overall greater impact on spectral signatures of individual pixels. Although it drastically reduces the amount of time conducting fieldwork, laboratory processing time needed to complete steps 2 through 5 can be considerably long.

3.3. Rock coating index, GIS, and data matrix creation

A traditional approach in interpreting qualitative, categorical observations of earth scientists has been to develop indices (Bach, 1995; Harden, 1982; Lancaster, 1988). The aim of my research and fieldwork was not only to gather particle size information, but also to quantify the spatial distribution the rock coatings hosted by these particles on a desert hillslope. This required the creation of an index to transform a subjective assessment of coating into numbers, a GIS containing the knob to facilitate the overlaying of remotely sensed imagery and observation points, and the compilation of a comprehensive data matrix to facilitate graphical and statistical analyses.

3.3.1. Rock coating identification

I examined printed color copies of each raw image in order to identify the different coatings for each selected particle in Step 2. Because the geographic integrity of each particle is maintained in NIH/Scion Image's outlined and numerically cataloged image, each corresponding rock in the original image could be identified according to its rock coating type(s) (i.e. rock varnish, iron skin, or no coating). In spreadsheet format this is accomplished by assigning a '1' or a '0' (1=present, 0=not present) in three rock coating columns. In cases where a combination of these three classifications existed on a rock, I rank ordered the two most dominant coating types in terms of areal coverage on a particle and assigned them 75% and 25% values of 1, respectively. Total value sum of rock coatings for each observation is always 30.

3.3.2. *Weightings*

I assigned each particle and its associated coating a weighting ranging from 1 to 4, where 1 is representative of weaker coatings and 4 of strong coatings. For instance, rocks with dark varnish are weighted as a 4, as long as it is one of the two more dominant coatings of an individual particle. Rocks with no coating, thus exhibiting a higher albedo value, are not weighted (or the same as a weight of "1").

3.3.3. *Rock coating index*

Fig. 3.4 shows the criterion and formulae for a rock coating index (RCI), where each digital photograph (observation) is assigned three values pertaining to its intensity of varnished particles, iron skins, and highly weathered rocks. Varnish and iron skin rock coating index values have a possible range of 0 to 120, where high numbers signify a

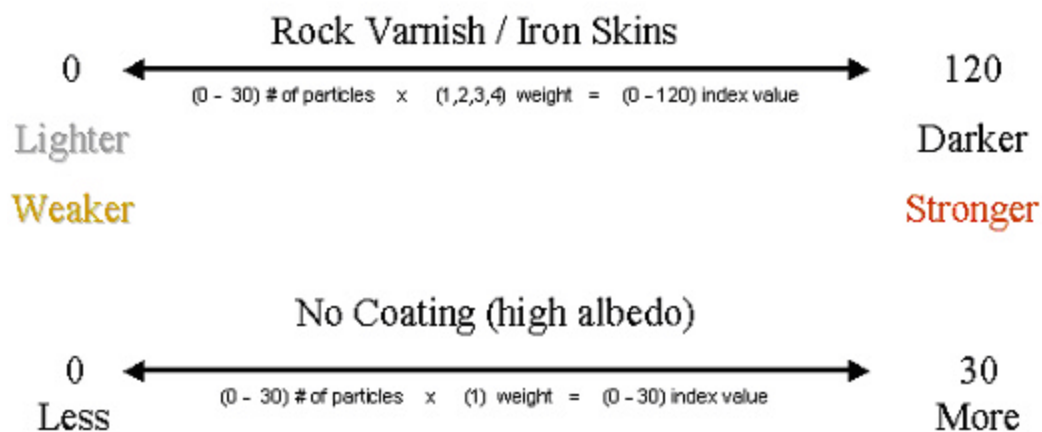


Fig. 3.4. Rock Coating Index (RCI) continuum for rock varnish, iron films (or iron skins), and particles eroding too fast to have either varnish or iron films. Each field observation at a field of view of approximately 0.5 meters can have a RCI score of 0-120 for varnish and iron skins, and a score between 0-30 for no coating RCI. RCI is an indicator for rock coating strength.

higher, more intense degree of coating. Rock albedo index values can vary from 0 to 30 (no weightings).

3.3.4. *GIS*

I created a GIS of the study site in order to facilitate the comparison of the rock coating index and remotely sensed imagery. Using the georeferenced digital orthophotograph at 1-meter resolution of the region containing the basaltic knob as a theme in ArcView, I could locate the start and end-points of the transects from coordinates (UTM) obtained with a Global Positioning System (GPS) unit in the field — thus creating a new line theme (Fig. 3.5). Then, the “ruler” tool aided in measuring and marking known interval distances for observations along each transect in a point theme.

ArcGIS instantly reconciles and re-projects layers of different coordinate systems and projections into the same ‘map’, facilitating the addition of Thematic Mapper Simulator data as a layer, and the addition of overlaid observation points (Fig. 3.6). I then queried each point for its corresponding digital number (DN) for the TMS bands 2, 7, and 10. In other words, points are classified according to an overlaid 30 x 30 meter pixel value (0-255) and entered into the spreadsheet. DNs from the digital orthophotograph are extracted in the same fashion.

3.3.4. *Data matrix creation*

Data collection using the digital image processing technique and classifying each particle according to its rock coating type, as described above, facilitates linkages of these data with a myriad of meaningful descriptors. For instance, presence (1) and non-

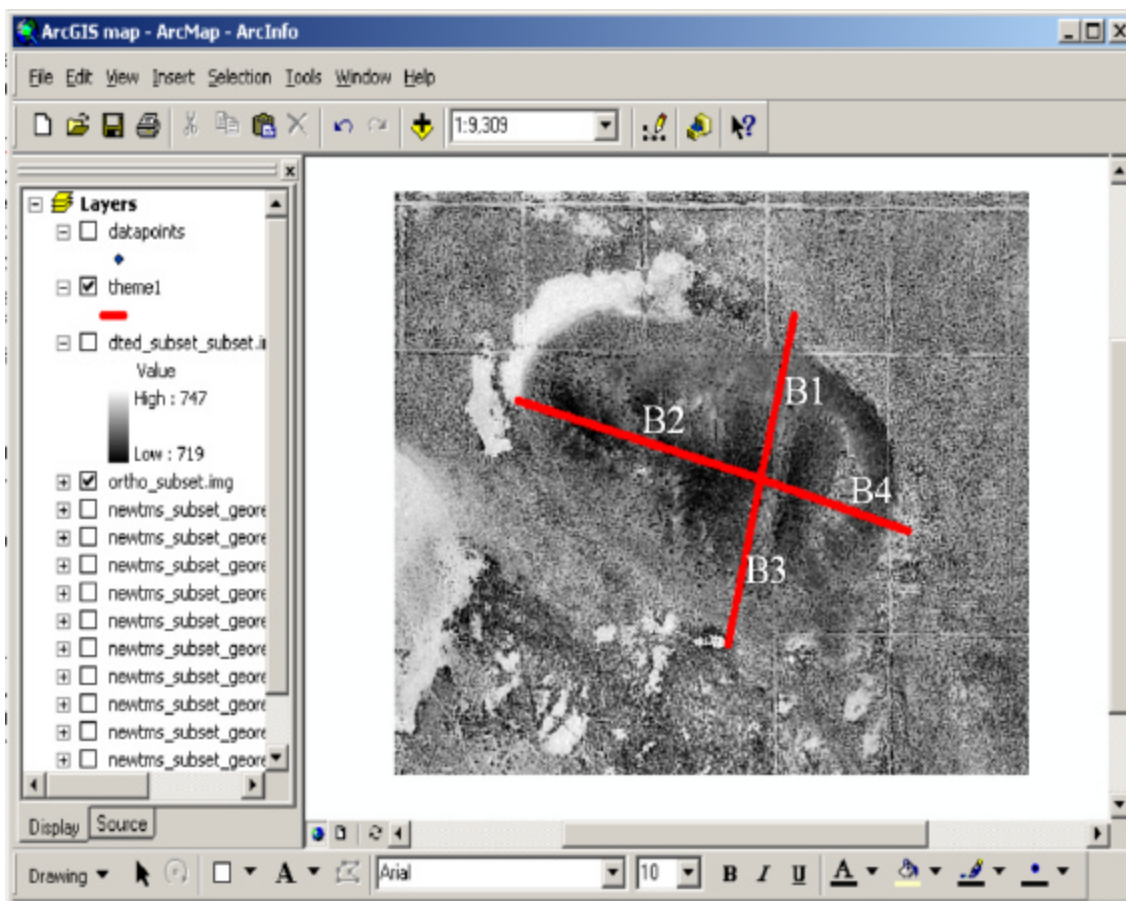


Fig. 3.5. ArcGIS map showing the line theme representing transects beginning at origin (intersection) on the top of the hill and extending in (magnetic) north, west, south, and east directions for transects B1, B2, B3, and B4, respectively. The image is a 1-meter resolution digital orthophotograph. As depicted here, the line for transect B1 extends roughly 800 feet.

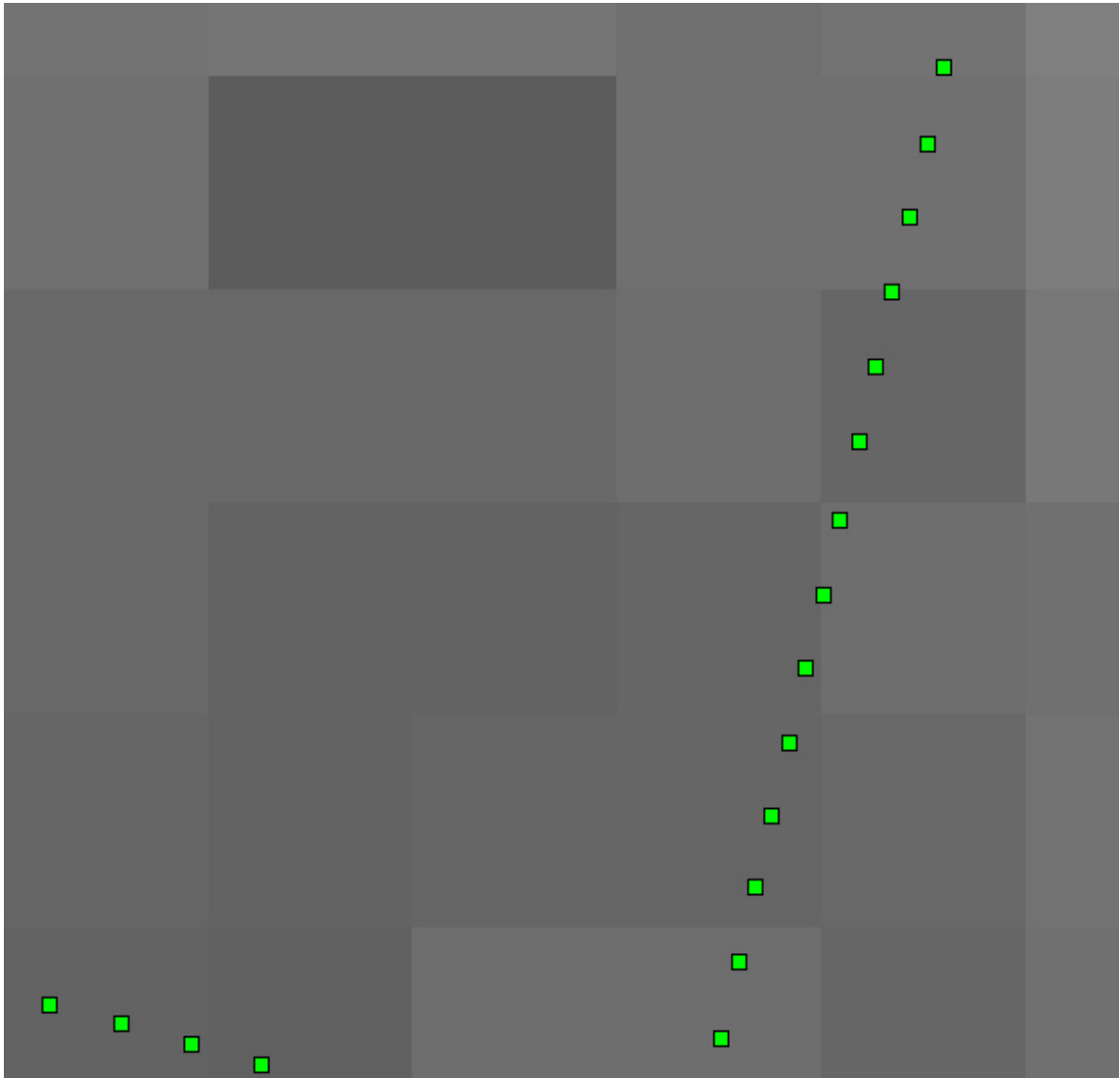


Fig. 3.6. Close-up view of higher resolution (~0.5 meter) observation points (small squares) 'overlaid' on top of TMS data (larger gray squares) at 25 meter resolution. This is a visual depiction of how a GIS can integrate isolated field observations and contiguous remotely sensed data of different scales. Transect B1 extends from bottom to top and a portion of B2 is in the lower left corner.

presence (0) of coatings can be multiplied by particle areas (mm^2), the output of NIH/Scion Image's measurements, and summed to give the total area coverage of rock varnish, iron skins, and no-coating particles at each observation. These and other descriptors are the focus of statistical analyses in the next chapter.

3.4. Method results in this study

This method enabled my measurement and classification of 2,760 individual particles from a cumulative of one day taking digital pictures in the field. Appendix B shows a portion of data produced from the field image processing exercise, as well as other slope metrics.

4. Results and discussion

4.1. Introduction

This chapter presents an interpretation of the first quantitative data on rock coating catenas, as exemplified for a specific hill in the western Mojave Desert. The emphasis of this chapter results in statistical analysis to yield meaningful information missed by casual field observations. This chapter combines graphical depictions of descriptive statistics with statistical tests including a simple regression of particle size and slope, a difference of means test (one-sample t-test) of mean particle areas for three rock coating types, multiple regressions of TMS data and RCI values, and discriminant analyses of the north, south, and west-facing slope transects where variables are differentiated according to slope position. These data and analyses all focus on the basic question of how rock coatings vary spatially from the top to the bottom of a desert hillslope.

4.2. Data matrix

A Q-mode matrix arranges data 92 rows and 18 columns—areal units along transects and indices, respectively. Indices include the following variables: distance (feet), slope angle (degrees), geomorphic position (1,2,3), TMS band 10 albedo values (0-255), TMS band 7 albedo values (0-255), TMS band 2 albedo values (0-255), Digital Orthophotograph albedo values (0-255), rock varnish RCI (0-120), iron films RCI (0-120), ‘no-coating’ RCI (0-30), Smoothed rock varnish RCI (0-120), Smoothed iron films RCI (0-120), Smoothed ‘no-coating’ RCI (0-30), mean particle size (mm^2), median particle size (mm^2), sum of rock varnish particle sizes (mm^2), mean of iron skin

particle sizes (mm^2), and sum of iron skin particle sizes (mm^2). A 3x3 running mean calculated the three 'smoothed' RCI variables. Table 4.1 presents summary statistics for these variables.

Confirming normality is an important step before subjecting a data matrix to statistical procedures. The Kolmogorov-Smirnov One-Sample Test (Birnbaum, 1952; Birnbaum, 1953; Dixon, 1954; Kolmogorov, 1941; Massey, 1951; Smirnov, 1948) analyzes each variable against another variable defined as having a normal distribution. This test is especially suited for data sets with relatively low sample sizes, in this case $N=92$. All of the above 18 variables did not have a statistically significant Kolmogorov-Smirnov Z-scores (Table 4.2), which would have required the rejection of the hypothesis that the observed data follow a normal distribution. Furthermore, the null hypothesis that these variables are normally distributed could not be rejected because the standard errors of skewness and kurtosis rest between -2 and $+2$ (.247 and .490, respectively).

Visual analysis of TMS data plots warns of heteroscedasticity (Burt and Barber, 1996). I therefore transformed these three variables using weighted least squares before running multiple regressions. I used the statistical software package SPSS for Windows version 10.0 for all statistical tests and Microsoft Excel to produce the pie-chart slope profile diagrams.

4.3. Results

4.3.1. Simple regression and difference of means test

A simple regression function (Fig. 4.1) with mean particle areas as the dependent variable and slope angle in degrees as the predictor variable did not show a

Table 4.1. Descriptive statistics.

[illegible]

Table 4.2. Kolmogorov-Smirnov test.

		Distance(ft)	Slope*	ORTHO	TMS_band7	TMS_band2	TMS_band 10	Varn_index	VARN_3X3	Iron_index	IRON_3X3	Albedo_index	Albedo_3
N		92	92	92	92	92	92	92	92	92	92	92	92
Normal Parameters ^{a,b}	Mean	350.65	8.50	67.89	91.55	133.59	120.01	20.87	21.03	47.93	48.54	3.42	3.
	Std. Deviation	291.01	4.39	51.49	14.80	7.15	13.14	11.09	9.39	15.24	11.17	2.92	1.
Most Extreme Differences	Absolute	.167	.107	.094	.147	.129	.149	.090	.086	.067	.144	.144	.1
	Positive	.167	.107	.092	.147	.115	.149	.090	.086	.067	.144	.144	.1
	Negative	-.117	-.069	-.094	-.130	-.129	-.087	-.043	-.062	-.046	-.097	-.120	-.0
Kolmogorov-Smirnov Z		1.599	1.025	.898	1.409	1.237	1.427	.862	.822	.641	1.385	1.379	1.2
Asymp. Sig. (2-tailed)		.012	.245	.395	.038	.094	.034	.448	.508	.806	.043	.045	.0

a. Test distribution is Normal.

b. Calculated from data.

statistically significant relationship ($p = .426$). However, the resulting regression equation, $y = 1934.3 + 28.438x$, is consistent with slope literature which suggests that particle size is positively correlated with slope (Abrahams et al., 1988).

A difference of means test (one-sample t-test) for rock varnish, iron films, and ‘no-coating’ categories (Table 4.3) did show that varnished rocks are larger with a mean of $2542.48 \pm 3640.47 \text{ mm}^2$, iron films are not as large at $1655.183 \pm 1007.828 \text{ mm}^2$, compared to rocks lacking rock coatings that are generally small at $750.122 \pm 1081.748 \text{ mm}^2$ (Fig 4.2). These results are statistically significant ($p < .001$).

4.3.2. *Slope profiles*

Fig. 4.3a graphically represents RCI values as they change in increments of approximately 30 meters (100 feet) from the top to the bottom of the north-facing slope. Figure 4.3b is similar to 4.3a except pie charts here contain percent of total particle surface area. The slope profile derives from field measurements of slope and distance from origin at the top of the hill.

4.3.3. *Multiple regressions*

Setting albedo values of TMS bands 10, 7, and 2 as the exogenous variables in three separate multiple regressions against the three ‘smoothed’ RCI variables as endogenous variables produced R^2 values of .579, .527, and .444, respectively. Beta values for band 10 are -.426, -.973, and -.306 for ‘smoothed’ rock varnish, iron films, and no-coating RCIs, respectively. Similar ratios occurred for bands 7 and 2. Weighted least squares correction drastically lowered the root mean square error (root MSE) for all three tests.

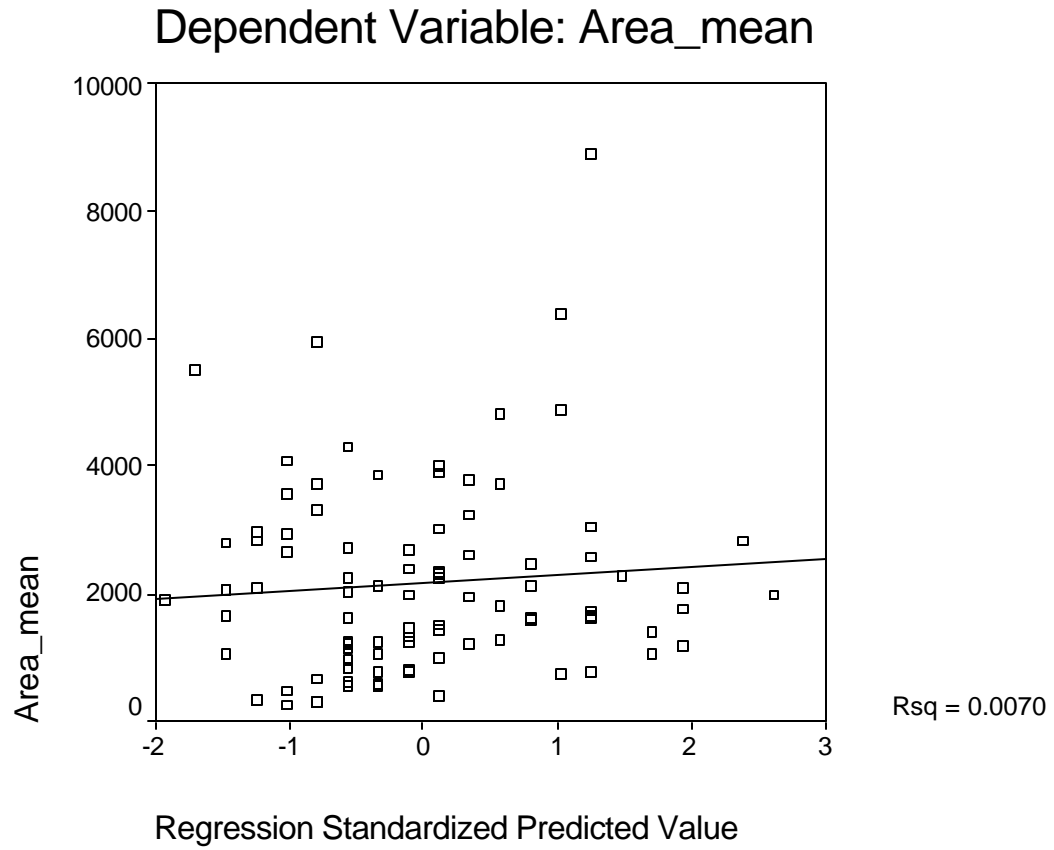


Fig. 4.1. Plot of mean particle size (mm^2) and standardized values for slope angle (degrees). This relationship is not statistically significant ($p=0.426$).

Table 4.3. Difference of means test.

	Test Value = 0					
	t	df	Sig. (2-tailed)	Mean Difference	95% Confidence Interval of the Difference	
					Lower	Upper
Varnish_area_mean	6.699	91	.000	2542.4836	1788.5635	3296.4037
Iron_area_mean	15.753	91	.000	1655.1838	1446.4685	1863.8991
Albedo_area_mean	6.651	91	.000	750.1223	526.0985	974.1461

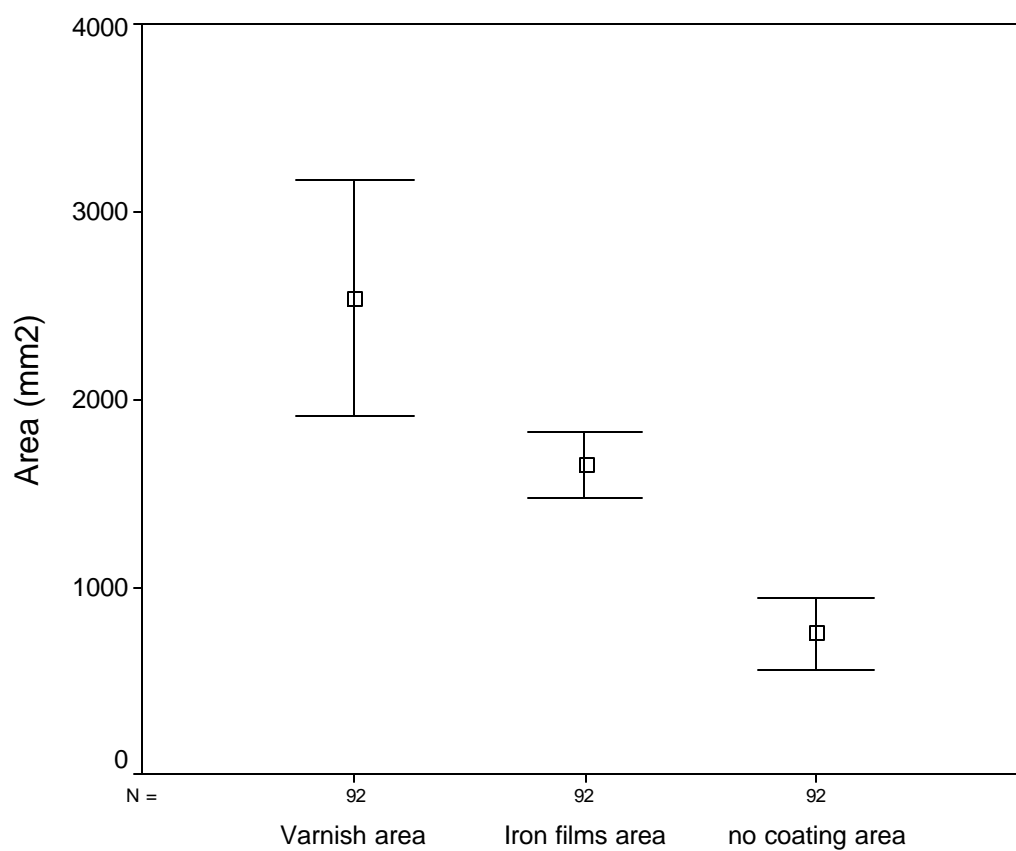


Fig. 4.2. Plot of mean varnish area, iron film area, and high albedo area and standard error bars at the 90% confidence interval, showing a statistically significant difference between the three. Varnished rocks are generally larger, and thus more resistant to overland flow (sheetwash). Iron films are, on average, not as large. Rocks without a coating are undergoing weathering at faster rates and are the smallest.

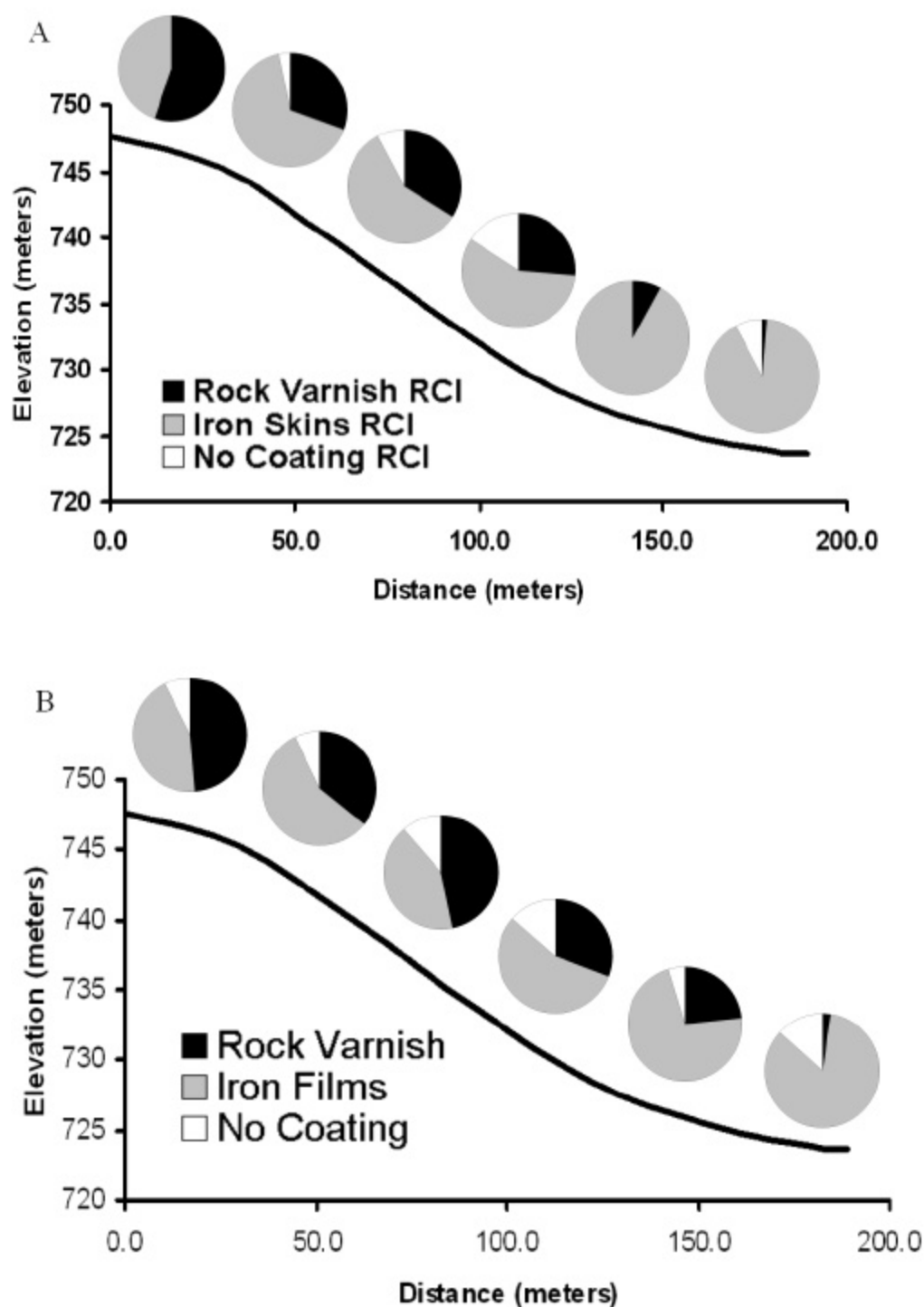


Fig. 4.3. RCI toposequence (A) for three rock coating types and % area toposequence (B) for three rock coating types. Note that in both case varnish is dominant at the top, iron films are present from top to bottom but increase in strength towards the bottom, and no coating rocks lack a slope position signal. 'A' is an average of RCI values every 30 meters (100 feet), and 'B' derives from a single observation every 30 meters.

For example, band 10 dropped from 9.22 before the correction to 9.879E-06 afterwards. The F-statistics, indicating the strength of the multiple regression equations, are 40.414, 32.668, and 23.438., respectively. All results are statistically significant at at least the 99% confidence interval. Plots appear in Fig. 4.4.

4.3.4. *Discriminant analyses*

Discriminant analysis evolved Figs. 4.5, 4.6, 4.7 and Table 4.4. The grouping variable is slope position indicated as upper convex, middle straight, and lower concave (1,2,3, respectively) portions of the slope (Fig. 4.8). All remaining 17 variables are entered simultaneously. For the north facing transect (B1), canonical correlation and eigenvalues for the first two canonical discriminant functions are 0.994 and 76.655, and 0.967 and 14.465, respectively. Wilk's Lamda (Λ) and Chi-square values are 0.001 and 99.272. For the west facing transect (B2), canonical correlation and eigenvalues are 0.984 and 31.307, and 0.920 and 5.534, respectively. Wilk's Lamda (Λ) and Chi-square values for B2 are 0.005 and 101.695. B3 is the south facing transect, which produced canonical correlation and eigenvalues of 0.995 and 91.480, and 0.839 and 2.382, respectively. Wilk's Lamda (Λ) and Chi-square values for B3 are 0.003 and 89.056. The fourth, east-facing transect, was not subject to a discriminant analysis because it did not have particles large enough for digital image processing at the lower concave portion of the slope profile.

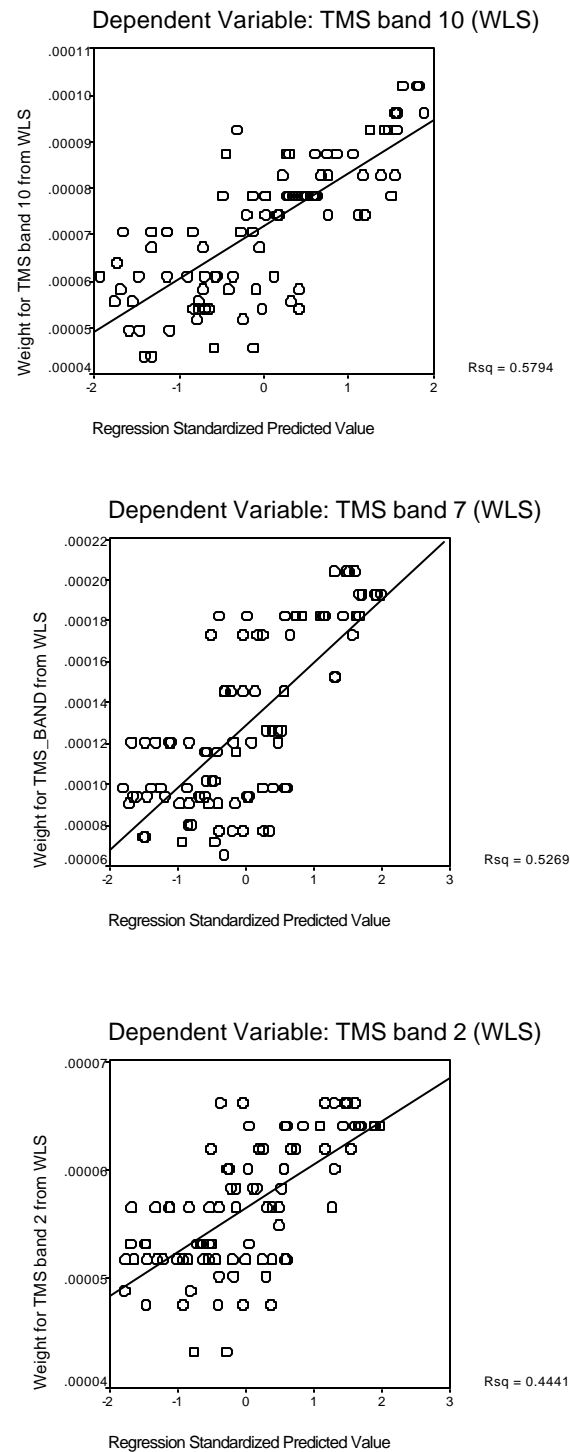


Fig. 4.4. Scatterplots of multiple regressions for weighted least squares corrected TMS band 10 (top right), TMS band 7 (top right), and TMS band 2 (bottom) against the three 'smoothed' RCI variables. These suggest a good correlation between isolated field observations of rock coatings and remotely sensed data, despite the jump in scale.

Canonical Discriminant Functions

Transect B1

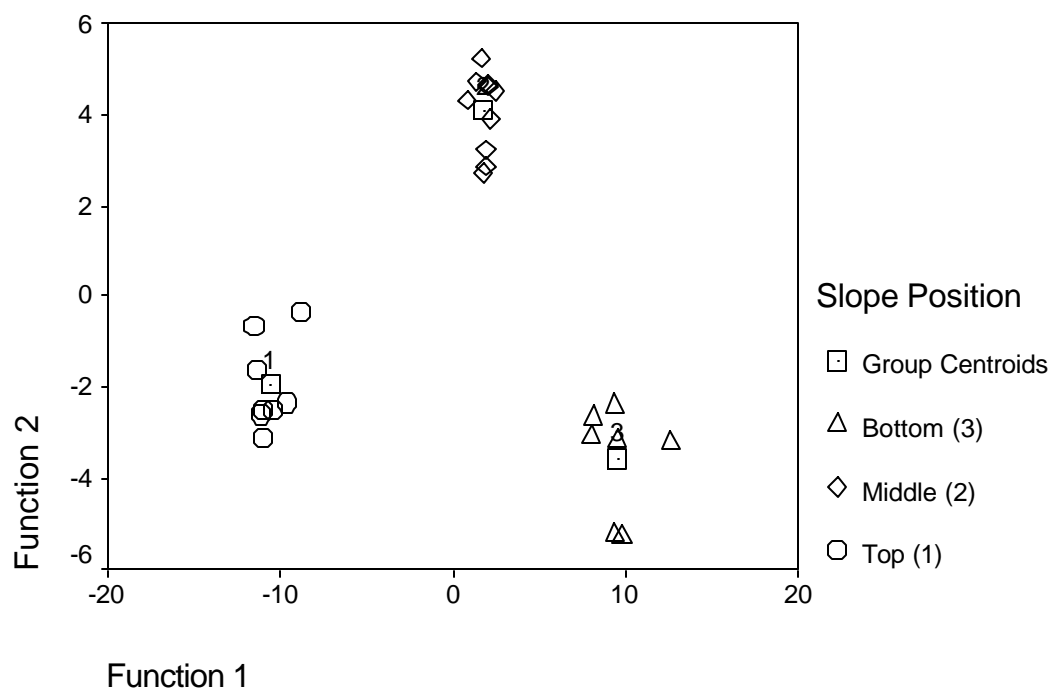


Fig. 4.5. Combined plot of the first two canonical discriminant functions for the north-facing catena (B1) showing an obvious separation (discriminant fence) between upper, middle, and lower slope positions. N=26.

Canonical Discriminant Functions

Transect B2

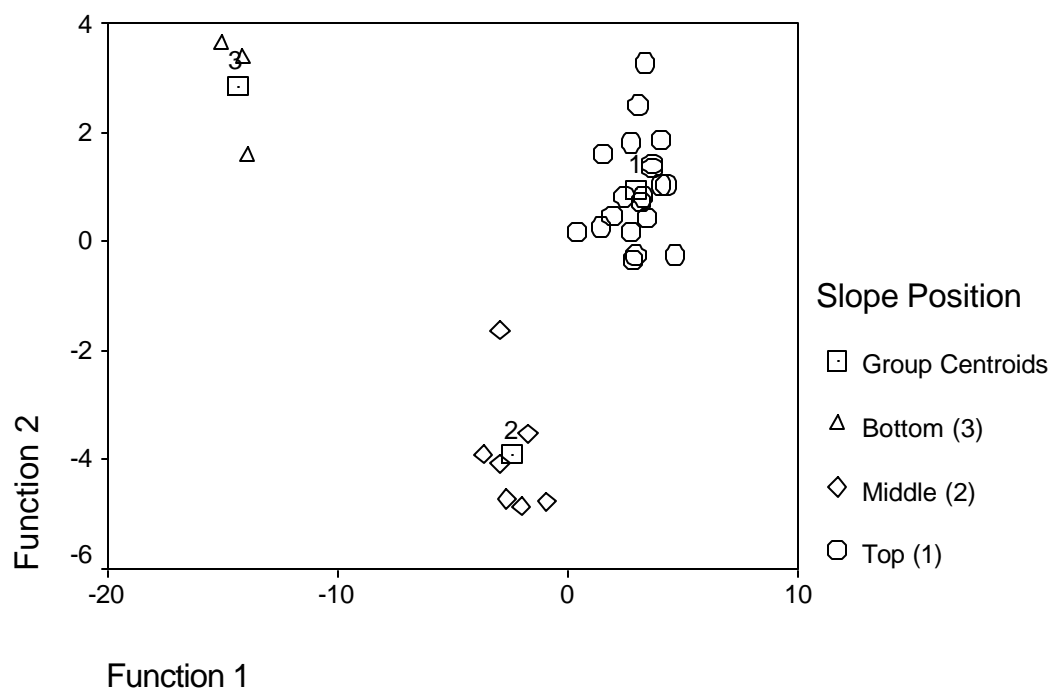


Fig 4.6. Combined plot of the first two canonical discriminant functions for the west-facing catena (B2) showing an obvious separation (discriminant fence) between upper, middle, and lower slope positions. N=30.

Canonical Discriminant Functions

Transect B3

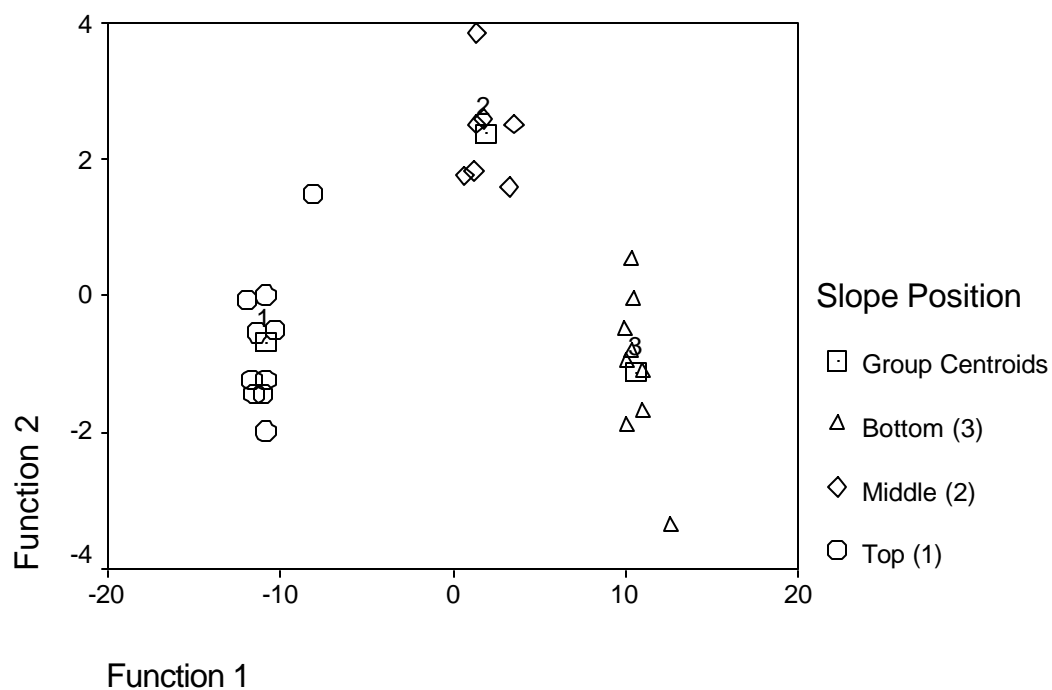


Fig. 4.7. Combined plot of the first two canonical discriminant functions for the south-facing catena (B3) showing an obvious separation (discriminant fence) between upper, middle, and lower slope positions. N=24.

Table 4.4. Structure Matrices for B1 (left), B2 (center), and B3 (right). Function 1 is renamed “stability”, in terms of slope position, or distance from the top of the hill and Function 2 relabeled “rock coating horizons”. Note the inverse relationship in the structure coefficients for rock coating and iron skins RCI variables.

	Function	
	1	2
Distance(ft)	.311*	-.114
ORTHO	.104*	.051
TMS_band7	.269	-.386*
TMS_band 10	.231	-.314*
IRON_3X3	.222	-.300*
Slope*	.010	.282*
Iron_index	.143	-.263*
TMS_band2	.205	-.260*
Area_mean	-.070	.206*
Varnish_area_su	-.071	.197*
VARN_3X3	-.140	.159*
Iron_area_mean	-.065	.153*
Area_median	-.065	.152*
Iron_area_sum	-.051	.138*
Varn_index	-.061	.128*
Albedo_index	-.004	.009*
Albedo_3x3	-.002	.006*

Pooled within-groups correlations between discriminant variables and standardized canonical discriminant functions. Variables ordered by absolute size of correlation within function.

*. Largest absolute correlation between each variable and any discriminant function

	Function	
	1	2
TMS_band 10	-.218*	-.087
Distance(ft)	-.161*	-.156
VARN_3X3	.088*	-.012
Albedo_3x3	-.027	-.448*
Albedo_index	.003	-.309*
Area_median	.038	.262*
IRON_3X3	-.206	.259*
TMS_band2	-.210	-.251*
Iron_index	-.129	.229*
TMS_band7	-.212	-.213*
Iron_area_sum	-.010	.197*
Area_mean	.030	.179*
Slope*	-.067	-.178*
Iron_area_mean	-.003	.158*
Varnish_area_sur	.067	.138*
ORTHO	-.039	.111*
Varn_index	.047	-.048*

Pooled within-groups correlations between discriminant variables and standardized canonical discriminant functions. Variables ordered by absolute size of correlation within function.

*. Largest absolute correlation between each variable and any discriminant function

	Function	
	1	2
Distance(ft)	.296*	-.094
TMS_band7	.136*	-.094
TMS_band2	.134*	-.044
TMS_band 10	.100*	-.069
IRON_3X3	.058	.504*
VARN_3X3	-.031	-.450*
Slope*	.019	.419*
Iron_index	.042	.328*
Varn_index	-.016	-.224*
Iron_area_sum	-.011	.174*
Area_mean	-.017	.161*
Area_median	-.073	-.160*
Iron_area_mean	-.038	.109*
Varnish_area_sur	.001	.099*
ORTHO	-.023	-.084*
Albedo_3x3	-.038	.075*
Albedo_index	-.021	.040*

Pooled within-groups correlations between discriminant variables and standardized canonical discriminant functions. Variables ordered by absolute size of correlation within function.

*. Largest absolute correlation between each variable and any discriminant function

a. This variable not used in the analysis.

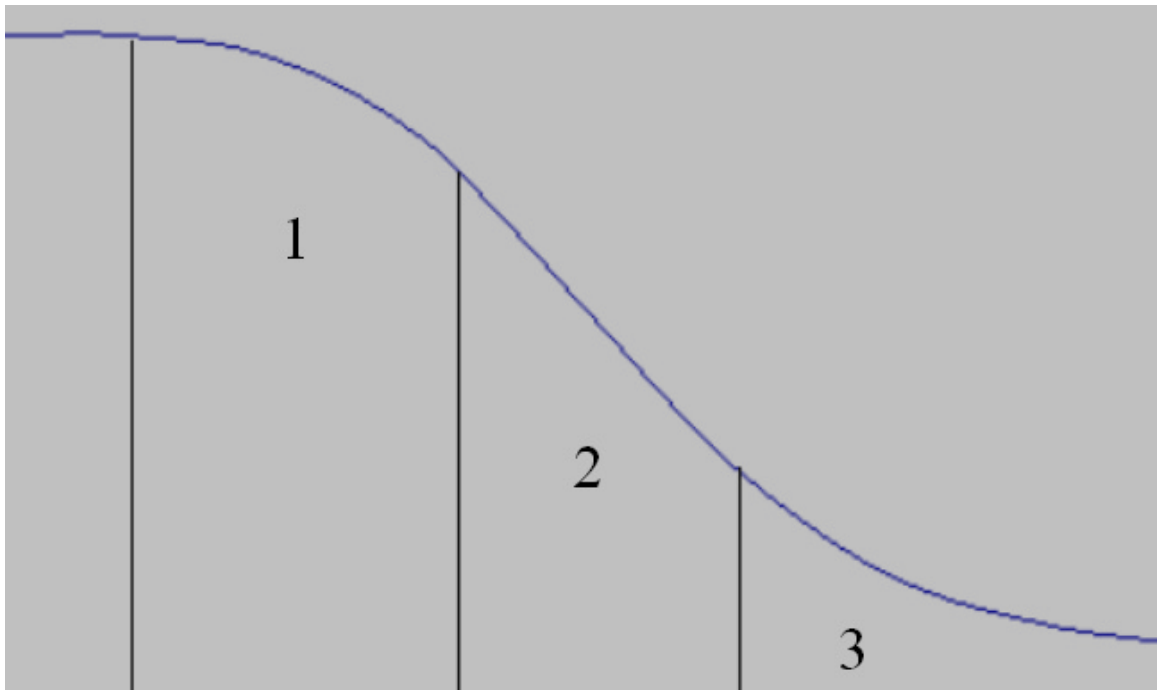


Fig. 4.8. Diagram showing the discriminant analysis grouping variable, slope position—top convex (1), middle straight (2), and bottom concave (3).

4.4. Discussion

This discussion focuses on answering the basic question of how rock coatings vary spatially from the top to the bottom of a desert hillslope. The order runs progressively from field-based perspectives towards aerial and statistical analyses—leading to the conclusion that rock coating catenas can be important indicators of slope stability.

Field based findings reveal a general preference scheme for the three types of rock surfaces studied here. Although statistically significant relationships do not exist between particle size and slope angle at this site, a noticeable decrease is obvious in digital images (Appendix A) as one moves from the top to the bottom of the slope transects. Comparison of means tests confirms what is also an easy deduction from site pictures—that particles hosting varnish are generally larger than iron film or no-coating particles. Larger particles resist transport processes such as overland flow (Hoggs, 1982; Yair and Lavee, 1982) to a much greater degree, thus being more amenable to conditions needed for manganiferous rock varnish accretion. In other words, larger particles are more stable and can hold more varnish. The formative environment for iron skins differs from that of rock varnish (Dorn, 1998). Iron skins begin to form in the sub-surface and are observable remnants on particles after they have been ‘ejected’, so to speak, outward onto the surface. This means that most likely every clast initially had an iron film coating, but depending on its size and weathering rate it may have developed a concealing varnish above or lost it because of disintegration and/or frequent spalling. In other words, rock varnish favors big rocks; iron films do not prefer any particular size; and smaller rocks fail to maintain stable enough surfaces to host rock coatings.

Hillslope position in a catena strongly influences the nature of rock coatings, where by Young's model articulates well to these findings. Young (1976) outlined the possible ways soils horizons may vary along a slope (Fig. 2.3)—such as increase, decrease, remain constant, deepen or rise, end or begin, be replaced, or gradually change in terms of properties but maintain the same identity. Catenary variations of rock coating intensity translated into a 'horizon' (not the actual micron-thick layer) will possibly match one of these scenarios.

RCI in this study generates values indicating the dominance of rock varnish, iron films, and rock eroding faster than coating accumulation in a field of view that is approximately a half-meter squared. RCI value and percent of total particle surface area slope profile diagrams both communicate the influence of slope position on rock coatings (Fig. 4.3). Rock varnish dominates on hilltops and decreases progressively until very little to no varnish occurs towards the lower end of the slope. In contrast, iron films occur at all slope positions but its signal is accentuated as varnish wanes, becoming strongly dominant in lower slope positions. "High albedo" rocks with no coatings also occur throughout the catena but without a clear slope position signal. In terms of Young's model, then, varnish 'horizons' decrease to almost nothing, iron film 'horizons' increase along the entire slope, and no-coating 'horizons' appear sporadically from top to bottom. The important finding here is that positions of least transport mobility, the top waxing convex portions (Dalrymple et al., 1968; Wood, 1942), correspond with rock varnish dominance. In other words, maps of rock coating character in general, and rock varnish abundance in particular, do appear to provide a proxy for slope stability.

Another fundamental problem addressed here is whether essentially higher resolution ground observations link statistically to lower resolution observations gathered from aerial and satellite platforms. No prior investigators have attempted to link ground and aerial views of rock coatings, despite the importance of rock coatings in influencing such large-expenditure items as Martian remote sensing.

Results from multiple regression analyses show strong, highly statistically significant relations. 25-meter scale TMS band 10 maintains an especially strong correlation with ground-based RCI values, as smoothed rock coating indices could account for almost 58% of explained variance. TMS Band 10 in the mid infrared is equivalent to Landsat TM band 7, useful for discriminating minerals and rock types. This finding gives further weight to the argument that geologic mapping can be misleading without first accounting for the presence and variation of rock coatings, as the high majority of particles in this study hosted one of two, or both types of rock coatings. Smoothed RCI values could account for slightly less variance in TMS band 7 in the near infrared (52.7 %) and the least in TMS band 2 in the red visible region (44.4%). Testing these bands was an effort to see how other bands suited for jobs other than geologic sensing perceived rock coatings. Although these other bands do not perform as well, they still convey the point that rock coating signals dominate image pixels. Also, ratios of standardized Beta values show that iron film strength (RCI) is generally twice as important as varnish strength (RCI) in contributing to explained variance in TMS bands.

Discriminant analysis facilitates separation between different groups of data, in this case slope position, and provides a 'multi' approach perspective. Data evaluated for the various slope positions include: TMS albedo values for the aforementioned three bands;

panchromatic orthophotograph albedo at 1-meter resolution; RCI values for rock varnish, iron film, and the ‘no coating’ categories; a 3x3 running mean for the RCI values; particle size descriptive statistics of mean and median; and are on the particles of rock varnish, iron film, and the lack of coating. These variables represent a combination of low-resolution data from TMS, medium resolution data from the orthophotograph albedo, and higher resolution data obtained from digital image processing of the individual particles.

A clear distinct discriminant fence occurs between the top convex (1), middle straight (2), and bottom concave (3) sections of the studied transect slopes. This statistical delineation further clarifies pie-chart slope profile catenas derived from descriptive statistics. Signals imposed by slow-forming manganiferous rock varnish on larger particles are strongest at the top, indicating that these hill portions are the most stable. These signals are a combination of scales, testifying to the ability of the multi approach. Darker 25-meter TMS albedo and larger, more varnished particles ground observation scales, both at higher slope positions, combine to advocate slope stability. Middle and lower slopes are less stable as erosion sheds iron films formed in subsurface environments. Additional evidence of continual weathering comes from ‘no coating’ smaller particles that obviously derive from erosion of larger clasts, most likely driving the slight decrease in particle sizes down the slopes.

The structure matrices (Table 4.4) list discriminant function coefficients that are similar to what factor loadings indicate in a factor analysis. Function 1 generally contains high ‘loadings’ for the slope position descriptor variable “distance(ft)” and thus I give it the more meaningful label of “Stability”. I rename Function 2 as “Rock Coating

Horizons” as it has the highest structure coefficients in the variables that can describe rock coatings in a catena. The important finding here is that discriminant function coefficients for both raw and smoothed varnish RCI and iron films RCI are inversely related. In other words, iron films are more likely to be dominant where rock varnish is weaker. This is consistent with the literature, suggesting that rock varnish forms in areas of low disturbance (Dorn and Krinsley, 1994; Lui and Dorn, 1996).

Future researchers can now predict surficial rock coating catenas using remotely sensed values, at least for homogenous hills of basaltic lithologies. In other words, slopes that are extraordinarily stable would maintain a very different remote sensing signature, as would very unstable slopes. Applications of this technique are driven by the need for data on slope stability. A greater understanding of the spatial distribution of rock coatings will help in endeavors such as environmental impact statements, tectonic stability studies, rock art and rock monument preservation, and other frameworks needing a general perspective on rock coating stability.

Just as we strive to preserve ‘old growth forests’, we need to preserve stable slopes, as restoration is difficult once the balance is turned. The Air Force, for example, can potentially make initial assessments of bombing range damage, where efforts to repair and restore natural environments are a huge concern, through remote sensing linked with an understanding of the catenary variation of rock coatings.

Natural erosion also removes much of the priceless histories etched in rocks and rock coatings by prehistoric peoples (Francis and Loendorf, 2002; Lee and Stasack, 1999). Understanding where to act first and what is likely to be preserved is of utmost

importance in terms of selecting the sites to conserve. The incorporation of a rock coating index and remotely sensed data will aid this time-constrained effort.

As mentioned earlier, rock coatings drastically influence the aesthetic appearance of the desert. However, attempts to mimic the desert in artificial home, park, or industrial landscapes sometimes apply ‘fake’ coatings that do not match nature. For example, in a new housing development in the Phoenix area a desert landscaper would have known it inappropriate to darken the rocks in a stream bed wash (Dorn 1998) if the developer understood natural distributions of rock coatings in desert environments.

This case study of rock coating catenas at one location of one lithology reveals the feasibility of this research. Further research of this type will help to formulate more general conclusions that are safe to apply to similar slopes near this specific study site in the western Mojave Desert (Parsons and Abrahams, 1987), and eventually other regions of the earth where rock coatings are present on slopes. This study also suggests that multi-scale approach methodologies will justify studies of increasingly more complex rock coating and slope situations in different settings where remote sensing is used to map Martian and terrestrial contexts.

5. Conclusion

Desert hillslopes around Earth and on Mars host a variety of rock coatings. No matter whether the study site is the Outback of Ayers Rock in Australia, the domed inselbergs of Namibia, South Mountain Park in Phoenix, or Martian slopes, rock coatings do vary down slopes. Those attempting to map geology on Earth and Mars, those interested in rock coatings as proxies for slope stability, and those simply interested in what rock coatings convey regarding environmental change have simply not focused on the simple task of mapping rock coating distributions on desert hillslopes. Such a task is not simple, perhaps explaining why investigators simply ignore or assume away the importance of slope variations in rock coatings.

This thesis is the first-ever study of how rock coatings change down a slope. In such a feasibility study, it is important to constrain the study area to a relatively simple site. A basalt slope with minor and similar vegetation in the western Mojave Desert demonstrates the feasibility of examining rock coatings them a multi-scale approach. The specific conclusions relevant to this location and particular lithology are that rock varnish accumulates on larger basalt clasts at more-stable hilltops, iron skins are dominant at the lower erosional zones, and ‘no coating’ particles indicate the fast-rate ongoing weathering of smaller particles. A new digital image processing technique allows for a more robust analysis of the study site and minimal time spent in the field. This method obtains a high degree of consistency because individual particles are measured in controlled conditions in the laboratory. The resulting rock coating index

communicates complexities inherent in rock coatings distributions, such that numbers in a catena may now express slope stability.

Geographers have long been interested in connecting scales (Church and Mark, 1980). Scale linkages, and critical jumps in scale are almost always a fundamental question that needs to be reconciled (Phillips, 1999). Implications for understanding the systematic change of rock coatings at a local field scale help bridge the gap between rock weathering and rock coating accretion processes dominant at the micro-scale and a more holistic view. The statistically significant correlation of TMS bands and the RCI categories, thus, provide the first step towards linking kilometer-scale remotely sensed and meter-scale field observations of rock coatings. Future research and improvements in the spatial precision of satellite and aerial image data will further increase the amount of confidence we can place in remote sensing's ability to express spatially isolated ground observations contiguously across the surface. However, this thesis demonstrates for the first time the ability of investigators to link rock weathering changes normally studied at the microscopic scale with satellite images used to study large areas in such endeavors as geologic mapping and land-use planning.

I foresee that the Air Force and other land managers could use my research by incorporating a rock coating index and satellite imagery in a variety of applications from base planning to bombing-range environmental damage assessment. Refinement of the methodology presented here may also be important to remote sensing specialists and geologists who are now concentrating on studying humanly inaccessible extraterrestrial surfaces, where rock coatings control abrasion and erosion rates (Kraft and Greeley, 2000). My findings will also interest rock coating specialists seeking to understand how

rock coatings can be used as important indicators of the physical geography and geochemical nature of a slope, as in a recent study of watersheds in the Arctic by geographers at the University of Illinois and the University of Arkansas (Dixon et al., 2002).

REFERENCES

- Abrahams, A.D., Parsons, A.J., Luk, S.-H., 1988. Hydrolic and sediment responses to simulated rainfall on desert hillslopes in southern Arizona. *Catena*. 15: 103-117.
- Abrams, M., Abbott, E., Kahle, A., 1991. Combined use of visible, reflected infrared, and thermal infrared images for mapping Hawaiian lava flows. *Journal of Geophysical Research-Solid Earth and Planets*. 96(B1): 475-484.
- Arvidson, R.E., 1974. Wind blown streaks, splotches, and associated craters on Mars: statistical analysis of Mariner 9 photographs. *Icarus*. 21: 12-27.
- Asner, G.P., Wessman, C.A., Bateson, C.A., Privette, J.L., 2000. Impact of tissue, canopy, and landscape factors on the hyperspectral reflectance variability of arid ecosystems. *Remote Sensing of Environment*. 74(1): 69-84.
- Bach, A.J., 1995. *Climatic controls on aeolian activity in the Mojave and Colorado deserts, California*. Dissertation Thesis, Arizona State University, Tempe.
- Bayr, K.J., Hall, D.K., Kovalick, W.M., 1994. Observations on glaciers in the eastern Austrian Alps using satellite data. *International Journal of Remote Sensing*. 15(9): 1733-1742.
- Beach, T., 1998. Soil catenas, tropical deforestation, and ancient and contemporary soil erosion in the Peten, Guatemala. *Physical Geography*. 19(5): 378-405.
- Birkeland, P.W., Gerson, R., 1991. Soil-catena development with time in a hot desert, southern Israel field data and salt distribution. *Journal of Arid Environments*. 21(2): 267-281.
- Birnbaum, Z.W., 1952. Numerical Tabulation of the distribution of Kolmogorov's statistic for finite sample values. *Journal of the American Statistical Association*. 47: 425-411.
- Birnbaum, Z.W., 1953. Distribution-free tests of fit for continuous distribution functions. *Annals of Mathematical Statistics*. 24: 1-8.
- Bishop, M.P., Shroder, J.F., Hickman, B.L., Copland, L., 1998. Scale-dependent analysis of satellite imagery for characterization of glacier surfaces in the Karakoram Himalaya. *Geomorphology*. 21((3-4)): 217-232.
- Breed, C.S., Grow, T., 1979. Morphology and distribution of dunes in sand seas observed by remote sensing. In: E.D. McKee (Editor), *A Study of Global Sand Seas*. U.S. Geologic Survey Professional Paper, 1052: 253-308.

- Bull, P.A., 1981. Image Analysis Instruments. In: A. Goudie et al. (Editors), *Geomorphological Techniques*. George Allen & Ulwin, London.
- Bunting, B.T., 1965. *The Geography of Soil*. Hutchinson, London.
- Buol, S.W., Hole, F.D., McCracken, R.J., 1973. *Soil Genesis and Classification*. Iowa State University Press, Ames.
- Burt, J.E., Barber, G.M., 1996. *Elementary Statistics for Geographers*. The Guilford Press, New York.
- Butler, J.B., Lane, S.N., Chandler, J.H., 2001. Automated extraction of grain-sized data from gravel surfaces using digital image processing. *Journal of Hydraulic Research*. 39(5): 519-529.
- Campbell, I.A., 1991. Classification of rock weathering at Writing-On-Stone Provincial Park, Alberta, Canada. *Earth Surface Processes and Landforms*. 16: 701-711.
- Cervený, N.V., 2000. Relationship between internal and external weathering characteristics of detrital quartz. MA Thesis, Arizona State University, Tempe.
- Christensen, P.R., Harrison, S.T., 1993. Thermal infrared emission spectroscopy of natural surfaces: application to desert varnish coating on rocks. *Journal of Geophysical Research*. 98(B11): 19,819-19,834.
- Christopherson, R.W., 2000. *Geosystems*. Prentice-Hall, Inc., Upper Saddle River, NJ.
- Church, M.A., Mark, D.M., 1980. On size and scale in geomorphology. *Progress in Physical Geography*. 4: 342-390.
- Colman, S.M., 1982. *Chemical Weathering of Basalts and Andesites: Evidence from Weathering Rinds*. Geological Survey Professional Paper 1246. United States Government Printing Office, Washington D.C.
- Cooke, R.U., Warren, A.S., Goudie, A.S., 1993. *Desert Geomorphology*. UCL Press Limited, London.
- Dalrymple, J.B., Blong, R.J., Conacher, A.J., 1968. A hypothetical nine-unit land-surface model. *Zeitschrift Geomorphologie*. 12: 60-76.
- Derbyshire, E., Lijun, L.F., Perrott, A., Xu, S., Waters, R.S., 1984. Quaternary glacial history of the Hunza Valley, Karakoram Mountains, Pakistan, The International Karakoram Project. Cambridge University Press, Cambridge.

- Dixon, J.C., Thorn, C.E., Darmody, R.G., Campbell, S.W., 2002. Weathering rinds and rock coatings from an Arctic alpine environment, northern Scandinavia. *GSA Bulletin*. 114(2): 226-238.
- Dixon, W.J., 1954. Power under normality of several non-parametric tests. *Annals of Mathematical Statistics*. 25: 610-614.
- Doehring, D.O. (Editor), 1980. *Geomorphology in Arid Regions*. George Allen & Ulwin, London, 272 pp.
- Dorn, R.I., 1995. Digital processing of back-scatter electron imagery: A microscopic approach to quantifying chemical weathering. *Geological Society of America Bulletin*. 107(6): 725-741.
- Dorn, R.I., 1998. *Rock Coatings. Developments in Earth Surface Processes 6*. Elsevier Science B. V., Amsterdam.
- Dorn, R.I., Krinsley, D.H., 1994. New perspectives on colluvial boulder deposits in the Southwest Great Basin, USA. *Physical Geography*. 15: 62-79.
- Dragovich, D., 1993. Fire-accelerated boulder weathering in the Pilbara, Western Australia. *Zeitschrift Geomorphologie*. 37: 295-307.
- Dunkerley, D.L., 1996. Stone cover on desert hillslopes: Extent of bias in diameters estimated from grid samples and procedures for bias correction. *Earth Surface Processes and Landforms*. 21(6): 573-580.
- Espizua, L.E., 1993. Quaternary glaciations in the Rio Mendoza Valley, Argentine Andes. *Quaternary Research*. 40(150-162).
- Espizua, L.E., Bengochea, J.D., 1990. Surge of Grande del Nevado Glacier (Mendoza, Argentina) in 1984: its evolution through satellite images. *Geographic Analysis*. 72(3/4): 255-259.
- Farr, T.G., Chadwick, O.A., 1996. Geomorphic processes and remote sensing signatures of alluvial fans in the Kun Lun mountains, China. *Journal of Geophysical Research-Planets*. 101(E10): 23091-23100.
- Fouache, E., Gruda, G., Mucaj, S., Nikolli, P., 2001. Recent geomorphological evolution of the deltas of the rivers Seman and Vjosa, Albania. *Earth Surface Processes and Landforms*. 26(7): 793-802.
- Francis, J., Loendorf, L., 2002. *Ancient Visions: Petroglyphs and Pictographs of the Wind River and Bighorn Country, Wyoming and Montana*. University of Utah Press, Salt Lake City.

- Gardiner, V., Dackombe, R., 1983. *Geomorphological Field Manual*. George Allen & Ulwin, Ltd., London.
- Gerrard, J., 1992. *Soil Geomorphology: An integration of pedology and geomorphology*. Chapman & Hall, London.
- Gordon, S.J., 1995. Assessing the effects of temperature of plagioclase weathering, Iztaccihuatl, Mexico. MA Thesis, Arizona State University, Tempe.
- Graef, F., van Duivenvooden, N., Stahr, K., 1998. Remote sensing and transect-based retrieval of spatial soil and terrain (SOTER) information in semi-arid Niger. *Journal of Arid Environments*. 39(4): 631-644.
- Graf, W.L., 1996. Transport and deposition of plutonium-contaminated sediments by fluvial processes, Los Alamos Canyon, New Mexico. *Geological Society of America Bulletin*. 108: 1342-1355.
- Gupta, A., Hock, L., Huang, X.J., Chen, P., 2002. Evaluation of part of the Mekong River using satellite imagery. *Geomorphology*. 44(3-4): 221-239.
- Harden, J.W., 1982. A quantitative index of soil development from field descriptions: Examples from a chronosequence in central California. *Geoderma*. 28(1): 1-28.
- Heywood, I., Cornelius, S., Carver, S., 1998. *An Introduction to Geographical Information Systems*. Pearsons Education Inc., New York.
- Hoggs, S.E., 1982. Sheetfloods, sheetwash, or sheetflow, or...? *Earth Science Reviews*. 18: 59-76.
- Hurst, V.J., Kelly, A.R., 1961. Patination of cultural flints. *Science*. 134: 251-256.
- Jensen, J.R., 1996. *Digital Image Processing: A Remote Sensing Perspective*. Prentice Hall Series in Geographic Information Science. Prentice Hall, Upper Saddle River.
- Johnson, W.C., 1994. Woodland expansion in the Platte River, Nebraska - Patterns and causes. *Ecological Monographs*. 64(1): 45-84.
- Kalliola, R., Puhakka, M., Salo, J., Toumisto, H., Ruokolainen, K., 1991. The dynamics, distribution and classification of swamp vegetation in Peruvian Amazonia. *Annales Botanici Fennici*. 28(3): 225-239.
- Kenea, N.H., 2001. Influence of desert varnish on the reflectance of gossans in the context of Landsat TM data, southern Red Sea Hills, Sudan. *International Journal of Remote Sensing*. 22: 1879-1894.

- Kochis, N.S., Lasca, N.P., 1994. Soil variation on north and south slope-catenas on a kame in southeast Wisconsin. *Physical Geography*. 15(6): 543-556.
- Kolmogorov, A., 1941. Confidence limits for an unknown distribution function. *Annals of Mathematical Statistics*. 12: 461-463.
- Kraft, M.D., Greeley, R., 2000. Rock coatings and aeolian abrasion on Mars: Application to the Pathfinder landing site. *Journal of Geophysical Research-Planets*. 105(E6): 15107-15116.
- Krimmel, R.M., Meier, M.F., 1973. Glacier applications of ERTS. *Journal of Glaciology*. 15(73): 391-402.
- Lancaster, N., 1988. Development of linear dunes in the southwestern Kalahari, Southern Africa. *Journal of Arid Environments*. 14: 233-244.
- Langley, S.K., Cheshire, H.M., Humes, K.S., 2001. A comparison of single date and multitemporal satellite image classifications in a semi-arid grassland. *Journal of Arid Environments*. 49(2): 401-411.
- Lee, G., Stasack, E., 1999. *The Spirit of Place: Petroglyphs of Hawaii*. Bearsville and Cloud Mountain Presses, Los Osos.
- Legg, C.A., 1992. *Remote Sensing and Geographic Information Systems*. Ellis Horwood, New York.
- Leopold, L.B., Emmett, W.W., Myrick, R.M., 1966. Channel and hillslope processes in a semiarid area, New Mexico, USGS Professional Paper 500A.
- Lillesand, T.M., Kiefer, R.W., 2000. *Remote Sensing and Image Interpretation*. John Wiley & Sons, Inc., New York.
- Lui, T.Z., Dorn, R.I., 1996. Understanding the spatial variability of environmental change in drylands with rock varnish microlaminations. *Annals of the Association of American Geographers*. 86(2): 187-212.
- Massey, F.J., Jr., 1951. The Kolmogorov-Smirnov test for goodness of fit. *Journal of the American Statistical Association*. 46: 68-78.
- McCalpin, J.P., Berry, M.E., 1996. Soil catenas to estimate ages of movements on normal fault scarps, with an example from the Wasatch fault zone, Utah, USA. *Catena*. 27(3-4): 265-286.
- McDermid, G.J., Franklin, S.I., 1995. Remote sensing and geomorphometric discrimination of slope processes. *Zeitschrift Geomorphologie*. 101: 165-185.

- Milana, J.P., 2000. Characterization of alluvial bajada facies distribution using TM imagery. *Sedimentology*. 47: 741-760.
- Miller, D.C., Birkeland, P.W., 1992. Soil catena variation along an alpine climatic transect, northern Peruvian Andes. *Geoderma*. 55(3-4): 211-223.
- Milne, G., 1935. Some suggested units of classification and mapping, particularly for East African soils. *Soils Research*. 4(3): 183-198.
- NASA, 1992. ER-2 Flight Summary Report, Flight 92-093, Aircraft Data Facility, NASA-Ames Research Center, Science and Applications Aircraft Division, Airborne Science and Applications Program, Moffett Field, California.
- Oberlander, T.M., 1989. Slope and Pediment Systems. In: D.S.G. Thomas (Editor), *Arid Zone Geomorphology*. Belhaven Press, London, 56-84.
- Ollier, C.D., 1976. Catenas in Different Climates. In: E. Derbyshire (Editor), *Geomorphology and Climate*. Wiley & Sons, London, 137-169.
- Parsons, A.J., Abrahams, A.D., 1987. Gradient-particle size relations on quartz monzonite debris slopes in the Mojave Desert. *Journal of Geology*. 95: 423-452.
- Phillips, J.D., 1999. *Earth Surface Systems: Complexity, Order, and Scale*. Blackwell Publishers, Malden.
- Pickup, G., Marks, A., 2000. Identifying large-scale erosion and deposition processes from airborne gamma radiometric and digital elevation models in a weathered landscape. *Earth Surface Processes and Landforms*. 25(5): 535-557.
- Pope, G., Dorn, R.I., Dixon, J., 1995. A new conceptual model for understanding geographical variations in weathering. *Annals of the Association of American Geographers*. 85: 38-64.
- Prigent, C., Rossow, W.B., Matthews, E., Marticorena, B., 1999. Microwave radiometric signatures of different surface types in deserts. *Journal of Geophysical Research-Atmospheres*. 104(D10): 12147-12158.
- Rhoads, B.L., Thorn, C.E., 1996. *The Scientific Nature of Geomorphology*. John Wiley and Sons.
- Sagan, C., Pollack, J.B., 1969. Windblown dust on Mars. *Nature*. 223: 791-794.
- Scambos, T.A., Dutkiewicz, M.J., Wilson, J.C., 1992. Application of image cross correlation to the measurement of glacier velocity using satellite image data. *Remote Sensing of Environment*. 42(3): 177-186.

- Schick, A.P., 1980. A Tentative Sediment Budget for and Extremely Arid Watershed in the Southern Negev. In: D.O. Doehring (Editor), *Geomorphology in Arid Regions*. George Allen & Unwin, London, 272.
- Short, N.M., 1999. Remote Sensing Tutorial. Applied Information Sciences Branch NASA/Goddard Space Flight Center.
- Short, N.M., Blair, R.W., Jr. (Editors), 1986. *Geomorphology from Space: A Global Overview of Regional Landforms*. National Aeronautics and Space Administration, Washington, DC, 717 pp.
- Sharon, D., 1962. On the nature of hammadas in Israel. *Zeitschrift Geomorphologie*. 6:129-147.
- Simon, M., Sanchez, S., Garcia, I., 2000. Soil-landscape evolution on a Mediterranean high mountain. *Catena*. 39(3): 211-231.
- Simonett, D.S. (Editor), 1983. *Manual of Remote Sensing*, 1. American Society of Photogrammetry, Falls Church.
- Smirnov, N.V., 1948. Table for estimating the goodness of fit of empirical distributions. *Annals of Mathematical Statistics*. 19: 279-281.
- Spatz, D.M., Taranik, J.V., Hsu, L.C., 1989. Differentiating volcanic rock assemblages using Landsat thematic mapper data; influence of petrochemistry and desert varnish. *Advances in Space Research*. 1: 93-98.
- Sultan, M., Arvidson, R.E., Sturchio, N.C., Guinness, E.A., 1987. Lithologic mapping in arid regions with Landsat thematic mapper; Meatiq dome, Egypt. *Geological Society of America Bulletin*. 99: 748-762.
- Thomas, D.S.G. (Editor), 1989. *Arid Zone Geomorphology*. Halsted Press, New York, 372 pp.
- Walsh, S.J., Butler, D.R., Malanson, G.P., 1998. An overview of scale, pattern, process relationships in geomorphology: a remote sensing and GIS perspective. *Geomorphology*. 21: 183-205.
- White, K., 1991. Geomorphological analysis of piedmont landforms in the Tunisian southern atals using ground data and satellite imagery. *Geographical Journal*. 157: 279-294.
- White, K., 1993. Image processing of Thematic Mapper data for discriminating piedmont surficial materials in the Tunisian Southern Atlas. *International Journal of Remote Sensing*. 14: 961-977.

- White, K., Walden, J., Drake, N., Eckardt, F., Settle, J., 1997. Mapping the iron content of dun sands, Namib Sand Sea, Namibia, using Landsat Thematic Mapper data. *Remote Sensing of the Environment*. 62: 30-39.
- Whitley, D.S., Baird, J., Bennet, J., Tuck, R.G., 1984. The use of relative repatination in the chronological ordering of petroglyph assemblages. *journal of New World Archaeology*. 6(3): 19-25.
- Wood, A., 1942. The development of hillside slopes. *Process Geology Association*. 53: 128-140.
- Wood, J.A., Lasserre, M., Fedosejevs, G., 1989. Analysis of mid-infrared spectral characteristics of rock outcrops and an evaluation of the Kahle model in predicting outcrop thermal inertias. *Remote Sensing of the Environment*. 11: 705-725.
- Yair, A., Lavee, H., 1982. Factors affecting the spatial variability of runoff generation over arid hillslopes, southern Israel. *Israel Journal of Earth Sciences*. 31: 133-143.
- Young, A., 1960. Soil movement by denudational processes on slopes. *Nature*. 188.
- Young, A., 1976. *Tropical Soils and Soil Survey*. Cambridge University Press, Cambridge.
- Zumsprekel, H., Prinz, T., 2000. Computer-enhanced multispectral remote sensing data: a useful tool for the geological mapping of Achaean terrains in (semi)arid environments. *Computers & Geosciences*. 26(1): 87-100.

APPENDIX A

DIGITAL IMAGES

Original digital images from field observations. Transects are labeled B1, B2, B3, and B4 for the north, west, south, and east-facing transects, respectively. Frame numbers follow the transect ID. For example, image number 32 on the west transect is labeled B2_32.





Fig. A.1. B1_01.

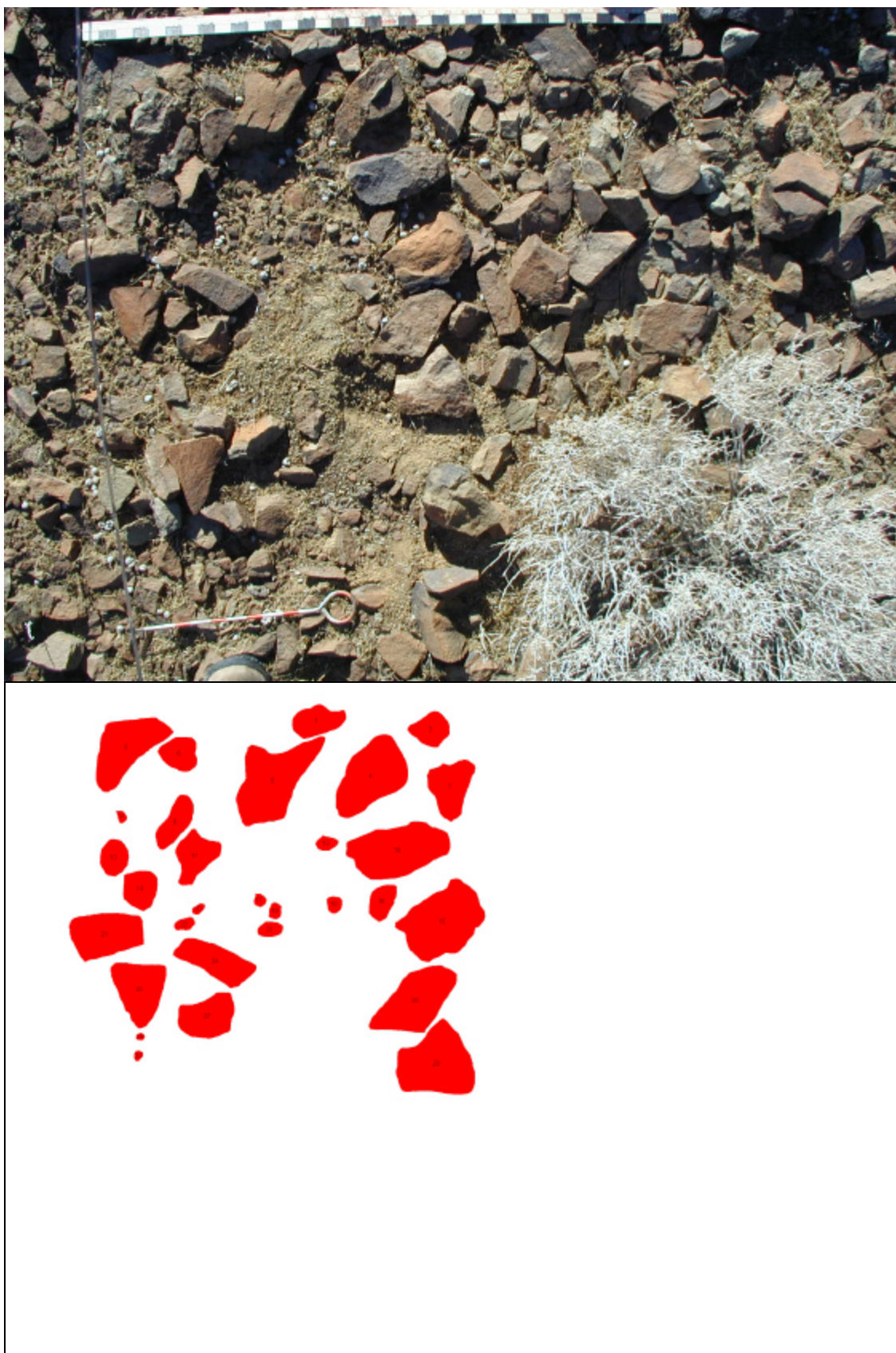


Fig. A.2. B1_02.



Fig. A.3. B1_03.



Fig. A.4. B1_04.



Fig. A.5. B1_05.



Fig. A.6. B1_06.

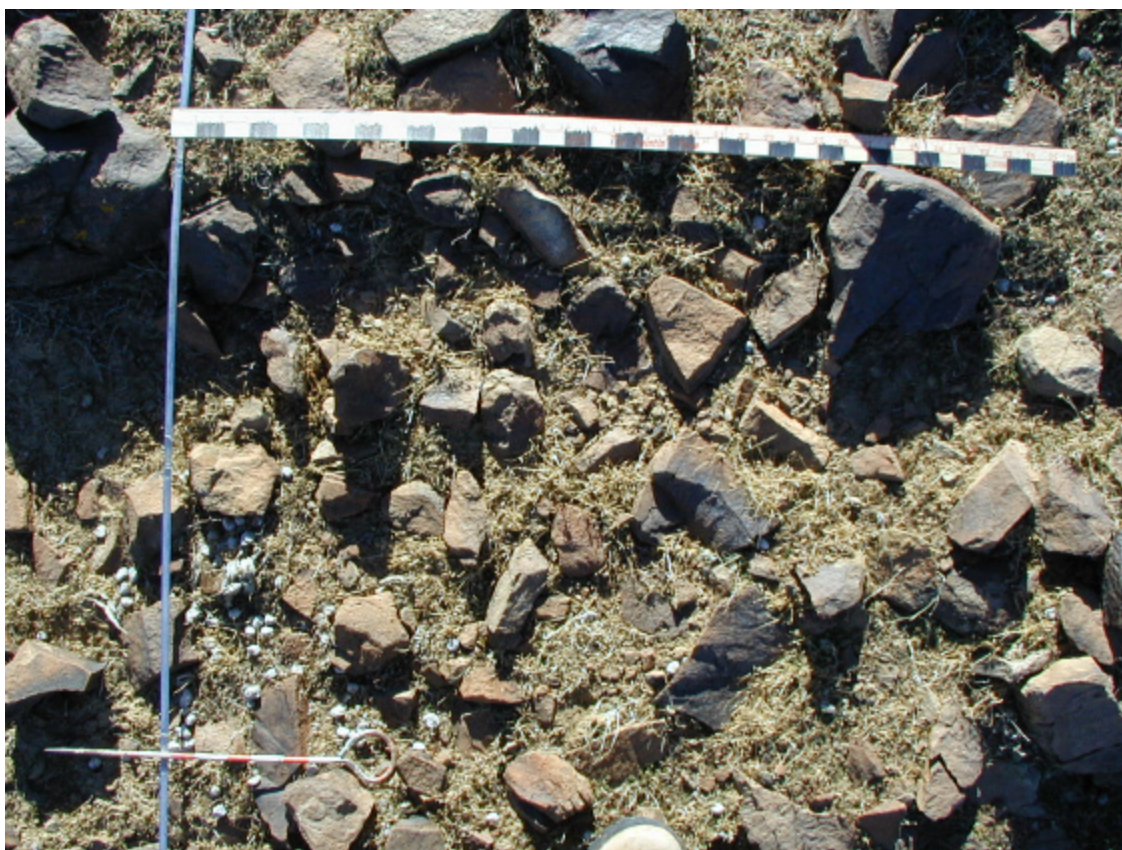


Fig. A.7. B1_07.



Fig. A.8. B1_08.



Fig. A.9. B1_09.



Fig. A.10. B1_10.



Fig. A.11. B1_11.

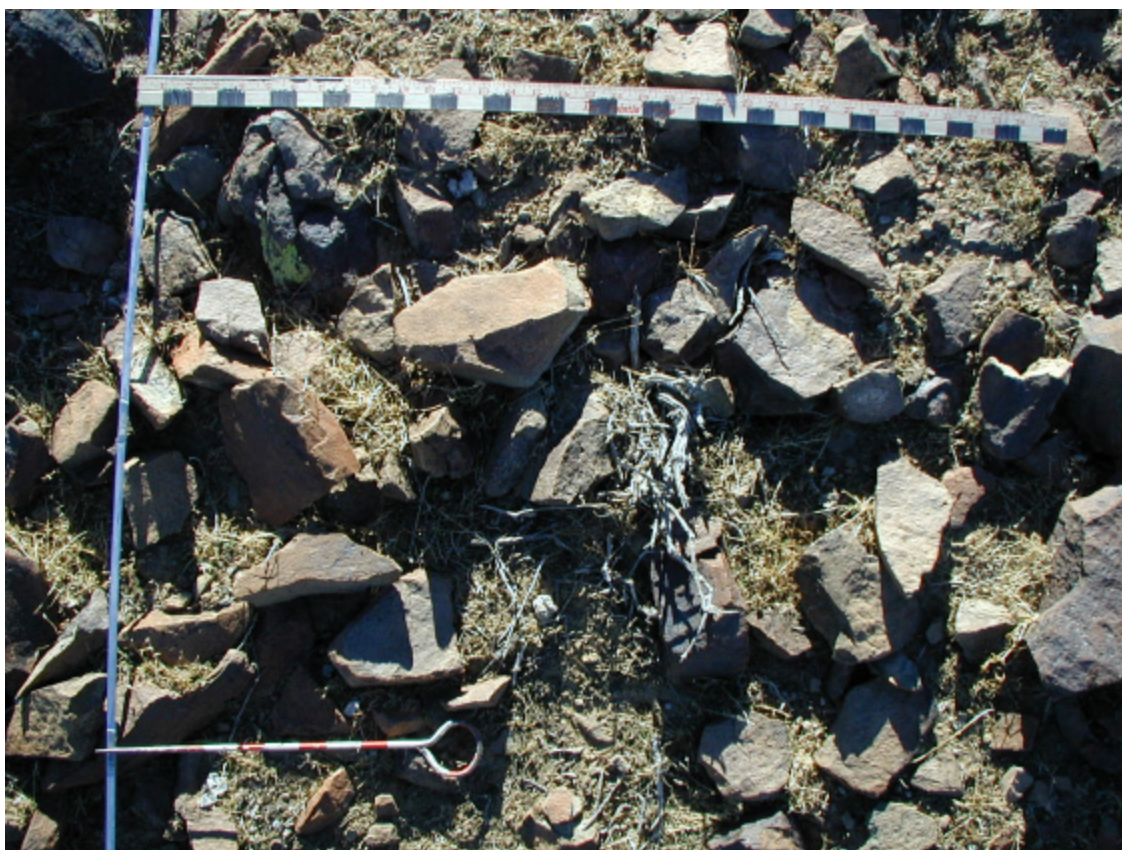


Fig. A.12. B1_12.



Fig. A.13. B1_13.

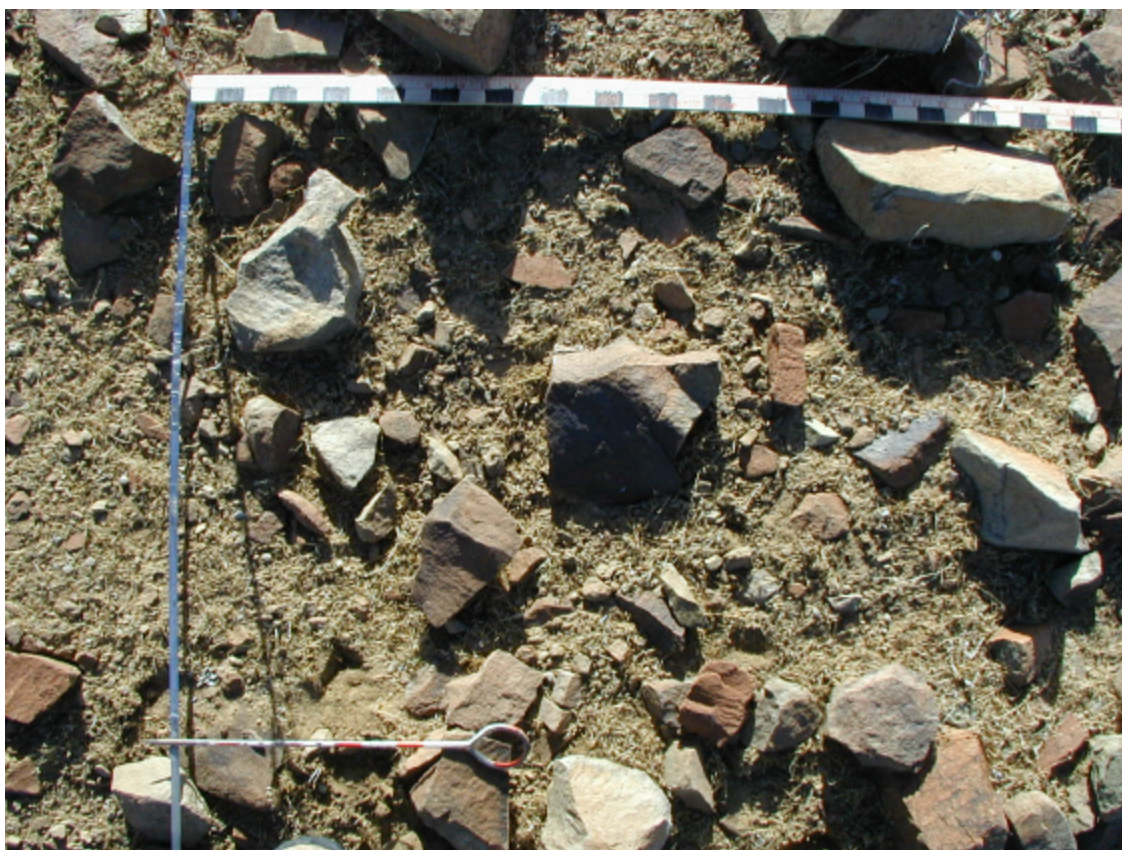


Fig. A.14. B1_14.

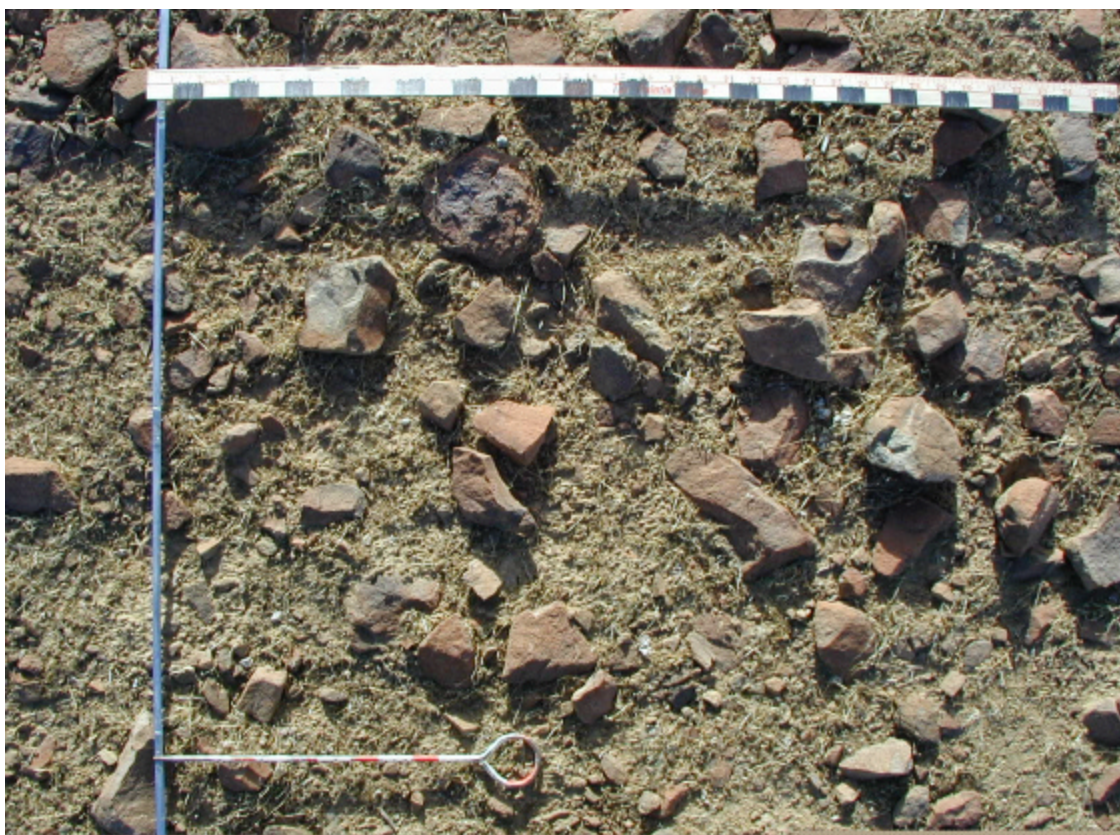


Fig. A.15. B1_15.

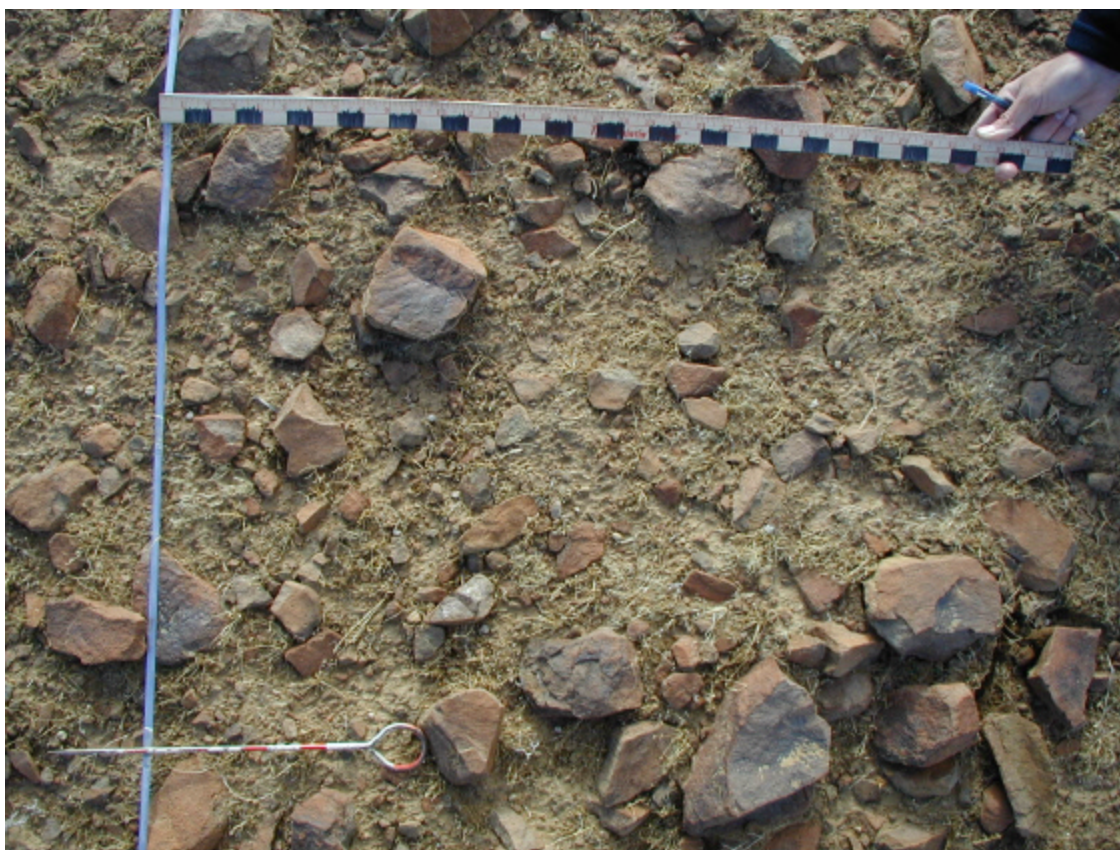


Fig. A.16. B1_17.

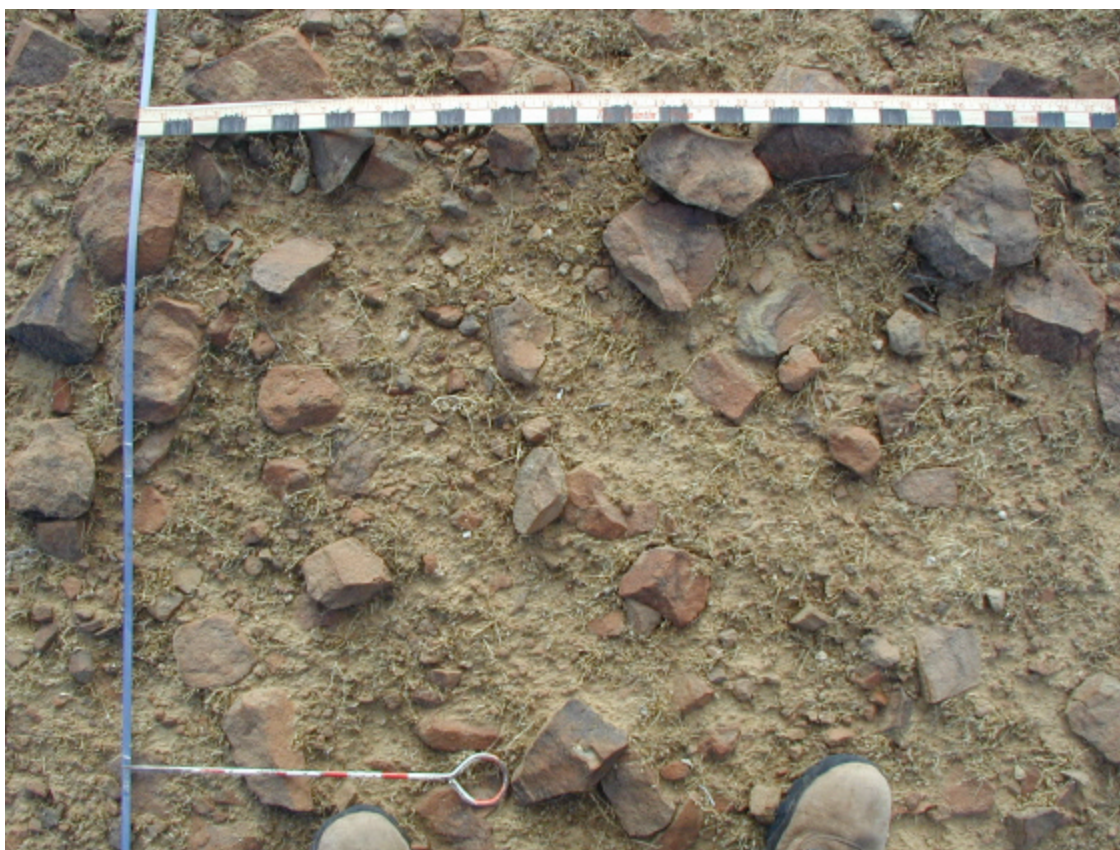


Fig. A.17. B1_18.



Fig. A.18. B1_19.

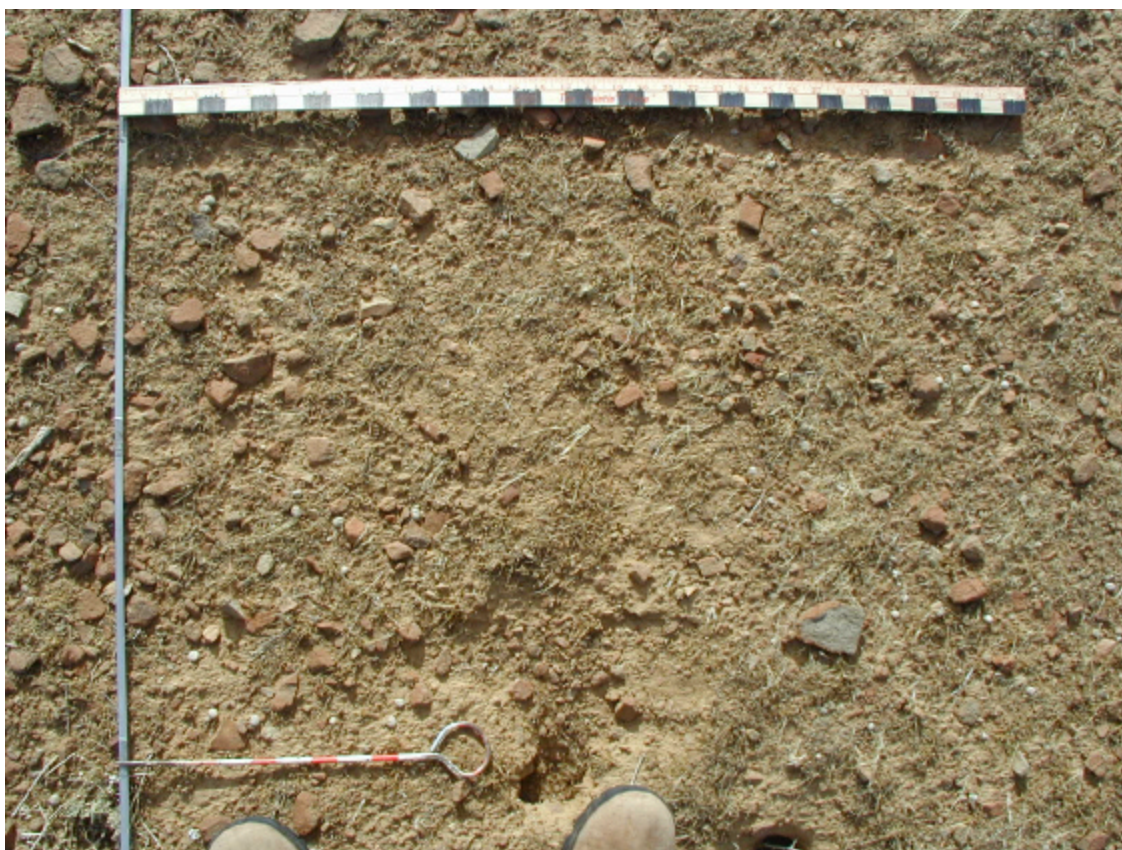


Fig. A.19. B1_20.

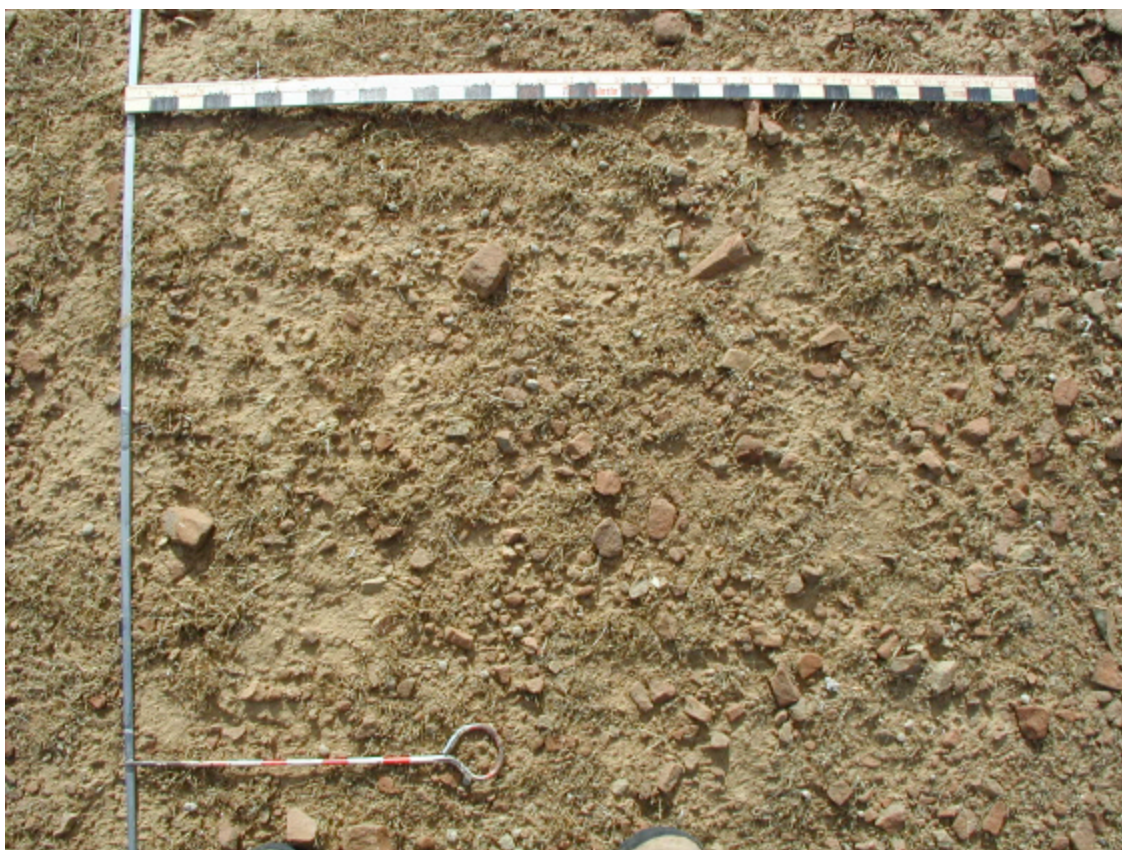


Fig. A.20. B1_21.

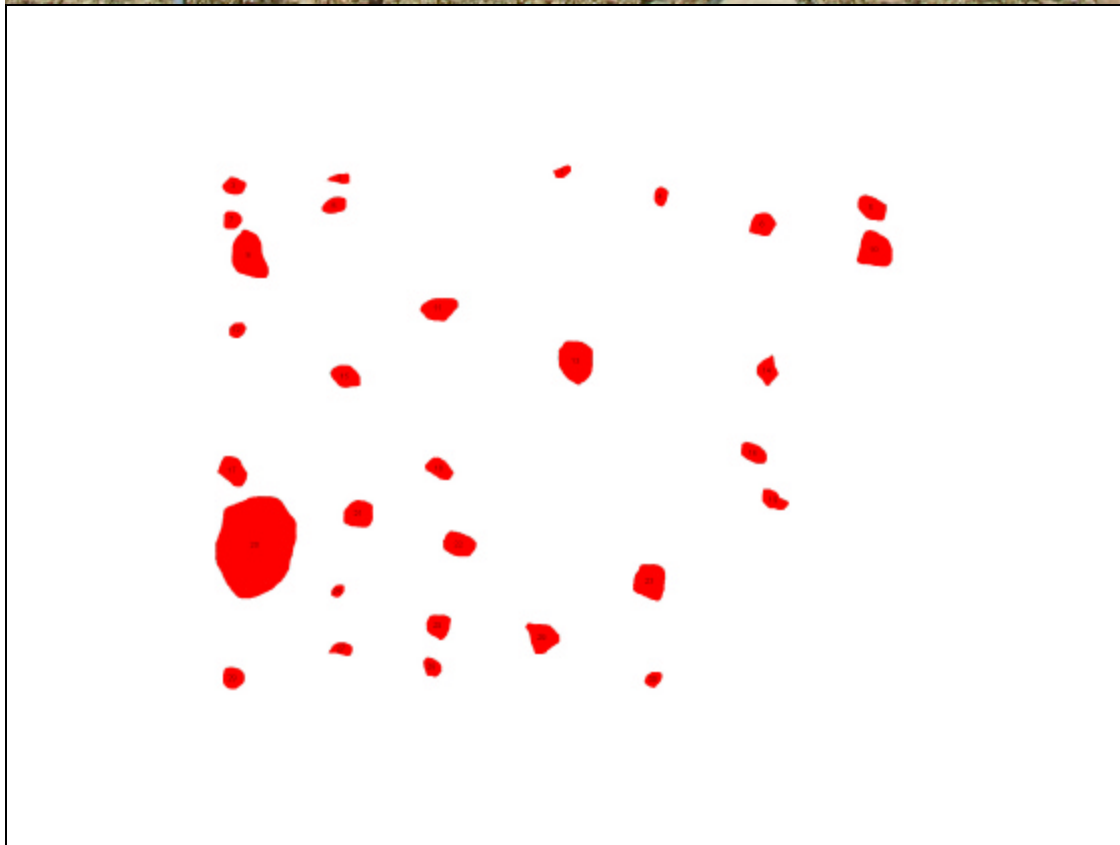
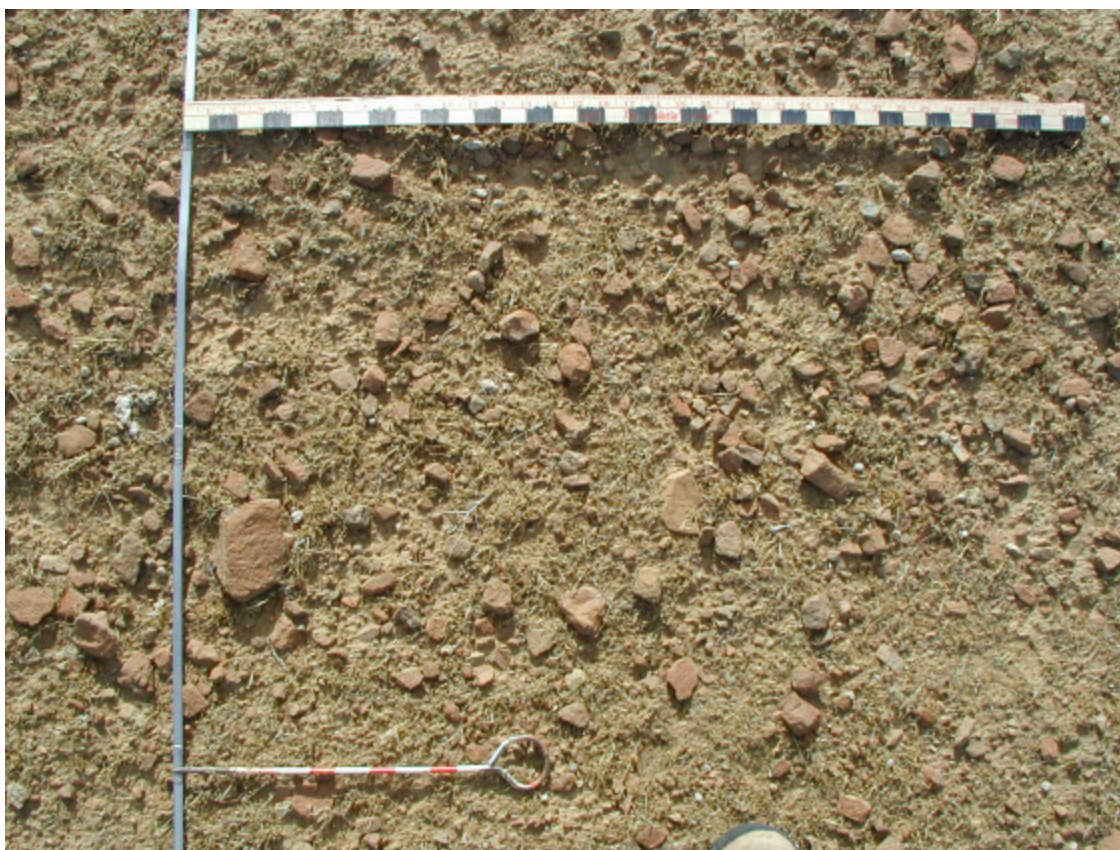


Fig. A.21. B1_22.

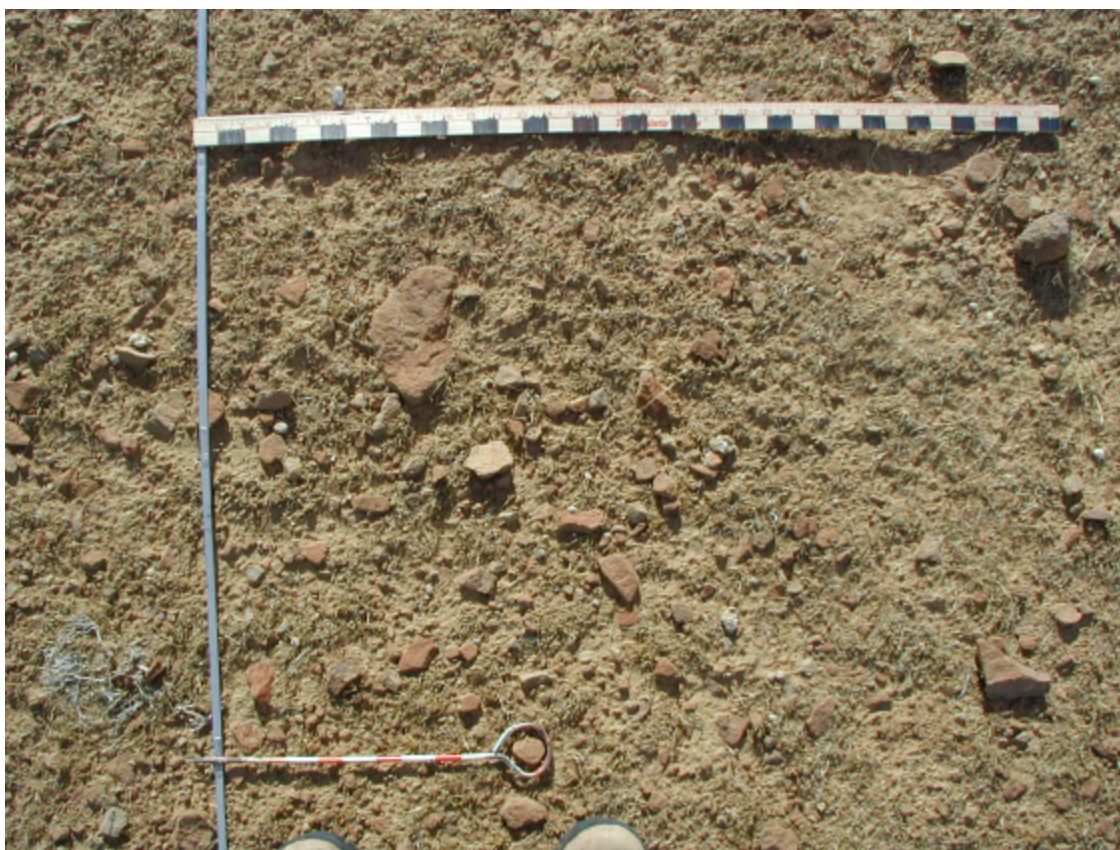


Fig. A.22. B1_24.



Fig. A.23. B1_25.



Fig. A.24. B1_26.

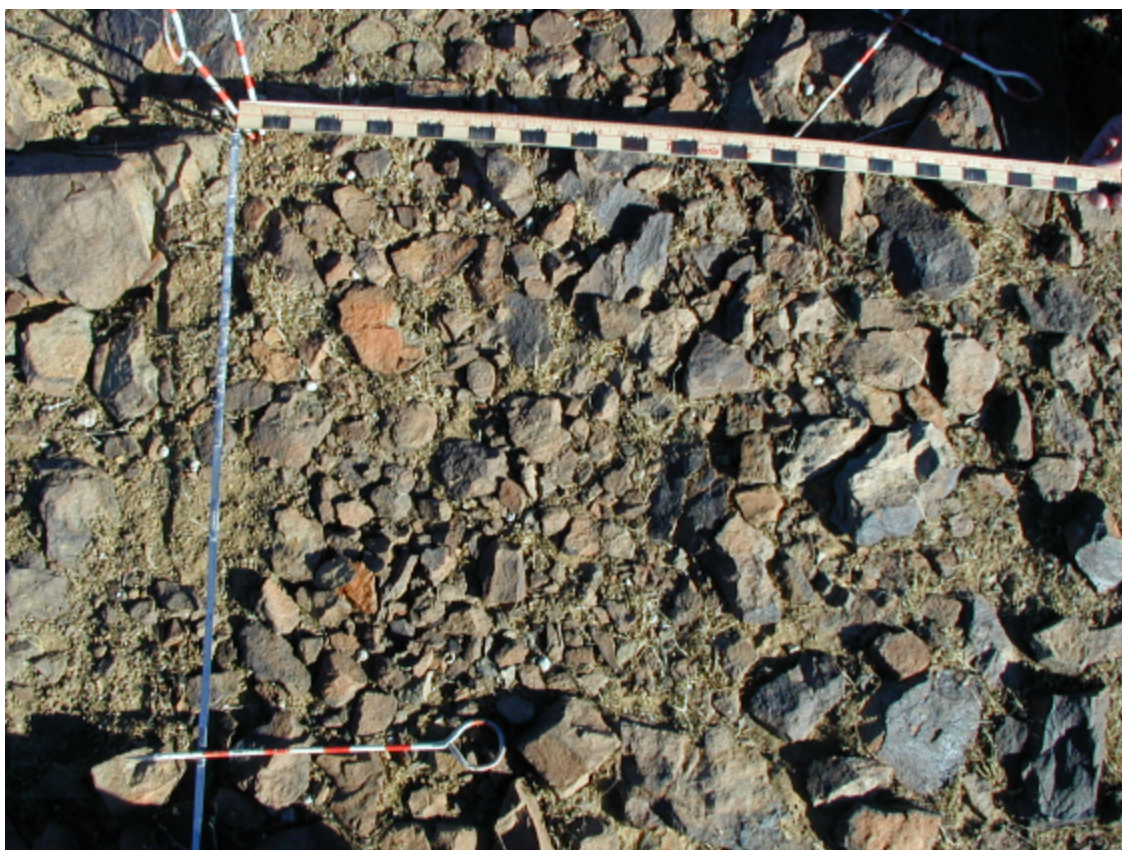


Fig. A.25. B2_32.



Fig. A.26. B2_33.



Fig. A.27. B2_34.

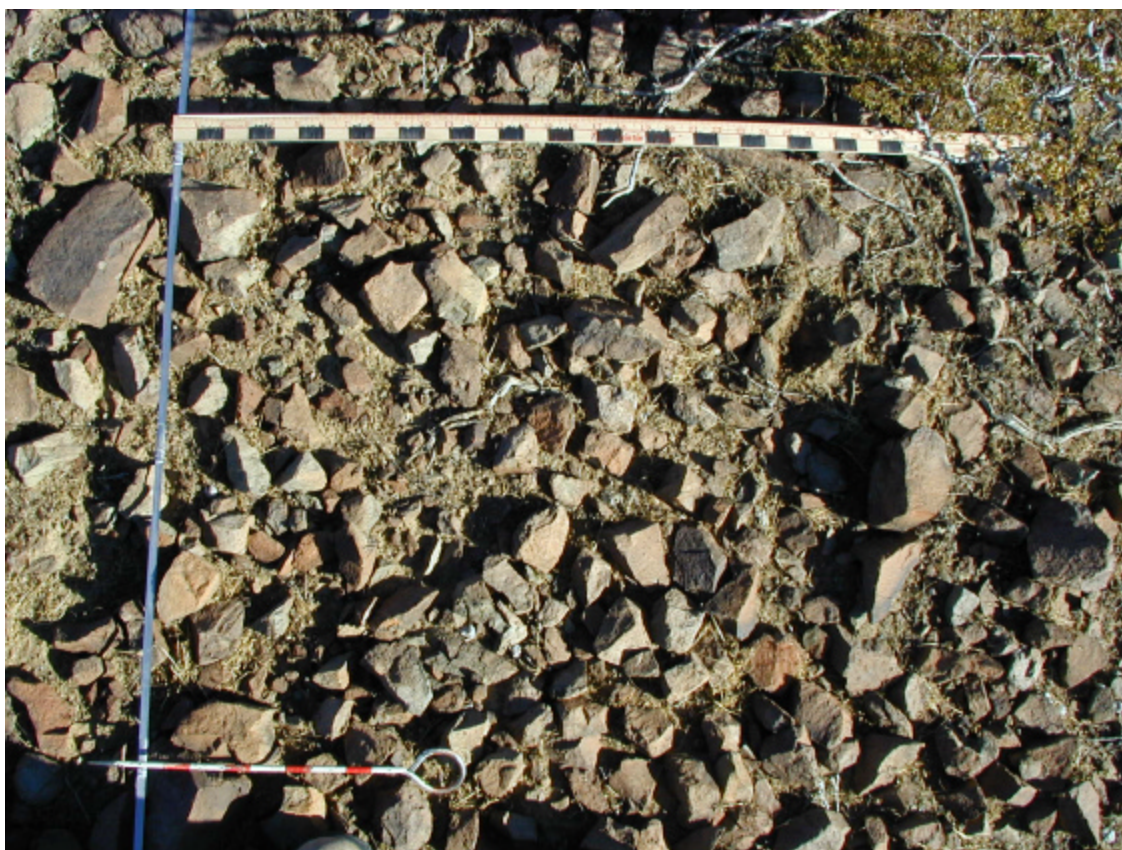


Fig. A.28. B2_35.

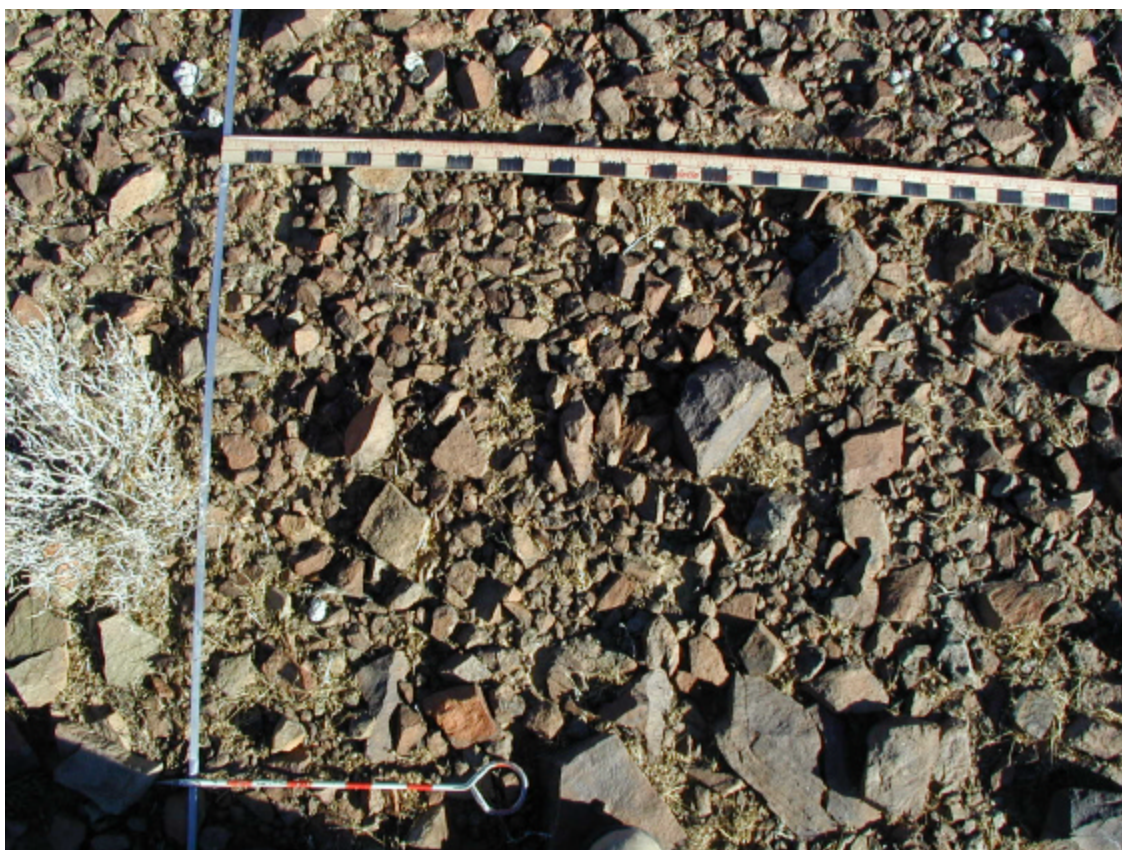


Fig. A.29. B1_36.

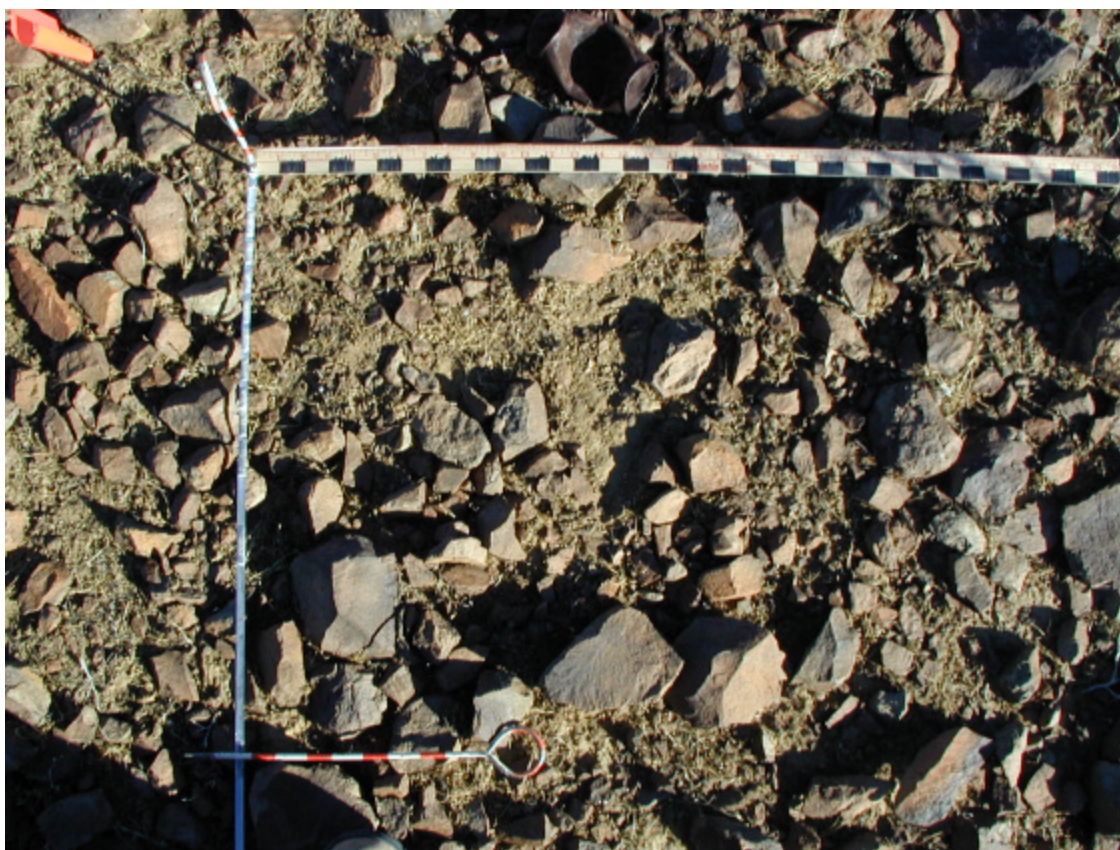


Fig. A.30. B2_37.

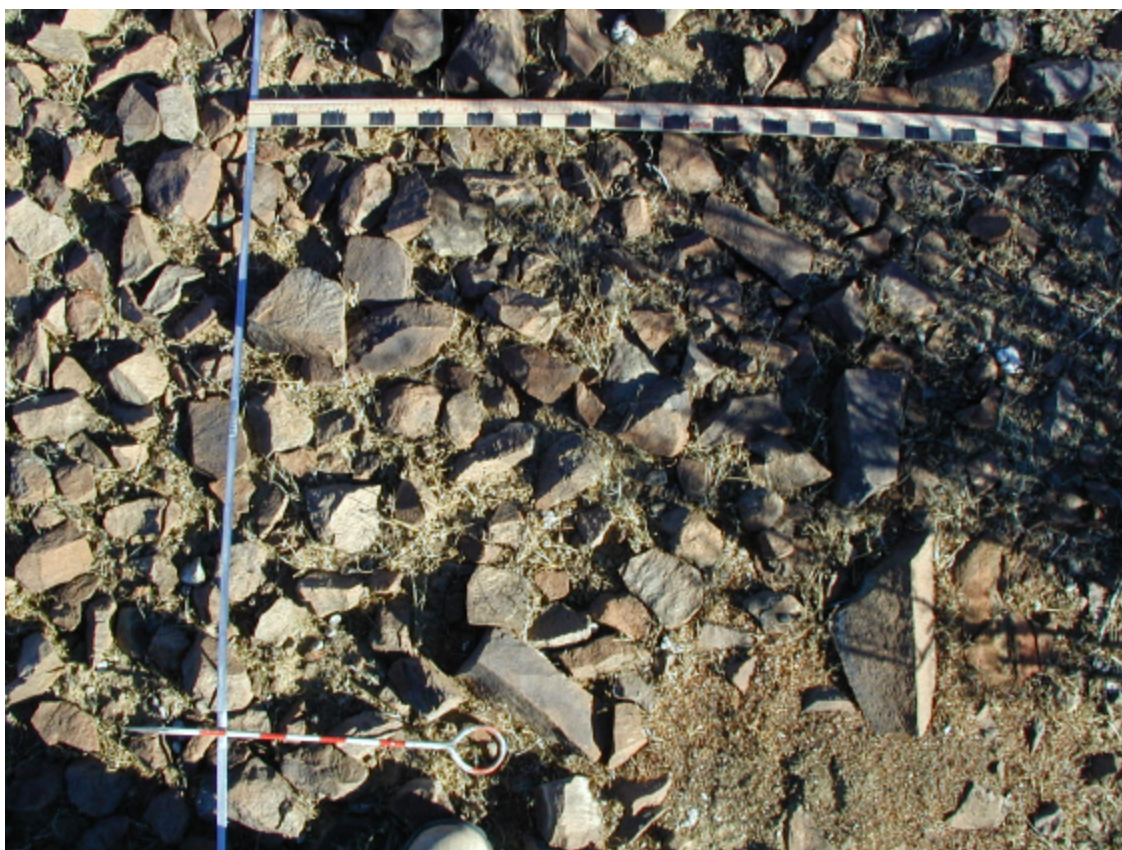


Fig. A.31. B2_38.

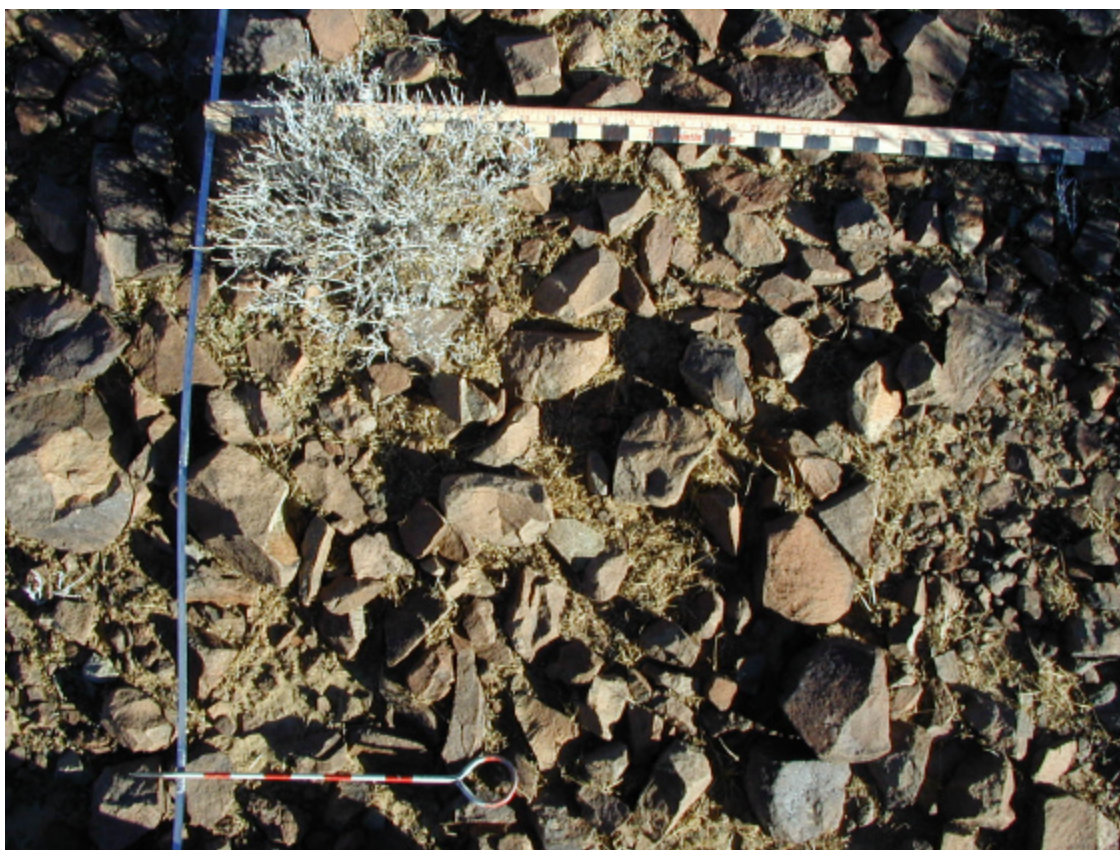


Fig. A.32. B2_39.

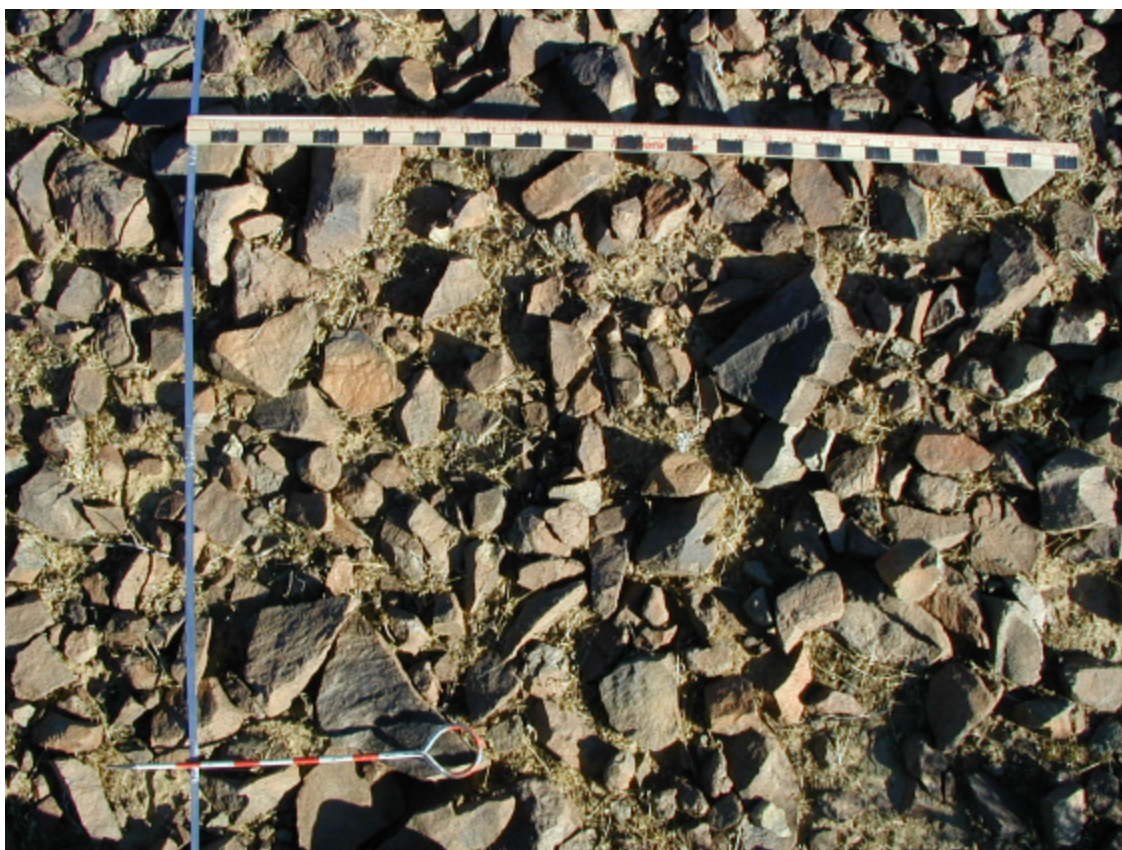


Fig. A.33. B2_40.



Fig. A.34. B2_41.

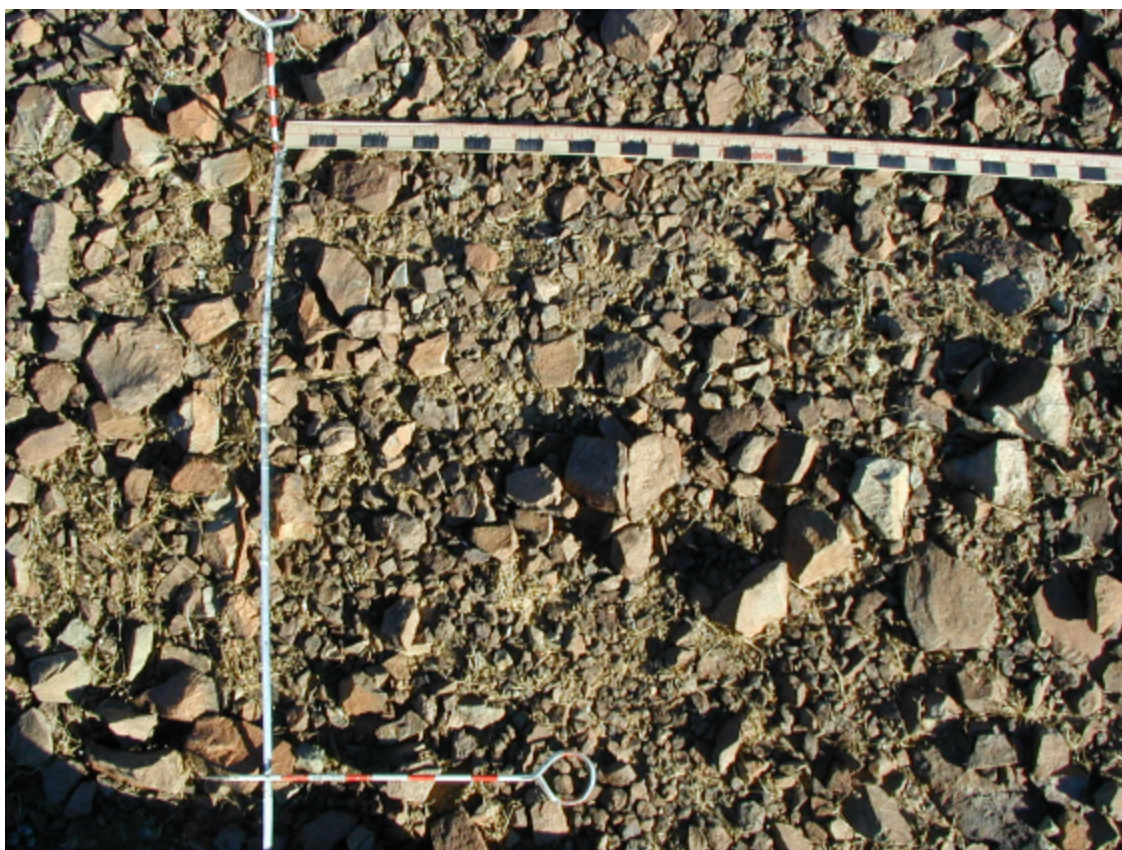


Fig. A.35. B2_42.

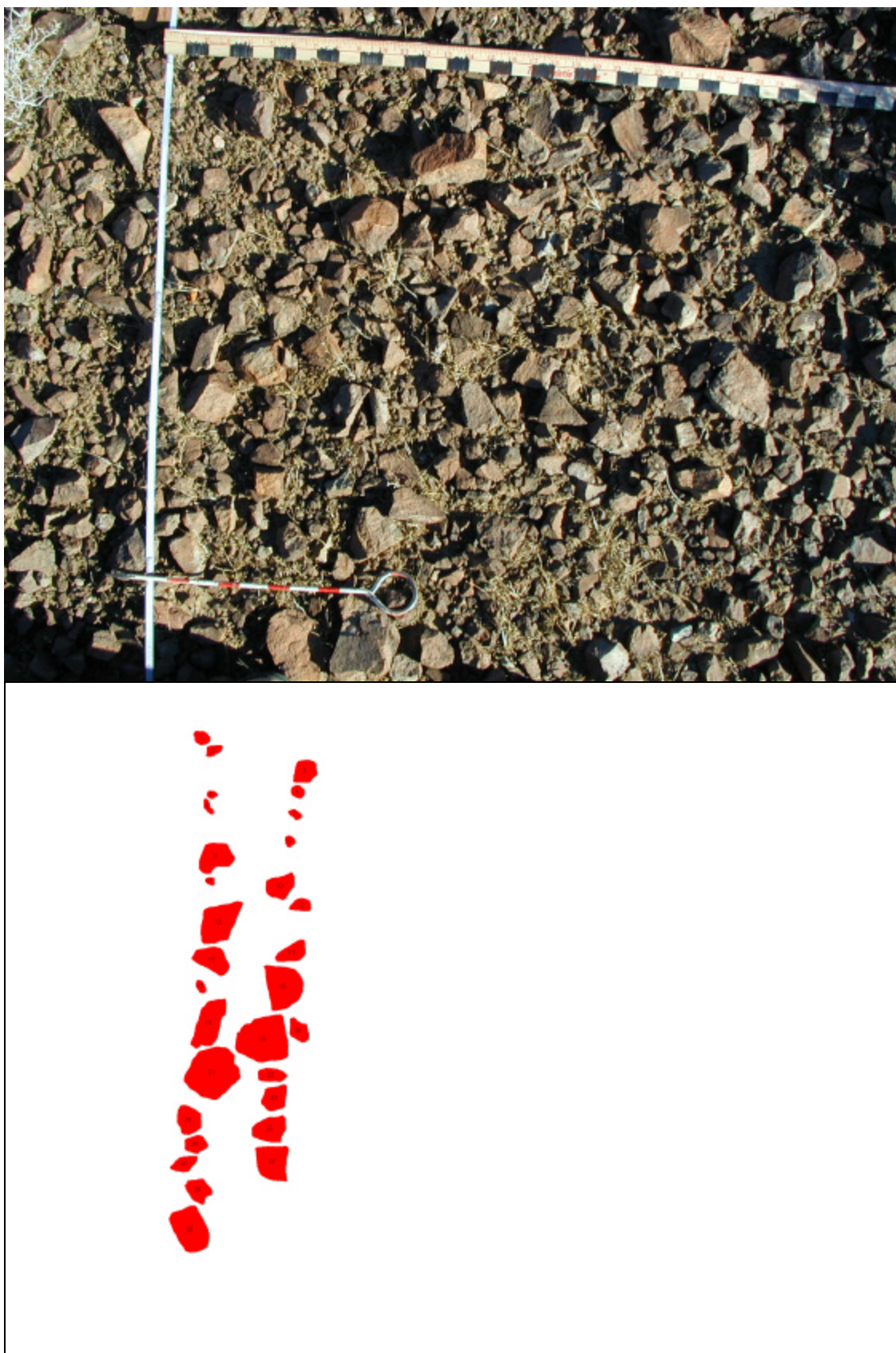


Fig. A.36. B2_43.

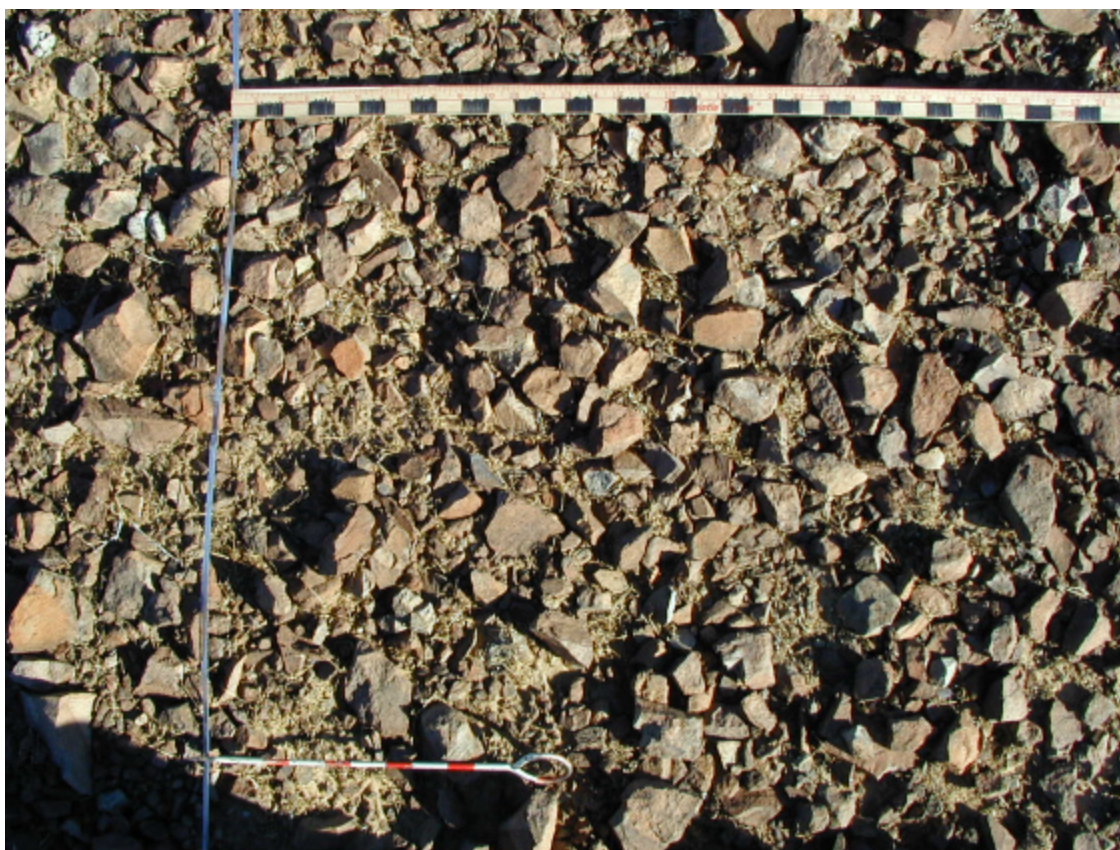


Fig. A.37. B2_44.



Fig. A.38. B2_45.

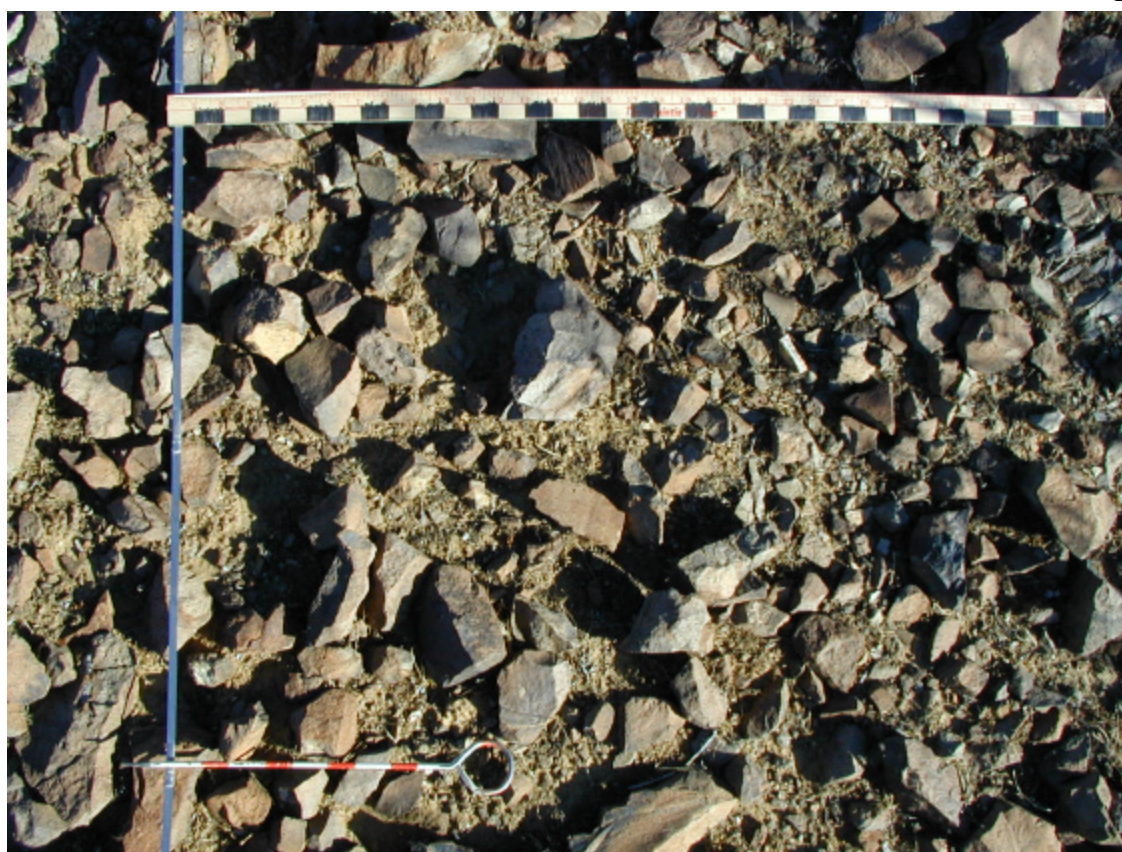


Fig. A.39. B2_46.



Fig. A.40. B2_47.

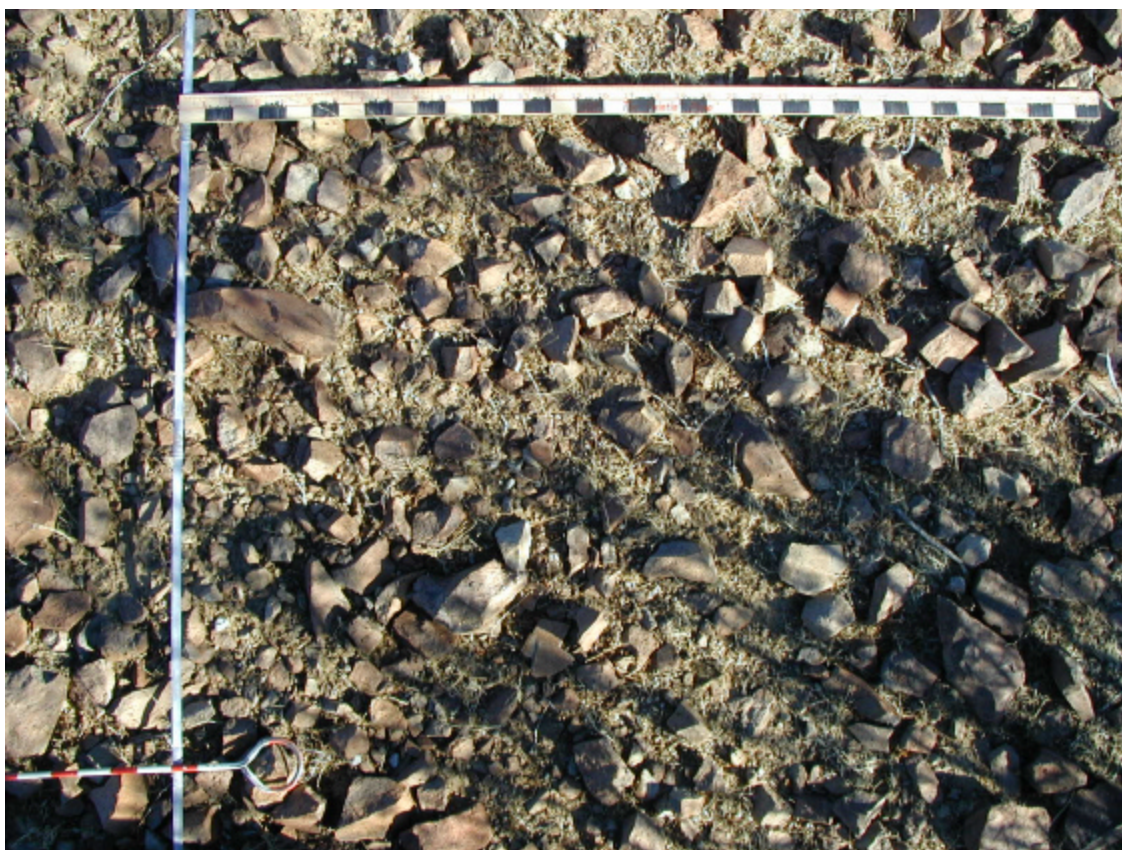


Fig. A.41. B2_48.

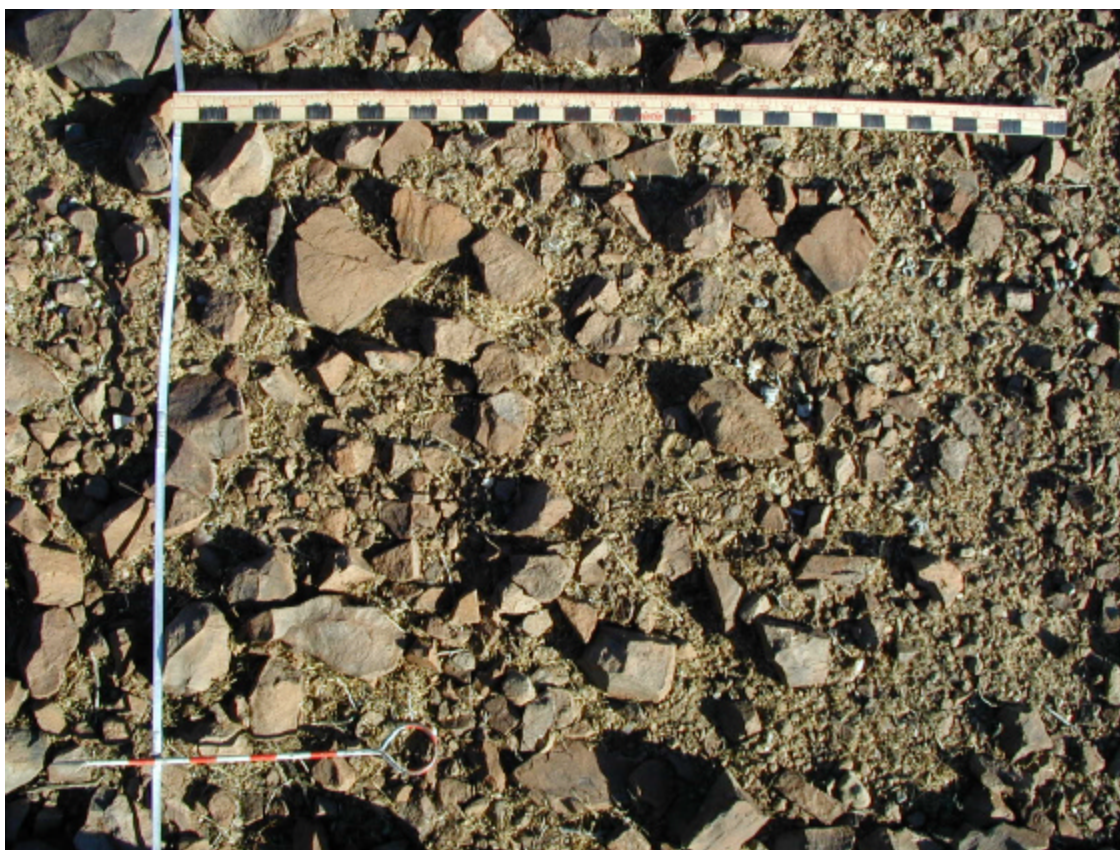


Fig. A.42. B2_49.



Fig. A.43. B2_55.

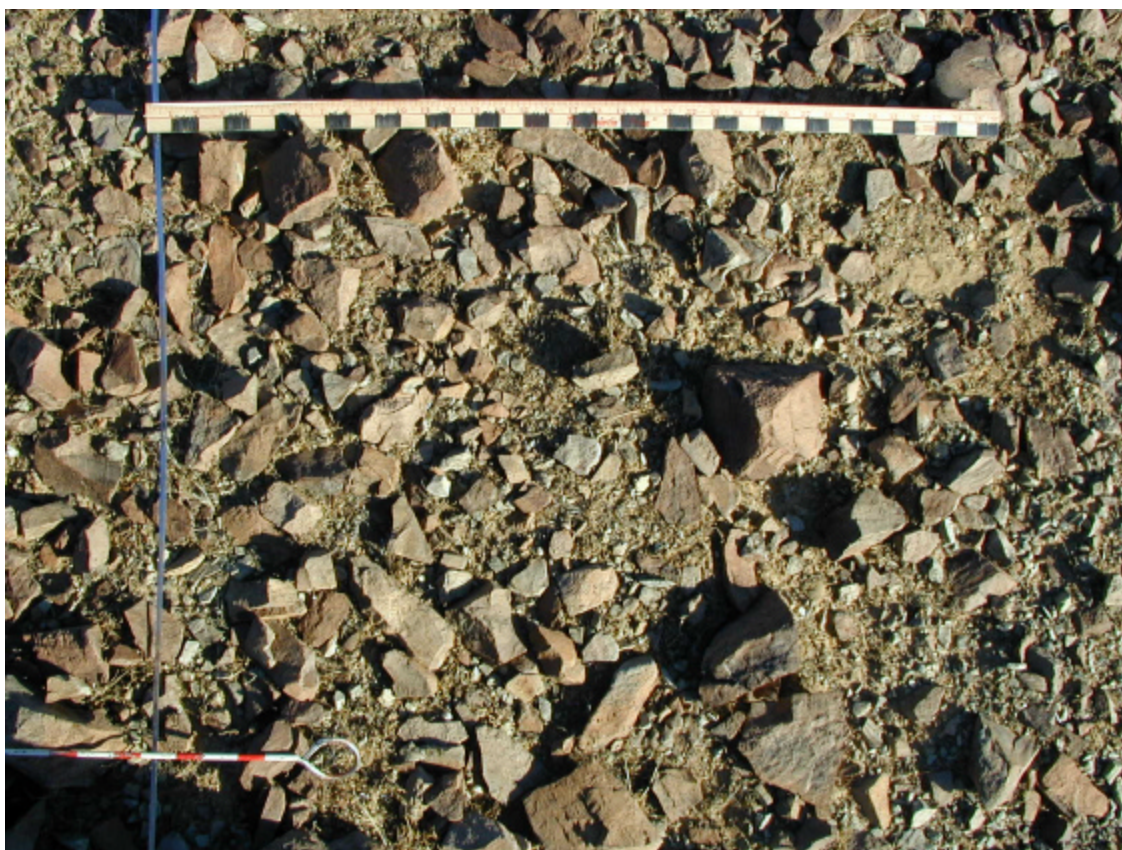


Fig. A.44. B2_56.

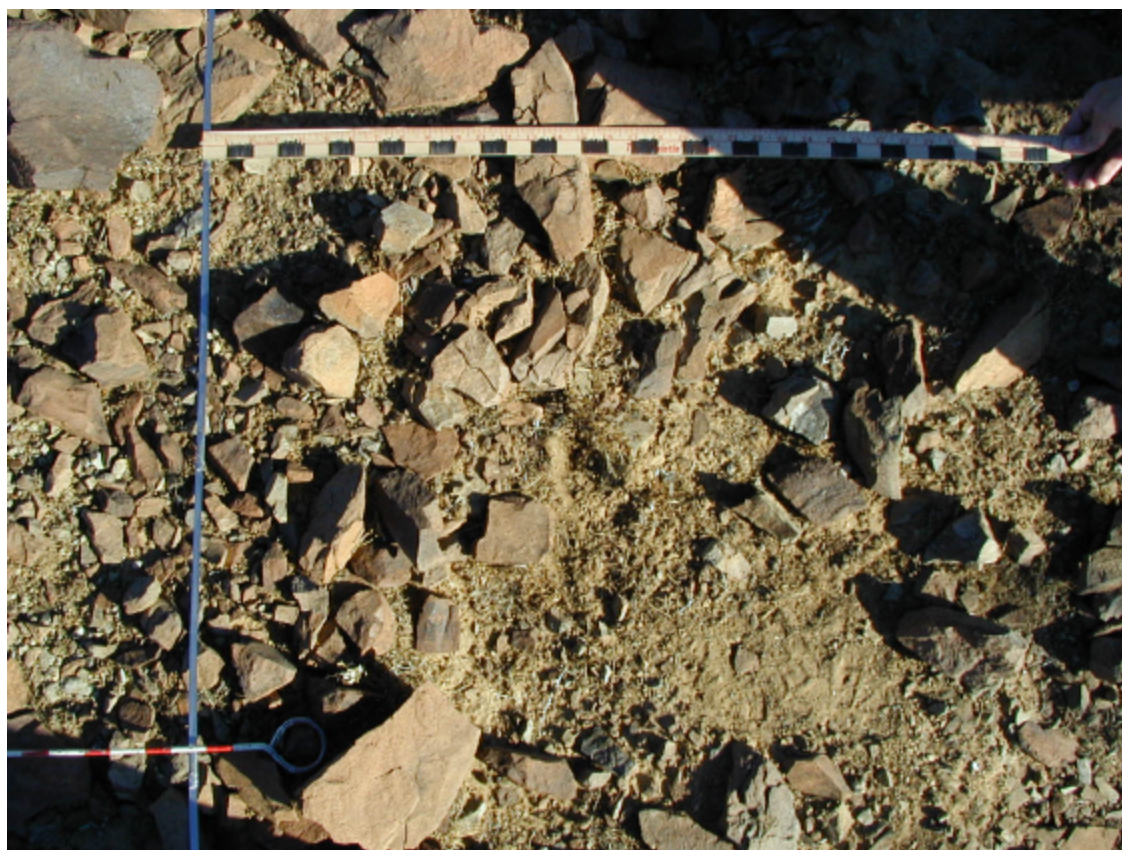


Fig. A.45. B2_57.

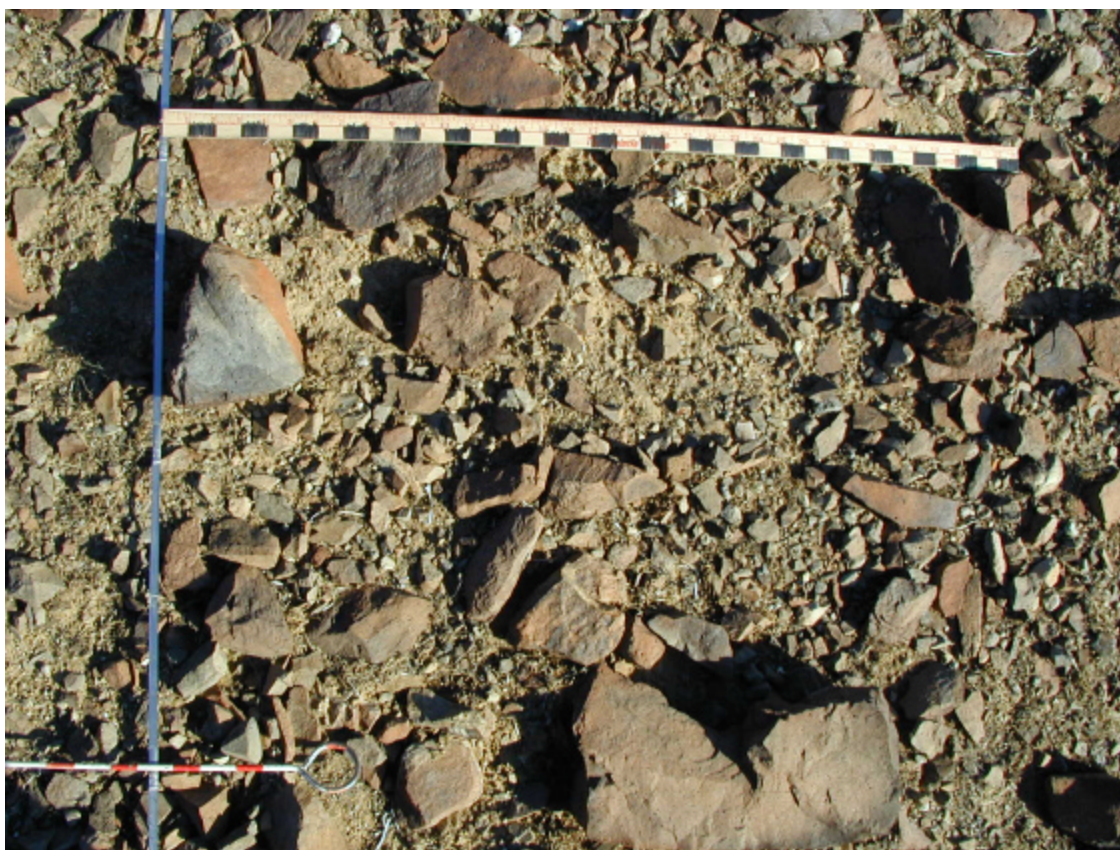


Fig. A.46. B2_58.



Fig. A.47. B2_59.

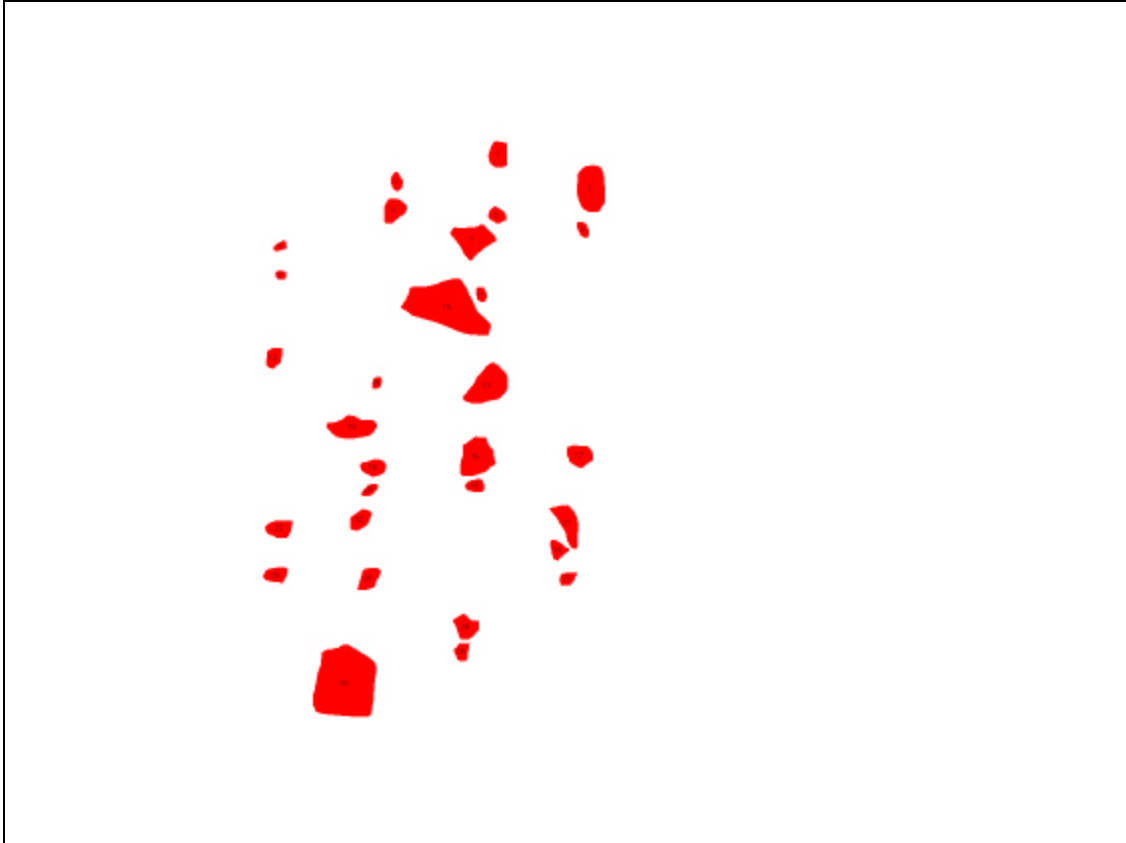


Fig. A.48. B2_60.

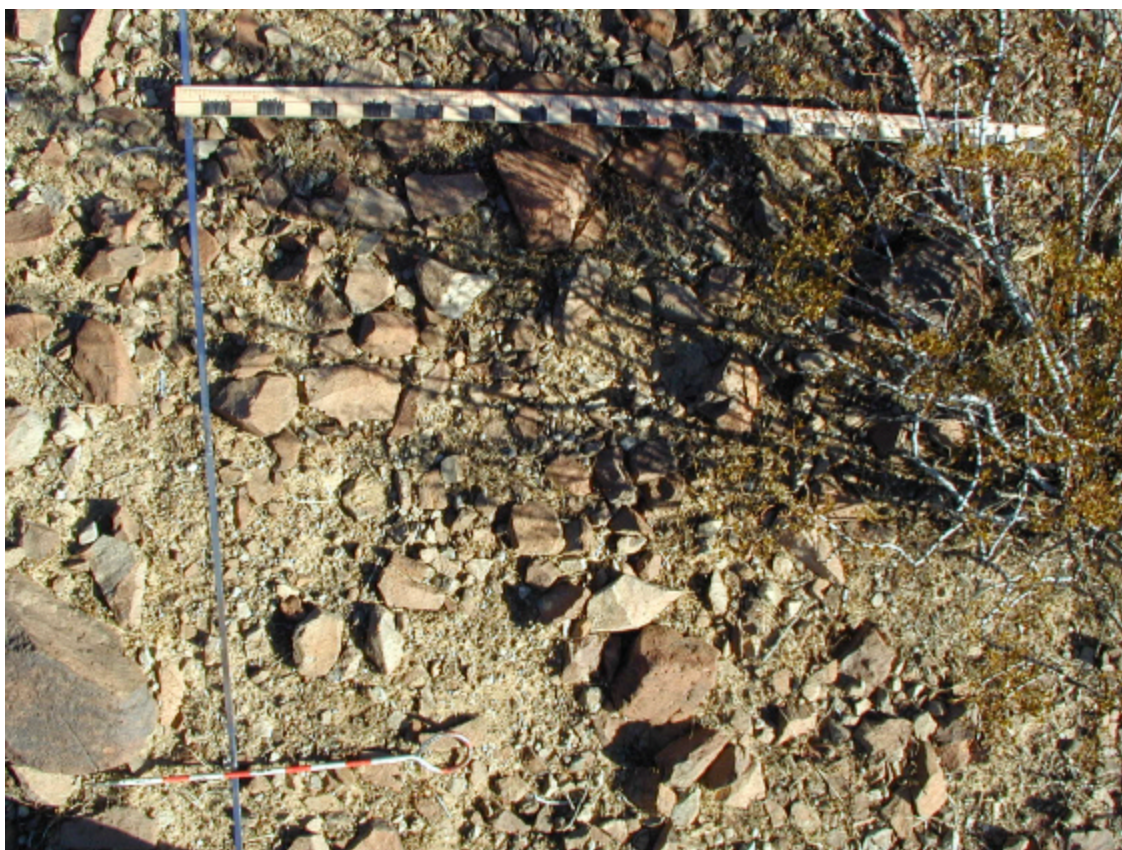


Fig. A.49. B2_61.

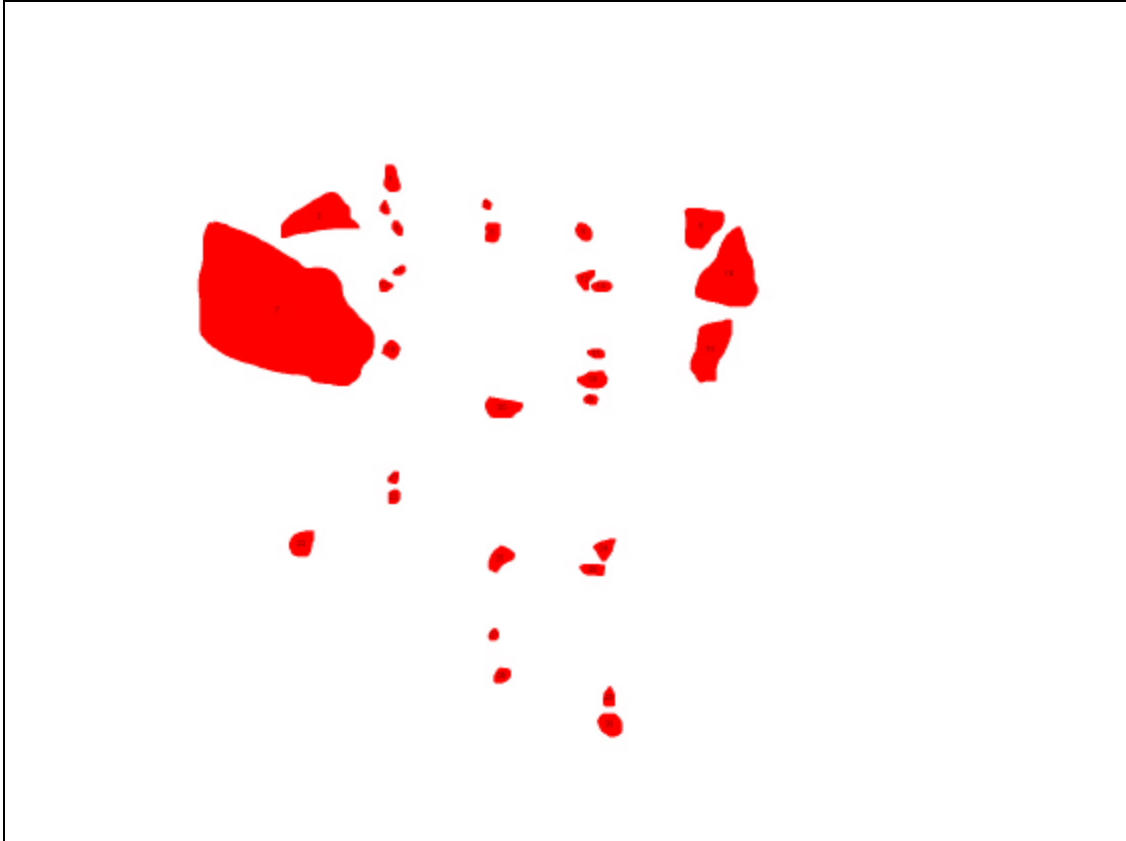


Fig. A.50. B2_62.



Fig. A.51. B2_63.

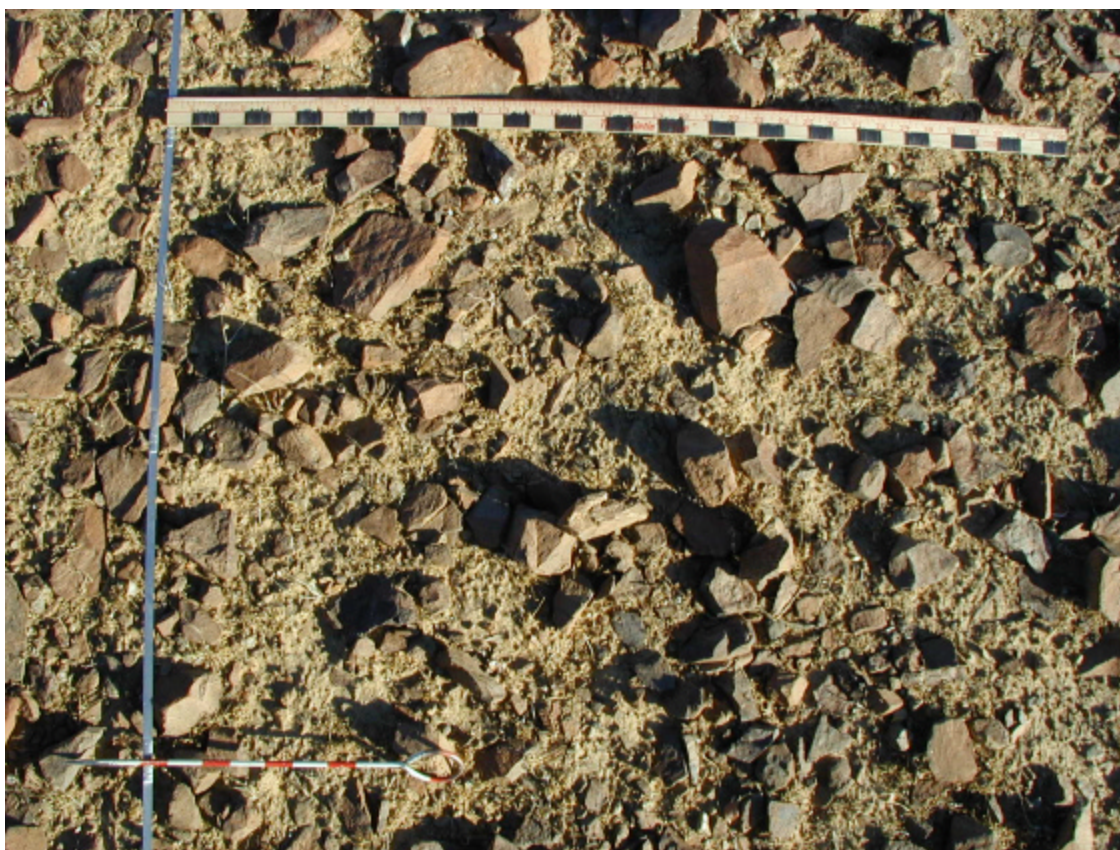


Fig. A.52. B2_64.

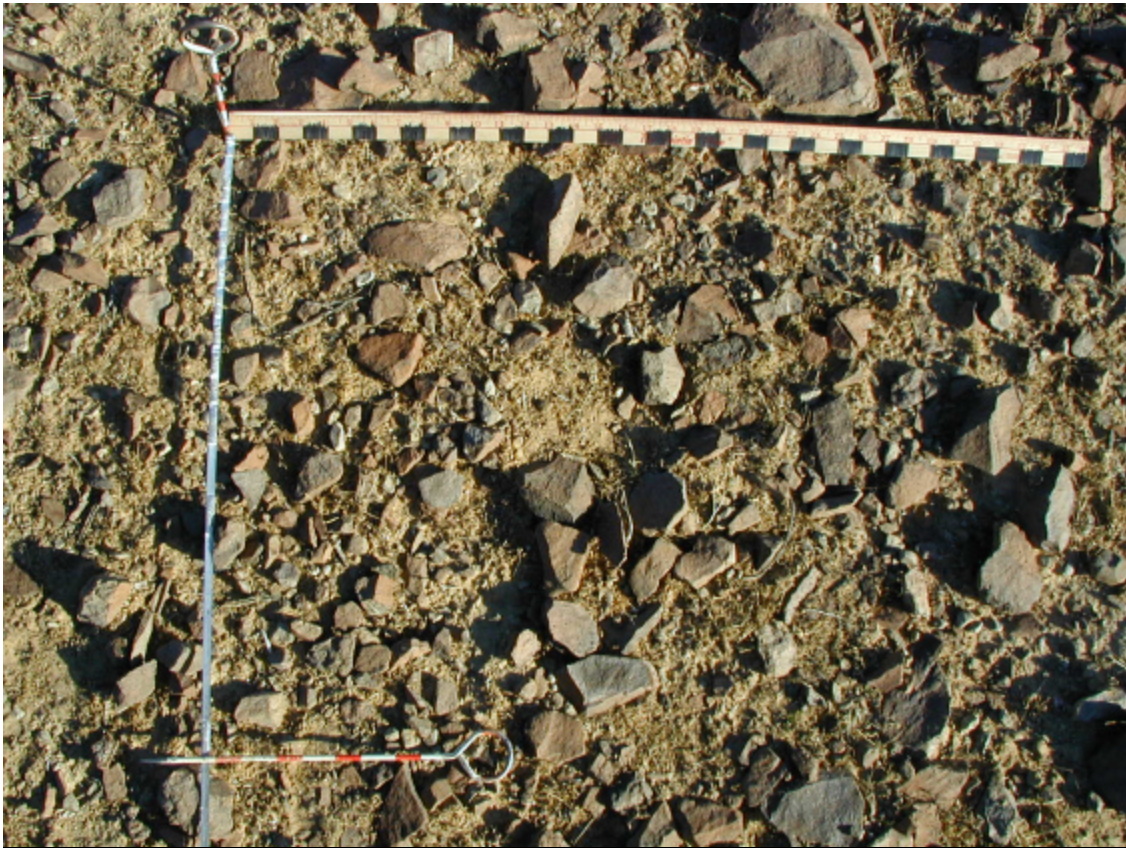


Fig. A.53. B2_65.



Fig. A.54. B2_68.

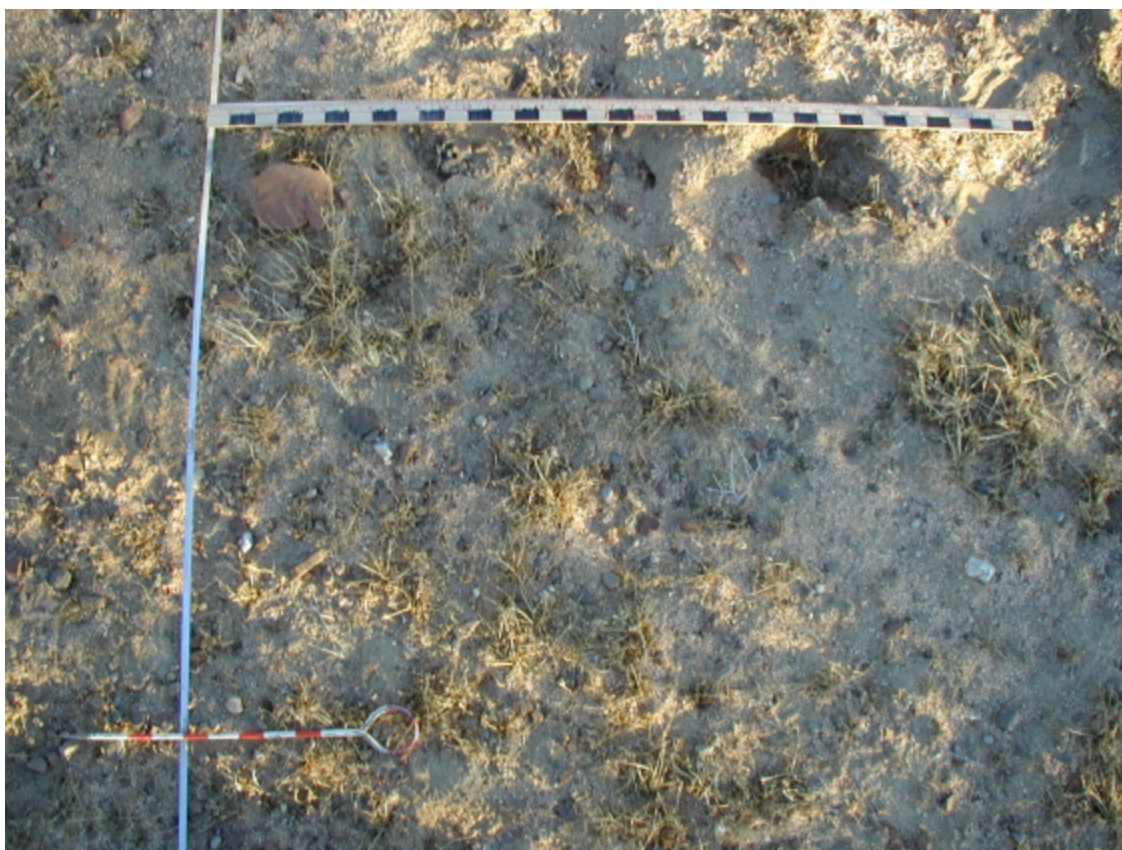


Fig. A.55. B2_73.



Fig. A.56. B3_80.

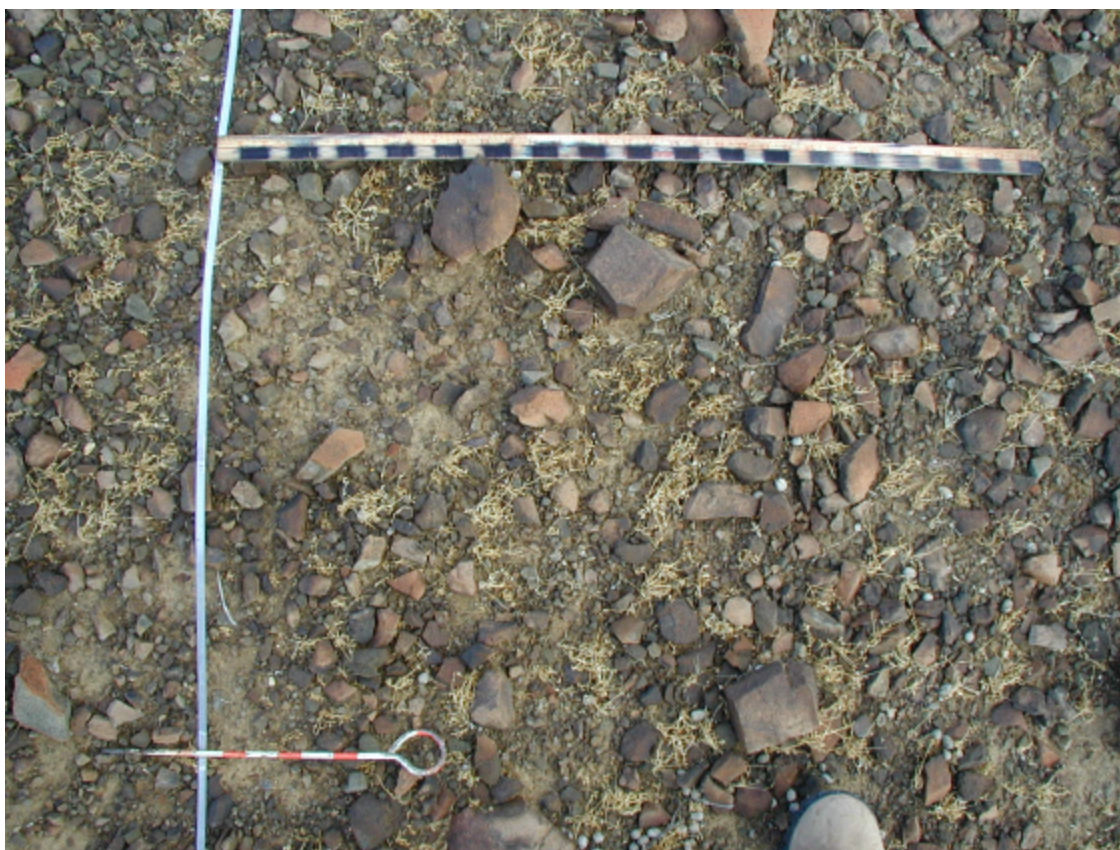


Fig. A.57. B3_81.



Fig. A.58. B3_82.

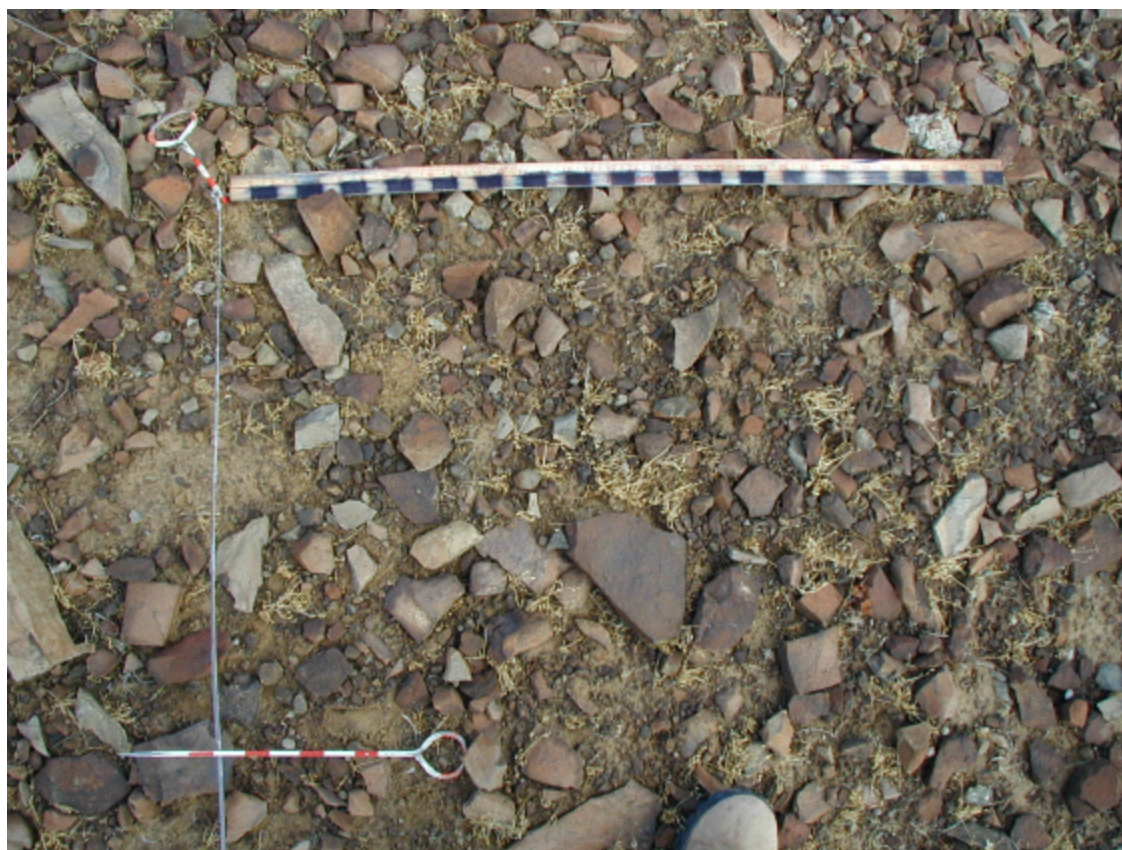


Fig. A.59. B3_83.

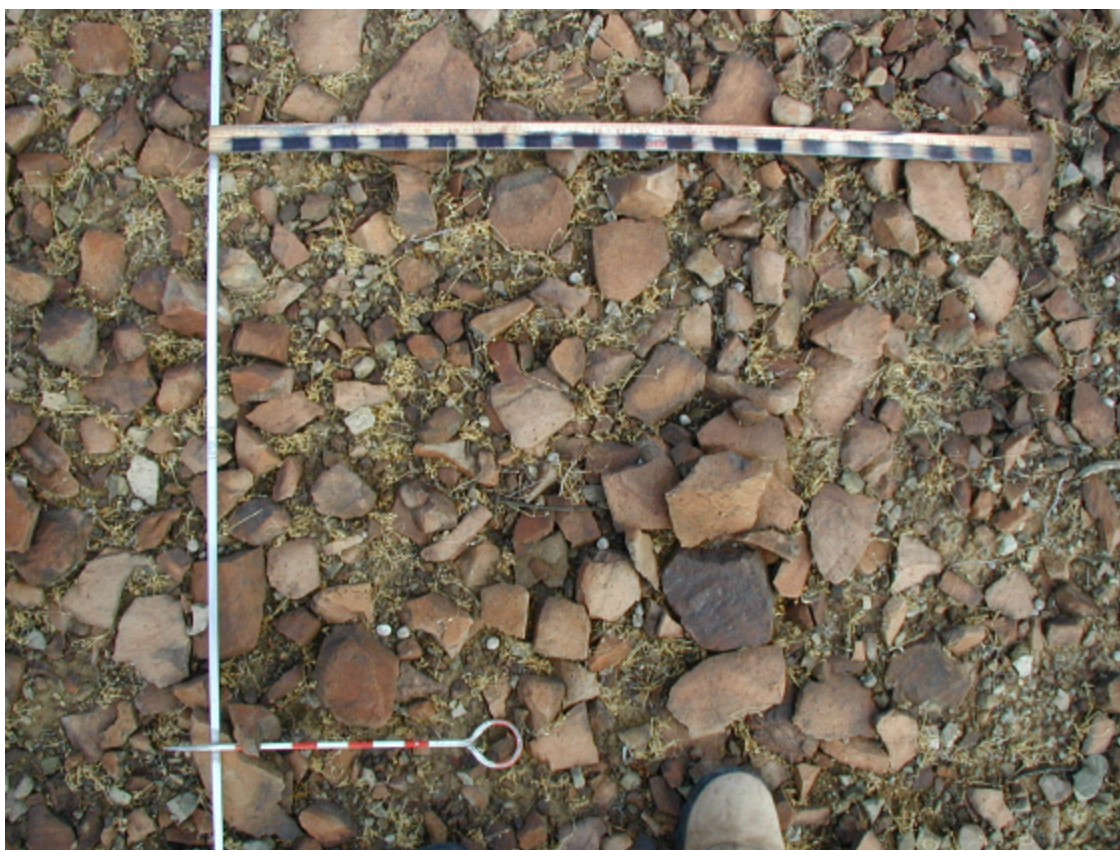


Fig. A.60. B3_84.



Fig. A.61. B3_85.



Fig. A.62. B3_86.

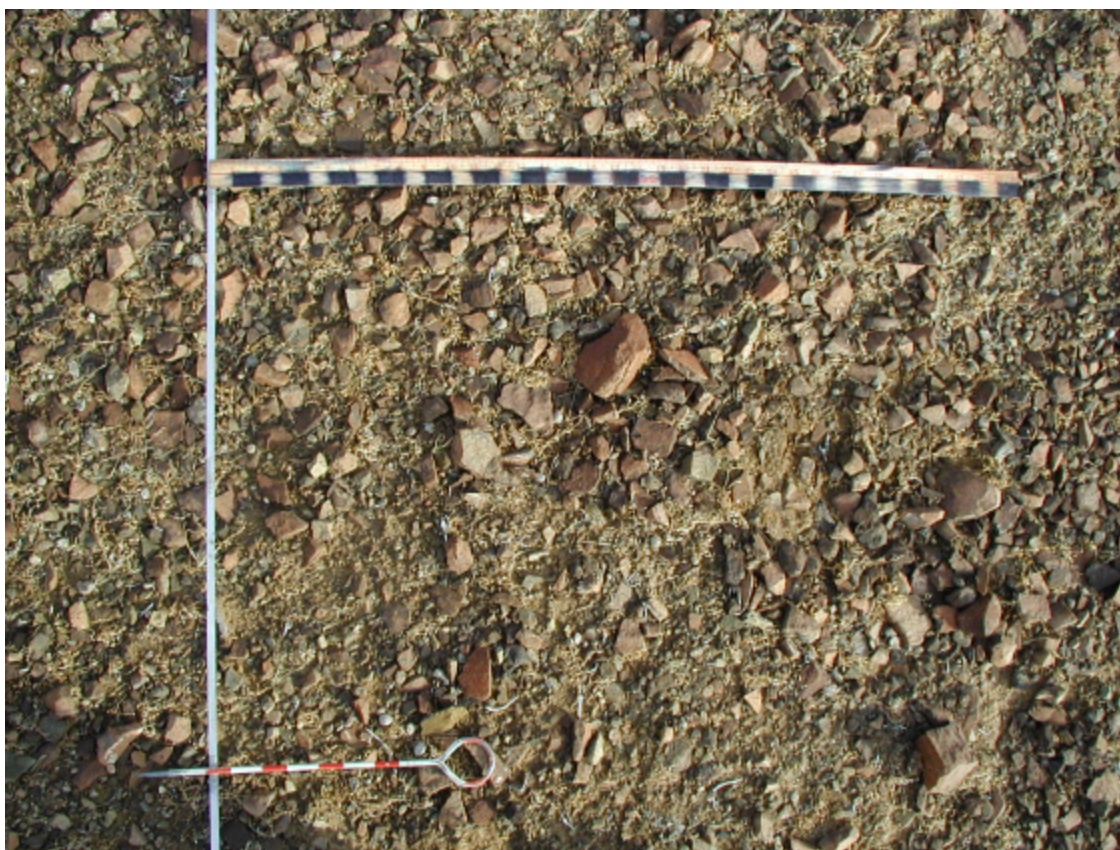


Fig. A.63. B3_87.

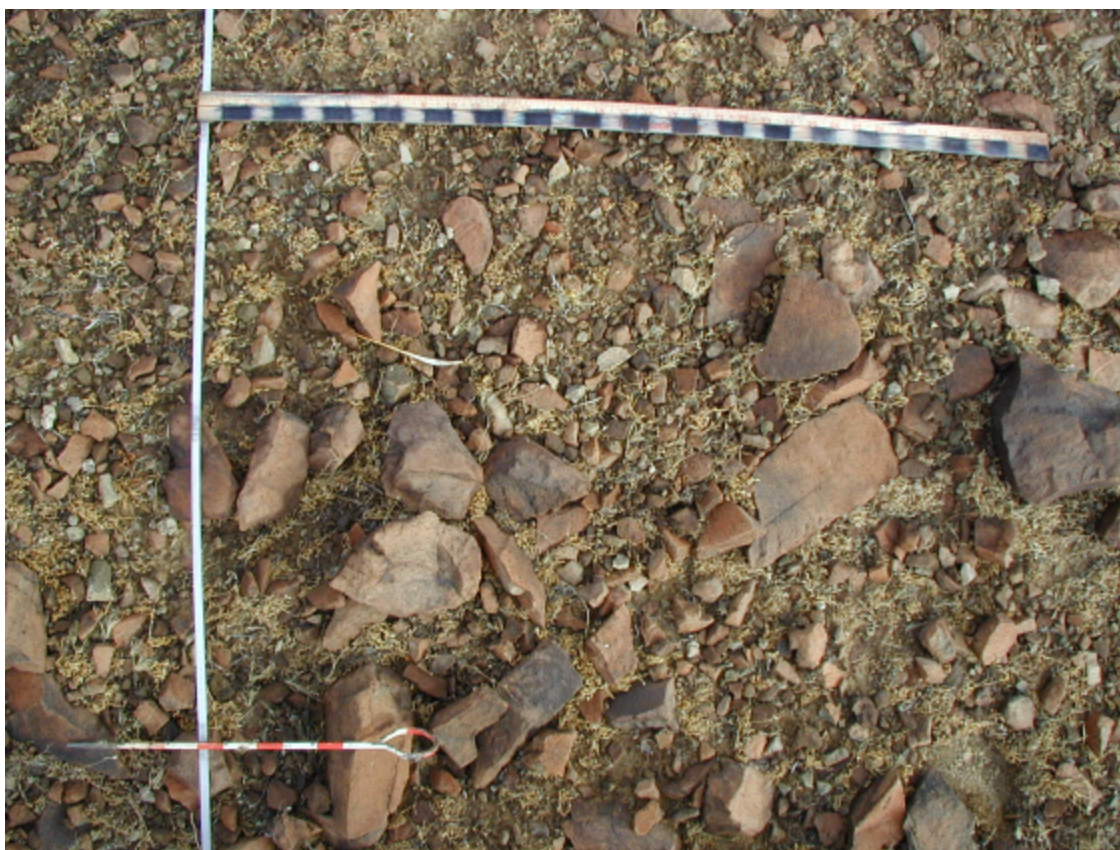


Fig. A.64. B3_89.



Fig. A.65. B3_90.

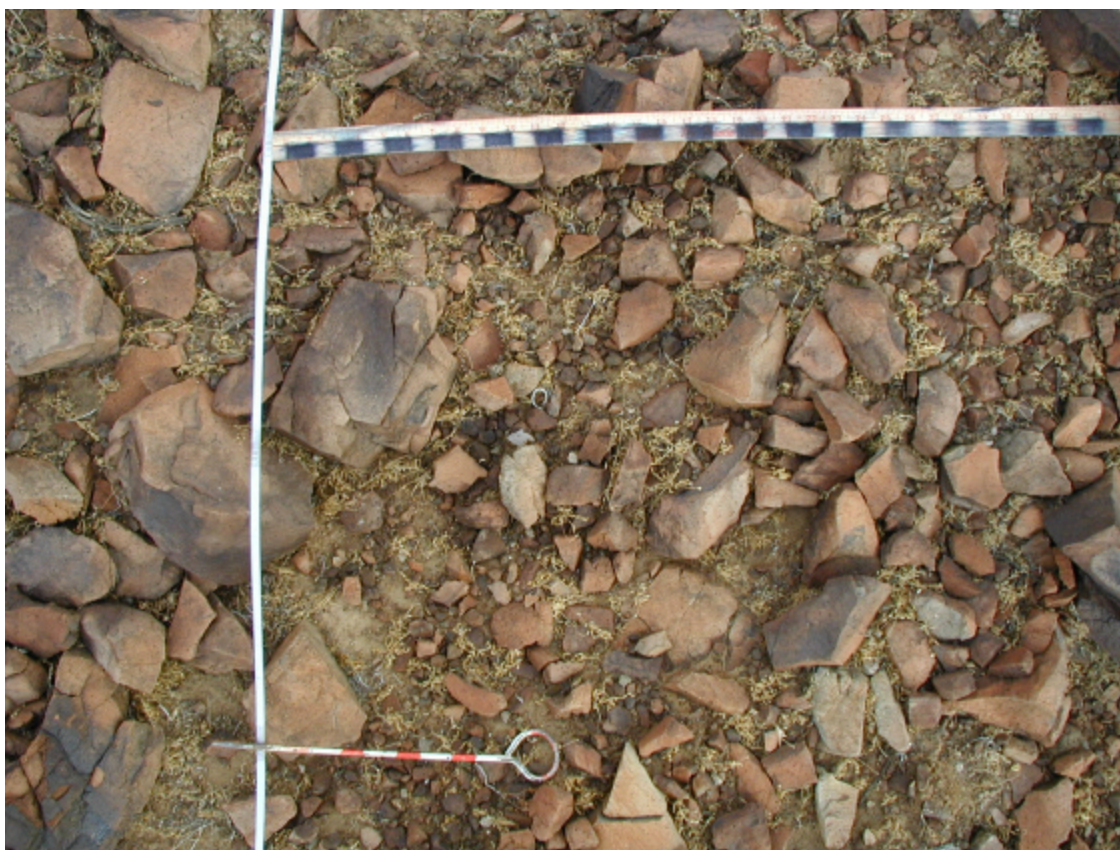


Fig. A.66. B3_91.

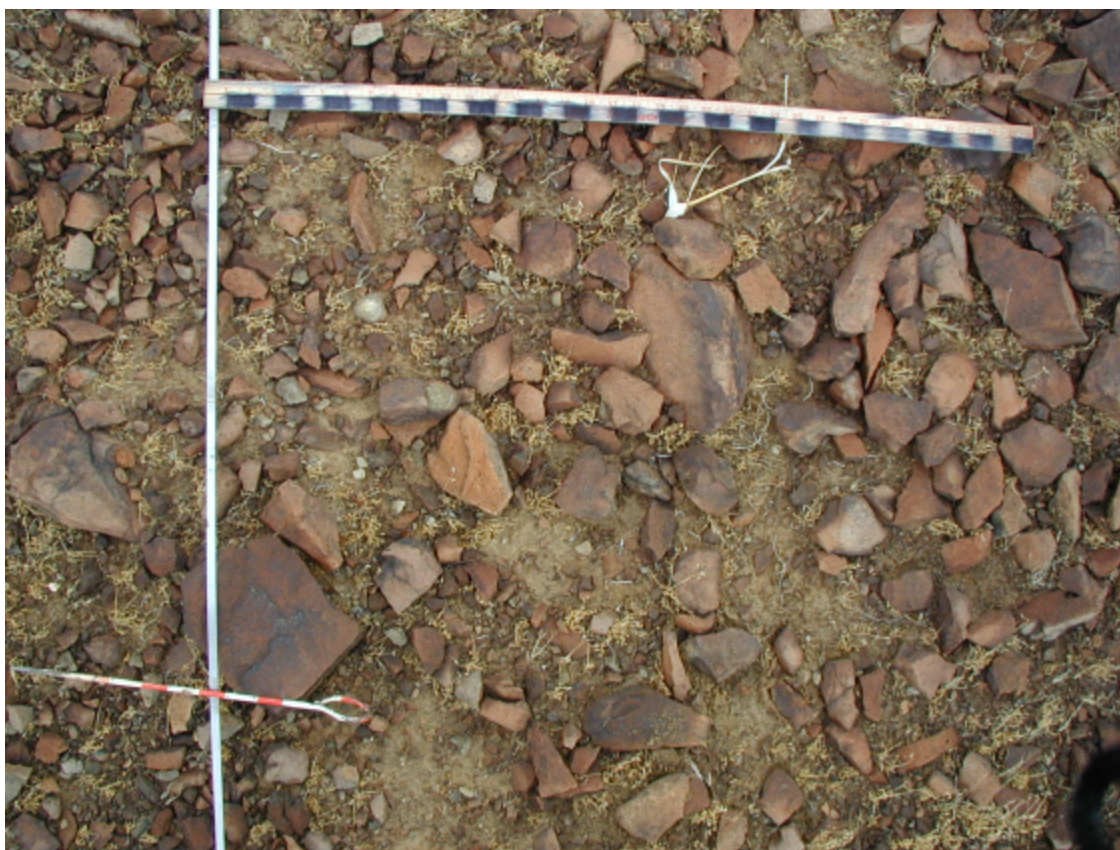


Fig. A.67. B3_92.

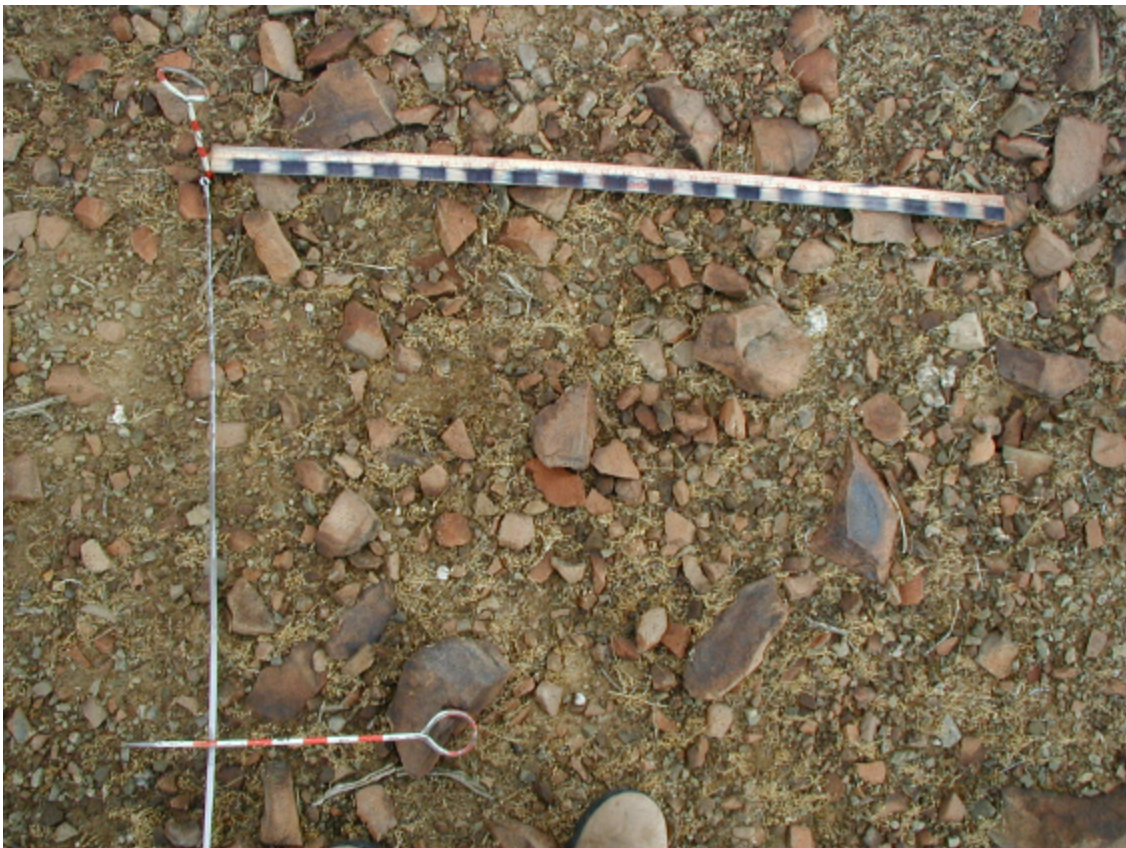


Fig. A.68. B3_93.

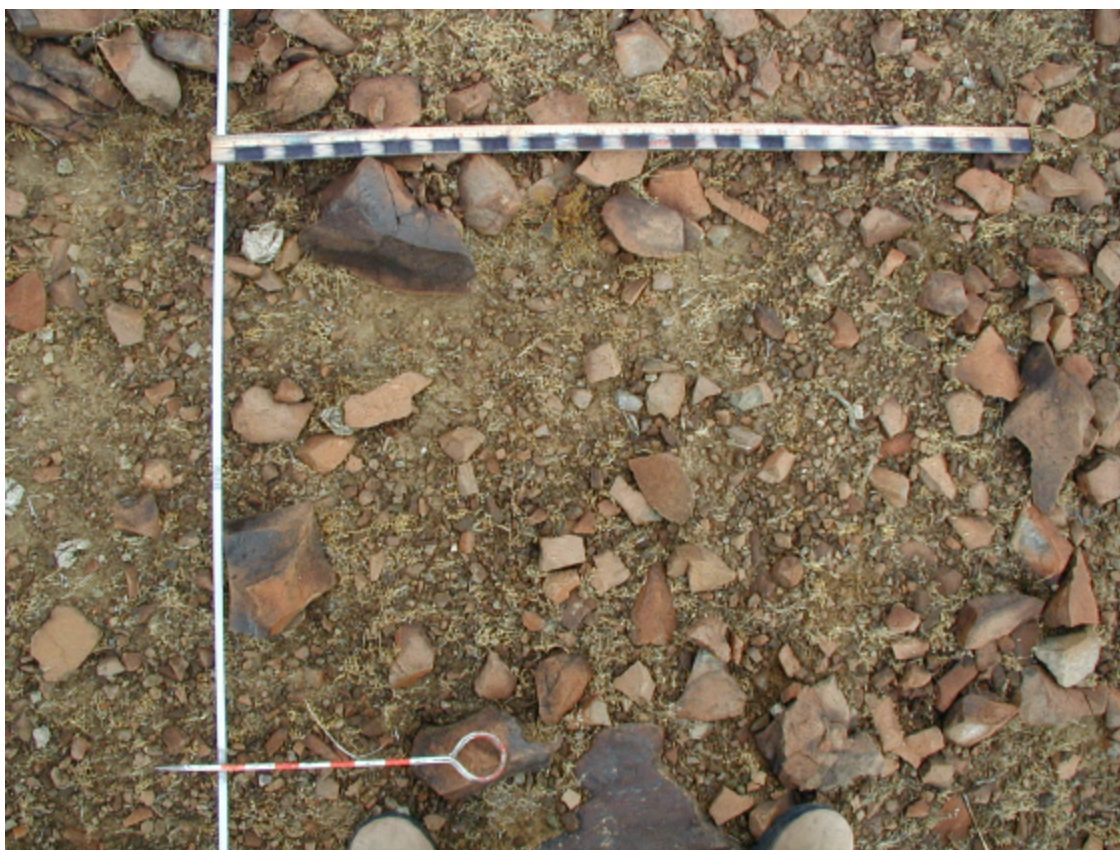


Fig. A.69. B3_94.

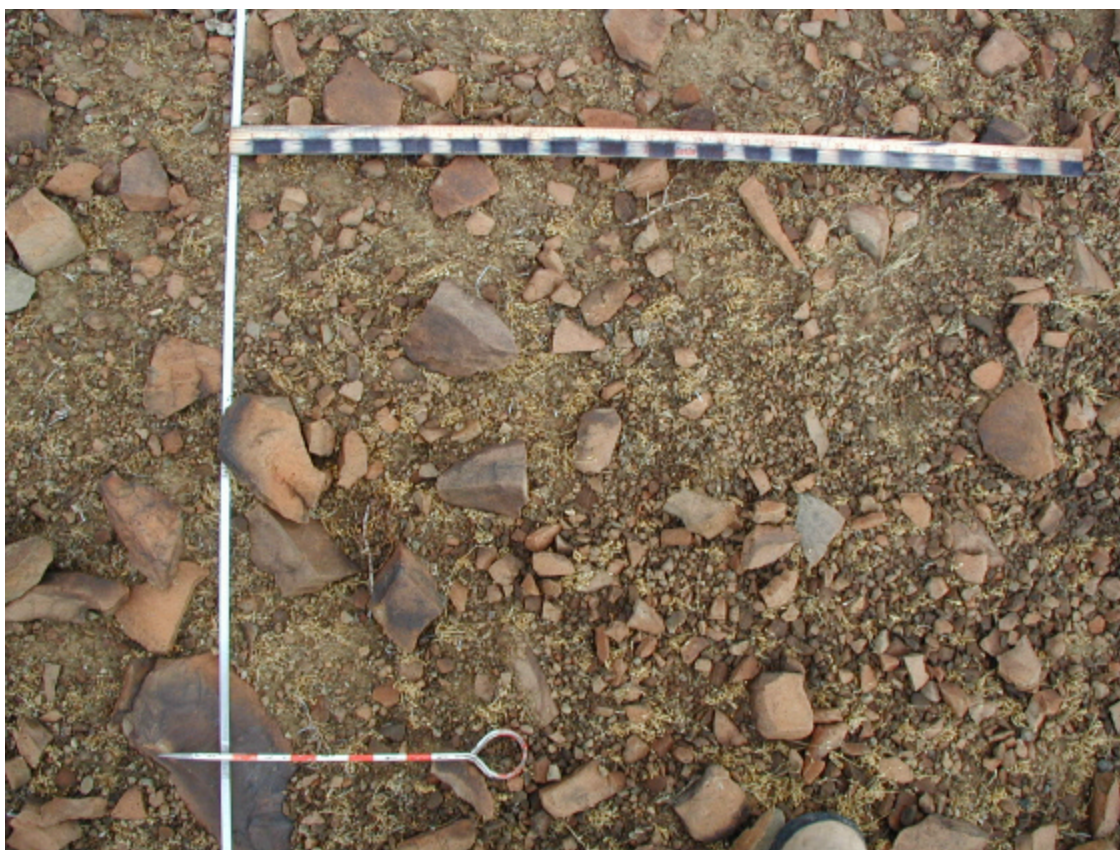


Fig. A.70. B3_95.

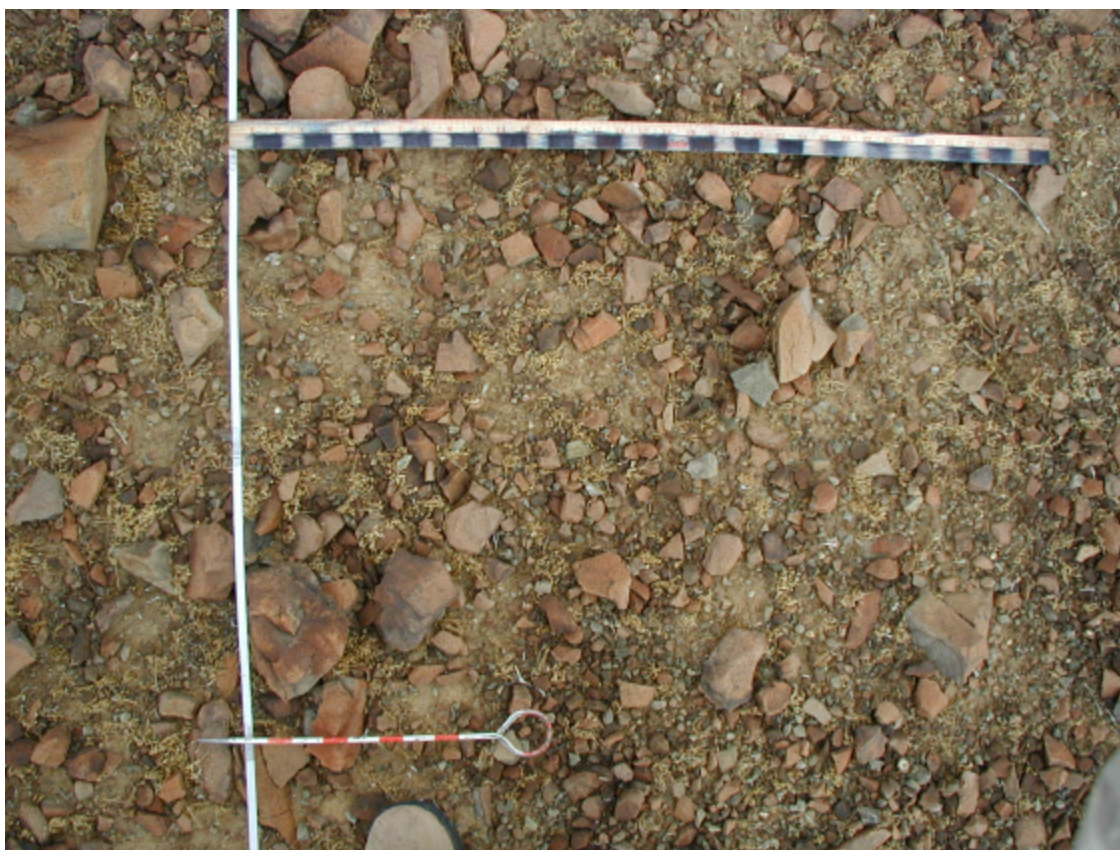


Fig. A.71. B3_96.

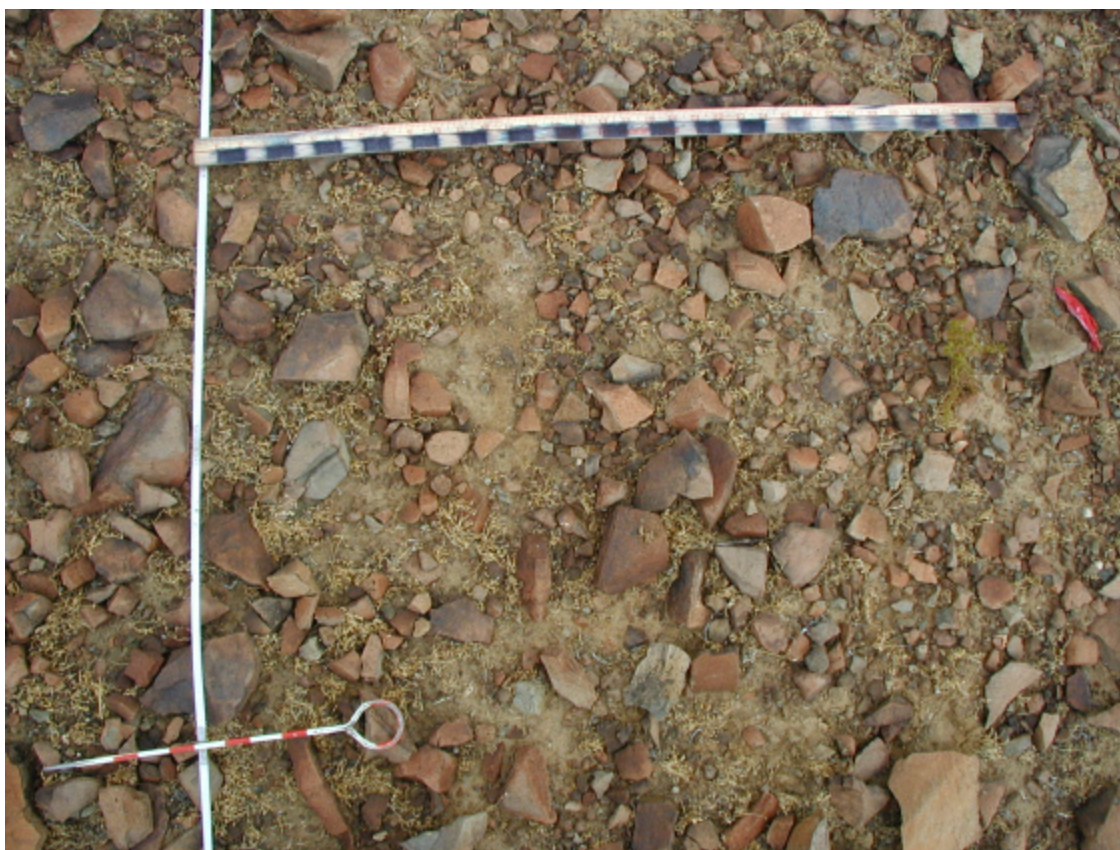


Fig. A.72. B3_97.

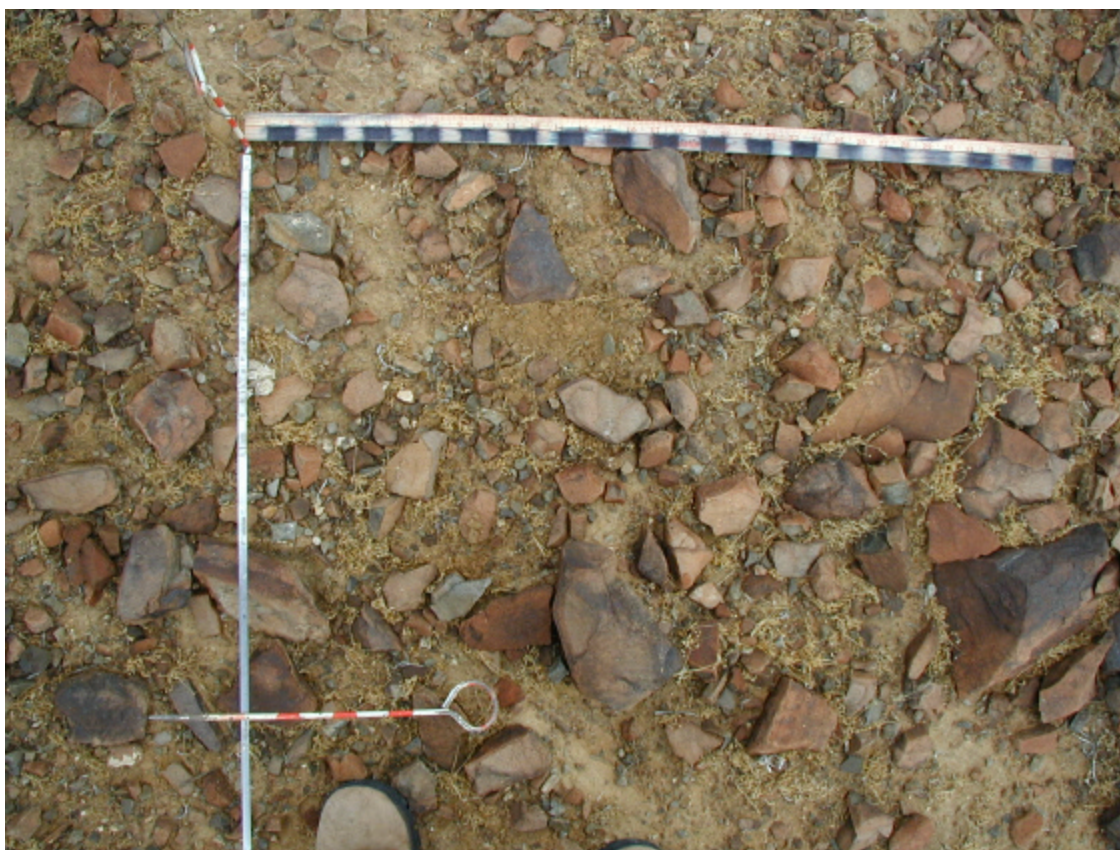


Fig. A.73. B3_98.

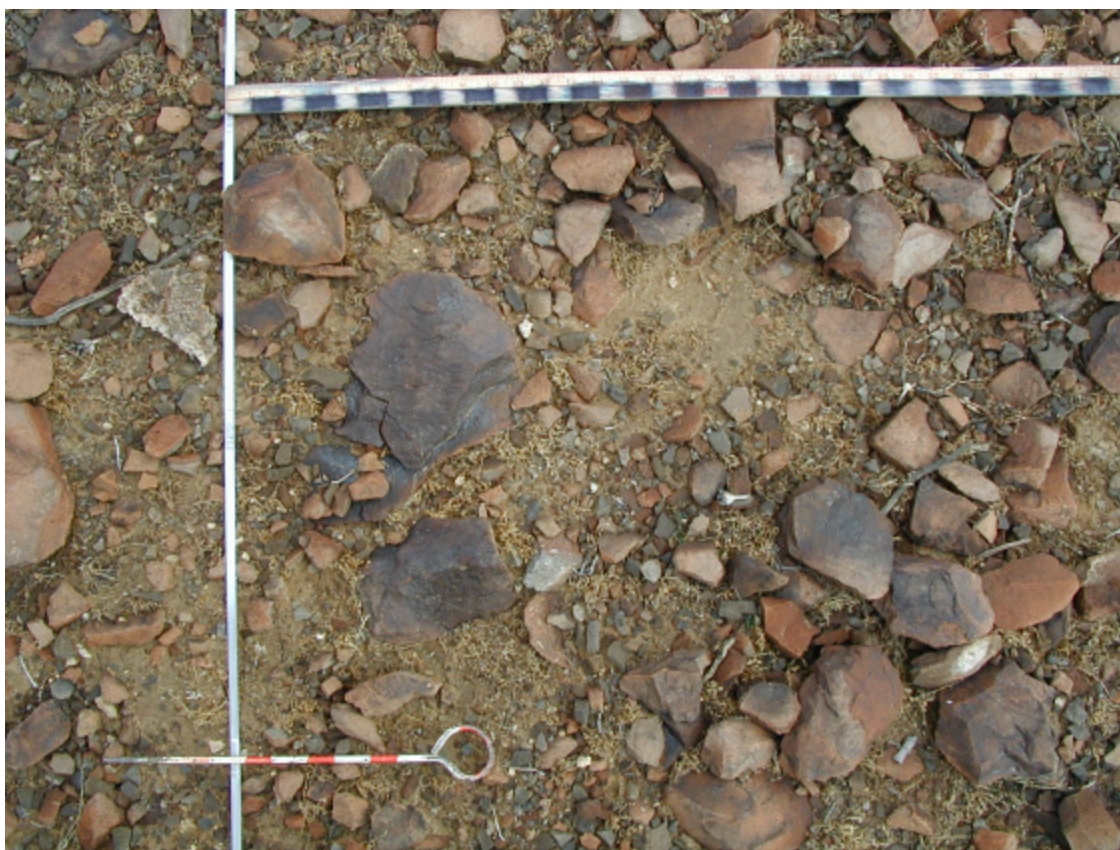


Fig. A.74. B3_99.

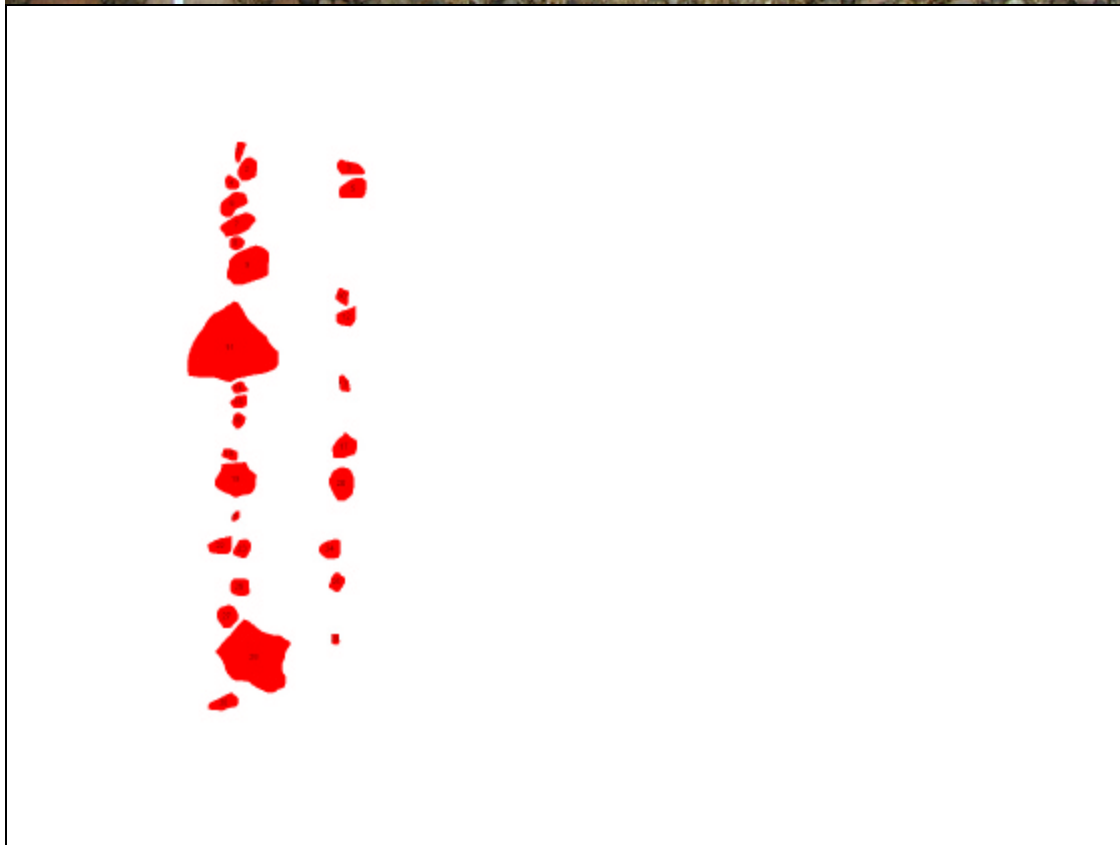
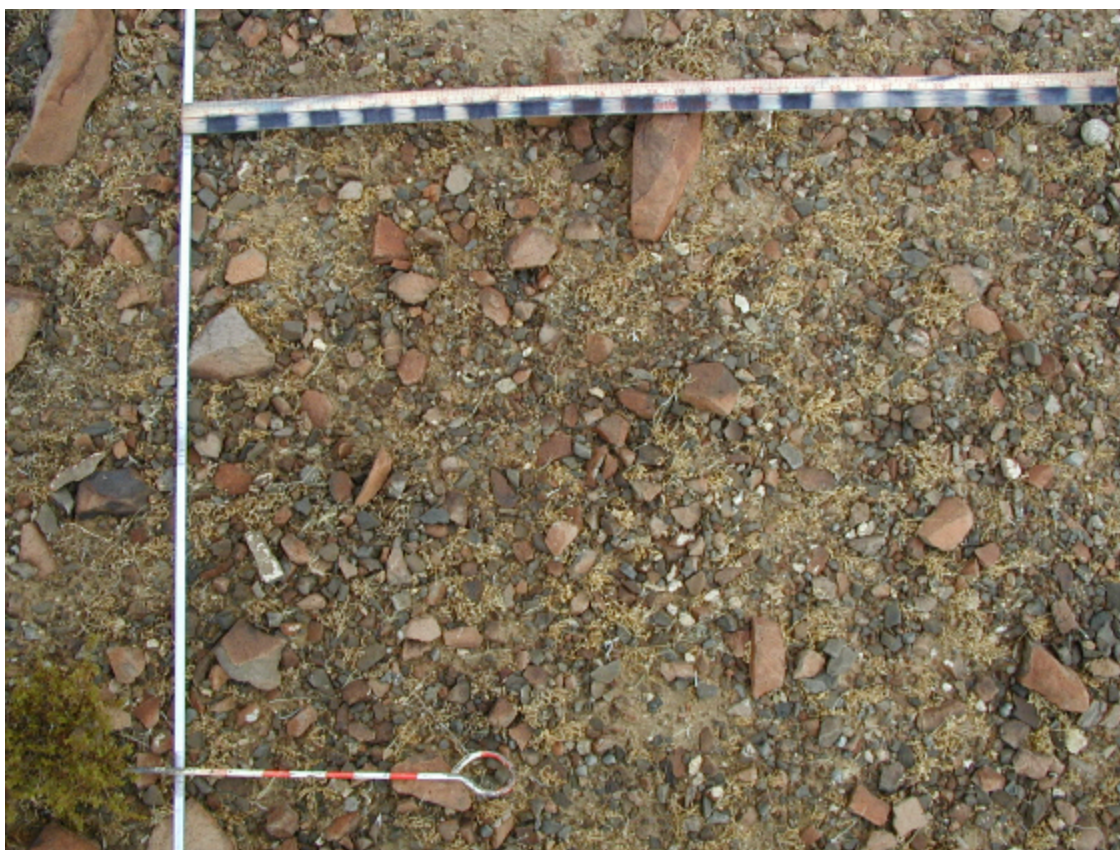


Fig. A.75. B3_100.

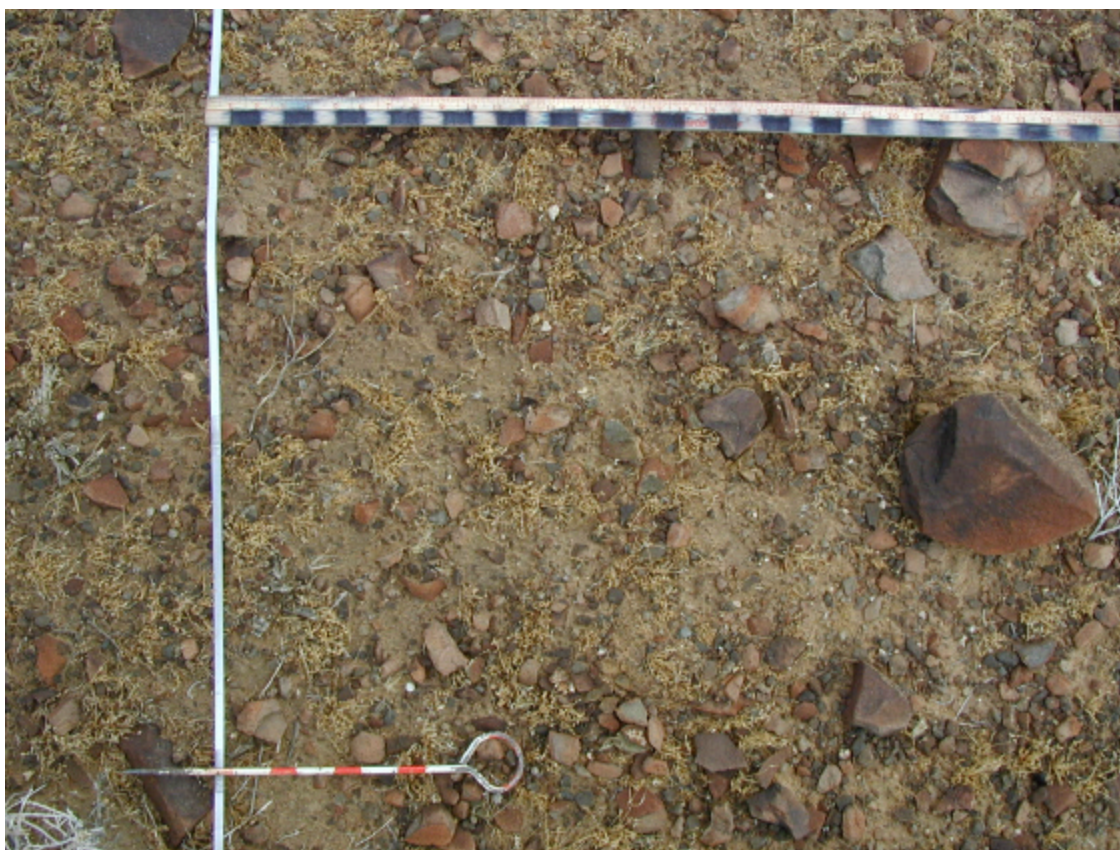


Fig. A.76. B3_101.

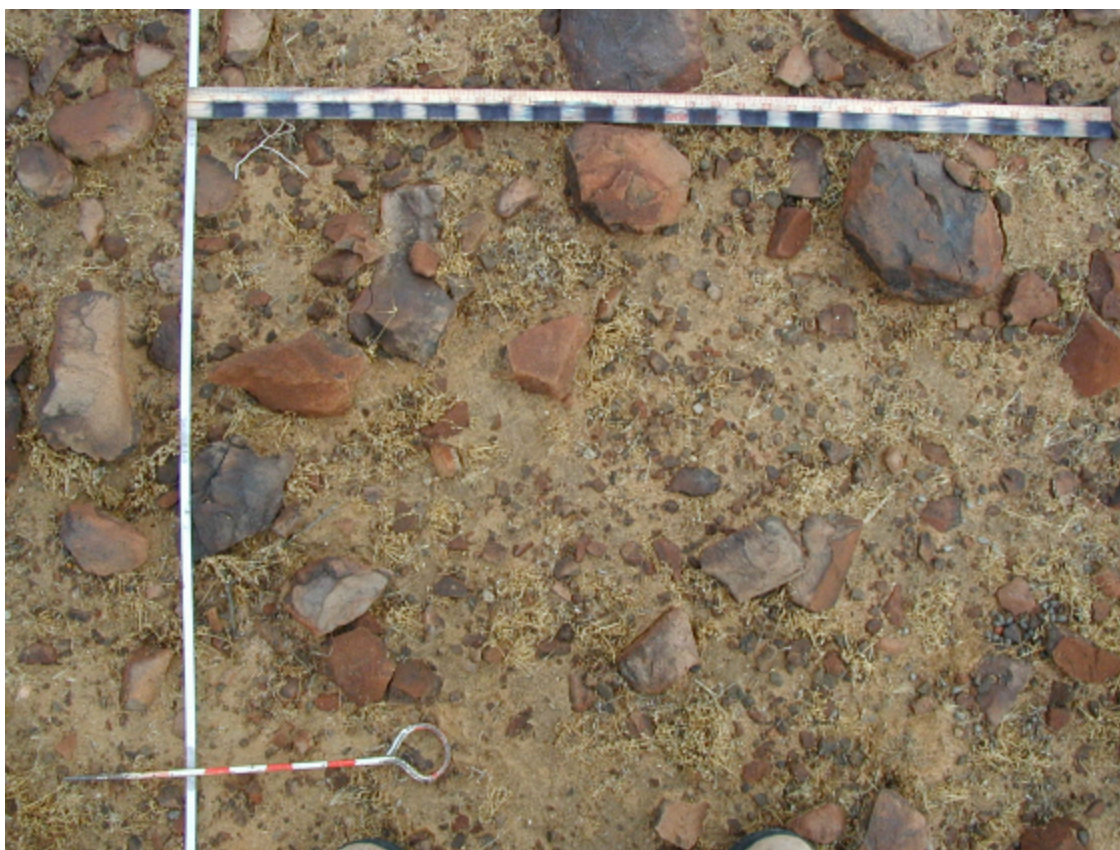


Fig. A.77. B3_102.

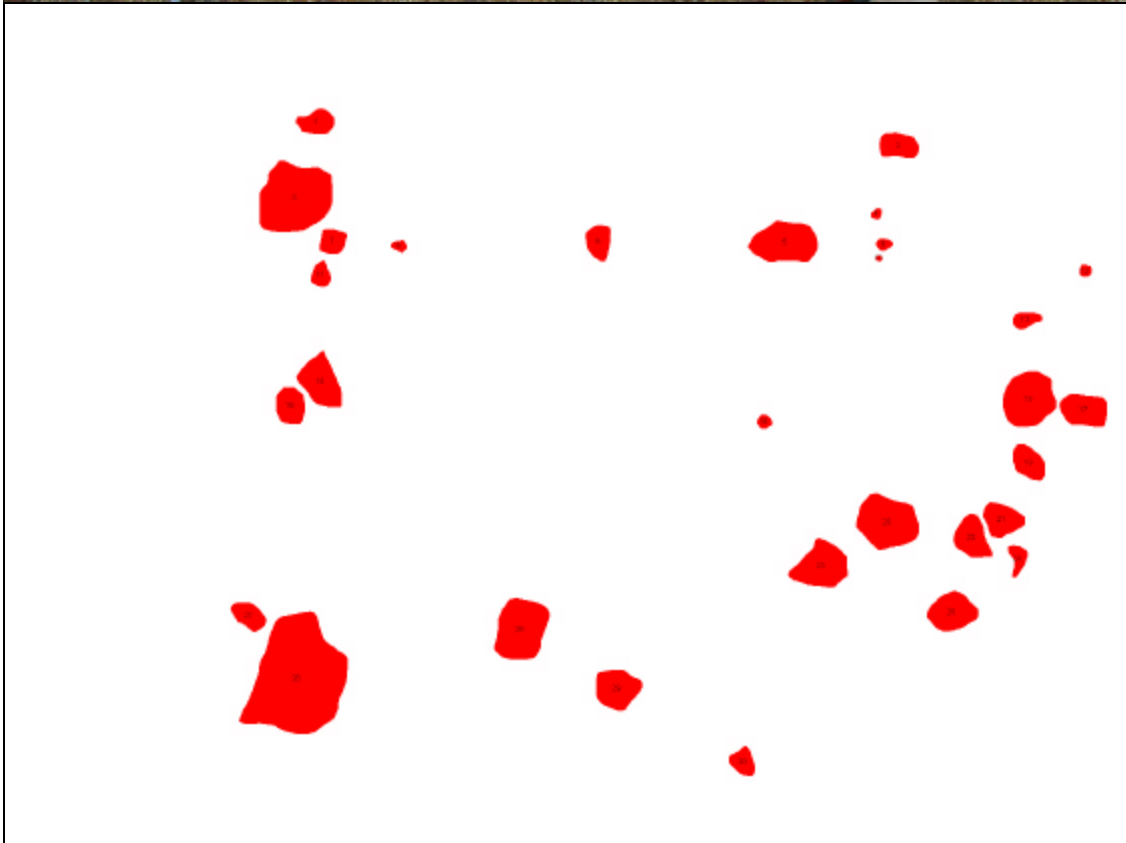
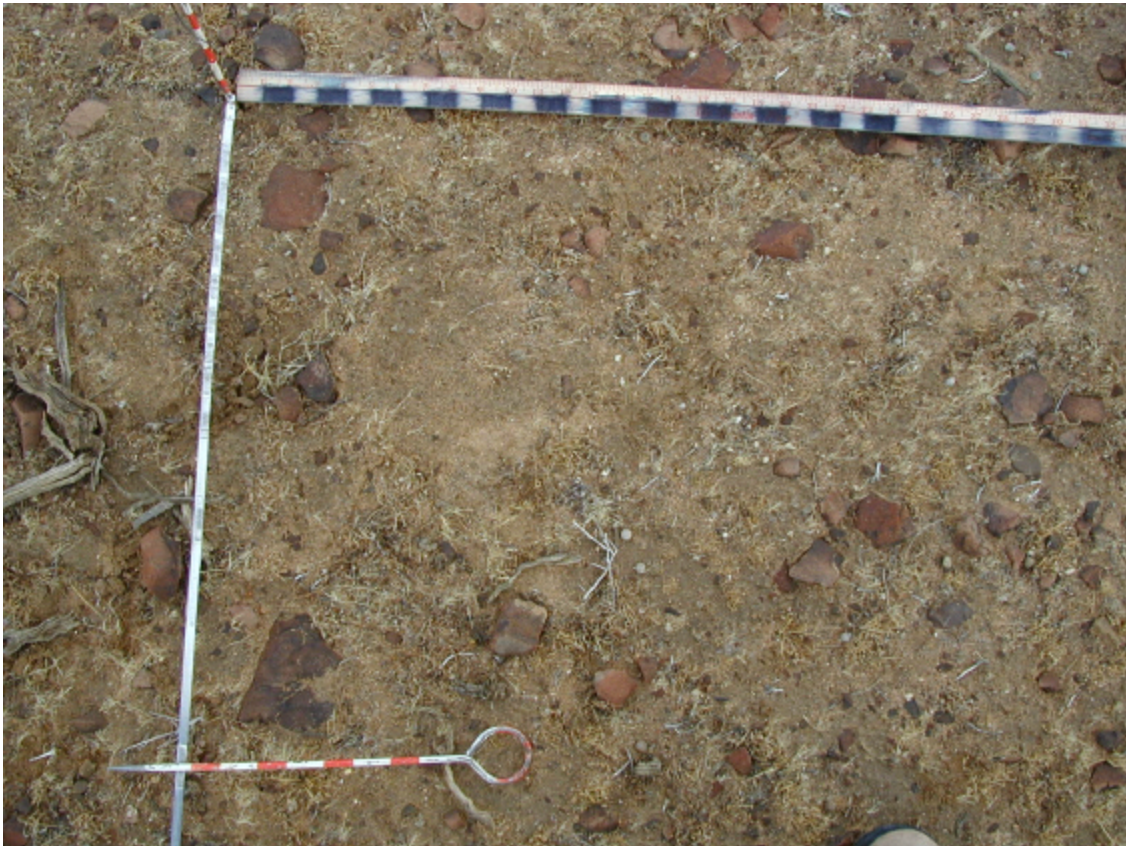


Fig. A.78. B3_103.

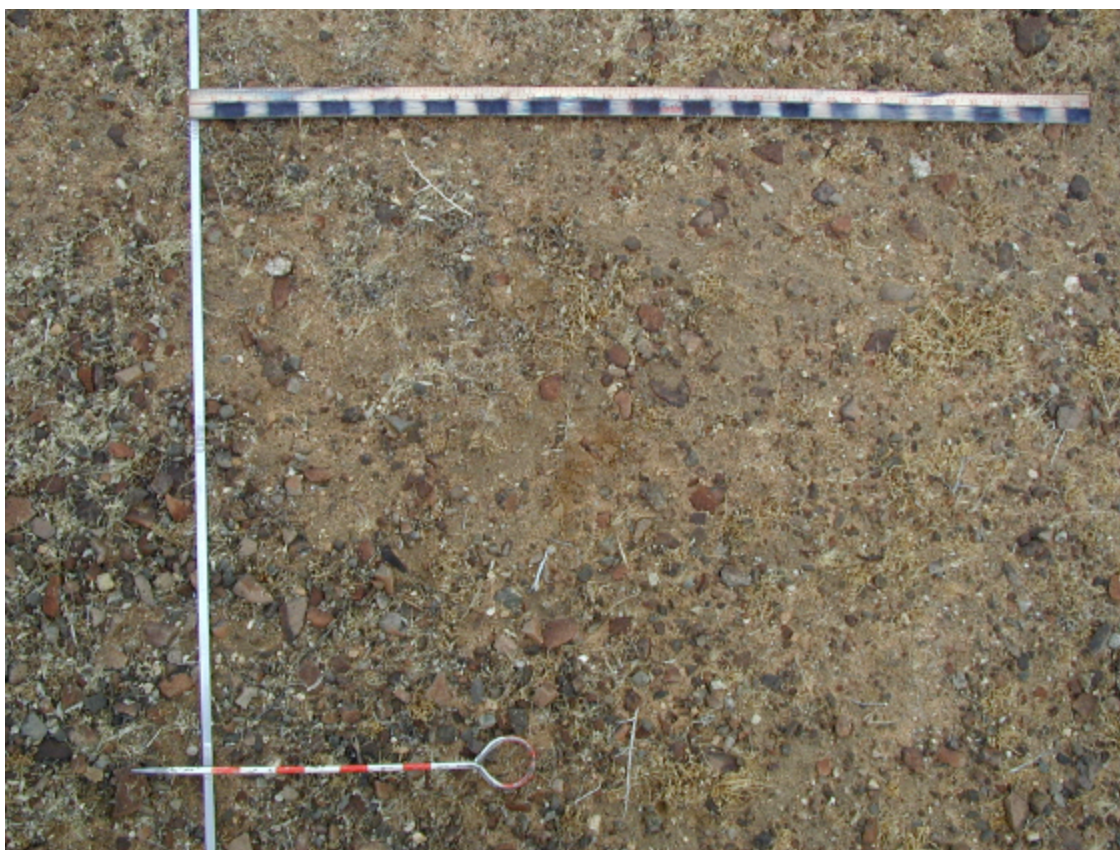


Fig. A.79. B3_104.



Fig. A.80. B4_108.

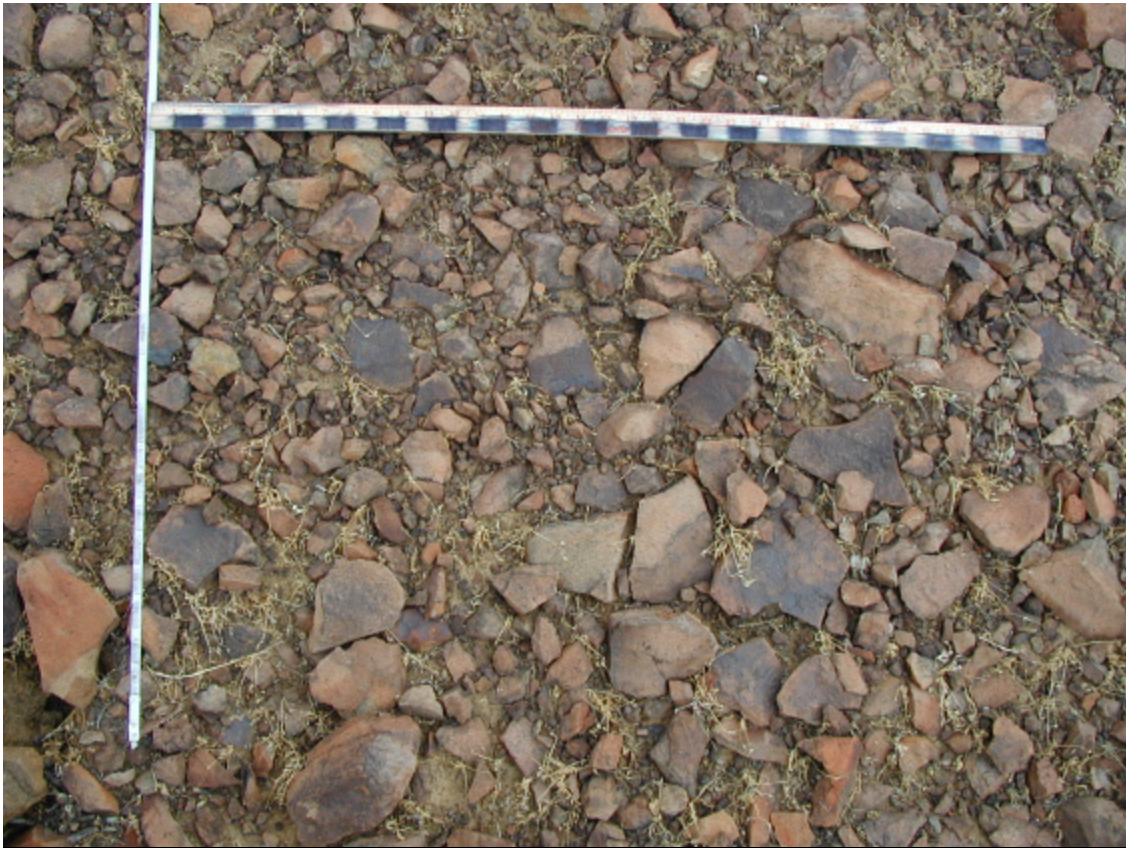


Fig. A.81. B4_109.



Fig. A.82. B4_110.

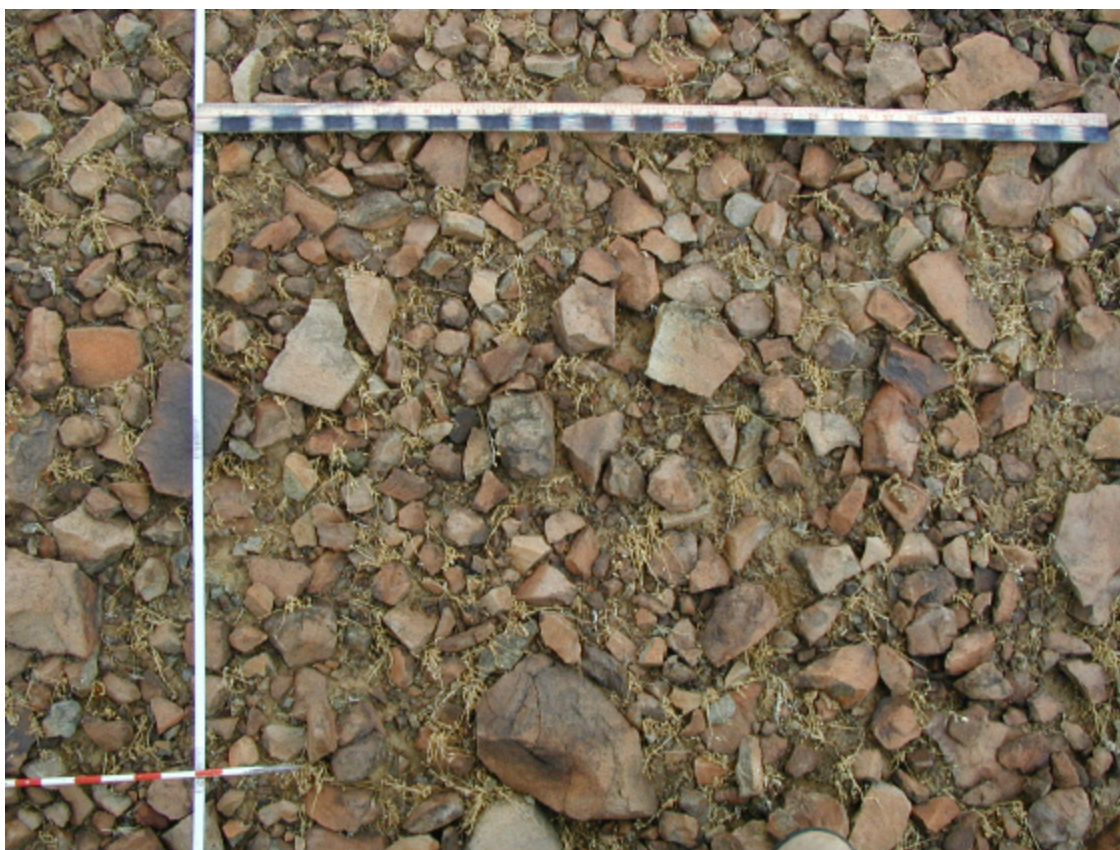


Fig. A.83. B4_111.



Fig. A.84. B4_112

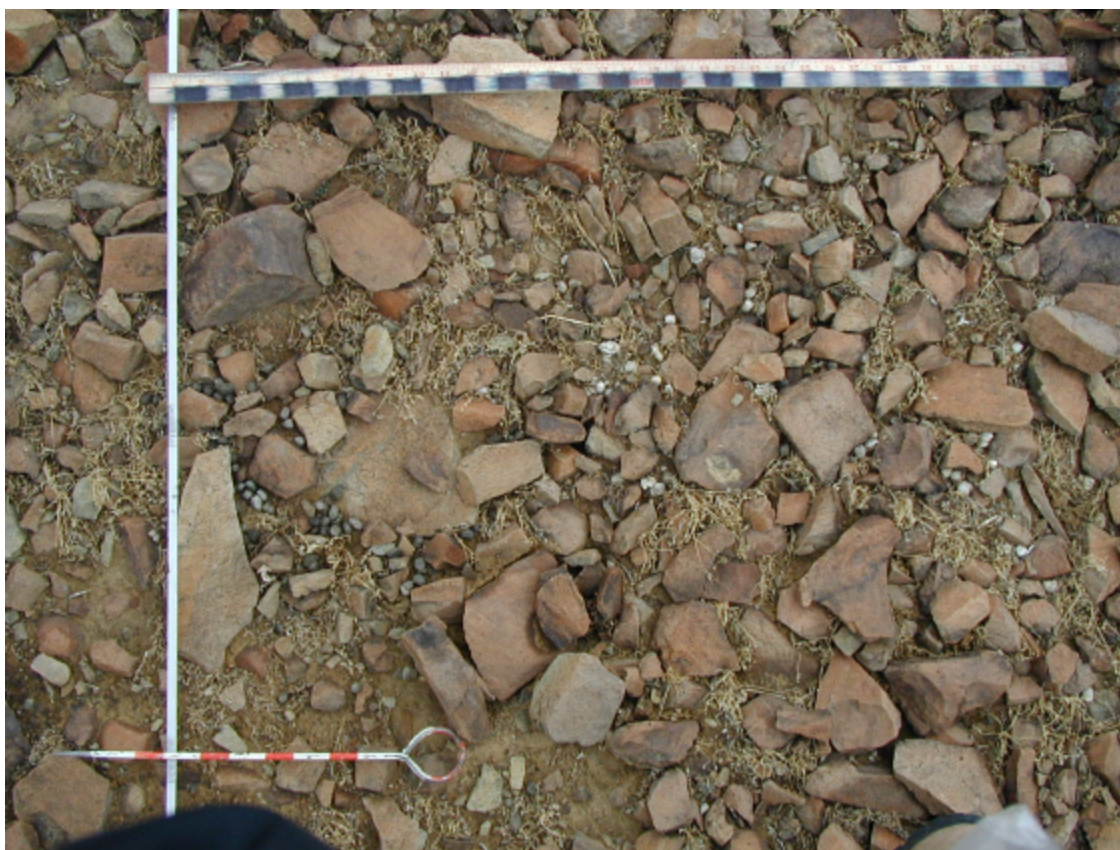


Fig. A.85. B4_113.

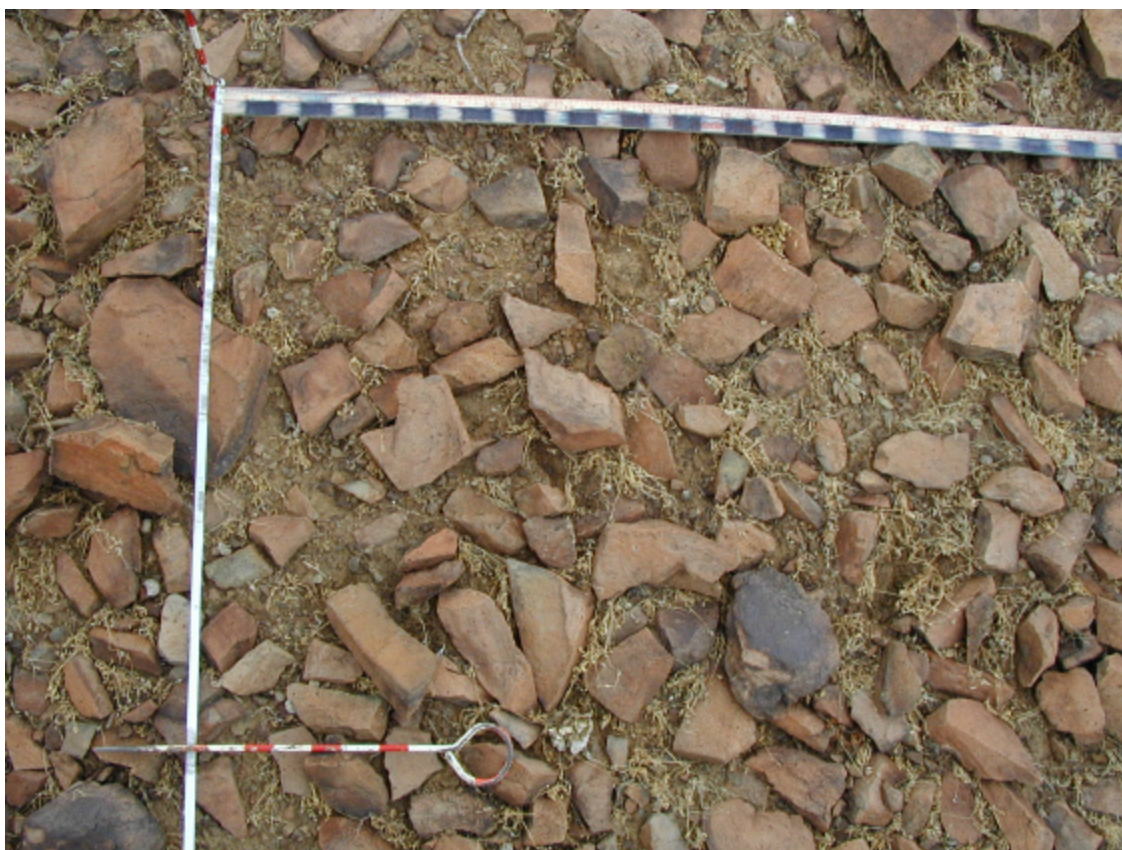


Fig. A.86. B4_114.

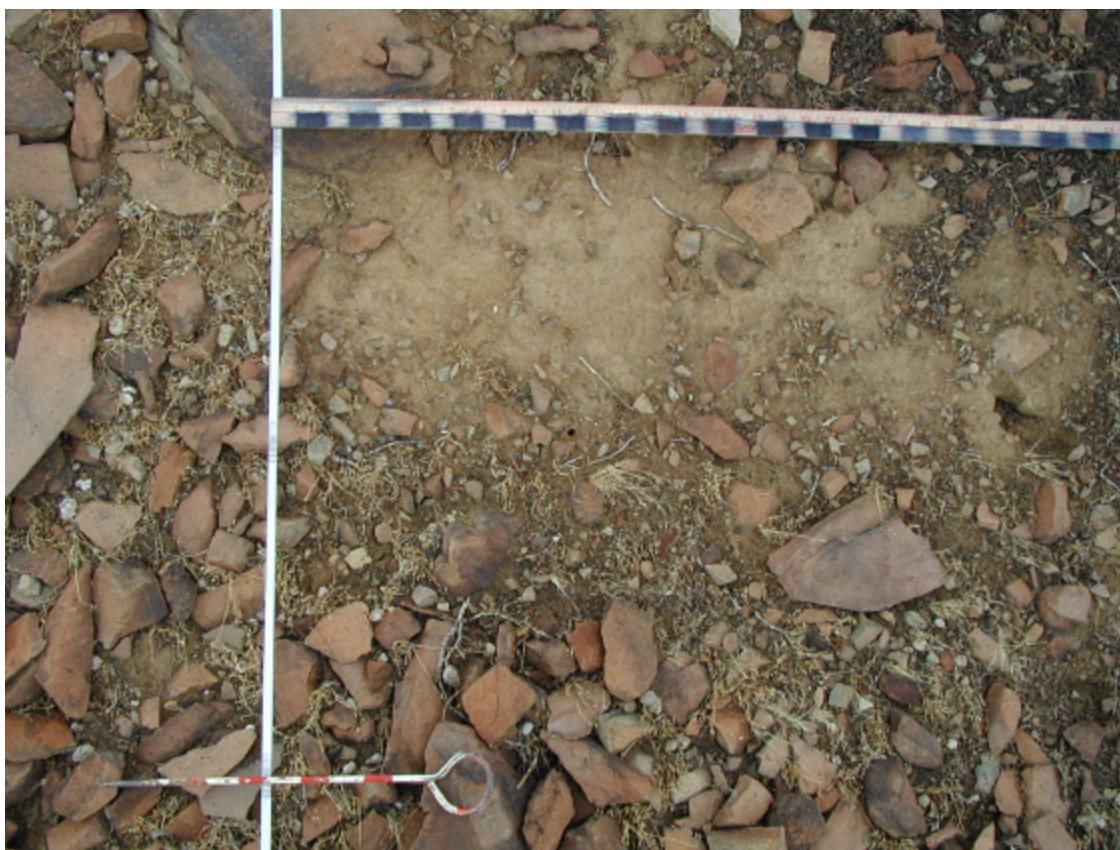


Fig. A.87. B4_115.

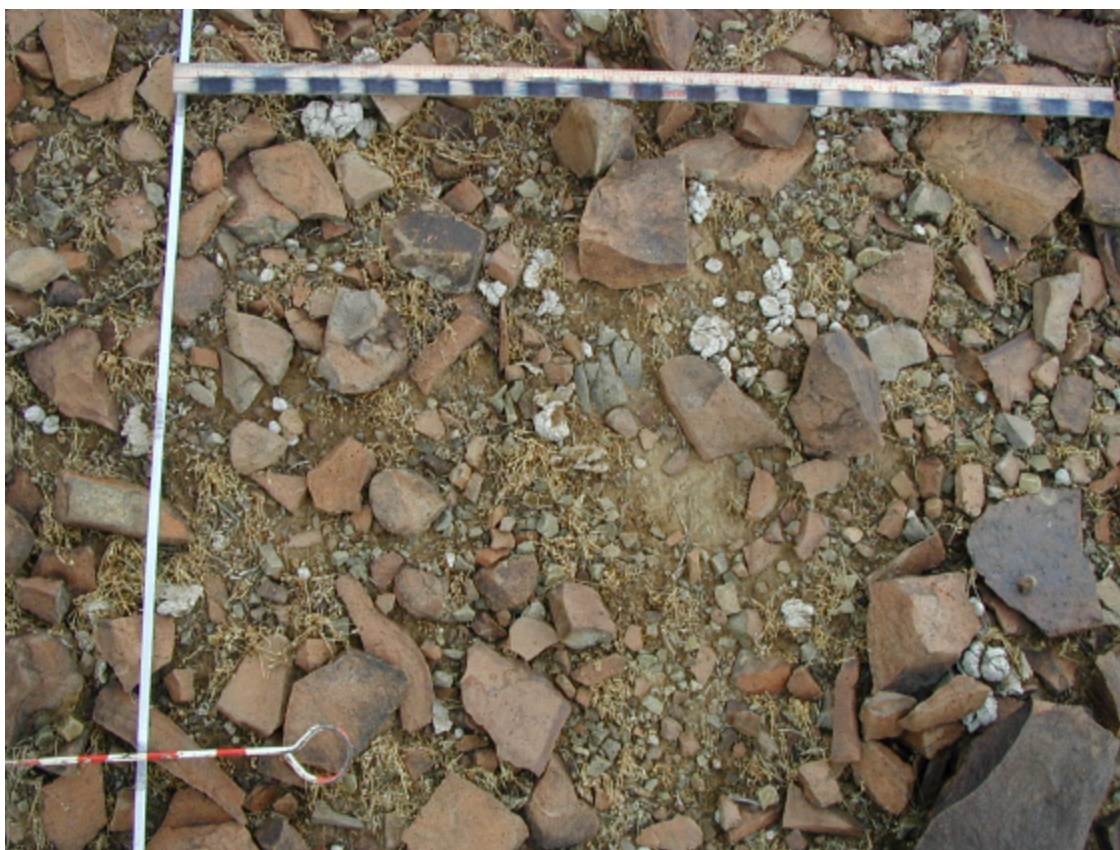


Fig. A.88. B4_116.

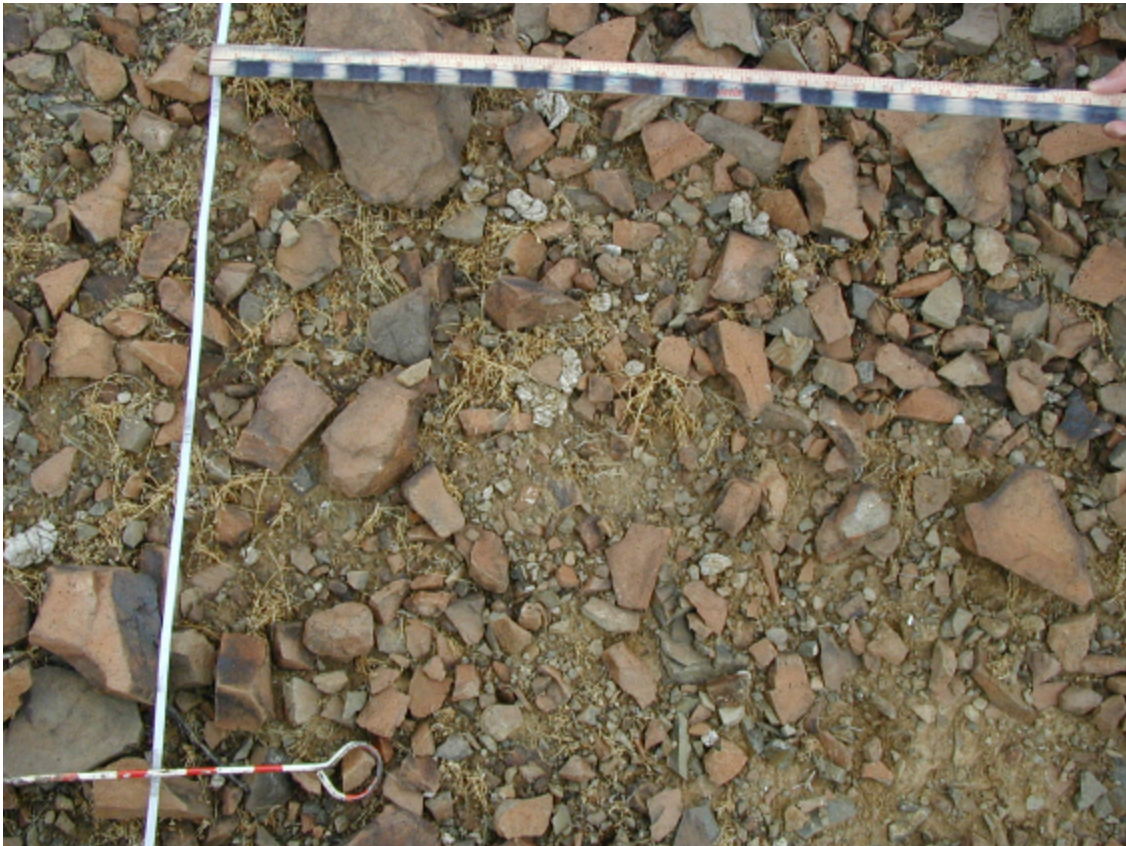


Fig. A.89. B4_117.

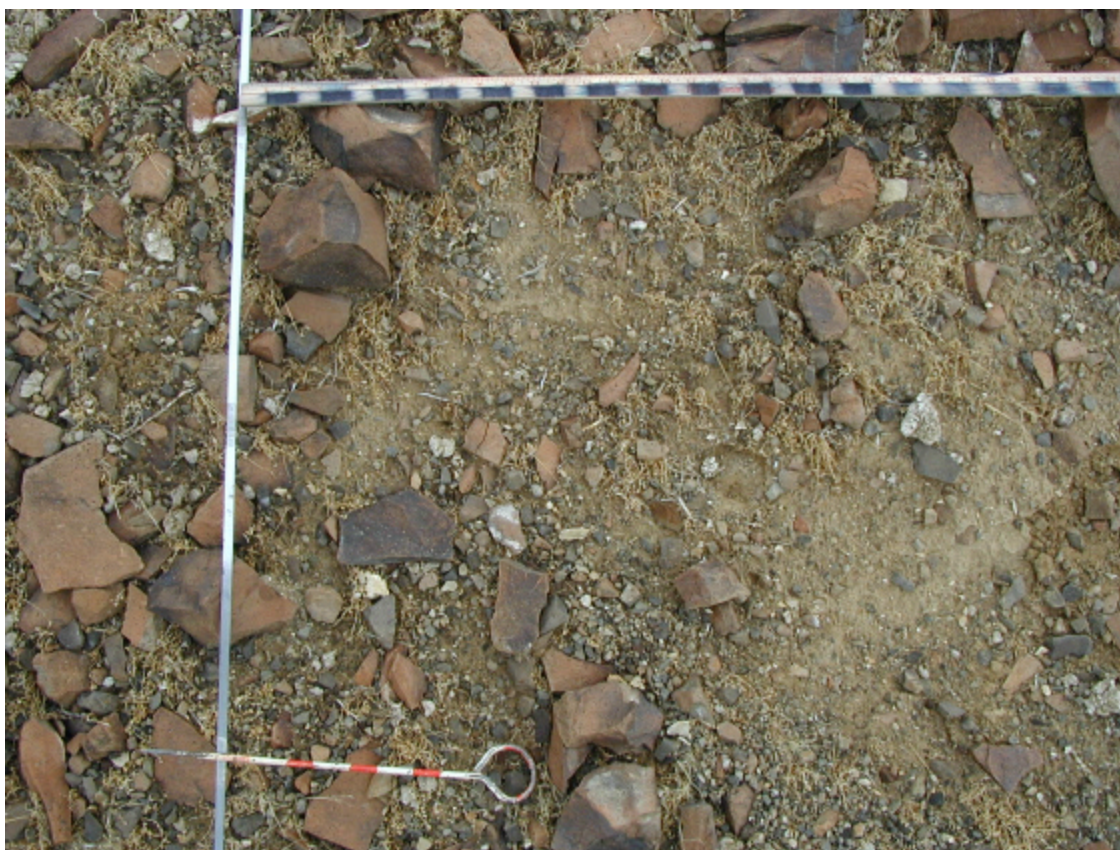


Fig. A.90. B4_118.



Fig. A.91. B4_119.



Fig. A.92. B4_120.

APPENDIX B

DATA TABLE

Table B.1. Partial data table from digital field sampling and digital image processing of 2760 basalt clasts.

Transect#_Frame#	Distance(ft)	Slope Angle (degrees)	Particle #	Area mm2	Rock Varnish Area	Iron Films Area	No Coating Area	Transect#_Frame#	Distance(ft)	Slope Angle (degrees)	Particle #	Area mm2	Rock Varnish Area	Iron Films Area	No Coating Area
B1_01	20	4	1	1052.3	0.0	0.0	1052.3	B2_59	980	13	1	171.2	0.0	0.0	171.2
B1_01	20	4	2	1126.6	0.0	1126.6	0.0	B2_59	980	13	2	171.7	0.0	171.7	0.0
B1_01	20	4	3	13854.6	13854.6	0.0	0.0	B2_59	980	13	3	805.8	0.0	805.8	0.0
B1_01	20	4	4	911.6	0.0	911.6	0.0	B2_59	980	13	4	235.4	0.0	235.4	0.0
B1_01	20	4	5	2132.0	0.0	0.0	2132.0	B2_59	980	13	5	304.9	0.0	304.9	0.0
B1_01	20	4	6	1046.1	0.0	0.0	1046.1	B2_59	980	13	6	9366.7	9366.7	0.0	0.0
B1_01	20	4	7	2391.3	0.0	0.0	2391.3	B2_59	980	13	7	160.1	160.1	0.0	0.0
B1_01	20	4	8	576.1	0.0	576.1	0.0	B2_59	980	13	8	264.4	264.4	0.0	0.0
B1_01	20	4	9	1416.0	0.0	1416.0	0.0	B2_59	980	13	9	308.6	308.6	0.0	0.0
B1_01	20	4	10	793.0	0.0	793.0	0.0	B2_59	980	13	10	280.7	280.7	0.0	0.0
B1_01	20	4	11	705.3	0.0	0.0	705.3	B2_59	980	13	11	297.0	0.0	0.0	297.0
B1_01	20	4	12	539.9	0.0	539.9	0.0	B2_59	980	13	12	1279.3	0.0	1279.3	0.0
B1_01	20	4	13	660.2	0.0	660.2	0.0	B2_59	980	13	13	358.7	89.7	269.0	0.0
B1_01	20	4	14	253.1	0.0	0.0	253.1	B2_59	980	13	14	558.8	558.8	0.0	0.0
B1_01	20	4	15	207.1	0.0	0.0	207.1	B2_59	980	13	15	145.4	0.0	0.0	145.4
B1_01	20	4	16	217.7	0.0	0.0	217.7	B2_59	980	13	16	254.9	0.0	254.9	0.0
B1_01	20	4	17	1418.7	0.0	0.0	1418.7	B2_59	980	13	17	185.4	0.0	0.0	185.4
B1_01	20	4	18	200.0	0.0	0.0	200.0	B2_59	980	13	18	337.6	337.6	0.0	0.0
B1_01	20	4	19	185.9	0.0	0.0	185.9	B2_59	980	13	19	352.9	352.9	0.0	0.0
B1_01	20	4	20	1722.2	0.0	1722.2	0.0	B2_59	980	13	20	178.5	0.0	178.5	0.0
B1_01	20	4	21	659.3	0.0	0.0	659.3	B2_59	980	13	21	494.5	0.0	0.0	494.5
B1_01	20	4	22	277.9	0.0	0.0	277.9	B2_59	980	13	22	122.7	122.7	0.0	0.0
B1_01	20	4	23	760.2	0.0	0.0	760.2	B2_59	980	13	23	988.0	0.0	988.0	0.0
B1_01	20	4	24	485.9	0.0	485.9	0.0	B2_59	980	13	24	163.8	0.0	0.0	163.8
B1_01	20	4	25	49606.7	49606.7	0.0	0.0	B2_59	980	13	25	117.5	0.0	0.0	117.5
B1_01	20	4	26	1286.8	0.0	1286.8	0.0	B2_59	980	13	26	593.0	593.0	0.0	0.0
B1_01	20	4	27	262.8	0.0	262.8	0.0	B2_59	980	13	27	433.4	0.0	433.4	0.0
B1_01	20	4	28	1370.0	0.0	0.0	1370.0	B2_59	980	13	28	154.3	0.0	154.3	0.0
B1_01	20	4	29	811.5	0.0	0.0	811.5	B2_59	980	13	29	2382.1	1786.6	595.5	0.0
B1_01	20	4	30	1526.6	0.0	0.0	1526.6	B2_59	980	13	30	173.3	0.0	173.3	0.0
B1_02	40	5	1	2822.2	0.0	2822.2	0.0	B2_60	1000	7	1	409.2	0.0	409.2	0.0
B1_02	40	5	2	2249.5	0.0	1687.1	562.4	B2_60	1000	7	2	1140.5	0.0	0.0	1140.5
B1_02	40	5	3	7146.3	7146.3	0.0	0.0	B2_60	1000	7	3	177.7	0.0	177.7	0.0
B1_02	40	5	4	8508.3	6381.2	2127.1	0.0	B2_60	1000	7	4	421.2	421.2	0.0	0.0
B1_02	40	5	5	9916.2	0.0	9916.2	0.0	B2_60	1000	7	5	216.1	0.0	0.0	216.1
B1_02	40	5	6	2298.9	0.0	2298.9	0.0	B2_60	1000	7	6	142.4	0.0	0.0	142.4
B1_02	40	5	7	4302.5	0.0	4302.5	0.0	B2_60	1000	7	7	946.8	0.0	946.8	0.0
B1_02	40	5	8	2581.4	2581.4	0.0	0.0	B2_60	1000	7	8	99.6	0.0	0.0	99.6
B1_02	40	5	9	203.6	203.6	0.0	0.0	B2_60	1000	7	9	78.7	78.7	0.0	0.0
B1_02	40	5	10	9448.1	9448.1	0.0	0.0	B2_60	1000	7	10	3014.2	0.0	3014.2	0.0
B1_02	40	5	11	3395.0	0.0	3395.0	0.0	B2_60	1000	7	11	130.4	0.0	0.0	130.4
B1_02	40	5	12	557.7	557.7	0.0	0.0	B2_60	1000	7	12	269.3	0.0	0.0	269.3
B1_02	40	5	13	1851.6	462.9	1388.7	0.0	B2_60	1000	7	13	1158.4	0.0	1158.4	0.0
B1_02	40	5	14	2499.7	624.9	1874.7	0.0	B2_60	1000	7	14	90.6	0.0	0.0	90.6
B1_02	40	5	15	10169.2	2542.3	7626.9	0.0	B2_60	1000	7	15	831.8	623.9	208.0	0.0
B1_02	40	5	16	1685.3	0.0	1685.3	0.0	B2_60	1000	7	16	1047.4	0.0	1047.4	0.0
B1_02	40	5	17	281.0	0.0	281.0	0.0	B2_60	1000	7	17	467.0	0.0	467.0	0.0
B1_02	40	5	18	483.2	0.0	483.2	0.0	B2_60	1000	7	18	340.5	255.4	85.1	0.0
B1_02	40	5	19	381.4	381.4	0.0	0.0	B2_60	1000	7	19	204.6	0.0	0.0	204.6
B1_02	40	5	20	210.0	210.0	0.0	0.0	B2_60	1000	7	20	137.4	0.0	0.0	137.4
B1_02	40	5	21	6284.6	0.0	6284.6	0.0	B2_60	1000	7	21	661.6	0.0	661.6	0.0
B1_02	40	5	22	461.7	0.0	461.7	0.0	B2_60	1000	7	22	327.1	327.1	0.0	0.0
B1_02	40	5	23	682.4	0.0	682.4	0.0	B2_60	1000	7	23	389.8	389.8	0.0	0.0
B1_02	40	5	24	4770.6	3578.0	1192.7	0.0	B2_60	1000	7	24	238.0	0.0	0.0	238.0
B1_02	40	5	25	5665.2	0.0	5665.2	0.0	B2_60	1000	7	25	301.7	301.7	0.0	0.0
B1_02	40	5	26	8010.1	0.0	8010.1	0.0	B2_60	1000	7	26	358.9	358.9	0.0	0.0
B1_02	40	5	27	4397.9	1099.5	3298.4	0.0	B2_60	1000	7	27	177.7	0.0	0.0	177.7
B1_02	40	5	28	9455.9	0.0	9455.9	0.0	B2_60	1000	7	28	443.1	0.0	0.0	443.1
B1_02	40	5	29	108.2	0.0	0.0	108.2	B2_60	1000	7	29	211.6	0.0	211.6	0.0
B1_02	40	5	30	156.3	156.3	0.0	0.0	B2_60	1000	7	30	3756.0	0.0	3756.0	0.0
B1_03	60	7	1	338.6	0.0	338.6	0.0	B2_61	1020	17	1	7606.6	1901.6	5704.9	0.0
B1_03	60	7	2	4594.1	1148.5	3445.6	0.0	B2_61	1020	17	2	585.3	0.0	585.3	0.0
B1_03	60	7	3	4112.7	0.0	4112.7	0.0	B2_61	1020	17	3	1336.3	0.0	1336.3	0.0

Table B.1., cont.

B1_03	60	7	4	1550.0	1162.5	387.5	0.0	B2_61	1020	17	4	6877.9	0.0	6877.9	0.0
B1_03	60	7	5	575.1	0.0	0.0	575.1	B2_61	1020	17	5	419.5	0.0	419.5	0.0
B1_03	60	7	6	4742.6	0.0	4742.6	0.0	B2_61	1020	17	6	3011.4	0.0	3011.4	0.0
B1_03	60	7	7	905.3	0.0	905.3	0.0	B2_61	1020	17	7	558.9	0.0	558.9	0.0
B1_03	60	7	8	1843.9	1843.9	0.0	0.0	B2_61	1020	17	8	949.0	0.0	949.0	0.0
B1_03	60	7	9	1804.4	0.0	0.0	1804.4	B2_61	1020	17	9	3059.6	2294.7	764.9	0.0
B1_03	60	7	10	233.3	0.0	233.3	0.0	B2_61	1020	17	10	2011.9	0.0	2011.9	0.0
B1_03	60	7	11	1374.1	343.5	1030.5	0.0	B2_61	1020	17	11	2735.2	0.0	683.8	2051.4
B1_03	60	7	12	3243.7	810.9	2432.8	0.0	B2_61	1020	17	12	704.6	528.4	176.1	0.0
B1_03	60	7	13	1978.7	0.0	0.0	1978.7	B2_61	1020	17	13	1086.1	0.0	1086.1	0.0
B1_03	60	7	14	9188.7	9188.7	0.0	0.0	B2_61	1020	17	14	247.1	0.0	247.1	0.0
B1_03	60	7	15	3065.7	2299.3	766.4	0.0	B2_61	1020	17	15	4429.9	0.0	4429.9	0.0
B1_03	60	7	16	11171.1	8378.3	2792.8	0.0	B2_61	1020	17	16	3704.8	0.0	3704.8	0.0
B1_03	60	7	17	2264.7	0.0	0.0	2264.7	B2_61	1020	17	17	1300.2	0.0	1300.2	0.0
B1_03	60	7	18	1901.8	475.4	1426.3	0.0	B2_61	1020	17	18	809.1	0.0	809.1	0.0
B1_03	60	7	19	2657.0	0.0	2657.0	0.0	B2_61	1020	17	19	900.3	0.0	900.3	0.0
B1_03	60	7	20	2712.3	0.0	2712.3	0.0	B2_61	1020	17	20	382.0	0.0	382.0	0.0
B1_03	60	7	21	1530.0	0.0	0.0	1530.0	B2_61	1020	17	21	1008.4	756.3	252.1	0.0
B1_03	60	7	22	4485.6	0.0	4485.6	0.0	B2_61	1020	17	22	459.3	0.0	0.0	459.3
B1_03	60	7	23	1510.5	0.0	1510.5	0.0	B2_61	1020	17	23	457.1	0.0	0.0	457.1
B1_03	60	7	24	1784.3	0.0	1784.3	0.0	B2_61	1020	17	24	126.9	0.0	126.9	0.0
B1_03	60	7	25	21732.2	16299.2	5433.1	0.0	B2_61	1020	17	25	3368.3	842.1	0.0	2526.3
B1_03	60	7	26	5343.5	5343.5	0.0	0.0	B2_61	1020	17	26	1401.1	1050.8	350.3	0.0
B1_03	60	7	27	12348.7	12348.7	0.0	0.0	B2_61	1020	17	27	1819.3	0.0	0.0	1819.3
B1_03	60	7	28	591.4	0.0	0.0	591.4	B2_61	1020	17	28	348.5	0.0	348.5	0.0
B1_03	60	7	29	1667.9	0.0	1667.9	0.0	B2_61	1020	17	29	191.7	0.0	0.0	191.7
B1_03	60	7	30	4641.0	0.0	0.0	4641.0	B2_61	1020	17	30	1332.3	999.2	333.1	0.0
B1_04	80	8	1	8133.3	8133.3	0.0	0.0	B2_62	1020	17	1	377.6	0.0	377.6	0.0
B1_04	80	8	2	4775.8	1193.9	3581.8	0.0	B2_62	1040	17	2	2171.4	0.0	2171.4	0.0
B1_04	80	8	3	3333.3	3333.3	0.0	0.0	B2_62	1040	17	3	92.2	92.2	0.0	0.0
B1_04	80	8	4	4930.6	0.0	4930.6	0.0	B2_62	1040	17	4	119.6	0.0	0.0	119.6
B1_04	80	8	5	4743.1	0.0	4743.1	0.0	B2_62	1040	17	5	1323.5	0.0	1323.5	0.0
B1_04	80	8	6	3567.1	0.0	3567.1	0.0	B2_62	1040	17	6	145.9	0.0	145.9	0.0
B1_04	80	8	7	955.9	0.0	955.9	0.0	B2_62	1040	17	7	20210.2	5052.5	15157.6	0.0
B1_04	80	8	8	414.5	0.0	414.5	0.0	B2_62	1040	17	8	292.8	292.8	0.0	0.0
B1_04	80	8	9	1121.8	0.0	1121.8	0.0	B2_62	1040	17	9	259.7	0.0	259.7	0.0
B1_04	80	8	10	4428.2	0.0	4428.2	0.0	B2_62	1040	17	10	3394.4	3394.4	0.0	0.0
B1_04	80	8	11	2279.9	0.0	2279.9	0.0	B2_62	1040	17	11	109.6	0.0	0.0	109.6
B1_04	80	8	12	3492.8	873.2	2619.6	0.0	B2_62	1040	17	12	259.1	0.0	0.0	259.1
B1_04	80	8	13	3301.7	0.0	825.4	2476.2	B2_62	1040	17	13	150.6	150.6	0.0	0.0
B1_04	80	8	14	651.0	0.0	651.0	0.0	B2_62	1040	17	14	209.6	209.6	0.0	0.0
B1_04	80	8	15	5689.0	4266.8	1422.3	0.0	B2_62	1040	17	15	1839.1	1839.1	0.0	0.0
B1_04	80	8	16	1680.6	0.0	0.0	1680.6	B2_62	1040	17	16	266.5	0.0	266.5	0.0
B1_04	80	8	17	1066.5	0.0	1066.5	0.0	B2_62	1040	17	17	154.3	154.3	0.0	0.0
B1_04	80	8	18	3815.7	3815.7	0.0	0.0	B2_62	1040	17	18	447.1	447.1	0.0	0.0
B1_04	80	8	19	493.5	0.0	493.5	0.0	B2_62	1040	17	19	144.3	0.0	144.3	0.0
B1_04	80	8	20	3041.0	3041.0	0.0	0.0	B2_62	1040	17	20	638.3	0.0	638.3	0.0
B1_04	80	8	21	586.7	586.7	0.0	0.0	B2_62	1040	17	21	121.1	0.0	121.1	0.0
B1_04	80	8	22	2255.2	2255.2	0.0	0.0	B2_62	1040	17	22	164.3	0.0	0.0	164.3
B1_04	80	8	23	316.5	0.0	316.5	0.0	B2_62	1040	17	23	560.4	560.4	0.0	0.0
B1_04	80	8	24	2108.2	0.0	2108.2	0.0	B2_62	1040	17	24	335.0	83.7	251.2	0.0
B1_04	80	8	25	1783.3	445.8	1337.5	0.0	B2_62	1040	17	25	470.3	0.0	470.3	0.0
B1_04	80	8	26	2205.7	0.0	2205.7	0.0	B2_62	1040	17	26	282.3	282.3	0.0	0.0
B1_04	80	8	27	327.1	0.0	327.1	0.0	B2_62	1040	17	27	110.6	0.0	0.0	110.6
B1_04	80	8	28	6225.2	0.0	6225.2	0.0	B2_62	1040	17	28	238.1	238.1	0.0	0.0
B1_04	80	8	29	2473.2	0.0	2473.2	0.0	B2_62	1040	17	29	212.3	212.3	0.0	0.0
B1_04	80	8	30	278.1	0.0	0.0	278.1	B2_62	1040	17	30	501.9	0.0	0.0	501.9
B1_05	100	9	1	2454.2	0.0	2454.2	0.0	B2_63	1060	8	1	7401.7	7401.7	0.0	0.0
B1_05	100	9	2	4960.2	1240.0	3720.1	0.0	B2_63	1060	8	2	873.2	654.9	218.3	0.0
B1_05	100	9	3	1682.1	0.0	1682.1	0.0	B2_63	1060	8	3	164.3	164.3	0.0	0.0
B1_05	100	9	4	14163.7	0.0	14163.7	0.0	B2_63	1060	8	4	134.8	134.8	0.0	0.0
B1_05	100	9	5	1063.3	0.0	0.0	1063.3	B2_63	1060	8	5	167.5	167.5	0.0	0.0
B1_05	100	9	6	2202.8	0.0	2202.8	0.0	B2_63	1060	8	6	1046.0	1046.0	0.0	0.0
B1_05	100	9	7	2578.2	0.0	2578.2	0.0	B2_63	1060	8	7	416.1	416.1	0.0	0.0
B1_05	100	9	8	10271.3	0.0	10271.3	0.0	B2_63	1060	8	8	240.2	0.0	0.0	240.2

Table B.1., cont.

B1_05	100	9	9	2565.7	2565.7	0.0	0.0	B2_63	1060	8	9	428.2	428.2	0.0	0.0
B1_05	100	9	10	513.7	0.0	513.7	0.0	B2_63	1060	8	10	223.8	0.0	0.0	223.8
B1_05	100	9	11	6138.0	0.0	6138.0	0.0	B2_63	1060	8	11	2357.4	1768.0	589.3	0.0
B1_05	100	9	12	1635.3	0.0	1635.3	0.0	B2_63	1060	8	12	189.1	0.0	0.0	189.1
B1_05	100	9	13	5118.5	0.0	5118.5	0.0	B2_63	1060	8	13	835.3	626.5	0.0	208.8
B1_05	100	9	14	761.2	0.0	761.2	0.0	B2_63	1060	8	14	304.9	304.9	0.0	0.0
B1_05	100	9	15	1381.9	1036.4	345.5	0.0	B2_63	1060	8	15	1207.6	0.0	1207.6	0.0
B1_05	100	9	16	1573.1	0.0	1573.1	0.0	B2_63	1060	8	16	273.9	0.0	0.0	273.9
B1_05	100	9	17	2883.8	2883.8	0.0	0.0	B2_63	1060	8	17	208.0	0.0	208.0	0.0
B1_05	100	9	18	4124.9	0.0	0.0	4124.9	B2_63	1060	8	18	962.2	0.0	0.0	962.2
B1_05	100	9	19	3854.6	3854.6	0.0	0.0	B2_63	1060	8	19	247.0	0.0	0.0	247.0
B1_05	100	9	20	287.7	0.0	287.7	0.0	B2_63	1060	8	20	1455.2	0.0	1455.2	0.0

B1_05	100	9	21	1493.9	0.0	1493.9	0.0	B2_63	1060	8	21	407.1	407.1	0.0	0.0
B1_05	100	9	22	10539.7	0.0	10539.7	0.0	B2_63	1060	8	22	154.3	154.3	0.0	0.0
B1_05	100	9	23	574.5	0.0	574.5	0.0	B2_63	1060	8	23	161.7	0.0	0.0	161.7
B1_05	100	9	24	1824.5	1824.5	0.0	0.0	B2_63	1060	8	24	395.5	0.0	0.0	395.5
B1_05	100	9	25	8156.6	0.0	8156.6	0.0	B2_63	1060	8	25	212.8	0.0	0.0	212.8
B1_05	100	9	26	5755.2	0.0	5755.2	0.0	B2_63	1060	8	26	420.8	0.0	420.8	0.0
B1_05	100	9	27	362.4	362.4	0.0	0.0	B2_63	1060	8	27	501.4	501.4	0.0	0.0
B1_05	100	9	28	2658.8	0.0	2658.8	0.0	B2_63	1060	8	28	1123.9	842.9	281.0	0.0
B1_05	100	9	29	2586.1	2586.1	0.0	0.0	B2_63	1060	8	29	368.1	368.1	0.0	0.0
B1_05	100	9	30	16558.7	0.0	12419.0	0.0	B2_63	1060	8	30	201.7	201.7	0.0	0.0
B1_06	120	5	1	47134.2	35350.7	0.0	0.0	B2_64	1080	11	1	2004.3	0.0	2004.3	0.0
B1_06	120	5	2	1523.8	0.0	1523.8	0.0	B2_64	1080	11	2	1670.6	1253.0	0.0	0.0
B1_06	120	5	3	3541.9	0.0	3541.9	0.0	B2_64	1080	11	3	2707.0	0.0	2707.0	0.0
B1_06	120	5	4	1441.2	0.0	1441.2	0.0	B2_64	1080	11	4	236.1	0.0	236.1	0.0
B1_06	120	5	5	5192.7	0.0	5192.7	0.0	B2_64	1080	11	5	585.8	585.8	0.0	0.0
B1_06	120	5	6	3765.4	0.0	3765.4	0.0	B2_64	1080	11	6	3699.0	2774.2	924.7	0.0
B1_06	120	5	7	7640.9	5730.7	0.0	0.0	B2_64	1080	11	7	8490.8	2122.7	6368.1	0.0
B1_06	120	5	8	7441.3	0.0	0.0	7441.3	B2_64	1080	11	8	2028.8	0.0	2028.8	0.0
B1_06	120	5	9	462.5	0.0	0.0	462.5	B2_64	1080	11	9	462.8	0.0	462.8	0.0
B1_06	120	5	10	6549.7	4912.3	0.0	0.0	B2_64	1080	11	10	877.5	877.5	0.0	0.0
B1_06	120	5	11	6998.2	0.0	6998.2	0.0	B2_64	1080	11	11	869.5	217.4	652.1	0.0
B1_06	120	5	12	5501.3	0.0	5501.3	0.0	B2_64	1080	11	12	431.2	431.2	0.0	0.0
B1_06	120	5	13	4192.1	0.0	0.0	4192.1	B2_64	1080	11	13	2084.4	0.0	2084.4	0.0
B1_06	120	5	14	4148.8	0.0	4148.8	0.0	B2_64	1080	11	14	1935.0	1935.0	0.0	0.0
B1_06	120	5	15	6391.9	0.0	4793.9	0.0	B2_64	1080	11	15	535.4	401.5	133.8	0.0
B1_06	120	5	16	1937.0	0.0	1937.0	0.0	B2_64	1080	11	16	624.4	624.4	0.0	0.0
B1_06	120	5	17	921.0	0.0	921.0	0.0	B2_64	1080	11	17	1867.2	0.0	1867.2	0.0
B1_06	120	5	18	13539.5	0.0	13539.5	0.0	B2_64	1080	11	18	2852.6	0.0	2852.6	0.0
B1_06	120	5	19	1993.2	0.0	1993.2	0.0	B2_64	1080	11	19	1687.6	0.0	1687.6	0.0
B1_06	120	5	20	602.4	0.0	0.0	602.4	B2_64	1080	11	20	3689.5	0.0	3689.5	0.0
B1_06	120	5	21	11830.0	0.0	11830.0	0.0	B2_64	1080	11	21	3338.9	2504.2	834.7	0.0
B1_06	120	5	22	2527.9	0.0	2527.9	0.0	B2_64	1080	11	22	647.1	0.0	647.1	0.0
B1_06	120	5	23	3052.6	0.0	3052.6	0.0	B2_64	1080	11	23	967.5	0.0	967.5	0.0
B1_06	120	5	24	8954.6	0.0	8954.6	0.0	B2_64	1080	11	24	2173.0	2173.0	0.0	0.0
B1_06	120	5	25	11206.2	0.0	11206.2	0.0	B2_64	1080	11	25	505.2	0.0	505.2	0.0
B1_06	120	5	26	2435.8	0.0	2435.8	0.0	B2_64	1080	11	26	1376.6	0.0	1376.6	0.0
B1_06	120	5	27	524.2	524.2	0.0	0.0	B2_64	1080	11	27	692.8	0.0	0.0	692.8
B1_06	120	5	28	1046.4	0.0	1046.4	0.0	B2_64	1080	11	28	4115.1	0.0	4115.1	0.0
B1_06	120	5	29	3539.4	0.0	3539.4	0.0	B2_64	1080	11	29	370.9	0.0	370.9	0.0
B1_06	120	5	30	2724.5	0.0	2724.5	0.0	B2_64	1080	11	30	350.2	0.0	350.2	0.0
B1_07	140	11	1	1916.2	0.0	1916.2	0.0	B2_65	1100	9	1	1896.0	0.0	1896.0	0.0
B1_07	140	11	2	23610.4	23610.4	0.0	0.0	B2_65	1100	9	2	470.3	470.3	0.0	0.0
B1_07	140	11	3	1473.2	1473.2	0.0	0.0	B2_65	1100	9	3	3937.9	2953.4	984.5	0.0
B1_07	140	11	4	3059.0	3059.0	0.0	0.0	B2_65	1100	9	4	2254.1	0.0	2254.1	0.0
B1_07	140	11	5	5193.8	1298.5	0.0	3895.4	B2_65	1100	9	5	4320.2	0.0	4320.2	0.0
B1_07	140	11	6	7480.9	7480.9	0.0	0.0	B2_65	1100	9	6	209.1	0.0	209.1	0.0
B1_07	140	11	7	3025.5	3025.5	0.0	0.0	B2_65	1100	9	7	116.4	0.0	0.0	116.4
B1_07	140	11	8	7229.7	0.0	7229.7	0.0	B2_65	1100	9	8	319.2	0.0	0.0	319.2
B1_07	140	11	9	3098.6	3098.6	0.0	0.0	B2_65	1100	9	9	377.1	377.1	0.0	0.0
B1_07	140	11	10	2607.0	0.0	2607.0	0.0	B2_65	1100	9	10	1484.1	0.0	1484.1	0.0
B1_07	140	11	11	2413.4	0.0	2413.4	0.0	B2_65	1100	9	11	2990.4	747.6	2242.8	0.0
B1_07	140	11	12	202.2	0.0	202.2	0.0	B2_65	1100	9	12	645.7	0.0	645.7	0.0
B1_07	140	11	13	2954.4	2215.8	738.6	0.0	B2_65	1100	9	13	268.1	0.0	268.1	0.0
B1_07	140	11	14	4425.7	0.0	4425.7	0.0	B2_65	1100	9	14	698.4	0.0	698.4	0.0
B1_07	140	11	15	11411.7	2852.9	8558.8	0.0	B2_65	1100	9	15	1385.7	1039.2	346.4	0.0
B1_07	140	11	16	1986.9	0.0	1986.9	0.0	B2_65	1100	9	16	873.7	0.0	873.7	0.0
B1_07	140	11	17	5494.0	5494.0	0.0	0.0	B2_65	1100	9	17	4842.7	3632.0	1210.7	0.0
B1_07	140	11	18	2238.5	0.0	2238.5	0.0	B2_65	1100	9	18	178.5	0.0	178.5	0.0

Table B.1., cont.

B1_07	140	11	19	2758.8	2069.1	689.7	0.0	B2_65	1100	9	19	1176.6	1176.6	0.0	0.0
B1_07	140	11	20	277.6	0.0	277.6	0.0	B2_65	1100	9	20	1896.0	1896.0	0.0	0.0
B1_07	140	11	21	3567.0	0.0	3567.0	0.0	B2_65	1100	9	21	753.1	0.0	753.1	0.0
B1_07	140	11	22	3330.9	3330.9	0.0	0.0	B2_65	1100	9	22	3541.3	885.3	2656.0	0.0
B1_07	140	11	23	781.8	0.0	781.8	0.0	B2_65	1100	9	23	415.5	0.0	415.5	0.0
B1_07	140	11	24	1288.0	0.0	1288.0	0.0	B2_65	1100	9	24	588.8	0.0	588.8	0.0
B1_07	140	11	25	314.3	0.0	314.3	0.0	B2_65	1100	9	25	1592.6	0.0	1592.6	0.0
B1_07	140	11	26	940.7	0.0	940.7	0.0	B2_65	1100	9	26	845.3	0.0	845.3	0.0
B1_07	140	11	27	1938.3	0.0	1938.3	0.0	B2_65	1100	9	27	1657.4	1243.1	414.4	0.0
B1_07	140	11	28	207.4	0.0	207.4	0.0	B2_65	1100	9	28	1045.4	0.0	1045.4	0.0
B1_07	140	11	29	5779.1	4334.3	1444.8	0.0	B2_65	1100	9	29	876.9	876.9	0.0	0.0
B1_07	140	11	30	607.0	0.0	607.0	0.0	B2_65	1100	9	30	1759.1	0.0	1759.1	0.0
B1_08	160	14	1	24676.6	6169.1	18507.4	0.0	B2_68	1140	9	1	5686.9	0.0	5686.9	0.0
B1_08	160	14	2	43756.2	10939.1	32817.2	0.0	B2_68	1140	9	2	7577.6	0.0	7577.6	0.0
B1_08	160	14	3	5354.3	0.0	5354.3	0.0	B2_68	1140	9	3	1331.4	0.0	1331.4	0.0
B1_08	160	14	4	4695.8	0.0	4695.8	0.0	B2_68	1140	9	4	312.8	234.6	78.2	0.0
B1_08	160	14	5	2000.7	0.0	2000.7	0.0	B2_68	1140	9	5	3166.8	0.0	3166.8	0.0
B1_08	160	14	6	37094.2	27820.6	9273.5	0.0	B2_68	1140	9	6	651.0	0.0	651.0	0.0
B1_08	160	14	7	1555.7	1166.8	388.9	0.0	B2_68	1140	9	7	1902.8	0.0	1902.8	0.0

B1_08	160	14	8	14408.5	14408.5	0.0	0.0	B2_68	1140	9	8	839.0	0.0	839.0	0.0
B1_08	160	14	9	25970.0	0.0	25970.0	0.0	B2_68	1140	9	9	4373.4	0.0	4373.4	0.0
B1_08	160	14	10	3790.6	0.0	0.0	3790.6	B2_68	1140	9	10	294.4	0.0	294.4	0.0
B1_08	160	14	11	438.8	0.0	438.8	0.0	B2_68	1140	9	11	957.5	239.4	718.1	0.0
B1_08	160	14	12	5589.3	0.0	0.0	5589.3	B2_68	1140	9	12	628.3	0.0	628.3	0.0
B1_08	160	14	13	1377.9	0.0	1377.9	0.0	B2_68	1140	9	13	4852.2	1213.0	3639.1	0.0
B1_08	160	14	14	3087.8	2315.8	771.9	0.0	B2_68	1140	9	14	4144.8	3108.6	1036.2	0.0
B1_08	160	14	15	755.5	0.0	755.5	0.0	B2_68	1140	9	15	516.1	0.0	516.1	0.0
B1_08	160	14	16	4318.7	0.0	4318.7	0.0	B2_68	1140	9	16	1807.0	0.0	1807.0	0.0
B1_08	160	14	17	3002.9	0.0	3002.9	0.0	B2_68	1140	9	17	9010.2	0.0	9010.2	0.0
B1_08	160	14	18	3185.6	3185.6	0.0	0.0	B2_68	1140	9	18	2452.7	0.0	2452.7	0.0
B1_08	160	14	19	21371.2	5342.8	16028.4	0.0	B2_68	1140	9	19	453.5	453.5	0.0	0.0
B1_08	160	14	20	6606.2	0.0	1651.6	4954.7	B2_68	1140	9	20	1176.0	0.0	1176.0	0.0
B1_08	160	14	21	6810.0	0.0	6810.0	0.0	B2_68	1140	9	21	1485.2	0.0	1485.2	0.0
B1_08	160	14	22	2658.8	0.0	2658.8	0.0	B2_68	1140	9	22	878.5	0.0	878.5	0.0
B1_08	160	14	23	18333.1	0.0	4583.3	13749.8	B2_68	1140	9	23	1279.8	0.0	1279.8	0.0
B1_08	160	14	24	1631.7	0.0	1631.7	0.0	B2_68	1140	9	24	7640.3	5730.2	1910.1	0.0
B1_08	160	14	25	6621.9	0.0	6621.9	0.0	B2_68	1140	9	25	4872.7	1218.2	3654.5	0.0
B1_08	160	14	26	2281.8	0.0	0.0	2281.8	B2_68	1140	9	26	813.7	0.0	813.7	0.0
B1_08	160	14	27	1247.4	0.0	1247.4	0.0	B2_68	1140	9	27	12652.0	3163.0	9489.0	0.0
B1_08	160	14	28	2107.5	0.0	2107.5	0.0	B2_68	1140	9	28	4092.7	0.0	4092.7	0.0
B1_08	160	14	29	11215.3	8411.5	2803.8	0.0	B2_68	1140	9	29	921.1	0.0	921.1	0.0
B1_08	160	14	30	1307.3	0.0	1307.3	0.0	B2_68	1140	9	30	3563.4	0.0	3563.4	0.0
B1_09	180	11	1	23633.1	17724.8	5908.3	0.0	B3_79	20	5	1	1542.1	0.0	1542.1	0.0
B1_09	180	11	2	4684.4	0.0	4684.4	0.0	B3_79	20	5	2	2776.2	0.0	2776.2	0.0
B1_09	180	11	3	4501.2	4501.2	0.0	0.0	B3_79	20	5	3	1077.1	0.0	1077.1	0.0
B1_09	180	11	4	16048.4	16048.4	0.0	0.0	B3_79	20	5	4	1751.8	0.0	1751.8	0.0
B1_09	180	11	5	4026.8	0.0	1006.7	3020.1	B3_79	20	5	5	115.5	0.0	0.0	115.5
B1_09	180	11	6	1851.9	0.0	1851.9	0.0	B3_79	20	5	6	241.1	0.0	241.1	0.0
B1_09	180	11	7	10770.6	10770.6	0.0	0.0	B3_79	20	5	7	53.3	0.0	53.3	0.0
B1_09	180	11	8	158.8	0.0	0.0	158.8	B3_79	20	5	8	16795.0	16795.0	0.0	0.0
B1_09	180	11	9	4246.3	0.0	4246.3	0.0	B3_79	20	5	9	1551.6	0.0	1551.6	0.0
B1_09	180	11	10	5106.0	5106.0	0.0	0.0	B3_79	20	5	10	3088.4	0.0	3088.4	0.0
B1_09	180	11	11	1773.2	1329.9	443.3	0.0	B3_79	20	5	11	10863.5	8147.6	2715.9	0.0
B1_09	180	11	12	13095.9	13095.9	0.0	0.0	B3_79	20	5	12	265.4	265.4	0.0	0.0
B1_09	180	11	13	205.1	0.0	0.0	205.1	B3_79	20	5	13	989.4	989.4	0.0	0.0
B1_09	180	11	14	7337.7	0.0	7337.7	0.0	B3_79	20	5	14	444.3	444.3	0.0	0.0
B1_09	180	11	15	1019.0	0.0	0.0	1019.0	B3_79	20	5	15	1366.8	341.7	1025.1	0.0
B1_09	180	11	16	2226.7	2226.7	0.0	0.0	B3_79	20	5	16	1975.2	493.8	1481.4	0.0
B1_09	180	11	17	1613.9	0.0	1613.9	0.0	B3_79	20	5	17	3530.9	0.0	3530.9	0.0
B1_09	180	11	18	1263.4	0.0	1263.4	0.0	B3_79	20	5	18	377.4	377.4	0.0	0.0
B1_09	180	11	19	4631.1	3473.3	1157.8	0.0	B3_79	20	5	19	440.8	440.8	0.0	0.0
B1_09	180	11	20	1262.0	315.5	946.5	0.0	B3_79	20	5	20	7962.3	7962.3	0.0	0.0
B1_09	180	11	21	3222.3	0.0	3222.3	0.0	B3_79	20	5	21	3114.4	3114.4	0.0	0.0
B1_09	180	11	22	4527.1	3395.3	0.0	1131.8	B3_79	20	5	22	252.4	252.4	0.0	0.0
B1_09	180	11	23	6793.1	0.0	6793.1	0.0	B3_79	20	5	23	3109.7	3109.7	0.0	0.0
B1_09	180	11	24	1467.6	0.0	1467.6	0.0	B3_79	20	5	24	885.1	885.1	0.0	0.0
B1_09	180	11	25	1285.4	0.0	1285.4	0.0	B3_79	20	5	25	17518.9	17518.9	0.0	0.0
B1_09	180	11	26	4156.7	0.0	4156.7	0.0	B3_79	20	5	26	2515.5	2515.5	0.0	0.0
B1_09	180	11	27	1978.8	1484.1	494.7	0.0	B3_79	20	5	27	5430.9	1357.7	4073.1	0.0
B1_09	180	11	28	5583.0	0.0	5583.0	0.0	B3_79	20	5	28	1538.0	384.5	1153.5	0.0

Table B.1., cont.

B1_09	180	11	29	3481.2	0.0	3481.2	0.0	B3_79	20	5	29	6943.4	5207.5	1735.8	0.0
B1_09	180	11	30	2330.3	2330.3	0.0	0.0	B3_79	20	5	30	305.7	0.0	305.7	0.0
B1_10	200	6	1	1595.9	1196.9	399.0	0.0	B3_80	40	6	1	6515.4	0.0	6515.4	0.0
B1_10	200	6	2	10217.6	7663.2	2554.4	0.0	B3_80	40	6	2	1281.4	1281.4	0.0	0.0
B1_10	200	6	3	1418.1	354.5	1063.6	0.0	B3_80	40	6	3	8878.0	0.0	8878.0	0.0
B1_10	200	6	4	5120.6	0.0	5120.6	0.0	B3_80	40	6	4	1155.5	866.6	288.9	0.0
B1_10	200	6	5	2348.8	0.0	2348.8	0.0	B3_80	40	6	5	1645.3	0.0	1645.3	0.0
B1_10	200	6	6	916.4	687.3	229.1	0.0	B3_80	40	6	6	1169.7	1169.7	0.0	0.0
B1_10	200	6	7	16511.5	12383.6	4127.9	0.0	B3_80	40	6	7	1151.3	1151.3	0.0	0.0
B1_10	200	6	8	1353.3	0.0	0.0	1353.3	B3_80	40	6	8	526.1	0.0	526.1	0.0
B1_10	200	6	9	9409.8	7057.4	2352.5	0.0	B3_80	40	6	9	1844.9	0.0	1844.9	0.0
B1_10	200	6	10	1414.1	1414.1	0.0	0.0	B3_80	40	6	10	4325.5	1081.4	3244.1	0.0
B1_10	200	6	11	6346.2	0.0	6346.2	0.0	B3_80	40	6	11	2401.1	2401.1	0.0	0.0
B1_10	200	6	12	1711.2	1711.2	0.0	0.0	B3_80	40	6	12	5600.5	0.0	5600.5	0.0
B1_10	200	6	13	774.3	0.0	0.0	774.3	B3_80	40	6	13	2546.9	0.0	2546.9	0.0
B1_10	200	6	14	1547.7	0.0	1547.7	0.0	B3_80	40	6	14	641.5	0.0	641.5	0.0
B1_10	200	6	15	4948.2	3711.1	1237.0	0.0	B3_80	40	6	15	410.8	0.0	410.8	0.0
B1_10	200	6	16	1675.9	419.0	1256.9	0.0	B3_80	40	6	16	508.8	0.0	0.0	508.8
B1_10	200	6	17	1924.3	0.0	1924.3	0.0	B3_80	40	6	17	1393.0	0.0	1393.0	0.0
B1_10	200	6	18	6772.4	6772.4	0.0	0.0	B3_80	40	6	18	2007.6	0.0	2007.6	0.0
B1_10	200	6	19	296.2	0.0	0.0	296.2	B3_80	40	6	19	2031.3	0.0	2031.3	0.0
B1_10	200	6	20	1764.4	0.0	1764.4	0.0	B3_80	40	6	20	150.1	150.1	0.0	0.0
B1_10	200	6	21	7225.9	0.0	7225.9	0.0	B3_80	40	6	21	2717.6	679.4	2038.2	0.0
B1_10	200	6	22	3322.3	0.0	3322.3	0.0	B3_80	40	6	22	625.7	0.0	625.7	0.0
B1_10	200	6	23	1402.0	0.0	0.0	1402.0	B3_80	40	6	23	439.8	439.8	0.0	0.0
B1_10	200	6	24	13927.7	0.0	13927.7	0.0	B3_80	40	6	24	1674.8	0.0	1674.8	0.0

B1_10	200	6	25	416.4	0.0	416.4	0.0	B3_80	40	6	25	605.1	0.0	605.1	0.0
B1_10	200	6	26	16551.7	12413.8	4137.9	0.0	B3_80	40	6	26	2844.0	2133.0	0.0	0.0
B1_10	200	6	27	1102.2	0.0	0.0	1102.2	B3_80	40	6	27	944.3	0.0	944.3	0.0
B1_10	200	6	28	3009.1	0.0	3009.1	0.0	B3_80	40	6	28	1727.5	0.0	1727.5	0.0
B1_10	200	6	29	3124.4	0.0	3124.4	0.0	B3_80	40	6	29	853.7	0.0	853.7	0.0
B1_10	200	6	30	496.4	124.1	372.3	0.0	B3_80	40	6	30	1564.2	1173.1	391.0	0.0
B1_11	220	13	1	1203.2	1203.2	0.0	0.0	B3_81	60	7	1	7291.1	5468.3	1822.8	0.0
B1_11	220	13	2	4918.3	0.0	0.0	0.0	B3_81	60	7	2	449.8	0.0	0.0	449.8
B1_11	220	13	3	2726.8	2045.1	681.7	0.0	B3_81	60	7	3	105.3	105.3	0.0	0.0
B1_11	220	13	4	3685.6	2764.2	921.4	0.0	B3_81	60	7	4	335.0	0.0	0.0	335.0
B1_11	220	13	5	4224.4	3168.3	1056.1	0.0	B3_81	60	7	5	650.4	650.4	0.0	0.0
B1_11	220	13	6	2987.7	2987.7	0.0	0.0	B3_81	60	7	6	196.5	196.5	0.0	0.0
B1_11	220	13	7	11832.8	8874.6	2958.2	0.0	B3_81	60	7	7	142.7	0.0	0.0	142.7
B1_11	220	13	8	2994.4	2994.4	0.0	0.0	B3_81	60	7	8	992.8	0.0	744.6	248.2
B1_11	220	13	9	428.5	0.0	0.0	428.5	B3_81	60	7	9	133.8	133.8	0.0	0.0
B1_11	220	13	10	6730.9	1682.7	5048.2	0.0	B3_81	60	7	10	388.2	388.2	0.0	0.0
B1_11	220	13	11	1965.4	0.0	1965.4	0.0	B3_81	60	7	11	416.6	0.0	416.6	0.0
B1_11	220	13	12	480.7	480.7	0.0	0.0	B3_81	60	7	12	342.3	0.0	342.3	0.0
B1_11	220	13	13	3225.8	0.0	3225.8	0.0	B3_81	60	7	13	467.2	467.2	0.0	0.0
B1_11	220	13	14	10885.6	0.0	10885.6	0.0	B3_81	60	7	14	520.3	520.3	0.0	0.0
B1_11	220	13	15	4721.7	4721.7	0.0	0.0	B3_81	60	7	15	191.7	191.7	0.0	0.0
B1_11	220	13	16	11175.5	2793.9	8381.6	0.0	B3_81	60	7	16	2455.3	0.0	2455.3	0.0
B1_11	220	13	17	13926.0	10444.5	3481.5	0.0	B3_81	60	7	17	302.3	302.3	0.0	0.0
B1_11	220	13	18	663.0	0.0	663.0	0.0	B3_81	60	7	18	447.1	447.1	0.0	0.0
B1_11	220	13	19	1699.1	0.0	1699.1	0.0	B3_81	60	7	19	794.2	0.0	0.0	794.2
B1_11	220	13	20	1632.1	1224.1	408.0	0.0	B3_81	60	7	20	545.1	545.1	0.0	0.0
B1_11	220	13	21	14475.1	0.0	14475.1	0.0	B3_81	60	7	21	359.2	359.2	0.0	0.0
B1_11	220	13	22	6896.6	5172.5	1724.2	0.0	B3_81	60	7	22	227.5	227.5	0.0	0.0
B1_11	220	13	23	3063.2	3063.2	0.0	0.0	B3_81	60	7	23	909.0	0.0	681.8	227.3
B1_11	220	13	24	2291.1	1718.3	572.8	0.0	B3_81	60	7	24	335.5	335.5	0.0	0.0
B1_11	220	13	25	658.6	0.0	658.6	0.0	B3_81	60	7	25	404.5	0.0	404.5	0.0
B1_11	220	13	26	4917.4	3688.0	1229.3	0.0	B3_81	60	7	26	536.7	536.7	0.0	0.0
B1_11	220	13	27	1933.7	1933.7	0.0	0.0	B3_81	60	7	27	1045.4	1045.4	0.0	0.0
B1_11	220	13	28	155.0	0.0	0.0	155.0	B3_81	60	7	28	101.1	101.1	0.0	0.0
B1_11	220	13	29	20038.0	15028.5	5009.5	0.0	B3_81	60	7	29	1333.5	1333.5	0.0	0.0
B1_11	220	13	30	251.5	0.0	251.5	0.0	B3_81	60	7	30	557.2	0.0	557.2	0.0
B1_12	240	13	1	6842.6	0.0	1710.6	5131.9	B3_82	80	6	1	2048.2	0.0	2048.2	0.0
B1_12	240	13	2	19690.4	19690.4	0.0	0.0	B3_82	80	6	2	2143.1	0.0	2143.1	0.0
B1_12	240	13	3	2419.4	0.0	0.0	2419.4	B3_82	80	6	3	1878.6	0.0	1878.6	0.0
B1_12	240	13	4	4869.6	0.0	0.0	4869.6	B3_82	80	6	4	877.9	877.9	0.0	0.0
B1_12	240	13	5	4787.3	3590.5	1196.8	0.0	B3_82	80	6	5	8108.6	2027.2	6081.5	0.0
B1_12	240	13	6	4454.9	0.0	4454.9	0.0	B3_82	80	6	6	2430.5	0.0	2430.5	0.0
B1_12	240	13	7	5141.2	5141.2	0.0	0.0	B3_82	80	6	7	962.7	0.0	0.0	962.7
B1_12	240	13	8	395.4	0.0	395.4	0.0	B3_82	80	6	8	4420.2	0.0	4420.2	0.0

Table B.1., cont.

B1_12	240	13	9	7695.0	1923.8	0.0	5771.3	B3_82	80	6	9	867.8	0.0	867.8	0.0
B1_12	240	13	10	3182.5	0.0	3182.5	0.0	B3_82	80	6	10	227.2	0.0	227.2	0.0
B1_12	240	13	11	16091.5	4022.9	12068.6	0.0	B3_82	80	6	11	498.9	498.9	0.0	0.0
B1_12	240	13	12	5216.3	5216.3	0.0	0.0	B3_82	80	6	12	600.0	0.0	600.0	0.0
B1_12	240	13	13	12642.8	12642.8	0.0	0.0	B3_82	80	6	13	1484.5	0.0	1484.5	0.0
B1_12	240	13	14	4388.8	4388.8	0.0	0.0	B3_82	80	6	14	392.3	0.0	0.0	392.3
B1_12	240	13	15	4947.3	0.0	1236.8	3710.5	B3_82	80	6	15	525.7	525.7	0.0	0.0
B1_12	240	13	16	620.1	0.0	620.1	0.0	B3_82	80	6	16	570.4	0.0	570.4	0.0
B1_12	240	13	17	6377.9	6377.9	0.0	0.0	B3_82	80	6	17	113.9	0.0	0.0	113.9
B1_12	240	13	18	12910.0	3227.5	9682.5	0.0	B3_82	80	6	18	248.4	248.4	0.0	0.0
B1_12	240	13	19	3598.9	0.0	899.7	2699.2	B3_82	80	6	19	1115.6	0.0	1115.6	0.0
B1_12	240	13	20	6990.9	0.0	0.0	6990.9	B3_82	80	6	20	2522.6	0.0	2522.6	0.0
B1_12	240	13	21	5906.1	0.0	5906.1	0.0	B3_82	80	6	21	129.5	0.0	0.0	129.5
B1_12	240	13	22	11945.8	8959.3	2986.4	0.0	B3_82	80	6	22	4644.5	3483.4	1161.1	0.0
B1_12	240	13	23	7666.9	5750.2	1916.7	0.0	B3_82	80	6	23	786.9	0.0	0.0	786.9
B1_12	240	13	24	10490.2	7867.6	2622.5	0.0	B3_82	80	6	24	146.8	146.8	0.0	0.0
B1_12	240	13	25	10653.2	0.0	0.0	10653.2	B3_82	80	6	25	791.4	0.0	791.4	0.0
B1_12	240	13	26	446.3	0.0	0.0	446.3	B3_82	80	6	26	2393.1	0.0	2393.1	0.0
B1_12	240	13	27	6215.7	0.0	6215.7	0.0	B3_82	80	6	27	4092.5	0.0	4092.5	0.0
B1_12	240	13	28	2274.2	1705.6	568.5	0.0	B3_82	80	6	28	1170.3	1170.3	0.0	0.0
B1_12	240	13	29	1528.0	0.0	0.0	1528.0	B3_82	80	6	29	999.0	0.0	999.0	0.0
B1_12	240	13	30	1018.2	0.0	1018.2	0.0	B3_82	80	6	30	1047.0	0.0	1047.0	0.0
B1_13	260	14	1	542.0	0.0	542.0	0.0	B3_83	100	7	1	820.9	0.0	0.0	820.9
B1_13	260	14	2	1809.2	0.0	1809.2	0.0	B3_83	100	7	2	1493.2	1493.2	0.0	0.0
B1_13	260	14	3	1075.4	0.0	1075.4	0.0	B3_83	100	7	3	1335.7	1001.8	333.9	0.0
B1_13	260	14	4	786.1	0.0	786.1	0.0	B3_83	100	7	4	500.3	0.0	500.3	0.0
B1_13	260	14	5	6734.9	0.0	6734.9	0.0	B3_83	100	7	5	6309.2	0.0	6309.2	0.0
B1_13	260	14	6	652.7	652.7	0.0	0.0	B3_83	100	7	6	1592.1	0.0	1592.1	0.0
B1_13	260	14	7	6278.7	0.0	0.0	6278.7	B3_83	100	7	7	221.1	0.0	221.1	0.0
B1_13	260	14	8	298.8	0.0	0.0	298.8	B3_83	100	7	8	129.2	129.2	0.0	0.0
B1_13	260	14	9	619.2	0.0	619.2	0.0	B3_83	100	7	9	890.3	890.3	0.0	0.0
B1_13	260	14	10	1919.0	1919.0	0.0	0.0	B3_83	100	7	10	164.4	0.0	164.4	0.0
B1_13	260	14	11	2501.0	0.0	625.3	1875.8	B3_83	100	7	11	771.8	0.0	771.8	0.0

B1_13	260	14	12	2573.6	0.0	2573.6	0.0	B3_83	100	7	12	446.7	0.0	0.0	446.7
B1_13	260	14	13	506.1	379.6	126.5	0.0	B3_83	100	7	13	1531.0	1531.0	0.0	0.0
B1_13	260	14	14	286.5	0.0	0.0	286.5	B3_83	100	7	14	477.6	0.0	477.6	0.0
B1_13	260	14	15	423.7	0.0	423.7	0.0	B3_83	100	7	15	798.9	798.9	0.0	0.0
B1_13	260	14	16	2195.2	0.0	2195.2	0.0	B3_83	100	7	16	289.8	289.8	0.0	0.0
B1_13	260	14	17	453.4	0.0	453.4	0.0	B3_83	100	7	17	369.2	369.2	0.0	0.0
B1_13	260	14	18	2459.5	1844.7	614.9	0.0	B3_83	100	7	18	145.5	145.5	0.0	0.0
B1_13	260	14	19	606.1	0.0	606.1	0.0	B3_83	100	7	19	210.4	210.4	0.0	0.0
B1_13	260	14	20	2565.1	2565.1	0.0	0.0	B3_83	100	7	20	1196.5	0.0	0.0	1196.5
B1_13	260	14	21	283.2	0.0	283.2	0.0	B3_83	100	7	21	2835.2	0.0	2126.4	0.0
B1_13	260	14	22	739.4	0.0	739.4	0.0	B3_83	100	7	22	454.9	0.0	454.9	0.0
B1_13	260	14	23	219.1	219.1	0.0	0.0	B3_83	100	7	23	330.8	0.0	0.0	330.8
B1_13	260	14	24	1658.4	1658.4	0.0	0.0	B3_83	100	7	24	1386.1	0.0	1386.1	0.0
B1_13	260	14	25	350.2	350.2	0.0	0.0	B3_83	100	7	25	263.4	263.4	0.0	0.0
B1_13	260	14	26	548.1	548.1	0.0	0.0	B3_83	100	7	26	4598.0	4598.0	0.0	0.0
B1_13	260	14	27	583.9	0.0	583.9	0.0	B3_83	100	7	27	236.3	236.3	0.0	0.0
B1_13	260	14	28	139.0	0.0	0.0	139.0	B3_83	100	7	28	945.1	945.1	0.0	0.0
B1_13	260	14	29	8558.2	6418.6	2139.5	0.0	B3_83	100	7	29	739.0	739.0	0.0	0.0
B1_13	260	14	30	1436.0	0.0	1436.0	0.0	B3_83	100	7	30	511.6	511.6	0.0	0.0
B1_14	300	9	1	5021.0	3765.8	1255.3	0.0	B3_84	120	11	1	415.5	0.0	415.5	0.0
B1_14	300	9	2	22894.3	0.0	0.0	22894.3	B3_84	120	11	2	174.3	0.0	0.0	174.3
B1_14	300	9	3	4883.4	4883.4	0.0	0.0	B3_84	120	11	3	455.6	0.0	455.6	0.0
B1_14	300	9	4	424.0	0.0	0.0	424.0	B3_84	120	11	4	984.3	0.0	984.3	0.0
B1_14	300	9	5	14903.5	0.0	3725.9	11177.6	B3_84	120	11	5	385.5	385.5	0.0	0.0
B1_14	300	9	6	1147.4	0.0	1147.4	0.0	B3_84	120	11	6	1801.7	0.0	1801.7	0.0
B1_14	300	9	7	1609.3	0.0	1609.3	0.0	B3_84	120	11	7	129.0	0.0	129.0	0.0
B1_14	300	9	8	949.4	0.0	949.4	0.0	B3_84	120	11	8	83.2	83.2	0.0	0.0
B1_14	300	9	9	735.0	0.0	735.0	0.0	B3_84	120	11	9	150.6	0.0	0.0	150.6
B1_14	300	9	10	286.4	0.0	0.0	286.4	B3_84	120	11	10	191.2	0.0	0.0	191.2
B1_14	300	9	11	2690.1	0.0	2690.1	0.0	B3_84	120	11	11	959.6	0.0	959.6	0.0
B1_14	300	9	12	20839.1	15629.3	5209.8	0.0	B3_84	120	11	12	851.6	0.0	851.6	0.0
B1_14	300	9	13	193.0	0.0	0.0	193.0	B3_84	120	11	13	141.7	0.0	0.0	141.7
B1_14	300	9	14	301.6	0.0	301.6	0.0	B3_84	120	11	14	1001.2	0.0	1001.2	0.0
B1_14	300	9	15	3575.7	3575.7	0.0	0.0	B3_84	120	11	15	68.5	0.0	0.0	68.5
B1_14	300	9	16	3400.1	0.0	0.0	3400.1	B3_84	120	11	16	662.0	662.0	0.0	0.0
B1_14	300	9	17	342.7	0.0	342.7	0.0	B3_84	120	11	17	2172.0	0.0	2172.0	0.0
B1_14	300	9	18	967.7	0.0	241.9	725.8	B3_84	120	11	18	656.2	0.0	656.2	0.0

Table B.1., cont.

B1_14	300	9	19	1105.4	0.0	1105.4	0.0	B3_84	120	11	19	2032.9	0.0	2032.9	0.0
B1_14	300	9	20	9200.3	6900.2	2300.1	0.0	B3_84	120	11	20	2367.4	591.8	1775.5	0.0
B1_14	300	9	21	1449.4	0.0	0.0	1449.4	B3_84	120	11	21	2394.7	0.0	2394.7	0.0
B1_14	300	9	22	1299.3	0.0	0.0	1299.3	B3_84	120	11	22	658.3	0.0	658.3	0.0
B1_14	300	9	23	966.0	0.0	966.0	0.0	B3_84	120	11	23	2012.9	0.0	2012.9	0.0
B1_14	300	9	24	2651.7	1988.8	0.0	0.0	B3_84	120	11	24	262.8	0.0	262.8	0.0
B1_14	300	9	25	460.2	0.0	460.2	0.0	B3_84	120	11	25	2856.6	2856.6	0.0	0.0
B1_14	300	9	26	5166.7	0.0	5166.7	0.0	B3_84	120	11	26	2602.2	1951.7	650.6	0.0
B1_14	300	9	27	4201.6	0.0	4201.6	0.0	B3_84	120	11	27	608.8	0.0	608.8	0.0
B1_14	300	9	28	531.7	0.0	531.7	0.0	B3_84	120	11	28	2354.2	0.0	2354.2	0.0
B1_14	300	9	29	3951.8	2963.9	988.0	0.0	B3_84	120	11	29	7387.5	0.0	7387.5	0.0
B1_14	300	9	30	729.6	0.0	729.6	0.0	B3_84	120	11	30	2149.3	537.3	1612.0	0.0
B1_15	320	10	1	1877.8	0.0	1877.8	0.0	B3_85	140	16	1	2954.0	0.0	2954.0	0.0
B1_15	320	10	2	3065.9	0.0	3065.9	0.0	B3_85	140	16	2	1027.5	0.0	1027.5	0.0
B1_15	320	10	3	1729.8	0.0	1729.8	0.0	B3_85	140	16	3	4368.8	0.0	4368.8	0.0
B1_15	320	10	4	9605.8	7204.3	2401.4	0.0	B3_85	140	16	4	120.5	120.5	0.0	0.0
B1_15	320	10	5	1029.9	0.0	1029.9	0.0	B3_85	140	16	5	194.6	194.6	0.0	0.0
B1_15	320	10	6	610.4	610.4	0.0	0.0	B3_85	140	16	6	198.1	0.0	0.0	198.1
B1_15	320	10	7	7015.4	5261.5	1753.8	0.0	B3_85	140	16	7	373.9	0.0	0.0	373.9
B1_15	320	10	8	547.6	0.0	547.6	0.0	B3_85	140	16	8	549.1	0.0	0.0	549.1
B1_15	320	10	9	384.3	0.0	384.3	0.0	B3_85	140	16	9	842.3	0.0	842.3	0.0
B1_15	320	10	10	4070.8	0.0	4070.8	0.0	B3_85	140	16	10	1251.5	0.0	1251.5	0.0
B1_15	320	10	11	5052.3	0.0	5052.3	0.0	B3_85	140	16	11	348.5	0.0	348.5	0.0
B1_15	320	10	12	531.5	0.0	531.5	0.0	B3_85	140	16	12	148.4	0.0	148.4	0.0
B1_15	320	10	13	1398.9	1398.9	0.0	0.0	B3_85	140	16	13	365.9	365.9	0.0	0.0
B1_15	320	10	14	692.7	0.0	692.7	0.0	B3_85	140	16	14	245.9	0.0	245.9	0.0
B1_15	320	10	15	1523.6	0.0	1523.6	0.0	B3_85	140	16	15	2129.1	0.0	2129.1	0.0
B1_15	320	10	16	4453.8	0.0	4453.8	0.0	B3_85	140	16	16	3287.5	821.9	2465.7	0.0
B1_15	320	10	17	3063.8	0.0	3063.8	0.0	B3_85	140	16	17	482.4	0.0	482.4	0.0
B1_15	320	10	18	572.6	0.0	572.6	0.0	B3_85	140	16	18	2686.2	0.0	2686.2	0.0
B1_15	320	10	19	3804.8	951.2	2853.6	0.0	B3_85	140	16	19	987.2	987.2	0.0	0.0
B1_15	320	10	20	9049.2	0.0	9049.2	0.0	B3_85	140	16	20	250.4	0.0	250.4	0.0
B1_15	320	10	21	2015.2	503.8	1511.4	0.0	B3_85	140	16	21	269.3	269.3	0.0	0.0
B1_15	320	10	22	321.5	0.0	321.5	0.0	B3_85	140	16	22	100.6	0.0	0.0	100.6
B1_15	320	10	23	4185.7	3139.3	1046.4	0.0	B3_85	140	16	23	241.4	0.0	241.4	0.0
B1_15	320	10	24	776.2	776.2	0.0	0.0	B3_85	140	16	24	799.5	0.0	0.0	799.5
B1_15	320	10	25	4954.3	0.0	4954.3	0.0	B3_85	140	16	25	1675.6	0.0	1675.6	0.0
B1_15	320	10	26	2805.9	0.0	2805.9	0.0	B3_85	140	16	26	295.2	295.2	0.0	0.0
B1_15	320	10	27	2434.3	0.0	2434.3	0.0	B3_85	140	16	27	767.1	0.0	767.1	0.0
B1_15	320	10	28	283.8	0.0	283.8	0.0	B3_85	140	16	28	1113.6	0.0	1113.6	0.0

B1_15	320	10	29	664.3	166.1	498.2	0.0	B3_85	140	16	29	434.6	0.0	434.6	0.0
B1_15	320	10	30	295.7	0.0	295.7	0.0	B3_85	140	16	30	3026.2	0.0	3026.2	0.0
B1_17	360	12	1	6606.0	4954.5	1651.5	0.0	B3_86	160	7	1	1787.0	0.0	1787.0	0.0
B1_17	360	12	2	1307.8	0.0	1307.8	0.0	B3_86	160	7	2	1660.6	0.0	1660.6	0.0
B1_17	360	12	3	3801.8	2851.3	950.4	0.0	B3_86	160	7	3	1422.5	0.0	1422.5	0.0
B1_17	360	12	4	82.6	0.0	0.0	82.6	B3_86	160	7	4	5584.7	1396.2	4188.6	0.0
B1_17	360	12	5	213.1	0.0	213.1	0.0	B3_86	160	7	5	2222.5	0.0	555.6	1666.9
B1_17	360	12	6	289.7	0.0	0.0	289.7	B3_86	160	7	6	2124.0	1593.0	531.0	0.0
B1_17	360	12	7	1179.3	0.0	1179.3	0.0	B3_86	160	7	7	443.5	443.5	0.0	0.0
B1_17	360	12	8	10045.8	7534.4	2511.5	0.0	B3_86	160	7	8	1819.1	0.0	1819.1	0.0
B1_17	360	12	9	2099.8	524.9	1574.8	0.0	B3_86	160	7	9	2070.8	0.0	2070.8	0.0
B1_17	360	12	10	216.6	0.0	216.6	0.0	B3_86	160	7	10	2094.0	0.0	1570.5	523.5
B1_17	360	12	11	2334.7	0.0	2334.7	0.0	B3_86	160	7	11	2320.0	1740.0	580.0	0.0
B1_17	360	12	12	158.8	0.0	158.8	0.0	B3_86	160	7	12	800.0	0.0	800.0	0.0
B1_17	360	12	13	744.2	744.2	0.0	0.0	B3_86	160	7	13	7356.4	5517.3	1839.1	0.0
B1_17	360	12	14	1278.9	0.0	1278.9	0.0	B3_86	160	7	14	5311.4	3983.6	1327.9	0.0
B1_17	360	12	15	893.1	0.0	893.1	0.0	B3_86	160	7	15	4090.6	0.0	4090.6	0.0
B1_17	360	12	16	4308.6	0.0	4308.6	0.0	B3_86	160	7	16	1478.9	0.0	1478.9	0.0
B1_17	360	12	17	107.5	0.0	107.5	0.0	B3_86	160	7	17	2366.3	0.0	2366.3	0.0
B1_17	360	12	18	1274.9	0.0	1274.9	0.0	B3_86	160	7	18	644.6	0.0	483.5	161.2
B1_17	360	12	19	1147.5	0.0	286.9	860.6	B3_86	160	7	19	1930.8	0.0	1930.8	0.0
B1_17	360	12	20	2280.0	0.0	570.0	1710.0	B3_86	160	7	20	296.0	0.0	296.0	0.0
B1_17	360	12	21	2692.7	0.0	2692.7	0.0	B3_86	160	7	21	182.2	0.0	0.0	182.2
B1_17	360	12	22	715.4	0.0	715.4	0.0	B3_86	160	7	22	1971.3	0.0	1971.3	0.0
B1_17	360	12	23	423.6	0.0	423.6	0.0	B3_86	160	7	23	3391.7	0.0	3391.7	0.0
B1_17	360	12	24	8291.5	6218.6	2072.9	0.0	B3_86	160	7	24	691.0	0.0	691.0	0.0
B1_17	360	12	25	415.7	0.0	415.7	0.0	B3_86	160	7	25	1362.5	340.6	1021.9	0.0
B1_17	360	12	26	2260.6	0.0	2260.6	0.0	B3_86	160	7	26	707.3	0.0	707.3	0.0
B1_17	360	12	27	325.6	0.0	325.6	0.0	B3_86	160	7	27	1752.7	1752.7	0.0	0.0
B1_17	360	12	28	1707.5	0.0	1707.5	0.0	B3_86	160	7	28	2649.6	0.0	662.4	1987.2

Table B.1., cont.

B1_17	360	12	29	271.3	0.0	271.3	0.0	B3_86	160	7	29	476.6	476.6	0.0	0.0
B1_17	360	12	30	6136.0	1534.0	4602.0	0.0	B3_86	160	7	30	2993.6	0.0	2993.6	0.0
B1_18	380	9	1	7897.9	1974.5	5923.4	0.0	B3_87	180	7	1	444.3	0.0	444.3	0.0
B1_18	380	9	2	1931.0	482.8	1448.3	0.0	B3_87	180	7	2	187.5	0.0	187.5	0.0
B1_18	380	9	3	2162.5	1621.8	540.6	0.0	B3_87	180	7	3	390.1	0.0	390.1	0.0
B1_18	380	9	4	1743.4	1743.4	0.0	0.0	B3_87	180	7	4	422.5	316.9	105.6	0.0
B1_18	380	9	5	319.5	0.0	0.0	319.5	B3_87	180	7	5	378.4	0.0	378.4	0.0
B1_18	380	9	6	9906.2	2476.5	7429.6	0.0	B3_87	180	7	6	588.8	0.0	588.8	0.0
B1_18	380	9	7	57.6	57.6	0.0	0.0	B3_87	180	7	7	813.7	0.0	610.3	203.4
B1_18	380	9	8	3017.2	0.0	3017.2	0.0	B3_87	180	7	8	149.0	149.0	0.0	0.0
B1_18	380	9	9	72.8	72.8	0.0	0.0	B3_87	180	7	9	237.8	237.8	0.0	0.0
B1_18	380	9	10	144.8	144.8	0.0	0.0	B3_87	180	7	10	412.4	0.0	0.0	412.4
B1_18	380	9	11	4307.9	3230.9	1077.0	0.0	B3_87	180	7	11	717.2	0.0	717.2	0.0
B1_18	380	9	12	9217.7	2304.4	6913.3	0.0	B3_87	180	7	12	613.9	0.0	613.9	0.0
B1_18	380	9	13	3018.5	0.0	3018.5	0.0	B3_87	180	7	13	598.3	0.0	598.3	0.0
B1_18	380	9	14	4160.9	0.0	4160.9	0.0	B3_87	180	7	14	452.1	339.0	113.0	0.0
B1_18	380	9	15	202.4	202.4	0.0	0.0	B3_87	180	7	15	817.1	0.0	817.1	0.0
B1_18	380	9	16	302.9	0.0	302.9	0.0	B3_87	180	7	16	2513.1	0.0	0.0	0.0
B1_18	380	9	17	1726.4	0.0	1726.4	0.0	B3_87	180	7	17	654.1	0.0	654.1	0.0
B1_18	380	9	18	4162.3	0.0	4162.3	0.0	B3_87	180	7	18	414.1	414.1	0.0	0.0
B1_18	380	9	19	97.9	0.0	97.9	0.0	B3_87	180	7	19	903.6	0.0	903.6	0.0
B1_18	380	9	20	159.1	0.0	159.1	0.0	B3_87	180	7	20	258.4	258.4	0.0	0.0
B1_18	380	9	21	678.2	0.0	678.2	0.0	B3_87	180	7	21	976.7	0.0	976.7	0.0
B1_18	380	9	22	403.9	0.0	403.9	0.0	B3_87	180	7	22	360.5	360.5	0.0	0.0
B1_18	380	9	23	743.0	0.0	743.0	0.0	B3_87	180	7	23	1124.6	0.0	1124.6	0.0
B1_18	380	9	24	743.0	0.0	743.0	0.0	B3_87	180	7	24	276.3	0.0	207.2	0.0
B1_18	380	9	25	4315.1	1078.8	3236.3	0.0	B3_87	180	7	25	97.1	0.0	0.0	97.1
B1_18	380	9	26	107.2	0.0	107.2	0.0	B3_87	180	7	26	308.1	0.0	308.1	0.0
B1_18	380	9	27	245.3	0.0	245.3	0.0	B3_87	180	7	27	186.4	0.0	0.0	186.4
B1_18	380	9	28	7335.8	1834.0	5501.9	0.0	B3_87	180	7	28	228.8	0.0	0.0	228.8
B1_18	380	9	29	248.0	0.0	248.0	0.0	B3_87	180	7	29	447.0	0.0	447.0	0.0
B1_18	380	9	30	64.3	0.0	64.3	0.0	B3_87	180	7	30	1029.1	0.0	1029.1	0.0
B1_19	400	9	1	314.1	0.0	314.1	0.0	B3_89	220	14	1	118.5	0.0	118.5	0.0
B1_19	400	9	2	6160.3	6160.3	0.0	0.0	B3_89	220	14	2	1242.9	0.0	1242.9	0.0
B1_19	400	9	3	307.8	0.0	307.8	0.0	B3_89	220	14	3	435.6	0.0	435.6	0.0
B1_19	400	9	4	2647.7	0.0	2647.7	0.0	B3_89	220	14	4	141.7	0.0	0.0	141.7
B1_19	400	9	5	3933.5	0.0	3933.5	0.0	B3_89	220	14	5	397.1	0.0	0.0	397.1
B1_19	400	9	6	174.3	0.0	174.3	0.0	B3_89	220	14	6	335.0	0.0	335.0	0.0
B1_19	400	9	7	1625.0	0.0	1625.0	0.0	B3_89	220	14	7	208.6	208.6	0.0	0.0
B1_19	400	9	8	5017.4	3763.1	1254.4	0.0	B3_89	220	14	8	774.2	0.0	774.2	0.0
B1_19	400	9	9	11868.0	8901.0	2967.0	0.0	B3_89	220	14	9	3051.0	0.0	3051.0	0.0
B1_19	400	9	10	775.2	0.0	775.2	0.0	B3_89	220	14	10	162.2	0.0	0.0	162.2
B1_19	400	9	11	152.8	0.0	152.8	0.0	B3_89	220	14	11	211.7	0.0	0.0	211.7
B1_19	400	9	12	377.5	0.0	377.5	0.0	B3_89	220	14	12	386.6	0.0	386.6	0.0
B1_19	400	9	13	4229.3	1057.3	3172.0	0.0	B3_89	220	14	13	2763.4	0.0	2763.4	0.0
B1_19	400	9	14	2551.2	0.0	2551.2	0.0	B3_89	220	14	14	424.0	0.0	424.0	0.0
B1_19	400	9	15	1159.4	0.0	1159.4	0.0	B3_89	220	14	15	357.1	357.1	0.0	0.0

B1_19	400	9	16	588.0	0.0	588.0	0.0	B3_89	220	14	16	1161.3	0.0	1161.3	0.0
B1_19	400	9	17	340.5	0.0	340.5	0.0	B3_89	220	14	17	691.5	0.0	518.6	172.9
B1_19	400	9	18	126.4	0.0	126.4	0.0	B3_89	220	14	18	566.2	0.0	566.2	0.0
B1_19	400	9	19	1060.7	0.0	1060.7	0.0	B3_89	220	14	19	746.3	0.0	746.3	0.0
B1_19	400	9	20	307.4	0.0	307.4	0.0	B3_89	220	14	20	426.6	0.0	426.6	0.0
B1_19	400	9	21	1653.6	0.0	1653.6	0.0	B3_89	220	14	21	9549.5	7162.1	2387.4	0.0
B1_19	400	9	22	5088.0	1272.0	3816.0	0.0	B3_89	220	14	22	133.3	0.0	133.3	0.0
B1_19	400	9	23	4678.8	0.0	4678.8	0.0	B3_89	220	14	23	526.1	0.0	526.1	0.0
B1_19	400	9	24	440.5	0.0	440.5	0.0	B3_89	220	14	24	3147.9	787.0	2360.9	0.0
B1_19	400	9	25	2697.7	0.0	2697.7	0.0	B3_89	220	14	25	6529.6	0.0	6529.6	0.0
B1_19	400	9	26	3244.1	2433.1	811.0	0.0	B3_89	220	14	26	12197.0	12197.0	0.0	0.0
B1_19	400	9	27	2968.5	0.0	2968.5	0.0	B3_89	220	14	27	460.8	0.0	460.8	0.0
B1_19	400	9	28	1936.4	0.0	1452.3	484.1	B3_89	220	14	28	457.1	0.0	457.1	0.0
B1_19	400	9	29	4166.3	1041.6	3124.7	0.0	B3_89	220	14	29	487.2	487.2	0.0	0.0
B1_19	400	9	30	187.2	0.0	187.2	0.0	B3_89	220	14	30	909.6	0.0	909.6	0.0
B1_20	420	4	1	1044.3	0.0	0.0	1044.3	B3_90	240	14	1	1058.7	0.0	1058.7	0.0
B1_20	420	4	2	454.3	113.6	340.7	0.0	B3_90	240	14	2	2888.7	722.2	2166.5	0.0
B1_20	420	4	3	544.8	0.0	544.8	0.0	B3_90	240	14	3	1044.2	0.0	1044.2	0.0
B1_20	420	4	4	309.6	0.0	0.0	309.6	B3_90	240	14	4	149.0	0.0	149.0	0.0
B1_20	420	4	5	94.7	0.0	94.7	0.0	B3_90	240	14	5	1751.3	0.0	1751.3	0.0
B1_20	420	4	6	605.6	0.0	605.6	0.0	B3_90	240	14	6	281.8	0.0	281.8	0.0
B1_20	420	4	7	991.5	0.0	991.5	0.0	B3_90	240	14	7	4660.1	0.0	4660.1	0.0
B1_20	420	4	8	583.0	0.0	0.0	583.0	B3_90	240	14	8	300.8	0.0	300.8	0.0

Table B.1., cont.

B1_20	420	4	9	564.6	0.0	564.6	0.0	B3_90	240	14	9	1168.1	292.0	876.1	0.0
B1_20	420	4	10	1439.7	359.9	1079.8	0.0	B3_90	240	14	10	111.6	0.0	111.6	0.0
B1_20	420	4	11	190.4	0.0	0.0	190.4	B3_90	240	14	11	98.2	0.0	98.2	0.0
B1_20	420	4	12	299.7	0.0	299.7	0.0	B3_90	240	14	12	197.0	0.0	197.0	0.0
B1_20	420	4	13	597.6	0.0	597.6	0.0	B3_90	240	14	13	963.8	0.0	963.8	0.0
B1_20	420	4	14	181.4	0.0	0.0	181.4	B3_90	240	14	14	856.1	0.0	856.1	0.0
B1_20	420	4	15	289.4	0.0	289.4	0.0	B3_90	240	14	15	324.3	0.0	324.3	0.0
B1_20	420	4	16	1095.2	0.0	1095.2	0.0	B3_90	240	14	16	288.5	0.0	288.5	0.0
B1_20	420	4	17	605.6	0.0	605.6	0.0	B3_90	240	14	17	154.0	0.0	154.0	0.0
B1_20	420	4	18	287.5	0.0	287.5	0.0	B3_90	240	14	18	279.6	279.6	0.0	0.0
B1_20	420	4	19	290.3	0.0	290.3	0.0	B3_90	240	14	19	666.9	666.9	0.0	0.0
B1_20	420	4	20	409.1	0.0	409.1	0.0	B3_90	240	14	20	552.0	0.0	552.0	0.0
B1_20	420	4	21	522.6	130.7	392.0	0.0	B3_90	240	14	21	154.6	0.0	115.9	38.6
B1_20	420	4	22	239.9	0.0	0.0	239.9	B3_90	240	14	22	218.8	164.1	54.7	0.0
B1_20	420	4	23	257.8	0.0	257.8	0.0	B3_90	240	14	23	420.3	0.0	420.3	0.0
B1_20	420	4	24	154.6	0.0	0.0	154.6	B3_90	240	14	24	89.9	89.9	0.0	0.0
B1_20	420	4	25	504.7	0.0	504.7	0.0	B3_90	240	14	25	552.5	0.0	552.5	0.0
B1_20	420	4	26	292.7	219.5	73.2	0.0	B3_90	240	14	26	439.8	439.8	0.0	0.0
B1_20	420	4	27	54.2	0.0	54.2	0.0	B3_90	240	14	27	593.3	0.0	593.3	0.0
B1_20	420	4	28	271.5	0.0	271.5	0.0	B3_90	240	14	28	414.1	414.1	0.0	0.0
B1_20	420	4	29	866.2	216.5	649.6	0.0	B3_90	240	14	29	975.0	975.0	0.0	0.0
B1_20	420	4	30	83.9	0.0	83.9	0.0	B3_90	240	14	30	1546.5	0.0	386.6	1159.9
B1_21	440	3	1	45.6	45.6	0.0	0.0	B3_91	260	14	1	13778.0	3444.5	10333.5	0.0
B1_21	440	3	2	1575.8	0.0	1575.8	0.0	B3_91	260	14	2	7962.1	0.0	7962.1	0.0
B1_21	440	3	3	1695.6	1271.7	423.9	0.0	B3_91	260	14	3	6407.4	1601.8	4805.5	0.0
B1_21	440	3	4	123.3	0.0	123.3	0.0	B3_91	260	14	4	177.0	0.0	0.0	177.0
B1_21	440	3	5	117.1	117.1	0.0	0.0	B3_91	260	14	5	617.8	0.0	617.8	0.0
B1_21	440	3	6	147.0	0.0	147.0	0.0	B3_91	260	14	6	144.3	0.0	144.3	0.0
B1_21	440	3	7	95.6	95.6	0.0	0.0	B3_91	260	14	7	5221.3	5221.3	0.0	0.0
B1_21	440	3	8	120.6	120.6	0.0	0.0	B3_91	260	14	8	371.3	0.0	371.3	0.0
B1_21	440	3	9	83.6	0.0	0.0	83.6	B3_91	260	14	9	199.1	199.1	0.0	0.0
B1_21	440	3	10	111.3	0.0	0.0	111.3	B3_91	260	14	10	27349.6	20512.2	6837.4	0.0
B1_21	440	3	11	62.6	62.6	0.0	0.0	B3_91	260	14	11	924.8	924.8	0.0	0.0
B1_21	440	3	12	139.8	139.8	0.0	0.0	B3_91	260	14	12	302.8	302.8	0.0	0.0
B1_21	440	3	13	263.6	0.0	263.6	0.0	B3_91	260	14	13	234.4	234.4	0.0	0.0
B1_21	440	3	14	566.5	0.0	566.5	0.0	B3_91	260	14	14	1133.9	0.0	1133.9	0.0
B1_21	440	3	15	127.3	127.3	0.0	0.0	B3_91	260	14	15	882.7	220.7	662.0	0.0
B1_21	440	3	16	1513.7	378.4	1135.3	0.0	B3_91	260	14	16	1239.8	0.0	1239.8	0.0
B1_21	440	3	17	167.6	0.0	167.6	0.0	B3_91	260	14	17	225.9	225.9	0.0	0.0
B1_21	440	3	18	844.0	844.0	0.0	0.0	B3_91	260	14	18	1244.0	0.0	1244.0	0.0
B1_21	440	3	19	351.6	0.0	351.6	0.0	B3_91	260	14	19	3568.7	0.0	2676.5	892.2
B1_21	440	3	20	245.3	0.0	245.3	0.0	B3_91	260	14	20	231.2	0.0	231.2	0.0
B1_21	440	3	21	152.4	0.0	152.4	0.0	B3_91	260	14	21	1728.0	432.0	1296.0	0.0
B1_21	440	3	22	420.0	0.0	420.0	0.0	B3_91	260	14	22	177.0	0.0	177.0	0.0
B1_21	440	3	23	243.1	0.0	0.0	243.1	B3_91	260	14	23	207.0	0.0	207.0	0.0
B1_21	440	3	24	125.6	0.0	125.6	0.0	B3_91	260	14	24	461.9	0.0	461.9	0.0
B1_21	440	3	25	41.1	0.0	41.1	0.0	B3_91	260	14	25	200.7	0.0	200.7	0.0
B1_21	440	3	26	69.3	0.0	69.3	0.0	B3_91	260	14	26	2241.0	0.0	2241.0	0.0
B1_21	440	3	27	124.7	0.0	124.7	0.0	B3_91	260	14	27	516.7	0.0	387.5	129.2
B1_21	440	3	28	84.9	0.0	0.0	84.9	B3_91	260	14	28	12432.9	0.0	12432.9	0.0
B1_21	440	3	29	124.7	0.0	124.7	0.0	B3_91	260	14	29	1672.7	0.0	1672.7	0.0
B1_21	440	3	30	153.3	0.0	153.3	0.0	B3_91	260	14	30	108.5	0.0	0.0	108.5
B1_22	460	6	1	140.3	0.0	0.0	0.0	B3_92	280	14	1	1751.3	0.0	1751.3	0.0
B1_22	460	6	2	147.9	0.0	0.0	0.0	B3_92	280	14	2	995.7	746.7	248.9	0.0

B1_22	460	6	3	275.7	275.7	0.0	0.0	B3_92	280	14	3	1037.5	0.0	1037.5	0.0
B1_22	460	6	4	185.9	185.9	0.0	0.0	B3_92	280	14	4	2032.0	0.0	2032.0	0.0
B1_22	460	6	5	485.2	0.0	0.0	0.0	B3_92	280	14	5	385.1	385.1	0.0	0.0
B1_22	460	6	6	279.2	0.0	0.0	0.0	B3_92	280	14	6	366.7	366.7	0.0	0.0
B1_22	460	6	7	244.8	0.0	244.8	0.0	B3_92	280	14	7	133.4	0.0	0.0	133.4
B1_22	460	6	8	418.6	0.0	418.6	0.0	B3_92	280	14	8	431.4	431.4	0.0	0.0
B1_22	460	6	9	1167.0	291.8	875.3	0.0	B3_92	280	14	9	395.1	395.1	0.0	0.0
B1_22	460	6	10	896.7	0.0	896.7	0.0	B3_92	280	14	10	240.0	240.0	0.0	0.0
B1_22	460	6	11	588.4	0.0	588.4	0.0	B3_92	280	14	11	384.0	384.0	0.0	0.0
B1_22	460	6	12	181.4	0.0	181.4	0.0	B3_92	280	14	12	1297.0	0.0	1297.0	0.0
B1_22	460	6	13	1063.8	0.0	1063.8	0.0	B3_92	280	14	13	1106.2	0.0	0.0	0.0
B1_22	460	6	14	361.0	0.0	361.0	0.0	B3_92	280	14	14	589.4	0.0	589.4	0.0
B1_22	460	6	15	451.7	0.0	451.7	0.0	B3_92	280	14	15	99.9	0.0	99.9	0.0
B1_22	460	6	16	353.4	0.0	353.4	0.0	B3_92	280	14	16	86.5	86.5	0.0	0.0
B1_22	460	6	17	543.7	0.0	543.7	0.0	B3_92	280	14	17	240.0	240.0	0.0	0.0
B1_22	460	6	18	377.1	0.0	377.1	0.0	B3_92	280	14	18	730.0	0.0	730.0	0.0

Table B.1., cont.

B1_22	460	6	19	336.4	0.0	336.4	0.0	B3_92	280	14	19	4391.7	3293.8	1097.9	0.0
B1_22	460	6	20	5758.7	0.0	5758.7	0.0	B3_92	280	14	20	6679.9	0.0	6679.9	0.0
B1_22	460	6	21	600.5	600.5	0.0	0.0	B3_92	280	14	21	279.1	0.0	0.0	279.1
B1_22	460	6	22	564.7	0.0	564.7	0.0	B3_92	280	14	22	768.5	768.5	0.0	0.0
B1_22	460	6	23	840.9	0.0	840.9	0.0	B3_92	280	14	23	751.2	0.0	751.2	0.0
B1_22	460	6	24	114.8	0.0	0.0	114.8	B3_92	280	14	24	160.7	0.0	0.0	160.7
B1_22	460	6	25	424.5	0.0	424.5	0.0	B3_92	280	14	25	22963.0	17222.2	5740.7	0.0
B1_22	460	6	26	630.4	0.0	630.4	0.0	B3_92	280	14	26	818.7	0.0	818.7	0.0
B1_22	460	6	27	203.3	0.0	203.3	0.0	B3_92	280	14	27	193.1	0.0	193.1	0.0
B1_22	460	6	28	241.3	0.0	241.3	0.0	B3_92	280	14	28	479.4	479.4	0.0	0.0
B1_22	460	6	29	351.2	0.0	351.2	0.0	B3_92	280	14	29	642.4	0.0	642.4	0.0
B1_22	460	6	30	181.8	0.0	181.8	0.0	B3_92	280	14	30	1511.3	377.8	1133.5	0.0
B1_24	480	6	1	269.1	269.1	0.0	0.0	B3_93	300	8	1	2345.0	0.0	2345.0	0.0
B1_24	480	6	2	310.6	0.0	310.6	0.0	B3_93	300	8	2	3394.0	0.0	3394.0	0.0
B1_24	480	6	3	149.4	0.0	149.4	0.0	B3_93	300	8	3	195.3	0.0	0.0	195.3
B1_24	480	6	4	8478.1	0.0	8478.1	0.0	B3_93	300	8	4	159.4	0.0	159.4	0.0
B1_24	480	6	5	636.7	0.0	636.7	0.0	B3_93	300	8	5	522.3	0.0	522.3	0.0
B1_24	480	6	6	1312.5	0.0	0.0	1312.5	B3_93	300	8	6	905.4	0.0	905.4	0.0
B1_24	480	6	7	321.9	0.0	0.0	321.9	B3_93	300	8	7	96.4	0.0	0.0	96.4
B1_24	480	6	8	758.3	0.0	758.3	0.0	B3_93	300	8	8	2939.1	0.0	2939.1	0.0
B1_24	480	6	9	218.2	0.0	0.0	218.2	B3_93	300	8	9	536.8	134.2	402.6	0.0
B1_24	480	6	10	387.4	0.0	387.4	0.0	B3_93	300	8	10	229.3	0.0	229.3	0.0
B1_24	480	6	11	178.6	0.0	178.6	0.0	B3_93	300	8	11	367.9	0.0	367.9	0.0
B1_24	480	6	12	640.9	0.0	640.9	0.0	B3_93	300	8	12	386.2	386.2	0.0	0.0
B1_24	480	6	13	245.1	0.0	0.0	245.1	B3_93	300	8	13	316.9	0.0	0.0	316.9
B1_24	480	6	14	477.9	0.0	477.9	0.0	B3_93	300	8	14	170.1	0.0	170.1	0.0
B1_24	480	6	15	82.5	0.0	82.5	0.0	B3_93	300	8	15	609.3	0.0	609.3	0.0
B1_24	480	6	16	599.5	0.0	599.5	0.0	B3_93	300	8	16	1174.4	0.0	1174.4	0.0
B1_24	480	6	17	947.7	0.0	947.7	0.0	B3_93	300	8	17	403.9	0.0	403.9	0.0
B1_24	480	6	18	344.5	344.5	0.0	0.0	B3_93	300	8	18	791.3	0.0	791.3	0.0
B1_24	480	6	19	1270.5	0.0	1270.5	0.0	B3_93	300	8	19	187.8	0.0	0.0	187.8
B1_24	480	6	20	369.5	0.0	0.0	369.5	B3_93	300	8	20	1078.0	0.0	1078.0	0.0
B1_24	480	6	21	679.1	509.3	169.8	0.0	B3_93	300	8	21	4259.7	1064.9	3194.8	0.0
B1_24	480	6	22	101.3	0.0	0.0	101.3	B3_93	300	8	22	1534.2	0.0	1534.2	0.0
B1_24	480	6	23	2609.9	0.0	2609.9	0.0	B3_93	300	8	23	87.0	0.0	0.0	87.0
B1_24	480	6	24	912.8	0.0	912.8	0.0	B3_93	300	8	24	158.1	0.0	0.0	158.1
B1_24	480	6	25	279.0	0.0	279.0	0.0	B3_93	300	8	25	694.9	173.7	521.2	0.0
B1_24	480	6	26	1022.7	767.0	255.7	0.0	B3_93	300	8	26	4623.9	3467.9	1156.0	0.0
B1_24	480	6	27	396.3	0.0	396.3	0.0	B3_93	300	8	27	2708.6	677.1	2031.4	0.0
B1_24	480	6	28	911.0	0.0	911.0	0.0	B3_93	300	8	28	439.1	0.0	439.1	0.0
B1_24	480	6	29	108.9	0.0	108.9	0.0	B3_93	300	8	29	5567.1	4175.3	1391.8	0.0
B1_24	480	6	30	381.7	0.0	381.7	0.0	B3_93	300	8	30	958.9	239.7	719.2	0.0
B1_25	500	5	1	246.0	0.0	246.0	0.0	B3_94	320	12	1	16957.5	12718.1	4239.4	0.0
B1_25	500	5	2	367.1	0.0	0.0	367.1	B3_94	320	12	2	4333.4	1083.3	3250.0	0.0
B1_25	500	5	3	395.5	0.0	395.5	0.0	B3_94	320	12	3	210.1	0.0	210.1	0.0
B1_25	500	5	4	682.6	0.0	682.6	0.0	B3_94	320	12	4	102.2	0.0	102.2	0.0
B1_25	500	5	5	310.2	0.0	310.2	0.0	B3_94	320	12	5	112.2	0.0	112.2	0.0
B1_25	500	5	6	704.2	0.0	0.0	704.2	B3_94	320	12	6	149.1	0.0	149.1	0.0
B1_25	500	5	7	75.8	0.0	75.8	0.0	B3_94	320	12	7	113.8	0.0	113.8	0.0
B1_25	500	5	8	421.9	0.0	421.9	0.0	B3_94	320	12	8	95.3	0.0	95.3	0.0
B1_25	500	5	9	419.2	0.0	419.2	0.0	B3_94	320	12	9	192.8	0.0	192.8	0.0
B1_25	500	5	10	171.2	0.0	171.2	0.0	B3_94	320	12	10	3185.3	0.0	3185.3	0.0
B1_25	500	5	11	481.9	0.0	481.9	0.0	B3_94	320	12	11	93.2	0.0	93.2	0.0
B1_25	500	5	12	61.1	0.0	61.1	0.0	B3_94	320	12	12	3816.2	0.0	3816.2	0.0
B1_25	500	5	13	648.9	0.0	648.9	0.0	B3_94	320	12	13	264.9	0.0	264.9	0.0
B1_25	500	5	14	114.3	0.0	0.0	114.3	B3_94	320	12	14	1361.4	0.0	1361.4	0.0
B1_25	500	5	15	332.3	0.0	332.3	0.0	B3_94	320	12	15	395.5	98.9	296.6	0.0
B1_25	500	5	16	296.5	0.0	296.5	0.0	B3_94	320	12	16	694.7	0.0	694.7	0.0
B1_25	500	5	17	321.8	0.0	321.8	0.0	B3_94	320	12	17	215.4	0.0	215.4	0.0
B1_25	500	5	18	165.4	0.0	165.4	0.0	B3_94	320	12	18	12258.1	9193.6	3064.5	0.0
B1_25	500	5	19	99.0	0.0	0.0	99.0	B3_94	320	12	19	196.5	0.0	196.5	0.0

B1_25	500	5	20	41.1	0.0	41.1	0.0	B3_94	320	12	20	285.5	285.5	0.0	0.0
B1_25	500	5	21	260.7	0.0	260.7	0.0	B3_94	320	12	21	1584.7	0.0	1584.7	0.0
B1_25	500	5	22	145.9	145.9	0.0	0.0	B3_94	320	12	22	337.6	0.0	337.6	0.0
B1_25	500	5	23	54.3	0.0	54.3	0.0	B3_94	320	12	23	237.0	0.0	237.0	0.0
B1_25	500	5	24	226.5	0.0	226.5	0.0	B3_94	320	12	24	1139.2	0.0	1139.2	0.0
B1_25	500	5	25	273.9	0.0	0.0	273.9	B3_94	320	12	25	173.8	0.0	173.8	0.0
B1_25	500	5	26	286.0	0.0	286.0	0.0	B3_94	320	12	26	174.3	0.0	0.0	174.3
B1_25	500	5	27	62.7	0.0	62.7	0.0	B3_94	320	12	27	82.2	0.0	0.0	82.2
B1_25	500	5	28	177.0	0.0	0.0	177.0	B3_94	320	12	28	67.9	0.0	67.9	0.0

Table B.1., cont.

B1_25	500	5	29	350.8	0.0	350.8	0.0	B3_94	320	12	29	57.9	0.0	57.9	0.0
B1_25	500	5	30	141.7	0.0	141.7	0.0	B3_94	320	12	30	148.5	0.0	148.5	0.0
B1_26	520	5	1	260.6	0.0	260.6	0.0	B3_95	340	12	1	3450.2	862.5	2587.6	0.0
B1_26	520	5	2	186.2	186.2	0.0	0.0	B3_95	340	12	2	498.2	0.0	498.2	0.0
B1_26	520	5	3	493.9	0.0	493.9	0.0	B3_95	340	12	3	676.2	0.0	676.2	0.0
B1_26	520	5	4	113.1	113.1	0.0	0.0	B3_95	340	12	4	181.2	0.0	181.2	0.0
B1_26	520	5	5	132.4	0.0	0.0	132.4	B3_95	340	12	5	628.8	0.0	628.8	0.0
B1_26	520	5	6	221.5	0.0	221.5	0.0	B3_95	340	12	6	285.5	0.0	0.0	285.5
B1_26	520	5	7	107.5	0.0	107.5	0.0	B3_95	340	12	7	67.4	67.4	0.0	0.0
B1_26	520	5	8	284.2	0.0	284.2	0.0	B3_95	340	12	8	7961.0	7961.0	0.0	0.0
B1_26	520	5	9	178.6	0.0	178.6	0.0	B3_95	340	12	9	275.4	275.4	0.0	0.0
B1_26	520	5	10	393.5	0.0	393.5	0.0	B3_95	340	12	10	248.6	0.0	248.6	0.0
B1_26	520	5	11	251.7	0.0	251.7	0.0	B3_95	340	12	11	215.4	215.4	0.0	0.0
B1_26	520	5	12	986.8	0.0	986.8	0.0	B3_95	340	12	12	118.5	0.0	118.5	0.0
B1_26	520	5	13	100.4	0.0	100.4	0.0	B3_95	340	12	13	141.2	141.2	0.0	0.0
B1_26	520	5	14	434.0	0.0	434.0	0.0	B3_95	340	12	14	9907.1	2476.8	7430.3	0.0
B1_26	520	5	15	70.7	0.0	70.7	0.0	B3_95	340	12	15	70.6	0.0	70.6	0.0
B1_26	520	5	16	1165.9	0.0	1165.9	0.0	B3_95	340	12	16	65.8	0.0	65.8	0.0
B1_26	520	5	17	276.6	0.0	276.6	0.0	B3_95	340	12	17	65.3	0.0	0.0	65.3
B1_26	520	5	18	245.1	0.0	245.1	0.0	B3_95	340	12	18	570.9	0.0	570.9	0.0
B1_26	520	5	19	215.4	0.0	215.4	0.0	B3_95	340	12	19	620.9	0.0	620.9	0.0
B1_26	520	5	20	342.1	0.0	342.1	0.0	B3_95	340	12	20	5767.0	5767.0	0.0	0.0
B1_26	520	5	21	163.1	0.0	0.0	163.1	B3_95	340	12	21	383.4	0.0	383.4	0.0
B1_26	520	5	22	453.4	0.0	453.4	0.0	B3_95	340	12	22	7842.5	7842.5	0.0	0.0
B1_26	520	5	23	167.3	0.0	0.0	0.0	B3_95	340	12	23	5535.2	4151.4	1383.8	0.0
B1_26	520	5	24	136.7	0.0	0.0	136.7	B3_95	340	12	24	234.4	234.4	0.0	0.0
B1_26	520	5	25	993.4	0.0	993.4	0.0	B3_95	340	12	25	72.2	0.0	72.2	0.0
B1_26	520	5	26	175.8	0.0	0.0	175.8	B3_95	340	12	26	26425.3	19819.0	6606.3	0.0
B1_26	520	5	27	97.1	0.0	97.1	0.0	B3_95	340	12	27	143.3	0.0	143.3	0.0
B1_26	520	5	28	225.3	0.0	225.3	0.0	B3_95	340	12	28	664.1	0.0	664.1	0.0
B1_26	520	5	29	189.0	0.0	189.0	0.0	B3_95	340	12	29	50.6	0.0	50.6	0.0
B1_26	520	5	30	264.9	0.0	264.9	0.0	B3_95	340	12	30	277.6	0.0	277.6	0.0
B2_32	0	0	1	3545.4	2659.1	886.4	0.0	B3_96	360	9	1	953.8	953.8	0.0	0.0
B2_32	0	0	2	975.2	975.2	0.0	0.0	B3_96	360	9	2	735.8	735.8	0.0	0.0
B2_32	0	0	3	203.1	203.1	0.0	0.0	B3_96	360	9	3	269.7	0.0	269.7	0.0
B2_32	0	0	4	7834.5	7834.5	0.0	0.0	B3_96	360	9	4	470.8	0.0	470.8	0.0
B2_32	0	0	5	3109.8	2332.4	777.5	0.0	B3_96	360	9	5	483.5	0.0	483.5	0.0
B2_32	0	0	6	1139.0	854.2	284.7	0.0	B3_96	360	9	6	1629.5	0.0	1629.5	0.0
B2_32	0	0	7	1333.1	999.9	333.3	0.0	B3_96	360	9	7	230.2	0.0	230.2	0.0
B2_32	0	0	8	5687.5	0.0	5687.5	0.0	B3_96	360	9	8	106.4	0.0	106.4	0.0
B2_32	0	0	9	416.2	0.0	416.2	0.0	B3_96	360	9	9	458.7	0.0	458.7	0.0
B2_32	0	0	10	1358.5	0.0	1358.5	0.0	B3_96	360	9	10	297.6	0.0	297.6	0.0
B2_32	0	0	11	992.6	0.0	992.6	0.0	B3_96	360	9	11	176.4	0.0	176.4	0.0
B2_32	0	0	12	799.5	0.0	799.5	0.0	B3_96	360	9	12	209.1	0.0	0.0	209.1
B2_32	0	0	13	5270.3	3952.7	1317.6	0.0	B3_96	360	9	13	93.2	0.0	93.2	0.0
B2_32	0	0	14	2704.6	2028.5	676.2	0.0	B3_96	360	9	14	89.5	0.0	89.5	0.0
B2_32	0	0	15	459.5	0.0	459.5	0.0	B3_96	360	9	15	419.8	0.0	419.8	0.0
B2_32	0	0	16	3710.2	3710.2	0.0	0.0	B3_96	360	9	16	98.0	0.0	0.0	98.0
B2_32	0	0	17	272.8	272.8	0.0	0.0	B3_96	360	9	17	167.5	0.0	167.5	0.0
B2_32	0	0	18	1836.4	1377.3	459.1	0.0	B3_96	360	9	18	218.0	218.0	0.0	0.0
B2_32	0	0	19	827.9	0.0	827.9	0.0	B3_96	360	9	19	333.9	0.0	333.9	0.0
B2_32	0	0	20	1238.6	309.6	928.9	0.0	B3_96	360	9	20	696.8	696.8	0.0	0.0
B2_32	0	0	21	468.4	0.0	0.0	0.0	B3_96	360	9	21	291.8	0.0	291.8	0.0
B2_32	0	0	22	1340.1	0.0	1340.1	0.0	B3_96	360	9	22	240.2	0.0	240.2	0.0
B2_32	0	0	23	1892.7	0.0	1892.7	0.0	B3_96	360	9	23	162.2	0.0	162.2	0.0
B2_32	0	0	24	1317.2	329.3	987.9	0.0	B3_96	360	9	24	183.3	0.0	183.3	0.0
B2_32	0	0	25	375.4	0.0	375.4	0.0	B3_96	360	9	25	565.6	0.0	565.6	0.0
B2_32	0	0	26	3370.7	3370.7	0.0	0.0	B3_96	360	9	26	255.4	0.0	255.4	0.0
B2_32	0	0	27	501.8	376.3	125.4	0.0	B3_96	360	9	27	1422.5	0.0	1422.5	0.0
B2_32	0	0	28	2067.9	517.0	1550.9	0.0	B3_96	360	9	28	629.9	0.0	629.9	0.0
B2_32	0	0	29	353.9	353.9	0.0	0.0	B3_96	360	9	29	6413.2	1603.3	4809.9	0.0
B2_32	0	0	30	1746.8	1310.1	436.7	0.0	B3_96	360	9	30	11361.2	2840.3	8520.9	0.0
B2_33	20	1	1	2189.5	547.4	1642.1	0.0	B3_97	380	9	1	254.5	0.0	254.5	0.0
B2_33	20	1	2	3241.4	2431.0	810.3	0.0	B3_97	380	9	2	107.7	0.0	107.7	0.0
B2_33	20	1	3	567.4	0.0	567.4	0.0	B3_97	380	9	3	299.7	0.0	299.7	0.0
B2_33	20	1	4	4379.0	1094.8	3284.3	0.0	B3_97	380	9	4	222.7	222.7	0.0	0.0
B2_33	20	1	5	1247.4	0.0	1247.4	0.0	B3_97	380	9	5	1438.8	0.0	1438.8	0.0
B2_33	20	1	6	1975.6	0.0	1975.6	0.0	B3_97	380	9	6	999.0	249.8	749.3	0.0

B2_33	20	1	7	3839.9	2879.9	960.0	0.0	B3_97	380	9	7	256.7	256.7	0.0	0.0
B2_33	20	1	8	1067.0	0.0	1067.0	0.0	B3_97	380	9	8	597.2	447.9	149.3	0.0

Table B.1., cont.

B2_33	20	1	9	3848.4	3848.4	0.0	0.0	B3_97	380	9	9	213.8	213.8	0.0	0.0
B2_33	20	1	10	23067.0	5766.8	17300.3	0.0	B3_97	380	9	10	438.1	0.0	438.1	0.0
B2_33	20	1	11	2588.7	0.0	2588.7	0.0	B3_97	380	9	11	782.5	586.8	195.6	0.0
B2_33	20	1	12	946.8	0.0	946.8	0.0	B3_97	380	9	12	310.3	0.0	310.3	0.0
B2_33	20	1	13	7966.7	0.0	7966.7	0.0	B3_97	380	9	13	2548.3	637.1	1911.2	0.0
B2_33	20	1	14	781.4	586.0	195.3	0.0	B3_97	380	9	14	224.9	0.0	224.9	0.0
B2_33	20	1	15	965.6	0.0	965.6	0.0	B3_97	380	9	15	6365.7	4774.3	1591.4	0.0
B2_33	20	1	16	3408.7	852.2	2556.5	0.0	B3_97	380	9	16	549.7	0.0	549.7	0.0
B2_33	20	1	17	4616.1	0.0	4616.1	0.0	B3_97	380	9	17	385.1	0.0	385.1	0.0
B2_33	20	1	18	50635.1	37976.3	12658.8	0.0	B3_97	380	9	18	1753.6	0.0	1753.6	0.0
B2_33	20	1	19	9809.4	0.0	9809.4	0.0	B3_97	380	9	19	1024.7	256.2	768.5	0.0
B2_33	20	1	20	2380.4	2380.4	0.0	0.0	B3_97	380	9	20	5834.4	5834.4	0.0	0.0
B2_33	20	1	21	374.2	0.0	374.2	0.0	B3_97	380	9	21	108.8	108.8	0.0	0.0
B2_33	20	1	22	589.6	0.0	589.6	0.0	B3_97	380	9	22	1550.4	0.0	1550.4	0.0
B2_33	20	1	23	6808.4	0.0	6808.4	0.0	B3_97	380	9	23	467.7	0.0	467.7	0.0
B2_33	20	1	24	1703.2	0.0	1703.2	0.0	B3_97	380	9	24	252.8	0.0	252.8	0.0
B2_33	20	1	25	18401.5	18401.5	0.0	0.0	B3_97	380	9	25	5225.5	1306.4	3919.1	0.0
B2_33	20	1	26	540.1	0.0	540.1	0.0	B3_97	380	9	26	329.3	0.0	329.3	0.0
B2_33	20	1	27	1547.2	0.0	1547.2	0.0	B3_97	380	9	27	2670.0	2670.0	0.0	0.0
B2_33	20	1	28	2576.9	0.0	2576.9	0.0	B3_97	380	9	28	617.8	0.0	617.8	0.0
B2_33	20	1	29	1401.1	0.0	1401.1	0.0	B3_97	380	9	29	8651.1	6488.3	2162.8	0.0
B2_33	20	1	30	1786.1	0.0	1786.1	0.0	B3_97	380	9	30	895.8	0.0	895.8	0.0
B2_34	40	2	1	1853.5	0.0	1853.5	0.0	B3_98	400	12	1	286.3	0.0	0.0	286.3
B2_34	40	2	2	803.0	803.0	0.0	0.0	B3_98	400	12	2	599.4	0.0	599.4	0.0
B2_34	40	2	3	1690.0	1267.5	422.5	0.0	B3_98	400	12	3	529.1	132.3	396.8	0.0
B2_34	40	2	4	1627.8	0.0	1627.8	0.0	B3_98	400	12	4	2125.2	0.0	2125.2	0.0
B2_34	40	2	5	762.0	0.0	0.0	762.0	B3_98	400	12	5	344.9	0.0	0.0	344.9
B2_34	40	2	6	1141.9	0.0	1141.9	0.0	B3_98	400	12	6	2650.4	0.0	0.0	0.0
B2_34	40	2	7	394.5	0.0	0.0	394.5	B3_98	400	12	7	495.6	495.6	0.0	0.0
B2_34	40	2	8	2719.2	0.0	2719.2	0.0	B3_98	400	12	8	4849.9	0.0	4849.9	0.0
B2_34	40	2	9	2489.7	0.0	622.4	1867.3	B3_98	400	12	9	211.5	0.0	0.0	211.5
B2_34	40	2	10	893.5	0.0	893.5	0.0	B3_98	400	12	10	233.3	0.0	0.0	233.3
B2_34	40	2	11	2930.8	0.0	2198.1	732.7	B3_98	400	12	11	985.0	0.0	985.0	0.0
B2_34	40	2	12	772.4	0.0	772.4	0.0	B3_98	400	12	12	500.6	0.0	500.6	0.0
B2_34	40	2	13	2821.0	0.0	2821.0	0.0	B3_98	400	12	13	2124.7	0.0	2124.7	0.0
B2_34	40	2	14	1630.1	0.0	1630.1	0.0	B3_98	400	12	14	269.6	0.0	269.6	0.0
B2_34	40	2	15	2832.8	0.0	2832.8	0.0	B3_98	400	12	15	429.7	0.0	0.0	429.7
B2_34	40	2	16	1589.6	0.0	0.0	1589.6	B3_98	400	12	16	482.8	482.8	0.0	0.0
B2_34	40	2	17	4251.8	4251.8	0.0	0.0	B3_98	400	12	17	643.5	0.0	643.5	0.0
B2_34	40	2	18	1261.6	0.0	1261.6	0.0	B3_98	400	12	18	3720.9	930.2	2790.6	0.0
B2_34	40	2	19	1367.1	0.0	1367.1	0.0	B3_98	400	12	19	560.3	0.0	560.3	0.0
B2_34	40	2	20	2309.2	0.0	2309.2	0.0	B3_98	400	12	20	1155.3	0.0	866.5	288.8
B2_34	40	2	21	543.8	0.0	0.0	543.8	B3_98	400	12	21	110.0	0.0	110.0	0.0
B2_34	40	2	22	6664.2	0.0	6664.2	0.0	B3_98	400	12	22	241.7	0.0	0.0	241.7
B2_34	40	2	23	1884.1	0.0	1884.1	0.0	B3_98	400	12	23	240.5	0.0	240.5	0.0
B2_34	40	2	24	1595.7	0.0	0.0	1595.7	B3_98	400	12	24	464.9	464.9	0.0	0.0
B2_34	40	2	25	1248.4	0.0	0.0	1248.4	B3_98	400	12	25	1439.3	0.0	1439.3	0.0
B2_34	40	2	26	574.0	0.0	574.0	0.0	B3_98	400	12	26	525.7	0.0	0.0	525.7
B2_34	40	2	27	5689.6	0.0	5689.6	0.0	B3_98	400	12	27	9810.8	2452.7	7358.1	0.0
B2_34	40	2	28	639.5	0.0	0.0	639.5	B3_98	400	12	28	2407.1	0.0	2407.1	0.0
B2_34	40	2	29	4332.8	3249.6	1083.2	0.0	B3_98	400	12	29	1988.0	1491.0	497.0	0.0
B2_34	40	2	30	2243.7	0.0	2243.7	0.0	B3_98	400	12	30	6591.2	4943.4	1647.8	0.0
B2_35	60	2	1	884.1	0.0	884.1	0.0	B3_99	420	14	1	782.3	0.0	782.3	0.0
B2_35	60	2	2	6328.2	4746.1	0.0	1582.0	B3_99	420	14	2	2475.2	2475.2	0.0	0.0
B2_35	60	2	3	468.4	0.0	468.4	0.0	B3_99	420	14	3	3031.9	0.0	3031.9	0.0
B2_35	60	2	4	1443.7	0.0	1443.7	0.0	B3_99	420	14	4	10320.8	2580.2	7740.6	0.0
B2_35	60	2	5	432.1	0.0	432.1	0.0	B3_99	420	14	5	1155.4	0.0	1155.4	0.0
B2_35	60	2	6	1290.3	1290.3	0.0	0.0	B3_99	420	14	6	2476.1	0.0	2476.1	0.0
B2_35	60	2	7	640.7	0.0	640.7	0.0	B3_99	420	14	7	440.5	0.0	330.4	110.1
B2_35	60	2	8	4373.8	0.0	4373.8	0.0	B3_99	420	14	8	235.5	0.0	235.5	0.0
B2_35	60	2	9	1553.7	1553.7	0.0	0.0	B3_99	420	14	9	2775.5	693.9	2081.6	0.0
B2_35	60	2	10	1193.3	894.9	298.3	0.0	B3_99	420	14	10	235.5	0.0	235.5	0.0
B2_35	60	2	11	116.0	0.0	0.0	116.0	B3_99	420	14	11	24983.5	24983.5	0.0	0.0
B2_35	60	2	12	1457.6	1457.6	0.0	0.0	B3_99	420	14	12	1746.9	1746.9	0.0	0.0
B2_35	60	2	13	228.5	0.0	228.5	0.0	B3_99	420	14	13	295.3	0.0	0.0	295.3
B2_35	60	2	14	1125.6	0.0	0.0	1125.6	B3_99	420	14	14	176.0	176.0	0.0	0.0
B2_35	60	2	15	166.8	0.0	166.8	0.0	B3_99	420	14	15	819.4	0.0	819.4	0.0
B2_35	60	2	16	1531.3	0.0	382.8	1148.5	B3_99	420	14	16	851.6	0.0	851.6	0.0
B2_35	60	2	17	207.6	207.6	0.0	0.0	B3_99	420	14	17	322.1	322.1	0.0	0.0
B2_35	60	2	18	312.1	0.0	312.1	0.0	B3_99	420	14	18	663.9	663.9	0.0	0.0

Table B.1., cont.

B2_35	60	2	19	1684.1	0.0	1684.1	0.0	B3_99	420	14	19	341.4	341.4	0.0	0.0
B2_35	60	2	20	1583.5	0.0	1583.5	0.0	B3_99	420	14	20	281.0	0.0	281.0	0.0
B2_35	60	2	21	470.9	470.9	0.0	0.0	B3_99	420	14	21	429.8	0.0	429.8	0.0

B2_35	60	2	22	402.7	402.7	0.0	0.0	B3_99	420	14	22	303.4	303.4	0.0	0.0
B2_35	60	2	23	2110.7	0.0	2110.7	0.0	B3_99	420	14	23	13702.1	13702.1	0.0	0.0
B2_35	60	2	24	1406.3	0.0	0.0	1406.3	B3_99	420	14	24	179.6	0.0	179.6	0.0
B2_35	60	2	25	3279.1	0.0	3279.1	0.0	B3_99	420	14	25	443.2	443.2	0.0	0.0
B2_35	60	2	26	2463.7	1847.7	615.9	0.0	B3_99	420	14	26	1090.2	817.6	272.5	0.0
B2_35	60	2	27	3216.9	3216.9	0.0	0.0	B3_99	420	14	27	2418.0	0.0	604.5	1813.5
B2_35	60	2	28	3406.5	3406.5	0.0	0.0	B3_99	420	14	28	904.8	0.0	904.8	0.0
B2_35	60	2	29	176.7	0.0	176.7	0.0	B3_99	420	14	29	416.0	416.0	0.0	0.0
B2_35	60	2	30	6221.6	1555.4	4666.2	0.0	B3_99	420	14	30	2576.6	1932.5	644.2	0.0
B2_36	80	2	1	316.6	237.5	79.2	0.0	B3_100	440	6	1	145.2	145.2	0.0	0.0
B2_36	80	2	2	1839.4	1379.6	459.9	0.0	B3_100	440	6	2	330.8	0.0	0.0	0.0
B2_36	80	2	3	142.4	142.4	0.0	0.0	B3_100	440	6	3	296.4	0.0	296.4	0.0
B2_36	80	2	4	640.7	480.5	160.2	0.0	B3_100	440	6	4	153.2	0.0	153.2	0.0
B2_36	80	2	5	561.5	0.0	561.5	0.0	B3_100	440	6	5	434.0	0.0	434.0	0.0
B2_36	80	2	6	180.2	135.2	45.1	0.0	B3_100	440	6	6	422.3	422.3	0.0	0.0
B2_36	80	2	7	211.1	158.3	52.8	0.0	B3_100	440	6	7	498.1	0.0	498.1	0.0
B2_36	80	2	8	223.5	0.0	223.5	0.0	B3_100	440	6	8	157.9	0.0	157.9	0.0
B2_36	80	2	9	846.3	634.7	211.6	0.0	B3_100	440	6	9	1196.1	0.0	1196.1	0.0
B2_36	80	2	10	162.8	122.1	40.7	0.0	B3_100	440	6	10	162.1	162.1	0.0	0.0
B2_36	80	2	11	3144.7	3144.7	0.0	0.0	B3_100	440	6	11	4518.0	3388.5	1129.5	0.0
B2_36	80	2	12	268.3	201.2	67.1	0.0	B3_100	440	6	12	268.6	268.6	0.0	0.0
B2_36	80	2	13	2708.1	0.0	2708.1	0.0	B3_100	440	6	13	135.3	0.0	135.3	0.0
B2_36	80	2	14	673.5	0.0	673.5	0.0	B3_100	440	6	14	135.7	135.7	0.0	0.0
B2_36	80	2	15	2325.3	0.0	2325.3	0.0	B3_100	440	6	15	170.1	170.1	0.0	0.0
B2_36	80	2	16	980.7	0.0	980.7	0.0	B3_100	440	6	16	149.4	149.4	0.0	0.0
B2_36	80	2	17	395.3	0.0	395.3	0.0	B3_100	440	6	17	432.2	0.0	432.2	0.0
B2_36	80	2	18	4291.6	3218.7	1072.9	0.0	B3_100	440	6	18	147.5	147.5	0.0	0.0
B2_36	80	2	19	170.8	128.1	42.7	0.0	B3_100	440	6	19	1044.3	0.0	1044.3	0.0
B2_36	80	2	20	319.1	0.0	319.1	0.0	B3_100	440	6	20	621.1	155.3	465.8	0.0
B2_36	80	2	21	902.5	0.0	902.5	0.0	B3_100	440	6	21	65.5	0.0	65.5	0.0
B2_36	80	2	22	1063.3	0.0	1063.3	0.0	B3_100	440	6	22	307.7	307.7	0.0	0.0
B2_36	80	2	23	1001.1	0.0	1001.1	0.0	B3_100	440	6	23	241.3	0.0	241.3	0.0
B2_36	80	2	24	403.2	0.0	403.2	0.0	B3_100	440	6	24	329.4	329.4	0.0	0.0
B2_36	80	2	25	882.6	220.7	662.0	0.0	B3_100	440	6	25	203.6	203.6	0.0	0.0
B2_36	80	2	26	561.0	420.8	140.3	0.0	B3_100	440	6	26	290.8	290.8	0.0	0.0
B2_36	80	2	27	1592.5	1592.5	0.0	0.0	B3_100	440	6	27	359.6	359.6	0.0	0.0
B2_36	80	2	28	498.3	0.0	498.3	0.0	B3_100	440	6	28	3260.2	815.1	2445.2	0.0
B2_36	80	2	29	1212.7	1212.7	0.0	0.0	B3_100	440	6	29	76.8	76.8	0.0	0.0
B2_36	80	2	30	3526.5	881.6	2644.9	0.0	B3_100	440	6	30	328.5	0.0	328.5	0.0
B2_37	100	3	1	3439.6	2579.7	859.9	0.0	B3_101	460	9	1	189.4	0.0	189.4	0.0
B2_37	100	3	2	4873.2	3654.9	1218.3	0.0	B3_101	460	9	2	105.0	0.0	105.0	0.0
B2_37	100	3	3	1881.8	0.0	1881.8	0.0	B3_101	460	9	3	193.0	193.0	0.0	0.0
B2_37	100	3	4	892.2	0.0	892.2	0.0	B3_101	460	9	4	244.0	244.0	0.0	0.0
B2_37	100	3	5	378.1	0.0	378.1	0.0	B3_101	460	9	5	123.3	123.3	0.0	0.0
B2_37	100	3	6	5432.5	4074.4	1358.1	0.0	B3_101	460	9	6	116.6	116.6	0.0	0.0
B2_37	100	3	7	533.0	0.0	533.0	0.0	B3_101	460	9	7	180.1	180.1	0.0	0.0
B2_37	100	3	8	827.4	620.5	206.8	0.0	B3_101	460	9	8	647.4	161.9	485.6	0.0
B2_37	100	3	9	4572.5	1143.1	0.0	3429.4	B3_101	460	9	9	155.5	0.0	155.5	0.0
B2_37	100	3	10	510.3	0.0	382.8	0.0	B3_101	460	9	10	374.9	0.0	374.9	0.0
B2_37	100	3	11	3745.6	2809.2	936.4	0.0	B3_101	460	9	11	2085.2	1563.9	521.3	0.0
B2_37	100	3	12	809.5	607.1	202.4	0.0	B3_101	460	9	12	509.3	509.3	0.0	0.0
B2_37	100	3	13	1052.8	0.0	1052.8	0.0	B3_101	460	9	13	1243.0	0.0	1243.0	0.0
B2_37	100	3	14	249.1	0.0	249.1	0.0	B3_101	460	9	14	92.0	92.0	0.0	0.0
B2_37	100	3	15	1831.2	0.0	1831.2	0.0	B3_101	460	9	15	870.3	0.0	870.3	0.0
B2_37	100	3	16	449.8	0.0	0.0	449.8	B3_101	460	9	16	176.0	176.0	0.0	0.0
B2_37	100	3	17	3471.2	0.0	3471.2	0.0	B3_101	460	9	17	264.1	264.1	0.0	0.0
B2_37	100	3	18	1002.8	0.0	1002.8	0.0	B3_101	460	9	18	218.0	0.0	0.0	218.0
B2_37	100	3	19	633.6	475.2	158.4	0.0	B3_101	460	9	19	155.0	155.0	0.0	0.0
B2_37	100	3	20	2378.9	0.0	2378.9	0.0	B3_101	460	9	20	525.0	0.0	525.0	0.0
B2_37	100	3	21	1443.6	0.0	1443.6	0.0	B3_101	460	9	21	337.8	0.0	337.8	0.0
B2_37	100	3	22	1149.2	0.0	1149.2	0.0	B3_101	460	9	22	232.3	0.0	232.3	0.0
B2_37	100	3	23	2300.5	0.0	2300.5	0.0	B3_101	460	9	23	94.3	94.3	0.0	0.0
B2_37	100	3	24	11725.1	8793.8	2931.3	0.0	B3_101	460	9	24	428.5	0.0	428.5	0.0
B2_37	100	3	25	373.4	0.0	0.0	373.4	B3_101	460	9	25	124.2	0.0	0.0	124.2
B2_37	100	3	26	1402.5	0.0	1402.5	0.0	B3_101	460	9	26	71.9	0.0	0.0	71.9
B2_37	100	3	27	11301.1	8475.9	2825.3	0.0	B3_101	460	9	27	265.0	0.0	265.0	0.0
B2_37	100	3	28	11271.1	2817.8	8453.3	0.0	B3_101	460	9	28	1587.4	396.9	1190.6	0.0

Table B.1., cont.

B2_37	100	3	29	3951.0	0.0	3951.0	0.0	B3_101	460	9	29	126.4	0.0	126.4	0.0
B2_37	100	3	30	1180.3	0.0	1180.3	0.0	B3_101	460	9	30	925.3	0.0	925.3	0.0
B2_38	120	3	1	3585.0	0.0	3585.0	0.0	B3_102	480	3	1	10273.9	2568.5	7705.4	0.0
B2_38	120	3	2	665.7	665.7	0.0	0.0	B3_102	480	3	2	347.6	347.6	0.0	0.0
B2_38	120	3	3	2452.7	0.0	2452.7	0.0	B3_102	480	3	3	202.4	0.0	202.4	0.0
B2_38	120	3	4	2283.6	0.0	2283.6	0.0	B3_102	480	3	4	791.7	197.9	593.8	0.0
B2_38	120	3	5	439.8	0.0	439.8	0.0	B3_102	480	3	5	12307.7	12307.7	0.0	0.0
B2_38	120	3	6	675.7	0.0	675.7	0.0	B3_102	480	3	6	181.4	181.4	0.0	0.0
B2_38	120	3	7	4737.9	4737.9	0.0	0.0	B3_102	480	3	7	1440.0	0.0	1440.0	0.0
B2_38	120	3	8	1438.8	1438.8	0.0	0.0	B3_102	480	3	8	296.7	296.7	0.0	0.0

B2_38	120	3	9	7587.6	7587.6	0.0	0.0	B3_102	480	3	9	231.4	231.4	0.0	0.0
B2_38	120	3	10	2886.6	2165.0	721.7	0.0	B3_102	480	3	10	590.7	590.7	0.0	0.0
B2_38	120	3	11	1602.6	0.0	1602.6	0.0	B3_102	480	3	11	389.2	0.0	389.2	0.0
B2_38	120	3	12	6399.5	4799.6	1599.9	0.0	B3_102	480	3	12	4512.1	0.0	4512.1	0.0
B2_38	120	3	13	395.5	0.0	395.5	0.0	B3_102	480	3	13	8241.9	2060.5	6181.4	0.0
B2_38	120	3	14	3414.4	2560.8	853.6	0.0	B3_102	480	3	14	210.0	0.0	210.0	0.0
B2_38	120	3	15	3549.7	0.0	3549.7	0.0	B3_102	480	3	15	396.3	396.3	0.0	0.0
B2_38	120	3	16	4469.8	0.0	4469.8	0.0	B3_102	480	3	16	1161.2	0.0	1161.2	0.0
B2_38	120	3	17	2132.5	1599.3	533.1	0.0	B3_102	480	3	17	118.9	118.9	0.0	0.0
B2_38	120	3	18	1327.2	0.0	1327.2	0.0	B3_102	480	3	18	86.2	0.0	86.2	0.0
B2_38	120	3	19	2933.5	733.4	2200.1	0.0	B3_102	480	3	19	8805.8	8805.8	0.0	0.0
B2_38	120	3	20	3699.3	0.0	3699.3	0.0	B3_102	480	3	20	945.0	0.0	945.0	0.0
B2_38	120	3	21	4112.7	4112.7	0.0	0.0	B3_102	480	3	21	426.2	426.2	0.0	0.0
B2_38	120	3	22	1216.6	0.0	1216.6	0.0	B3_102	480	3	22	268.1	0.0	268.1	0.0
B2_38	120	3	23	303.4	0.0	0.0	303.4	B3_102	480	3	23	248.4	0.0	248.4	0.0
B2_38	120	3	24	4694.7	0.0	0.0	4694.7	B3_102	480	3	24	516.5	387.4	129.1	0.0
B2_38	120	3	25	4063.7	4063.7	0.0	0.0	B3_102	480	3	25	5299.8	5299.8	0.0	0.0
B2_38	120	3	26	938.5	0.0	938.5	0.0	B3_102	480	3	26	557.6	557.6	0.0	0.0
B2_38	120	3	27	780.5	0.0	780.5	0.0	B3_102	480	3	27	237.2	0.0	237.2	0.0
B2_38	120	3	28	1696.9	0.0	1696.9	0.0	B3_102	480	3	28	269.9	269.9	0.0	0.0
B2_38	120	3	29	3024.6	0.0	3024.6	0.0	B3_102	480	3	29	3882.6	0.0	3882.6	0.0
B2_38	120	3	30	11744.6	8808.4	2936.1	0.0	B3_102	480	3	30	179.6	179.6	0.0	0.0
B2_39	140	4	1	529.9	0.0	529.9	0.0	B3_103	500	6	1	604.9	0.0	604.9	0.0
B2_39	140	4	2	1165.7	0.0	1165.7	0.0	B3_103	500	6	2	700.7	0.0	700.7	0.0
B2_39	140	4	3	964.2	723.1	241.0	0.0	B3_103	500	6	3	3562.2	0.0	3562.2	0.0
B2_39	140	4	4	663.9	0.0	663.9	0.0	B3_103	500	6	4	78.1	0.0	78.1	0.0
B2_39	140	4	5	4253.0	1063.2	3189.7	0.0	B3_103	500	6	5	1887.6	0.0	1887.6	0.0
B2_39	140	4	6	5772.1	0.0	5772.1	0.0	B3_103	500	6	6	595.1	0.0	595.1	0.0
B2_39	140	4	7	1864.9	0.0	1864.9	0.0	B3_103	500	6	7	473.8	0.0	473.8	0.0
B2_39	140	4	8	2181.2	0.0	0.0	2181.2	B3_103	500	6	8	129.8	0.0	129.8	0.0
B2_39	140	4	9	3902.7	0.0	3902.7	0.0	B3_103	500	6	9	120.5	0.0	120.5	0.0
B2_39	140	4	10	1894.4	473.6	1420.8	0.0	B3_103	500	6	10	32.7	0.0	0.0	32.7
B2_39	140	4	11	7261.2	5445.9	1815.3	0.0	B3_103	500	6	11	320.3	320.3	0.0	0.0
B2_39	140	4	12	3915.7	2936.7	978.9	0.0	B3_103	500	6	12	104.4	0.0	0.0	104.4
B2_39	140	4	13	11010.2	8257.7	2752.6	0.0	B3_103	500	6	13	308.8	0.0	308.8	0.0
B2_39	140	4	14	164.4	0.0	164.4	0.0	B3_103	500	6	14	1344.2	1344.2	0.0	0.0
B2_39	140	4	15	6170.2	0.0	6170.2	0.0	B3_103	500	6	15	1981.3	1981.3	0.0	0.0
B2_39	140	4	16	1893.5	0.0	0.0	1893.5	B3_103	500	6	16	755.0	0.0	755.0	0.0
B2_39	140	4	17	2389.9	0.0	2389.9	0.0	B3_103	500	6	17	1095.6	0.0	1095.6	0.0
B2_39	140	4	18	240.8	0.0	240.8	0.0	B3_103	500	6	18	137.9	137.9	0.0	0.0
B2_39	140	4	19	635.8	0.0	635.8	0.0	B3_103	500	6	19	737.6	737.6	0.0	0.0
B2_39	140	4	20	2524.4	0.0	2524.4	0.0	B3_103	500	6	20	2208.7	0.0	2208.7	0.0
B2_39	140	4	21	4049.7	0.0	4049.7	0.0	B3_103	500	6	21	878.9	659.2	219.7	0.0
B2_39	140	4	22	1709.4	0.0	1709.4	0.0	B3_103	500	6	22	968.0	0.0	968.0	0.0
B2_39	140	4	23	1989.1	1989.1	0.0	0.0	B3_103	500	6	23	1613.1	1613.1	0.0	0.0
B2_39	140	4	24	706.4	0.0	706.4	0.0	B3_103	500	6	24	320.7	0.0	320.7	0.0
B2_39	140	4	25	1994.0	0.0	1994.0	0.0	B3_103	500	6	25	1233.1	1233.1	0.0	0.0
B2_39	140	4	26	3192.3	3192.3	0.0	0.0	B3_103	500	6	26	2240.5	2240.5	0.0	0.0
B2_39	140	4	27	1764.4	1764.4	0.0	0.0	B3_103	500	6	27	586.6	0.0	586.6	0.0
B2_39	140	4	28	563.9	563.9	0.0	0.0	B3_103	500	6	28	7571.0	7571.0	0.0	0.0
B2_39	140	4	29	3722.2	0.0	3722.2	0.0	B3_103	500	6	29	1222.5	0.0	1222.5	0.0
B2_39	140	4	30	331.1	331.1	0.0	0.0	B3_103	500	6	30	452.2	0.0	452.2	0.0
B2_40	160	2	1	3991.9	998.0	2994.0	0.0	B3_104	520	4	1	166.4	0.0	166.4	0.0
B2_40	160	2	2	932.9	932.9	0.0	0.0	B3_104	520	4	2	158.8	0.0	0.0	158.8
B2_40	160	2	3	2551.3	637.8	1913.5	0.0	B3_104	520	4	3	109.8	0.0	109.8	0.0
B2_40	160	2	4	1397.9	349.5	1048.4	0.0	B3_104	520	4	4	110.3	110.3	0.0	0.0
B2_40	160	2	5	1155.9	0.0	1155.9	0.0	B3_104	520	4	5	101.8	0.0	0.0	101.8
B2_40	160	2	6	4790.9	1197.7	3593.2	0.0	B3_104	520	4	6	266.7	0.0	266.7	0.0
B2_40	160	2	7	2583.1	645.8	1937.4	0.0	B3_104	520	4	7	106.0	0.0	106.0	0.0
B2_40	160	2	8	1707.0	426.7	1280.2	0.0	B3_104	520	4	8	603.7	603.7	0.0	0.0

Table B.1., cont.

B2_40	160	2	9	6738.4	0.0	6738.4	0.0	B3_104	520	4	9	315.3	0.0	315.3	0.0
B2_40	160	2	10	5570.0	1392.5	4177.5	0.0	B3_104	520	4	10	204.5	204.5	0.0	0.0
B2_40	160	2	11	2836.0	2127.0	709.0	0.0	B3_104	520	4	11	109.3	109.3	0.0	0.0
B2_40	160	2	12	420.7	0.0	420.7	0.0	B3_104	520	4	12	242.2	0.0	242.2	0.0
B2_40	160	2	13	694.9	694.9	0.0	0.0	B3_104	520	4	13	106.5	0.0	106.5	0.0
B2_40	160	2	14	272.8	272.8	0.0	0.0	B3_104	520	4	14	93.3	0.0	0.0	93.3
B2_40	160	2	15	449.5	0.0	0.0	449.5	B3_104	520	4	15	86.7	86.7	0.0	0.0
B2_40	160	2	16	1635.8	409.0	1226.9	0.0	B3_104	520	4	16	333.2	333.2	0.0	0.0
B2_40	160	2	17	625.8	625.8	0.0	0.0	B3_104	520	4	17	305.9	0.0	305.9	0.0
B2_40	160	2	18	3272.1	818.0	2454.1	0.0	B3_104	520	4	18	318.6	0.0	318.6	0.0
B2_40	160	2	19	208.1	0.0	208.1	0.0	B3_104	520	4	19	65.0	0.0	65.0	0.0
B2_40	160	2	20	1658.2	1243.7	414.6	0.0	B3_104	520	4	20	156.0	156.0	0.0	0.0
B2_40	160	2	21	1823.5	0.0	1823.5	0.0	B3_104	520	4	21	787.5	0.0	787.5	0.0
B2_40	160	2	22	1724.9	0.0	1724.9	0.0	B3_104	520	4	22	125.4	0.0	125.4	0.0
B2_40	160	2	23	887.6	0.0	887.6	0.0	B3_104	520	4	23	862.9	0.0	862.9	0.0
B2_40	160	2	24	3483.2	0.0	3483.2	0.0	B3_104	520	4	24	82.5	0.0	0.0	82.5
B2_40	160	2	25	1233.6	0.0	1233.6	0.0	B3_104	520	4	25	143.7	0.0	0.0	143.7

B2_40	160	2	26	8629.6	2157.4	6472.2	0.0	B3_104	520	4	26	99.9	0.0	99.9	0.0
B2_40	160	2	27	14906.9	14906.9	0.0	0.0	B3_104	520	4	27	288.4	288.4	0.0	0.0
B2_40	160	2	28	2564.7	1923.5	641.2	0.0	B3_104	520	4	28	342.6	0.0	342.6	0.0
B2_40	160	2	29	654.1	0.0	654.1	0.0	B3_104	520	4	29	338.8	0.0	338.8	0.0
B2_40	160	2	30	4084.0	0.0	4084.0	0.0	B3_104	520	4	30	372.3	0.0	372.3	0.0
B2_41	180	6	1	437.1	0.0	437.1	0.0	B4_108	100	2	1	1583.9	0.0	1583.9	0.0
B2_41	180	6	2	1534.3	0.0	1534.3	0.0	B4_108	100	2	2	1249.3	0.0	1249.3	0.0
B2_41	180	6	3	4127.9	0.0	4127.9	0.0	B4_108	100	2	3	1038.2	0.0	1038.2	0.0
B2_41	180	6	4	307.7	0.0	0.0	307.7	B4_108	100	2	4	9246.2	0.0	9246.2	0.0
B2_41	180	6	5	5229.0	5229.0	0.0	0.0	B4_108	100	2	5	294.1	0.0	294.1	0.0
B2_41	180	6	6	583.9	0.0	583.9	0.0	B4_108	100	2	6	2584.9	1938.7	646.2	0.0
B2_41	180	6	7	1512.4	1134.3	378.1	0.0	B4_108	100	2	7	1408.1	0.0	1408.1	0.0
B2_41	180	6	8	1412.3	0.0	1412.3	0.0	B4_108	100	2	8	472.2	0.0	0.0	472.2
B2_41	180	6	9	1892.2	0.0	1892.2	0.0	B4_108	100	2	9	4371.5	1092.9	3278.6	0.0
B2_41	180	6	10	1177.3	0.0	1177.3	0.0	B4_108	100	2	10	591.0	0.0	591.0	0.0
B2_41	180	6	11	1215.2	1215.2	0.0	0.0	B4_108	100	2	11	1497.2	374.3	1122.9	0.0
B2_41	180	6	12	4795.9	0.0	4795.9	0.0	B4_108	100	2	12	697.9	0.0	697.9	0.0
B2_41	180	6	13	1679.1	0.0	1679.1	0.0	B4_108	100	2	13	3173.5	793.4	2380.1	0.0
B2_41	180	6	14	3557.4	0.0	3557.4	0.0	B4_108	100	2	14	8315.5	0.0	8315.5	0.0
B2_41	180	6	15	2178.9	1634.2	544.7	0.0	B4_108	100	2	15	706.4	0.0	706.4	0.0
B2_41	180	6	16	2096.3	1572.2	524.1	0.0	B4_108	100	2	16	603.2	0.0	603.2	0.0
B2_41	180	6	17	434.1	434.1	0.0	0.0	B4_108	100	2	17	323.3	0.0	323.3	0.0
B2_41	180	6	18	3153.1	0.0	3153.1	0.0	B4_108	100	2	18	707.8	0.0	707.8	0.0
B2_41	180	6	19	3114.3	0.0	3114.3	0.0	B4_108	100	2	19	5414.4	0.0	5414.4	0.0
B2_41	180	6	20	11960.9	11960.9	0.0	0.0	B4_108	100	2	20	143.7	0.0	0.0	143.7
B2_41	180	6	21	660.6	0.0	660.6	0.0	B4_108	100	2	21	1076.4	1076.4	0.0	0.0
B2_41	180	6	22	1256.0	0.0	1256.0	0.0	B4_108	100	2	22	725.3	0.0	725.3	0.0
B2_41	180	6	23	644.2	483.1	161.0	0.0	B4_108	100	2	23	599.0	0.0	599.0	0.0
B2_41	180	6	24	526.7	0.0	526.7	0.0	B4_108	100	2	24	212.5	0.0	212.5	0.0
B2_41	180	6	25	310.1	0.0	310.1	0.0	B4_108	100	2	25	599.0	0.0	0.0	599.0
B2_41	180	6	26	1534.8	0.0	1534.8	0.0	B4_108	100	2	26	121.1	121.1	0.0	0.0
B2_41	180	6	27	2785.3	2088.9	696.3	0.0	B4_108	100	2	27	3174.4	0.0	3174.4	0.0
B2_41	180	6	28	6267.9	4700.9	1567.0	0.0	B4_108	100	2	28	1998.6	0.0	1998.6	0.0
B2_41	180	6	29	240.9	0.0	0.0	240.9	B4_108	100	2	29	6842.3	0.0	6842.3	0.0
B2_41	180	6	30	418.2	313.6	104.5	0.0	B4_108	100	2	30	1461.4	0.0	1461.4	0.0
B2_42	200	5	1	3136.7	2352.6	784.2	0.0	B4_109	200	6	1	1669.2	1669.2	0.0	0.0
B2_42	200	5	2	395.9	395.9	0.0	0.0	B4_109	200	6	2	382.8	0.0	382.8	0.0
B2_42	200	5	3	220.6	0.0	220.6	0.0	B4_109	200	6	3	1808.1	452.0	1356.0	0.0
B2_42	200	5	4	91.0	91.0	0.0	0.0	B4_109	200	6	4	1595.0	398.7	1196.2	0.0
B2_42	200	5	5	139.0	0.0	139.0	0.0	B4_109	200	6	5	1435.2	0.0	1435.2	0.0
B2_42	200	5	6	131.5	131.5	0.0	0.0	B4_109	200	6	6	260.4	0.0	260.4	0.0
B2_42	200	5	7	2899.7	724.9	2174.8	0.0	B4_109	200	6	7	846.3	211.6	634.7	0.0
B2_42	200	5	8	670.6	0.0	670.6	0.0	B4_109	200	6	8	609.3	457.0	152.3	0.0
B2_42	200	5	9	511.8	0.0	0.0	511.8	B4_109	200	6	9	861.2	861.2	0.0	0.0
B2_42	200	5	10	51.4	0.0	0.0	51.4	B4_109	200	6	10	2199.8	2199.8	0.0	0.0
B2_42	200	5	11	223.9	0.0	223.9	0.0	B4_109	200	6	11	1850.4	0.0	1850.4	0.0
B2_42	200	5	12	1356.3	0.0	1356.3	0.0	B4_109	200	6	12	4608.7	4608.7	0.0	0.0
B2_42	200	5	13	2517.0	0.0	1887.8	629.3	B4_109	200	6	13	2266.0	0.0	2266.0	0.0
B2_42	200	5	14	1349.2	1349.2	0.0	0.0	B4_109	200	6	14	344.5	344.5	0.0	0.0
B2_42	200	5	15	144.2	0.0	144.2	0.0	B4_109	200	6	15	322.6	0.0	322.6	0.0
B2_42	200	5	16	1090.5	0.0	1090.5	0.0	B4_109	200	6	16	261.4	0.0	261.4	0.0
B2_42	200	5	17	294.5	294.5	0.0	0.0	B4_109	200	6	17	396.8	396.8	0.0	0.0
B2_42	200	5	18	320.0	0.0	320.0	0.0	B4_109	200	6	18	419.7	419.7	0.0	0.0

Table B.1., cont.

B2_42	200	5	19	339.8	339.8	0.0	0.0	B4_109	200	6	19	992.1	0.0	992.1	0.0
B2_42	200	5	20	205.9	0.0	205.9	0.0	B4_109	200	6	20	829.9	829.9	0.0	0.0
B2_42	200	5	21	167.8	167.8	0.0	0.0	B4_109	200	6	21	881.1	881.1	0.0	0.0
B2_42	200	5	22	105.1	0.0	0.0	105.1	B4_109	200	6	22	1014.5	0.0	1014.5	0.0
B2_42	200	5	23	506.6	380.0	126.7	0.0	B4_109	200	6	23	506.3	0.0	506.3	0.0
B2_42	200	5	24	209.2	0.0	0.0	209.2	B4_109	200	6	24	7343.2	5507.4	1835.8	0.0
B2_42	200	5	25	461.8	0.0	461.8	0.0	B4_109	200	6	25	1248.5	0.0	1248.5	0.0
B2_42	200	5	26	156.0	0.0	156.0	0.0	B4_109	200	6	26	210.1	0.0	210.1	0.0
B2_42	200	5	27	331.8	331.8	0.0	0.0	B4_109	200	6	27	532.7	0.0	532.7	0.0
B2_42	200	5	28	424.6	424.6	0.0	0.0	B4_109	200	6	28	261.4	0.0	261.4	0.0
B2_42	200	5	29	492.5	0.0	492.5	0.0	B4_109	200	6	29	569.0	569.0	0.0	0.0
B2_42	200	5	30	402.5	402.5	0.0	0.0	B4_109	200	6	30	1090.2	0.0	1090.2	0.0
B2_43	220	8	1	249.0	249.0	0.0	0.0	B4_110	220	4	1	15214.1	15214.1	0.0	0.0
B2_43	220	8	2	194.3	0.0	194.3	0.0	B4_110	220	4	2	1753.8	0.0	1753.8	0.0
B2_43	220	8	3	603.6	0.0	603.6	0.0	B4_110	220	4	3	5083.6	3812.7	1270.9	0.0
B2_43	220	8	4	189.2	0.0	189.2	0.0	B4_110	220	4	4	6644.3	1661.1	4983.2	0.0
B2_43	220	8	5	95.4	95.4	0.0	0.0	B4_110	220	4	5	396.8	0.0	396.8	0.0
B2_43	220	8	6	125.1	125.1	0.0	0.0	B4_110	220	4	6	3463.3	3463.3	0.0	0.0
B2_43	220	8	7	129.0	129.0	0.0	0.0	B4_110	220	4	7	2781.8	695.4	2086.3	0.0
B2_43	220	8	8	125.6	125.6	0.0	0.0	B4_110	220	4	8	380.8	380.8	0.0	0.0
B2_43	220	8	9	1054.9	263.7	791.2	0.0	B4_110	220	4	9	5217.6	0.0	1304.4	0.0
B2_43	220	8	10	745.7	0.0	745.7	0.0	B4_110	220	4	10	4294.1	1073.5	3220.6	0.0
B2_43	220	8	11	81.0	81.0	0.0	0.0	B4_110	220	4	11	5878.7	1469.7	4409.0	0.0
B2_43	220	8	12	305.4	305.4	0.0	0.0	B4_110	220	4	12	478.4	119.6	358.8	0.0

B2_43	220	8	13	1653.0	0.0	1239.7	413.2	B4_110	220	4	13	310.1	310.1	0.0	0.0
B2_43	220	8	14	601.9	0.0	601.9	0.0	B4_110	220	4	14	2969.4	2969.4	0.0	0.0
B2_43	220	8	15	942.1	0.0	942.1	0.0	B4_110	220	4	15	1504.4	0.0	1504.4	0.0
B2_43	220	8	16	1798.9	1349.2	449.7	0.0	B4_110	220	4	16	28400.6	28400.6	0.0	0.0
B2_43	220	8	17	134.0	0.0	134.0	0.0	B4_110	220	4	17	676.5	0.0	676.5	0.0
B2_43	220	8	18	1465.5	1099.1	366.4	0.0	B4_110	220	4	18	377.3	0.0	377.3	0.0
B2_43	220	8	19	2660.4	665.1	1995.3	0.0	B4_110	220	4	19	659.1	164.8	494.3	0.0
B2_43	220	8	20	456.0	114.0	0.0	342.0	B4_110	220	4	20	350.5	0.0	350.5	0.0
B2_43	220	8	21	2819.0	0.0	2819.0	0.0	B4_110	220	4	21	1393.9	0.0	1393.9	0.0
B2_43	220	8	22	445.0	445.0	0.0	0.0	B4_110	220	4	22	8521.0	2130.3	6390.8	0.0
B2_43	220	8	23	688.9	172.2	516.6	0.0	B4_110	220	4	23	375.4	0.0	375.4	0.0
B2_43	220	8	24	763.5	190.9	572.6	0.0	B4_110	220	4	24	1796.1	1796.1	0.0	0.0
B2_43	220	8	25	933.6	933.6	0.0	0.0	B4_110	220	4	25	2825.6	0.0	2825.6	0.0
B2_43	220	8	26	430.1	0.0	430.1	0.0	B4_110	220	4	26	490.3	490.3	0.0	0.0
B2_43	220	8	27	1298.8	0.0	1298.8	0.0	B4_110	220	4	27	238.5	0.0	238.5	0.0
B2_43	220	8	28	397.5	0.0	397.5	0.0	B4_110	220	4	28	3030.2	3030.2	0.0	0.0
B2_43	220	8	29	614.6	0.0	614.6	0.0	B4_110	220	4	29	297.2	0.0	297.2	0.0
B2_43	220	8	30	1755.2	0.0	1316.4	438.8	B4_110	220	4	30	1527.3	1527.3	0.0	0.0
B2_44	240	6	1	72.1	0.0	0.0	72.1	B4_111	240	6	1	1200.8	300.2	900.6	0.0
B2_44	240	6	2	279.0	209.2	69.7	0.0	B4_111	240	6	2	322.8	0.0	322.8	0.0
B2_44	240	6	3	579.2	144.8	434.4	0.0	B4_111	240	6	3	1010.9	0.0	1010.9	0.0
B2_44	240	6	4	115.5	115.5	0.0	0.0	B4_111	240	6	4	1953.9	1465.4	488.5	0.0
B2_44	240	6	5	1785.6	1339.2	446.4	0.0	B4_111	240	6	5	1100.4	0.0	1100.4	0.0
B2_44	240	6	6	971.3	0.0	0.0	971.3	B4_111	240	6	6	1420.9	1065.7	355.2	0.0
B2_44	240	6	7	1381.3	0.0	1381.3	0.0	B4_111	240	6	7	793.1	594.9	198.3	0.0
B2_44	240	6	8	562.2	562.2	0.0	0.0	B4_111	240	6	8	1507.1	0.0	1507.1	0.0
B2_44	240	6	9	1934.1	0.0	1934.1	0.0	B4_111	240	6	9	3209.3	0.0	3209.3	0.0
B2_44	240	6	10	780.9	585.7	195.2	0.0	B4_111	240	6	10	6845.1	1711.3	5133.8	0.0
B2_44	240	6	11	201.7	201.7	0.0	0.0	B4_111	240	6	11	478.8	478.8	0.0	0.0
B2_44	240	6	12	208.8	208.8	0.0	0.0	B4_111	240	6	12	2284.2	1713.2	571.1	0.0
B2_44	240	6	13	1072.1	268.0	804.1	0.0	B4_111	240	6	13	317.6	0.0	317.6	0.0
B2_44	240	6	14	1148.5	1148.5	0.0	0.0	B4_111	240	6	14	541.0	0.0	0.0	541.0
B2_44	240	6	15	313.4	313.4	0.0	0.0	B4_111	240	6	15	412.8	0.0	412.8	0.0
B2_44	240	6	16	923.2	0.0	923.2	0.0	B4_111	240	6	16	1300.7	0.0	1300.7	0.0
B2_44	240	6	17	492.9	0.0	492.9	0.0	B4_111	240	6	17	459.5	0.0	459.5	0.0
B2_44	240	6	18	826.6	826.6	0.0	0.0	B4_111	240	6	18	639.5	479.6	0.0	159.9
B2_44	240	6	19	1299.3	0.0	1299.3	0.0	B4_111	240	6	19	1044.3	0.0	1044.3	0.0
B2_44	240	6	20	289.4	0.0	289.4	0.0	B4_111	240	6	20	2050.0	0.0	2050.0	0.0
B2_44	240	6	21	1026.9	256.7	770.2	0.0	B4_111	240	6	21	1044.3	0.0	1044.3	0.0
B2_44	240	6	22	1026.9	256.7	770.2	0.0	B4_111	240	6	22	253.5	0.0	0.0	253.5
B2_44	240	6	23	2415.2	603.8	1811.4	0.0	B4_111	240	6	23	485.9	485.9	0.0	0.0
B2_44	240	6	24	733.8	733.8	0.0	0.0	B4_111	240	6	24	2394.0	0.0	2394.0	0.0
B2_44	240	6	25	972.7	243.2	729.5	0.0	B4_111	240	6	25	816.2	0.0	816.2	0.0
B2_44	240	6	26	635.3	0.0	0.0	635.3	B4_111	240	6	26	759.2	0.0	759.2	0.0
B2_44	240	6	27	1108.0	1108.0	0.0	0.0	B4_111	240	6	27	661.7	661.7	0.0	0.0
B2_44	240	6	28	189.5	189.5	0.0	0.0	B4_111	240	6	28	552.3	0.0	552.3	0.0

Table B.1., cont.

B2_44	240	6	29	4634.4	3475.8	1158.6	0.0	B4_111	240	6	29	231.9	0.0	231.9	0.0
B2_44	240	6	30	253.1	0.0	253.1	0.0	B4_111	240	6	30	424.1	0.0	424.1	0.0
B2_45	260	8	1	3486.4	0.0	3486.4	0.0	B4_112	260	4	1	7246.2	7246.2	0.0	0.0
B2_45	260	8	2	1304.0	0.0	1304.0	0.0	B4_112	260	4	2	304.9	0.0	304.9	0.0
B2_45	260	8	3	6631.7	4973.7	1657.9	0.0	B4_112	260	4	3	172.0	0.0	172.0	0.0
B2_45	260	8	4	1499.1	1499.1	0.0	0.0	B4_112	260	4	4	3616.5	904.1	2712.4	0.0
B2_45	260	8	5	629.1	0.0	629.1	0.0	B4_112	260	4	5	3556.2	0.0	3556.2	0.0
B2_45	260	8	6	330.8	330.8	0.0	0.0	B4_112	260	4	6	24373.4	6093.3	18280.0	0.0
B2_45	260	8	7	1585.3	1585.3	0.0	0.0	B4_112	260	4	7	322.8	0.0	0.0	322.8
B2_45	260	8	8	1965.2	1473.9	491.3	0.0	B4_112	260	4	8	4663.6	3497.7	1165.9	0.0
B2_45	260	8	9	1878.0	0.0	1878.0	0.0	B4_112	260	4	9	265.3	0.0	265.3	0.0
B2_45	260	8	10	1447.7	0.0	1447.7	0.0	B4_112	260	4	10	6924.3	5193.2	1731.1	0.0
B2_45	260	8	11	5142.9	0.0	5142.9	0.0	B4_112	260	4	11	2424.7	0.0	2424.7	0.0
B2_45	260	8	12	2620.2	1965.2	655.1	0.0	B4_112	260	4	12	1404.8	0.0	1404.8	0.0
B2_45	260	8	13	289.4	289.4	0.0	0.0	B4_112	260	4	13	1136.2	0.0	0.0	1136.2
B2_45	260	8	14	1619.3	0.0	1619.3	0.0	B4_112	260	4	14	400.1	400.1	400.1	0.0
B2_45	260	8	15	2800.3	0.0	2800.3	0.0	B4_112	260	4	15	416.6	0.0	416.6	0.0
B2_45	260	8	16	1201.7	0.0	1201.7	0.0	B4_112	260	4	16	7912.6	0.0	7912.6	0.0
B2_45	260	8	17	2149.0	0.0	2149.0	0.0	B4_112	260	4	17	1822.9	455.7	1367.1	0.0
B2_45	260	8	18	576.8	0.0	576.8	0.0	B4_112	260	4	18	6711.3	5033.5	1677.8	0.0
B2_45	260	8	19	444.9	0.0	444.9	0.0	B4_112	260	4	19	6749.0	5061.7	1687.2	0.0
B2_45	260	8	20	882.7	0.0	882.7	0.0	B4_112	260	4	20	6262.7	0.0	6262.7	0.0
B2_45	260	8	21	6014.3	1503.6	4510.7	0.0	B4_112	260	4	21	9456.9	2364.2	7092.7	0.0
B2_45	260	8	22	4224.9	0.0	4224.9	0.0	B4_112	260	4	22	4174.5	0.0	4174.5	0.0
B2_45	260	8	23	578.2	0.0	578.2	0.0	B4_112	260	4	23	374.7	0.0	374.7	0.0
B2_45	260	8	24	2234.3	0.0	2234.3	0.0	B4_112	260	4	24	5180.2	1295.0	3885.1	0.0
B2_45	260	8	25	198.4	0.0	0.0	198.4	B4_112	260	4	25	779.0	0.0	779.0	0.0
B2_45	260	8	26	136.2	0.0	0.0	136.2	B4_112	260	4	26	173.0	173.0	0.0	0.0
B2_45	260	8	27	2985.5	0.0	2985.5	0.0	B4_112	260	4	27	2330.4	0.0	2330.4	0.0
B2_45	260	8	28	232.3	232.3	0.0	0.0	B4_112	260	4	28	410.9	0.0	410.9	0.0
B2_45	260	8	29	2262.6	2262.6	0.0	0.0	B4_112	260	4	29	1280.9	0.0	1280.9	0.0

B2_45	260	8	30	1999.6	0.0	1999.6	0.0	B4_112	260	4	30	11455.1	8591.3	2863.8	0.0
B2_46	280	6	1	8846.1	6634.6	2211.5	0.0	B4_113	280	9	1	5654.1	0.0	5654.1	0.0
B2_46	280	6	2	2703.2	2027.4	675.8	0.0	B4_113	280	9	2	1506.6	0.0	1506.6	0.0
B2_46	280	6	3	3252.5	813.1	2439.4	0.0	B4_113	280	9	3	1743.4	1307.5	435.8	0.0
B2_46	280	6	4	1692.0	1692.0	0.0	0.0	B4_113	280	9	4	878.4	658.8	219.6	0.0
B2_46	280	6	5	692.3	692.3	0.0	0.0	B4_113	280	9	5	7534.6	0.0	7534.6	0.0
B2_46	280	6	6	3538.4	884.6	2653.8	0.0	B4_113	280	9	6	219.8	0.0	0.0	219.8
B2_46	280	6	7	714.7	0.0	714.7	0.0	B4_113	280	9	7	10851.2	10851.2	0.0	0.0
B2_46	280	6	8	1129.6	0.0	0.0	1129.6	B4_113	280	9	8	137.2	137.2	0.0	0.0
B2_46	280	6	9	2514.1	2514.1	0.0	0.0	B4_113	280	9	9	981.6	981.6	0.0	0.0
B2_46	280	6	10	345.7	0.0	345.7	0.0	B4_113	280	9	10	250.2	0.0	250.2	0.0
B2_46	280	6	11	2537.0	2537.0	0.0	0.0	B4_113	280	9	11	819.0	204.7	614.2	0.0
B2_46	280	6	12	1996.1	499.0	1497.1	0.0	B4_113	280	9	12	507.6	0.0	507.6	0.0
B2_46	280	6	13	10322.2	7741.6	0.0	2580.5	B4_113	280	9	13	355.2	355.2	0.0	0.0
B2_46	280	6	14	548.5	0.0	548.5	0.0	B4_113	280	9	14	198.8	0.0	198.8	0.0
B2_46	280	6	15	4638.7	1159.7	3479.0	0.0	B4_113	280	9	15	1264.9	948.6	316.2	0.0
B2_46	280	6	16	1601.7	400.4	1201.3	0.0	B4_113	280	9	16	1906.0	0.0	1906.0	0.0
B2_46	280	6	17	229.5	229.5	0.0	0.0	B4_113	280	9	17	1142.4	0.0	1142.4	0.0
B2_46	280	6	18	288.0	288.0	0.0	0.0	B4_113	280	9	18	315.9	0.0	315.9	0.0
B2_46	280	6	19	3356.9	0.0	3356.9	0.0	B4_113	280	9	19	2326.0	0.0	2326.0	0.0
B2_46	280	6	20	2860.6	2145.5	715.2	0.0	B4_113	280	9	20	1526.2	1144.7	381.6	0.0
B2_46	280	6	21	4212.0	3159.0	1053.0	0.0	B4_113	280	9	21	11517.3	0.0	11517.3	0.0
B2_46	280	6	22	173.9	0.0	173.9	0.0	B4_113	280	9	22	1127.7	845.8	281.9	0.0
B2_46	280	6	23	7107.8	5330.9	1777.0	0.0	B4_113	280	9	23	3896.9	0.0	3896.9	0.0
B2_46	280	6	24	601.1	601.1	0.0	0.0	B4_113	280	9	24	1222.9	0.0	1222.9	0.0
B2_46	280	6	25	2327.8	2327.8	0.0	0.0	B4_113	280	9	25	789.0	0.0	789.0	0.0
B2_46	280	6	26	1458.3	1093.7	0.0	364.6	B4_113	280	9	26	2066.8	0.0	2066.8	0.0
B2_46	280	6	27	1714.9	428.7	1286.2	0.0	B4_113	280	9	27	5084.9	1271.2	3813.7	0.0
B2_46	280	6	28	4657.4	3493.0	1164.3	0.0	B4_113	280	9	28	148.3	148.3	0.0	0.0
B2_46	280	6	29	3136.3	784.1	2352.2	0.0	B4_113	280	9	29	883.8	662.8	220.9	0.0
B2_46	280	6	30	2106.9	1580.1	526.7	0.0	B4_113	280	9	30	584.4	0.0	584.4	0.0
B2_47	300	8	1	2108.8	2108.8	0.0	0.0	B4_114	300	10	1	2968.5	0.0	2968.5	0.0
B2_47	300	8	2	794.8	198.7	596.1	0.0	B4_114	300	10	2	1889.9	1889.9	0.0	0.0
B2_47	300	8	3	118.0	0.0	118.0	0.0	B4_114	300	10	3	3737.8	2803.4	934.5	0.0
B2_47	300	8	4	1686.6	421.7	1265.0	0.0	B4_114	300	10	4	3175.8	2381.8	793.9	0.0
B2_47	300	8	5	1927.5	1927.5	0.0	0.0	B4_114	300	10	5	361.9	0.0	361.9	0.0
B2_47	300	8	6	1332.3	0.0	1332.3	0.0	B4_114	300	10	6	3170.9	0.0	3170.9	0.0
B2_47	300	8	7	128.7	0.0	0.0	128.7	B4_114	300	10	7	2840.2	2840.2	0.0	0.0
B2_47	300	8	8	533.0	533.0	0.0	0.0	B4_114	300	10	8	1647.8	1647.8	0.0	0.0

Table B.1., cont.

B2_47	300	8	9	105.4	0.0	0.0	105.4	B4_114	300	10	9	3550.2	0.0	2662.6	887.5
B2_47	300	8	10	1306.0	0.0	1306.0	0.0	B4_114	300	10	10	2078.0	519.5	1558.5	0.0
B2_47	300	8	11	2279.1	569.8	1709.3	0.0	B4_114	300	10	11	23415.7	5853.9	17561.8	0.0
B2_47	300	8	12	5111.3	3833.4	1277.8	0.0	B4_114	300	10	12	3451.9	0.0	3451.9	0.0
B2_47	300	8	13	376.2	0.0	376.2	0.0	B4_114	300	10	13	2266.6	0.0	2266.6	0.0
B2_47	300	8	14	283.3	0.0	283.3	0.0	B4_114	300	10	14	128.7	128.7	0.0	0.0
B2_47	300	8	15	441.9	0.0	0.0	441.9	B4_114	300	10	15	6531.2	1632.8	4898.4	0.0
B2_47	300	8	16	2015.5	503.9	1511.6	0.0	B4_114	300	10	16	8938.9	0.0	8938.9	0.0
B2_47	300	8	17	463.3	463.3	0.0	0.0	B4_114	300	10	17	1192.0	1192.0	0.0	0.0
B2_47	300	8	18	1467.3	0.0	1467.3	0.0	B4_114	300	10	18	1605.3	1605.3	0.0	0.0
B2_47	300	8	19	1334.6	0.0	1000.9	333.6	B4_114	300	10	19	133.1	0.0	133.1	0.0
B2_47	300	8	20	4486.2	0.0	4486.2	0.0	B4_114	300	10	20	810.5	0.0	202.6	607.9
B2_47	300	8	21	218.9	0.0	218.9	0.0	B4_114	300	10	21	3623.0	0.0	3623.0	0.0
B2_47	300	8	22	109.5	0.0	109.5	0.0	B4_114	300	10	22	1699.6	0.0	1699.6	0.0
B2_47	300	8	23	946.7	946.7	0.0	0.0	B4_114	300	10	23	1149.1	0.0	1149.1	0.0
B2_47	300	8	24	238.6	0.0	0.0	238.6	B4_114	300	10	24	2384.5	0.0	2384.5	0.0
B2_47	300	8	25	265.8	265.8	0.0	0.0	B4_114	300	10	25	1781.8	0.0	0.0	1781.8
B2_47	300	8	26	6810.0	0.0	6810.0	0.0	B4_114	300	10	26	8528.3	2132.1	6396.2	0.0
B2_47	300	8	27	375.8	0.0	375.8	0.0	B4_114	300	10	27	7041.4	0.0	7041.4	0.0
B2_47	300	8	28	2644.5	0.0	1983.4	661.1	B4_114	300	10	28	6638.4	0.0	6638.4	0.0
B2_47	300	8	29	3858.5	964.6	2893.9	0.0	B4_114	300	10	29	2246.5	0.0	2246.5	0.0
B2_47	300	8	30	274.8	0.0	0.0	274.8	B4_114	300	10	30	4223.9	0.0	4223.9	0.0
B2_48	320	10	1	83.1	0.0	83.1	0.0	B4_115	320	7	1	532.1	0.0	532.1	0.0
B2_48	320	10	2	1558.0	0.0	1558.0	0.0	B4_115	320	7	2	4737.2	1184.3	3552.9	0.0
B2_48	320	10	3	550.4	0.0	550.4	0.0	B4_115	320	7	3	268.6	0.0	0.0	268.6
B2_48	320	10	4	1104.5	828.3	276.1	0.0	B4_115	320	7	4	1091.9	1091.9	0.0	0.0
B2_48	320	10	5	161.3	161.3	0.0	0.0	B4_115	320	7	5	279.9	0.0	279.9	0.0
B2_48	320	10	6	1634.8	0.0	1634.8	0.0	B4_115	320	7	6	271.9	0.0	0.0	271.9
B2_48	320	10	7	219.8	0.0	0.0	219.8	B4_115	320	7	7	1704.1	0.0	1704.1	0.0
B2_48	320	10	8	647.4	647.4	0.0	0.0	B4_115	320	7	8	353.9	0.0	0.0	353.9
B2_48	320	10	9	1269.8	0.0	1269.8	0.0	B4_115	320	7	9	563.2	0.0	563.2	0.0
B2_48	320	10	10	6921.2	5190.9	1730.3	0.0	B4_115	320	7	10	327.1	0.0	327.1	0.0
B2_48	320	10	11	391.8	0.0	391.8	0.0	B4_115	320	7	11	227.2	0.0	0.0	227.2
B2_48	320	10	12	1131.3	0.0	848.5	282.8	B4_115	320	7	12	1902.0	0.0	1902.0	0.0
B2_48	320	10	13	815.8	204.0	611.9	0.0	B4_115	320	7	13	376.5	0.0	376.5	0.0
B2_48	320	10	14	1403.8	0.0	351.0	1052.9	B4_115	320	7	14	587.7	0.0	587.7	0.0
B2_48	320	10	15	1468.2	1468.2	0.0	0.0	B4_115	320	7	15	112.6	112.6	0.0	0.0
B2_48	320	10	16	1108.0	0.0	1108.0	0.0	B4_115	320	7	16	86.7	0.0	0.0	86.7

B2_48	320	10	17	615.7	615.7	0.0	0.0	B4_115	320	7	17	490.1	0.0	490.1	0.0
B2_48	320	10	18	383.3	383.3	0.0	0.0	B4_115	320	7	18	5379.0	1344.8	4034.3	0.0
B2_48	320	10	19	1516.9	1137.6	379.2	0.0	B4_115	320	7	19	101.3	0.0	101.3	0.0
B2_48	320	10	20	752.8	0.0	752.8	0.0	B4_115	320	7	20	164.5	164.5	0.0	0.0
B2_48	320	10	21	173.4	173.4	0.0	0.0	B4_115	320	7	21	159.3	0.0	159.3	0.0
B2_48	320	10	22	420.0	420.0	0.0	0.0	B4_115	320	7	22	463.7	0.0	0.0	463.7
B2_48	320	10	23	2300.5	575.1	1725.4	0.0	B4_115	320	7	23	137.1	0.0	0.0	137.1
B2_48	320	10	24	5537.1	1384.3	0.0	4152.8	B4_115	320	7	24	206.9	0.0	0.0	206.9
B2_48	320	10	25	150.6	150.6	0.0	0.0	B4_115	320	7	25	4716.0	3537.0	1179.0	0.0
B2_48	320	10	26	2261.6	1696.2	565.4	0.0	B4_115	320	7	26	2838.4	0.0	2838.4	0.0
B2_48	320	10	27	421.3	0.0	421.3	0.0	B4_115	320	7	27	1879.4	0.0	1879.4	0.0
B2_48	320	10	28	288.2	288.2	0.0	0.0	B4_115	320	7	28	1432.2	0.0	1432.2	0.0
B2_48	320	10	29	542.0	0.0	542.0	0.0	B4_115	320	7	29	3887.5	0.0	3887.5	0.0
B2_48	320	10	30	324.8	0.0	0.0	324.8	B4_115	320	7	30	1824.3	0.0	1368.2	456.1
B2_49	360	8	1	4464.3	0.0	3348.2	1116.1	B4_116	340	15	1	305.2	305.2	0.0	0.0
B2_49	360	8	2	875.6	0.0	875.6	0.0	B4_116	340	15	2	5382.9	4037.2	1345.7	0.0
B2_49	360	8	3	673.4	0.0	673.4	0.0	B4_116	340	15	3	732.7	732.7	0.0	0.0
B2_49	360	8	4	699.4	524.5	174.8	0.0	B4_116	340	15	4	1638.4	0.0	1638.4	0.0
B2_49	360	8	5	4437.0	1109.2	3327.7	0.0	B4_116	340	15	5	4682.3	1170.6	3511.8	0.0
B2_49	360	8	6	11169.5	0.0	11169.5	0.0	B4_116	340	15	6	985.6	0.0	985.6	0.0
B2_49	360	8	7	3813.5	2860.1	953.4	0.0	B4_116	340	15	7	2586.0	0.0	2586.0	0.0
B2_49	360	8	8	450.1	112.5	337.5	0.0	B4_116	340	15	8	6978.4	6978.4	0.0	0.0
B2_49	360	8	9	2038.7	0.0	2038.7	0.0	B4_116	340	15	9	615.7	615.7	0.0	0.0
B2_49	360	8	10	2534.0	0.0	2534.0	0.0	B4_116	340	15	10	3600.2	2700.2	900.1	0.0
B2_49	360	8	11	366.2	366.2	0.0	0.0	B4_116	340	15	11	6878.3	5158.7	1719.6	0.0
B2_49	360	8	12	1443.0	0.0	1443.0	0.0	B4_116	340	15	12	2582.0	0.0	2582.0	0.0
B2_49	360	8	13	1990.6	1493.0	497.7	0.0	B4_116	340	15	13	242.6	0.0	242.6	0.0
B2_49	360	8	14	689.9	0.0	689.9	0.0	B4_116	340	15	14	506.7	0.0	506.7	0.0
B2_49	360	8	15	6017.6	4513.2	1504.4	0.0	B4_116	340	15	15	118.4	0.0	0.0	118.4
B2_49	360	8	16	1212.1	303.0	909.1	0.0	B4_116	340	15	16	494.2	0.0	0.0	494.2
B2_49	360	8	17	515.1	515.1	0.0	0.0	B4_116	340	15	17	125.1	0.0	0.0	125.1
B2_49	360	8	18	714.4	0.0	714.4	0.0	B4_116	340	15	18	745.7	0.0	745.7	0.0

Table B.1., cont.

B2_49	360	8	19	508.0	508.0	0.0	0.0	B4_116	340	15	19	250.7	0.0	0.0	250.7
B2_49	360	8	20	372.3	0.0	372.3	0.0	B4_116	340	15	20	3711.0	0.0	3711.0	0.0
B2_49	360	8	21	2501.0	625.3	1875.8	0.0	B4_116	340	15	21	435.6	435.6	0.0	0.0
B2_49	360	8	22	373.7	373.7	0.0	0.0	B4_116	340	15	22	3526.5	881.6	2644.9	0.0
B2_49	360	8	23	1101.4	0.0	1101.4	0.0	B4_116	340	15	23	455.3	0.0	0.0	455.3
B2_49	360	8	24	1896.8	1422.6	474.2	0.0	B4_116	340	15	24	440.5	0.0	440.5	0.0
B2_49	360	8	25	1944.4	0.0	1944.4	0.0	B4_116	340	15	25	2317.9	579.5	1738.5	0.0
B2_49	360	8	26	2439.3	2439.3	0.0	0.0	B4_116	340	15	26	5920.0	0.0	5920.0	0.0
B2_49	360	8	27	806.8	201.7	605.1	0.0	B4_116	340	15	27	974.0	0.0	974.0	0.0
B2_49	360	8	28	8714.6	6536.0	2178.7	0.0	B4_116	340	15	28	1033.0	0.0	1033.0	0.0
B2_49	360	8	29	5663.2	1415.8	4247.4	0.0	B4_116	340	15	29	9682.8	2420.7	7262.1	0.0
B2_49	360	8	30	954.3	0.0	954.3	0.0	B4_116	340	15	30	842.6	0.0	842.6	0.0
B2_55	900	10	1	3156.1	0.0	3156.1	0.0	B4_117	360	17	1	23254.9	23254.9	0.0	0.0
B2_55	900	10	2	3613.6	903.4	2710.2	0.0	B4_117	360	17	2	1400.0	350.0	1050.0	0.0
B2_55	900	10	3	899.1	0.0	899.1	0.0	B4_117	360	17	3	1624.6	0.0	1624.6	0.0
B2_55	900	10	4	2262.6	1696.9	565.6	0.0	B4_117	360	17	4	1169.8	1169.8	0.0	0.0
B2_55	900	10	5	11430.2	8572.7	2857.6	0.0	B4_117	360	17	5	306.1	0.0	306.1	0.0
B2_55	900	10	6	403.2	0.0	403.2	0.0	B4_117	360	17	6	1064.1	0.0	1064.1	0.0
B2_55	900	10	7	5977.7	4483.3	1494.4	0.0	B4_117	360	17	7	742.7	742.7	0.0	0.0
B2_55	900	10	8	2692.2	673.0	0.0	2019.1	B4_117	360	17	8	254.8	254.8	0.0	0.0
B2_55	900	10	9	495.8	0.0	495.8	0.0	B4_117	360	17	9	462.1	0.0	462.1	0.0
B2_55	900	10	10	5861.7	4396.3	1465.4	0.0	B4_117	360	17	10	244.4	0.0	244.4	0.0
B2_55	900	10	11	679.5	0.0	679.5	0.0	B4_117	360	17	11	5314.9	1328.7	3986.2	0.0
B2_55	900	10	12	1533.8	383.4	1150.3	0.0	B4_117	360	17	12	8433.1	2108.3	6324.8	0.0
B2_55	900	10	13	1183.8	887.8	295.9	0.0	B4_117	360	17	13	428.6	428.6	0.0	0.0
B2_55	900	10	14	2396.0	1797.0	599.0	0.0	B4_117	360	17	14	496.0	496.0	0.0	0.0
B2_55	900	10	15	1985.8	0.0	0.0	1985.8	B4_117	360	17	15	377.0	377.0	0.0	0.0
B2_55	900	10	16	1858.3	1858.3	0.0	0.0	B4_117	360	17	16	1344.8	336.2	1008.6	0.0
B2_55	900	10	17	5722.8	0.0	5722.8	0.0	B4_117	360	17	17	313.3	313.3	0.0	0.0
B2_55	900	10	18	3371.7	0.0	3371.7	0.0	B4_117	360	17	18	681.5	511.1	170.4	0.0
B2_55	900	10	19	251.4	0.0	251.4	0.0	B4_117	360	17	19	2296.8	574.2	1722.6	0.0
B2_55	900	10	20	474.4	0.0	474.4	0.0	B4_117	360	17	20	1140.7	0.0	1140.7	0.0
B2_55	900	10	21	5649.7	4237.2	1412.4	0.0	B4_117	360	17	21	74.2	0.0	0.0	74.2
B2_55	900	10	22	2218.7	2218.7	0.0	0.0	B4_117	360	17	22	1081.5	0.0	1081.5	0.0
B2_55	900	10	23	7527.9	5645.9	1882.0	0.0	B4_117	360	17	23	424.2	0.0	424.2	0.0
B2_55	900	10	24	1743.3	1307.5	0.0	435.8	B4_117	360	17	24	208.5	208.5	0.0	0.0
B2_55	900	10	25	1044.4	783.3	261.1	0.0	B4_117	360	17	25	858.5	0.0	858.5	0.0
B2_55	900	10	26	3303.5	2477.6	825.9	0.0	B4_117	360	17	26	2922.6	0.0	2922.6	0.0
B2_55	900	10	27	1601.0	0.0	1601.0	0.0	B4_117	360	17	27	414.1	0.0	414.1	0.0
B2_55	900	10	28	6522.8	0.0	1630.7	4892.1	B4_117	360	17	28	4431.9	3323.9	1108.0	0.0
B2_55	900	10	29	9746.1	2436.5	7309.6	0.0	B4_117	360	17	29	354.8	0.0	354.8	0.0
B2_55	900	10	30	1300.3	325.1	975.2	0.0	B4_117	360	17	30	687.9	0.0	687.9	0.0
B2_56	920	10	1	5959.8	4469.8	1489.9	0.0	B4_118	380	16	1	193.0	0.0	193.0	0.0
B2_56	920	10	2	6320.7	4740.5	1580.2	0.0	B4_118	380	16	2	179.2	0.0	179.2	0.0
B2_56	920	10	3	3208.4	802.1	2406.3	0.0	B4_118	380	16	3	125.6	0.0	125.6	0.0

B2_56	920	10	4	490.3	490.3	0.0	0.0	B4_118	380	16	4	11435.6	2858.9	8576.7	0.0
B2_56	920	10	5	2026.1	2026.1	0.0	0.0	B4_118	380	16	5	309.2	309.2	0.0	0.0
B2_56	920	10	6	754.7	0.0	754.7	0.0	B4_118	380	16	6	67.9	0.0	0.0	67.9
B2_56	920	10	7	1048.4	786.3	262.1	0.0	B4_118	380	16	7	69.7	69.7	0.0	0.0
B2_56	920	10	8	396.3	297.2	99.1	0.0	B4_118	380	16	8	73.3	0.0	0.0	73.3
B2_56	920	10	9	3638.5	0.0	3638.5	0.0	B4_118	380	16	9	2331.3	0.0	2331.3	0.0
B2_56	920	10	10	2236.7	1677.5	559.2	0.0	B4_118	380	16	10	430.7	0.0	430.7	0.0
B2_56	920	10	11	527.2	527.2	0.0	0.0	B4_118	380	16	11	1009.7	0.0	1009.7	0.0
B2_56	920	10	12	1380.4	345.1	1035.3	0.0	B4_118	380	16	12	201.5	0.0	0.0	201.5
B2_56	920	10	13	1068.8	801.6	267.2	0.0	B4_118	380	16	13	1138.0	0.0	1138.0	0.0
B2_56	920	10	14	186.7	0.0	186.7	0.0	B4_118	380	16	14	1204.5	1204.5	0.0	0.0
B2_56	920	10	15	635.2	0.0	0.0	635.2	B4_118	380	16	15	1217.5	913.1	304.4	0.0
B2_56	920	10	16	3960.1	0.0	2970.1	990.0	B4_118	380	16	16	863.6	0.0	863.6	0.0
B2_56	920	10	17	3002.8	2252.1	750.7	0.0	B4_118	380	16	17	155.9	155.9	0.0	0.0
B2_56	920	10	18	4105.4	1026.4	3079.1	0.0	B4_118	380	16	18	113.5	113.5	0.0	0.0
B2_56	920	10	19	2755.4	2755.4	0.0	0.0	B4_118	380	16	19	6453.4	6453.4	0.0	0.0
B2_56	920	10	20	2495.5	0.0	2495.5	0.0	B4_118	380	16	20	1277.4	0.0	1277.4	0.0
B2_56	920	10	21	842.8	0.0	842.8	0.0	B4_118	380	16	21	3905.4	2929.0	976.3	0.0
B2_56	920	10	22	1558.2	1168.6	389.5	0.0	B4_118	380	16	22	390.1	0.0	390.1	0.0
B2_56	920	10	23	708.9	708.9	0.0	0.0	B4_118	380	16	23	1193.4	1193.4	0.0	0.0
B2_56	920	10	24	2874.9	0.0	2874.9	0.0	B4_118	380	16	24	112.6	0.0	0.0	112.6
B2_56	920	10	25	397.8	0.0	0.0	397.8	B4_118	380	16	25	93.8	0.0	0.0	93.8
B2_56	920	10	26	740.7	740.7	0.0	0.0	B4_118	380	16	26	1315.8	0.0	1315.8	0.0
B2_56	920	10	27	3680.8	920.2	2760.6	0.0	B4_118	380	16	27	111.3	0.0	0.0	111.3
B2_56	920	10	28	428.1	0.0	0.0	428.1	B4_118	380	16	28	108.1	0.0	108.1	0.0

Table B.1., cont.

B2_56	920	10	29	164.3	0.0	0.0	164.3	B4_118	380	16	29	208.7	208.7	0.0	0.0
B2_56	920	10	30	1119.6	1119.6	0.0	0.0	B4_118	380	16	30	5693.0	4269.7	1423.2	0.0
B2_57	940	19	1	1568.1	1568.1	0.0	0.0	B4_119	400	8	1	1735.3	0.0	433.8	0.0
B2_57	940	19	2	1583.5	0.0	1583.5	0.0	B4_119	400	8	2	76.4	0.0	0.0	76.4
B2_57	940	19	3	107.0	0.0	107.0	0.0	B4_119	400	8	3	1192.5	0.0	1192.5	0.0
B2_57	940	19	4	4250.3	3187.7	1062.6	0.0	B4_119	400	8	4	92.5	92.5	0.0	0.0
B2_57	940	19	5	420.2	0.0	420.2	0.0	B4_119	400	8	5	216.7	216.7	0.0	0.0
B2_57	940	19	6	8313.9	2078.5	6235.5	0.0	B4_119	400	8	6	260.9	260.9	0.0	0.0
B2_57	940	19	7	3650.0	912.5	2737.5	0.0	B4_119	400	8	7	447.7	0.0	0.0	0.0
B2_57	940	19	8	3880.4	3880.4	0.0	0.0	B4_119	400	8	8	146.1	146.1	0.0	0.0
B2_57	940	19	9	141.4	0.0	141.4	0.0	B4_119	400	8	9	109.5	109.5	0.0	0.0
B2_57	940	19	10	4598.8	0.0	4598.8	0.0	B4_119	400	8	10	101.4	0.0	101.4	0.0
B2_57	940	19	11	4375.3	1093.8	3281.4	0.0	B4_119	400	8	11	2946.6	0.0	2946.6	0.0
B2_57	940	19	12	2503.0	1877.2	625.7	0.0	B4_119	400	8	12	142.1	142.1	0.0	0.0
B2_57	940	19	13	224.5	0.0	224.5	0.0	B4_119	400	8	13	1280.9	0.0	320.2	0.0
B2_57	940	19	14	534.7	0.0	0.0	534.7	B4_119	400	8	14	785.0	0.0	785.0	0.0
B2_57	940	19	15	2261.6	1696.2	565.4	0.0	B4_119	400	8	15	88.5	0.0	88.5	0.0
B2_57	940	19	16	646.2	646.2	0.0	0.0	B4_119	400	8	16	133.6	0.0	133.6	0.0
B2_57	940	19	17	909.0	909.0	0.0	0.0	B4_119	400	8	17	396.8	0.0	396.8	0.0
B2_57	940	19	18	1640.8	1230.6	410.2	0.0	B4_119	400	8	18	143.9	0.0	143.9	0.0
B2_57	940	19	19	3322.9	2492.2	830.7	0.0	B4_119	400	8	19	92.9	0.0	0.0	0.0
B2_57	940	19	20	100.1	0.0	100.1	0.0	B4_119	400	8	20	7735.7	7735.7	0.0	0.0
B2_57	940	19	21	5425.1	0.0	5425.1	0.0	B4_119	400	8	21	136.3	0.0	0.0	0.0
B2_57	940	19	22	736.8	0.0	736.8	0.0	B4_119	400	8	22	4899.5	3674.6	1224.9	0.0
B2_57	940	19	23	4906.4	1226.6	3679.8	0.0	B4_119	400	8	23	654.6	0.0	654.6	0.0
B2_57	940	19	24	660.1	0.0	660.1	0.0	B4_119	400	8	24	366.4	0.0	0.0	0.0
B2_57	940	19	25	281.3	0.0	281.3	0.0	B4_119	400	8	25	3715.5	928.9	2786.6	0.0
B2_57	940	19	26	3143.7	2357.8	785.9	0.0	B4_119	400	8	26	282.8	282.8	0.0	0.0
B2_57	940	19	27	2339.7	1754.8	584.9	0.0	B4_119	400	8	27	2994.8	0.0	2994.8	0.0
B2_57	940	19	28	570.0	570.0	0.0	0.0	B4_119	400	8	28	165.3	0.0	0.0	0.0
B2_57	940	19	29	2931.1	2198.3	732.8	0.0	B4_119	400	8	29	2878.7	0.0	2159.0	0.0
B2_57	940	19	30	18473.8	4618.4	13855.3	0.0	B4_119	400	8	30	5981.6	4486.2	1495.4	0.0
B2_58	960	14	1	14271.7	14271.7	14271.7	0.0	B4_120	420	20	1	531.2	0.0	531.2	0.0
B2_58	960	14	2	4089.0	3066.8	1022.3	0.0	B4_120	420	20	2	365.9	0.0	365.9	0.0
B2_58	960	14	3	16064.9	12048.6	4016.2	0.0	B4_120	420	20	3	870.3	870.3	0.0	0.0
B2_58	960	14	4	3866.5	2899.9	966.6	0.0	B4_120	420	20	4	617.0	0.0	617.0	0.0
B2_58	960	14	5	8129.8	6097.3	2032.4	0.0	B4_120	420	20	5	207.3	207.3	0.0	0.0
B2_58	960	14	6	240.9	0.0	240.9	0.0	B4_120	420	20	6	4223.9	4223.9	0.0	0.0
B2_58	960	14	7	1976.8	1482.6	494.2	0.0	B4_120	420	20	7	4899.9	1225.0	3674.9	0.0
B2_58	960	14	8	149.3	0.0	149.3	0.0	B4_120	420	20	8	159.1	159.1	0.0	0.0
B2_58	960	14	9	682.0	0.0	682.0	682.0	B4_120	420	20	9	2178.1	0.0	2178.1	0.0
B2_58	960	14	10	503.3	0.0	503.3	0.0	B4_120	420	20	10	1751.0	0.0	1751.0	0.0
B2_58	960	14	11	392.3	0.0	392.3	0.0	B4_120	420	20	11	3923.7	0.0	980.9	0.0
B2_58	960	14	12	4644.1	1161.0	3483.1	0.0	B4_120	420	20	12	193.0	0.0	193.0	0.0
B2_58	960	14	13	211.6	0.0	211.6	0.0	B4_120	420	20	13	533.5	400.1	0.0	0.0
B2_58	960	14	14	529.7	0.0	529.7	0.0	B4_120	420	20	14	506.7	506.7	0.0	0.0
B2_58	960	14	15	579.5	0.0	579.5	0.0	B4_120	420	20	15	227.0	227.0	0.0	0.0
B2_58	960	14	16	120.0	0.0	0.0	120.0	B4_120	420	20	16	229.7	229.7	0.0	0.0
B2_58	960	14	17	2518.4	0.0	2518.4	0.0	B4_120	420	20	17	391.8	0.0	391.8	0.0
B2_58	960	14	18	1085.2	0.0	1085.2	0.0	B4_120	420	20	18	215.8	215.8	0.0	0.0
B2_58	960	14	19	5217.6	5217.6	0.0	0.0	B4_120	420	20	19	1721.0	430.3	1290.8	0.0
B2_58	960	14	20	2836.0	2127.0	709.0	0.0	B4_120	420	20	20	291.8	0.0	291.8	0.0

B2_58	960	14	21	9493.8	2373.4	7120.3	0.0	B4_120	420	20	21	17023.5	12767.7	4255.9	0.0
B2_58	960	14	22	348.5	0.0	348.5	0.0	B4_120	420	20	22	1241.2	0.0	1241.2	0.0
B2_58	960	14	23	290.7	290.7	0.0	0.0	B4_120	420	20	23	397.2	397.2	0.0	0.0
B2_58	960	14	24	7349.2	1837.3	5511.9	0.0	B4_120	420	20	24	482.1	0.0	0.0	482.1
B2_58	960	14	25	182.7	0.0	0.0	182.7	B4_120	420	20	25	2664.7	0.0	2664.7	0.0
B2_58	960	14	26	1491.4	0.0	0.0	1491.4	B4_120	420	20	26	101.4	0.0	0.0	101.4
B2_58	960	14	27	230.5	0.0	230.5	0.0	B4_120	420	20	27	9563.1	9563.1	0.0	0.0
B2_58	960	14	28	940.9	0.0	940.9	0.0	B4_120	420	20	28	3951.4	3951.4	0.0	0.0
B2_58	960	14	29	2637.4	0.0	2637.4	0.0	B4_120	420	20	29	229.7	0.0	0.0	229.7
B2_58	960	14	30	663.1	0.0	663.1	0.0	B4_120	420	20	30	346.3	0.0	346.3	0.0